NEOGENE SEDIMENTARY HISTORY OF THE CILICIA BASIN, EASTERN MEDITERRANEAN

BAHAR KURTBOGAN

NEOGENE SEDIMENTARY HISTORY OF THE CILICIA BASIN, EASTERN MEDITERRANEAN

by

© Bahar Kurtbogan

A thesis submitted to the

School of Graduate Studies

in partial fulfillment of the requirements for the degree of

Master of Science

Department of Earth Sciences

Memorial University of Newfoundland

April, 2013

St. John's Newfoundland and Labrador

Abstract

The Miocene to Recent tectonic evolution of the Cilicia Basin near the present day mouth of the Göksu River is studied using ~2000 km of high-resolution 96-channel seismic reflection profiles collected in 2008 using the RV Koca Piri Reis of the Institute of Marine Sciences and Technology. Our project is intended to provide a history of deposition in one of the ultimate sinks: the eastern Mediterranean. We mapped the distribution of sediment deposits and delineated the structures that developed in the Cilicia Basin precisely in space and time. The focus of this research is on the basin-wide structures that developed near the Turkish continental slope and extend through the entire Cilicia Basin.

Detailed interpretation and mapping of the seismic reflection profiles showed that during the Miocene a major south- and southeast-verging fold-thrust belt developed across the entire Cilicia Basin. The leading portion of this fold-thrust belt is well imaged in the Inner Latakia Basin, south east of the present-day Misis-Kyrenia Fault Zone. The trailing portion of the fold-thrust belt is believed to constitute the thrust panels which form the core of the central Taurus Mountains of southern Turkey. A north- and northwest-verging fold-thrust belt is locally mapped in the Outer Cilicia Basin. The belt is overprinted by smaller positive flower structures all soling into the primary thrust surface(s), and showing tip points extending to the depositional surface. This structural architecture suggests

that they are developed within a transpressional regime during the Pliocene-Quaternary. Seismic stratigraphic correlations with deep offshore exploration wells provided the chronology for the seismic data. A thick evaporite succession is unconformably deposited over deeper portions of the fold-thrust belt. This evaporite succession presently forms numerous salt pillows and salt rollers in Inner Cilicia Basin, and salt diapirs and salt walls in the Outer Cilicia Basin.

Detailed mapping showed that Miocene contraction was followed by partitioned contraction and extension that is related to strike-slip fault activity along the Kozan Fault Zone, a major splay from the East Anatolian Transform Fault. Our results show that Pliocene-Quaternary extension occurs within the basin contemporaneously with the contractional or transpressional structures along the southern margin of the basin. A specific problem that is addressed in this study is to understand the relationship of contemporaneous contractional to extensional deformation in the study area.

Acknowledgements

I would like to thank to my supervisors, Dr. Jeremy Hall, and Dr. Ali Aksu for their continuous support and guidance during my program. I would also like to thank to the all the students and collaborators that work in the Eastern Mediterranean Project. The seismic data for this project was collected in the RV Koca Piri Reis in collaboration with the Institute of Marine Sciences and Technology (IMST) group at Dokuz Eylül University in Izmir, Turkey. Thank to all the staff, ship crew, scientific crew and the students at IMST for their help with the data collection. Once again I would like to thank to my supervisors A. Aksu & J. Hall for providing funding for this project through NSERC Discovery Grants. The seismic data processing software was kindly provided by Landmark Graphics.

Table of Contents

List of Figures

List of Plates

CHAPTER ONE

INTRODUCTION

1.0. Background

The Central Anatolian Plateau contains eastern and central portions of the Aegean-Anatolian Microplate and is an orogenic uplift structure which is a young example of continental collision (Fig. 1.1, Schildgen et al., 2011; Cosentio et al., 2011, Yildirim et al., 2011). The Aegean-Anatolian Microplate is in the early stages of collision in between converging African, Arabian and Eurasian plates (Ben-Avraham et al., 2006; Dilek and Sandvol, 2009; Robertson et al., 2012). The Cilicia Basin has evolved in the forearc region at the southern edge of the Aegean-Anatolian Microplate in the eastern Mediterranean Sea (Fig. 1.1; Biju-Duval et al., 1978; Aksu et al., 1992, 2005; Bridge et al., 2005). The basin lies close to the eastern edge of the microplate within strands of the East Anatolian Transform Fault which forms the plate boundary with the Arabian and African plates (Fig. 1.2). Convergence of African and Arabian plates to the north has resulted in subduction of the African Plate along the Cyprus and Hellenic arcs, and the collision of the Arabian Microplate with the Aegean-Anatolian Microplate (Şengör et al., 1979; Ben-Avraham et al., 1988, 2006; McClusky et al., 2000). This convergence has resulted in the westward tectonic escape of the Aegean-Anatolian Microplate (Şengör et al., 1979, McClusky et al., 2000, Ben-Avraham et al., 2006).

Previous workers established that the Cilicia Basin has active tectonic structures resulting in contraction in some areas and extension in others (Evans et al., 1978; Aksu et

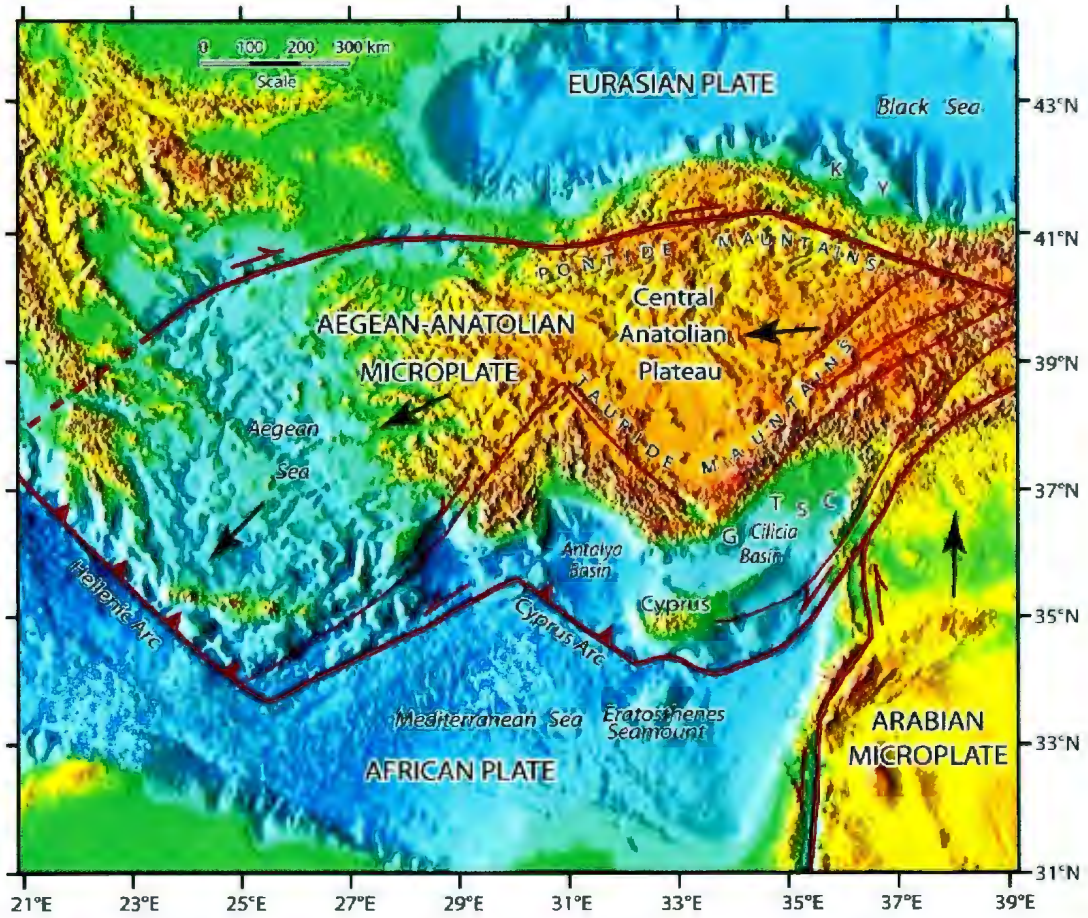

Figure 1.1: Physiographic map of the eastern Mediterranean showing simplified tectonic elements, Tauride and Pontide Mountains, Central Anatolian Plateau and the mouths of major rivers (C- Ceyhan, G- Göksu, K- Kızılırmak, S- Seyhan, T- Tarsus, and Y- Yeşilırmak). Large arrows indicate the sense of plate motion relative to a fixed Eurasian plate; half arrows indicate transform-strike-slip faults (Hall et al., 2008).

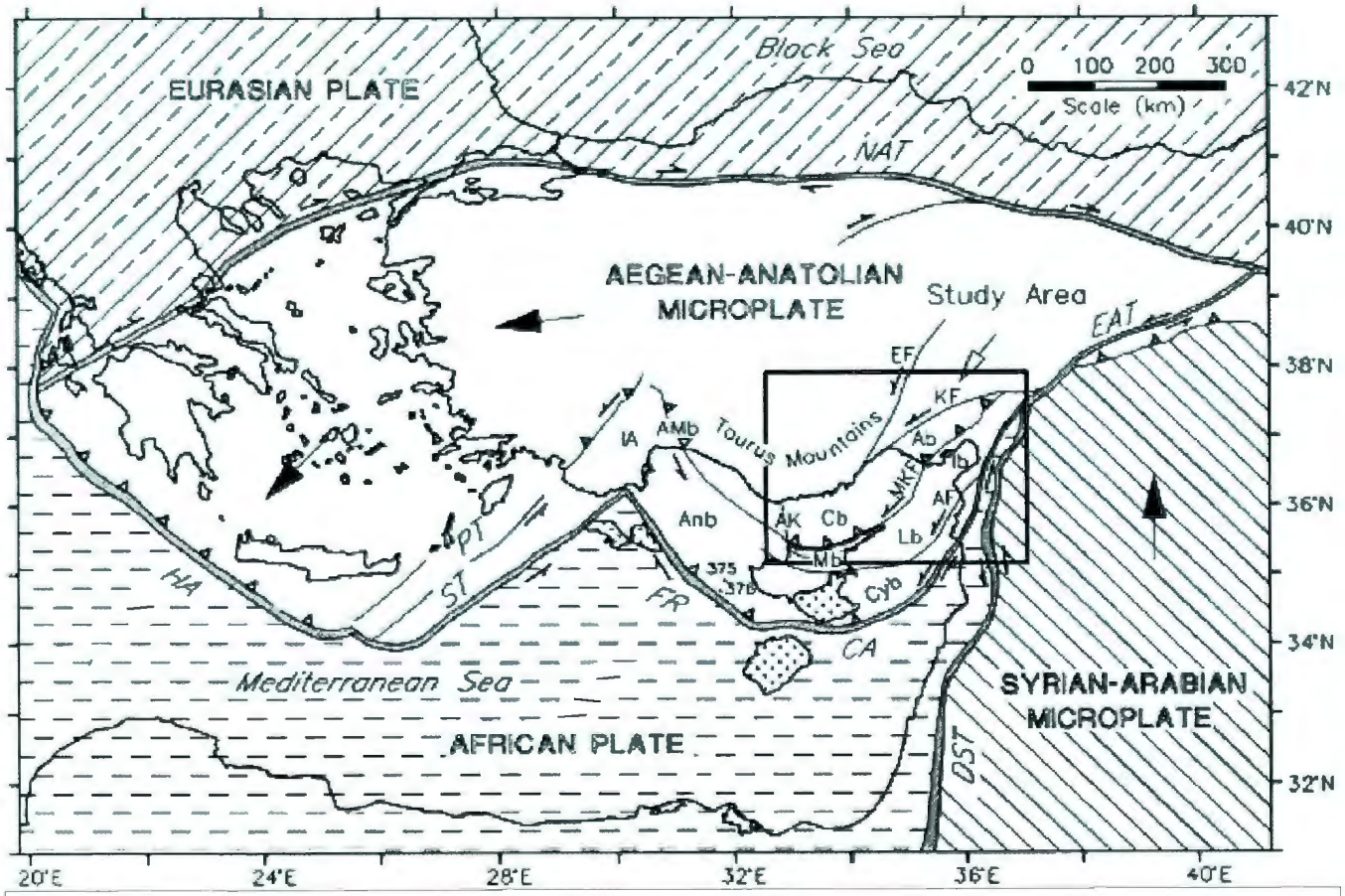

Figure 1.2: Eastern Mediterranean plate tectonics and plate motions relative to a fixed Eurasian plate. (Ab=Adana Basin, AF=Amanos Fault, AK=Anamur Kormakiti zone, Anb=Antalya Basin, CA=Cyprus Arc, Cb=Cilicia Basin, Cyb=Cyprus Basin, DST=Dead Sea Transform Fault, EAT=East Anatolian Transform Fault, EF=Ecemiş Fault, FR=Florence Rise, HA=Hellenic Arc, IA=Isparta Angle, Ib=Iskenderun Basin, KF=Kozan Fault, Lb=Latakia Basin, Mb=Mesaoria Basin, MKF=Misis-Kyrenia Fault, NAT=North Anatolian Transform Fault, PT=Pliny Trench, ST= Strabo Trench, Aksu et al., 2005)

al., 1992a, 2005b; Ergin et al., 2004, Bridge et al., 2005, Piercey 2011). The objective of this thesis is to map and interpret the active offshore structures in the central portion of Cilicia Basin, using multichannel seismic reflection images, so as to explain how the different kinds of strain overlap in time in the Pliocene-Quaternary.

Approximately 2500 km of high-resolution multichannel seismic reflection profiles were acquired for this project from the Cilicia Basin in a 30-day cruise in 2008 by a research team from the Memorial University of Newfoundland and the Dokuz Eylül University in Turkey. Seismic profiles are positioned as a fan, spreading out from the present-day Göksu River mouth, toward the northern Cyprus (Fig. 1.3). The seismic grid was tied to two offshore exploration wells: Seyhan-1 (S1) and Karataş-1 (K1) (Fig. 1.3). The data for my research are positioned at the middle of the study area covering northeastern Outer Cilicia Basin, and southwestern Inner Cilicia Basin, including the transition zone in between (Fig. 1.3). In addition, this project also ties to previous data from four major research cruises by the research team from Memorial University of Newfoundland and Dokuz Eylül University in 1991, 1992, 2001 and 2007, and seismic data from Turkish Petroleum Corporation (Fig. 1.3).

1.1. Geological Setting

The eastern Mediterranean Sea is the remnant of a larger Tethys Ocean that evolved during the Mesozoic (Robertson, 1998). The present day tectonic processes in the region are largely controlled by the continental collision of the Arabian and Eurasian plates (Biju-Duval et al., 1978, McClusky et al., 2000, Dilek and Sandvol 2009). The

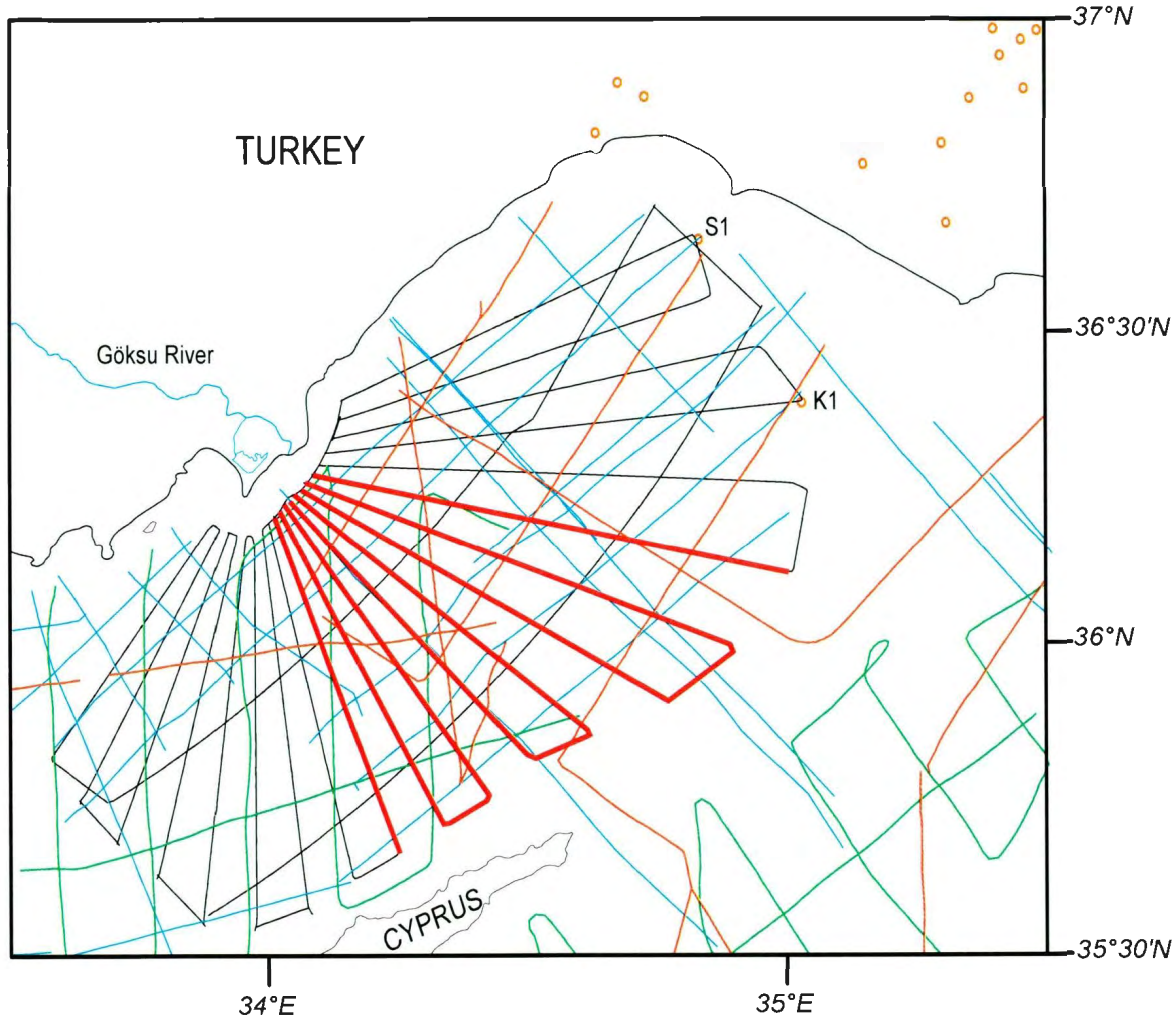

Figure 1.3: Location map showing the available data in the Cilicia Basin. Black lines are 2008 data, orange lines are 1991 data, green lines are 1992 data and light blue lines are the industry seismic reflection profiles. Thick red lines are the seismic data from the 2008 dataset that is used in this thesis. S1 and K1 are the Seyhan-1 and Karataş-1 exploration wells in the Inner Cilicia Basin.

relative northward movement of the African Plate and Arabian Microplate with respect to the Eurasian Plate resulted in westwards escape of the small Aegean-Anatolian Microplate along the North Anatolian and East Anatolian Transform faults in a counter-clockwise rotation (Fig. 1.2, Şengör et al., 1985, Dewey et al., 1986). The North Anatolian Transform Fault delineates the boundary between the Eurasian Plate and Aegean-Anatolian Microplate in a right lateral strike slip movement, where the East Anatolian Transform Fault shows a left lateral strike slip motion (Fig 1.2; Şengör et al., 1985). Sinistral strike-slip motion on the East Anatolian Transfom Fault is a major control on the structural elements of the Cilicia Basin. Two main fault zones characterising the Neogene evolution of the basin, Kozan and Misis-Kyrenia fault zones, are major splays from the East Anatolian Transform Fault.

The terminal continental collision of the Arabian Microplate and Eurasian Plate that occurred in the Miocene resulted in the development of the the Bitlis-Zagros suture zone (Şengör et al., 1979, 1981). Continuing convergence of the Arabian Microplate and Eurasion Plate resulted in N-S shortening and thickening, associated with rapidly rising elevations in the eastern portion of the Aegean-Anatolian Microplate (Şengör et al., 1981). Subsequently, in the late Miocene the westward escape of the Aegean Anatolian Microplate initiated along the North and East Anatolian transform faults (Şengör et al., 1981). The Hellenic Arc and the Pliny-Strabo Trenches delineate the convergent boundary between the African Plate and the Aegean-Anatolian Microplate in the west where the subduction is still active and the subduction zone is steepening and/or rolling back causing the pervasive extension in the back arc region (i.e., the Aegean Sea and

western Anatolia; Fig. 1.2; McKenzie and Yılmaz, 1991; Spakman and Wortel, 2004). The Florence Rise and Cyprus Arc delineates the boundary between the African Plate and the Aegean-Anatolian Microplate in the east where subduction has essentially stopped along the Cyprus arc due to initiation of collision of micro-continental blocks on the northern edge of the subducting lower portion of the African Plate (Fig. 1.2; Ben-Avraham et al., 1988, 1995, Woodside et al., 2002, Sellier et al., 2011, 2012)

1.2. Study Area

There are several large basins on the southeastern edge of the Aegean-Anatolian Microplate in the northeast Mediterranean. The Adana and Mesoria basins are the onland extensions of the marine Cilicia and Latakia-Iskenderun basins, respectively. The Kyrenia Range and its marine extension Misis-Kyrenia fault zone separate the Cilicia-Adana basin complex from the Latakia-Iskenderun-Mesoria basin complex (Aksu et al., 1992, 2005; Hall et al., 2005; Calon et al., 2005). Cilicia Basin lies directly between Cyprus and Turkey in the eastern Mediterranean Sea, bounded by Taurides Mountains in the north, and Kyrenia Range and its marine extension in the south and southeast (Fig. 1.2). The evolution of the Cilicia-Adana basin complex started in the Oligocene to early Miocene in a foredeep setting in front of the Tauride fold-thrust belt (Williams et al., 1995; Calon et al., 2005 a; Aksu et al., 2005). Tectonic evolution of this basin complex is related with the subduction of the Africa Plate beneath the Eurasia Plate along the Cyprus and Hellenic arcs (Biju-Duval et al., 1978). Subduction changed to collision along the Cyprus Arc when the Eratosthenes Seamount collided with the subduction zone; however subduction is still active along the Hellenic Arc (Ben-Avraham et al., 1995; McClusky et

al., 2000, Sellier et al., 2012. The present study of the Cilicia Basin provides better understanding of tectonic and stratigraphic controls on young collisional systems, transition of subduction to collision, and Neogene evolution of a fore-arc basin in this transition.

The Cilicia Basin formed in the mid-to-late Miocene in a fore arc region associated with the subduction of the African Plate beneath the Aegean-Anatolian Microplate along the Cyprus Arc (Biju-Duval et al., 1978). On its western margin, the Cilicia Basin is separated from the Antalya Basin by the N-S trending Anamur-Kormakti zone across which the water depth significantly drops westward from ~1000 metres to ~2200 metres (Figs. 1.2, 1.4). In the northeast section of the eastern Mediterranean, the morphology of the sea-floor is largely controlled by the major tectonic features and by the sediment input from the surrounding rivers which include the Seyhan, Ceyhan, Tarsus and Göksu (Aksu et al., 2005). In the Cilicia Basin, the sea-floor gradually deepens from the Turkish shelf; reaching its maximum depth of 1000 metres in the central portion of the Outer Cilicia Basin (Fig. 1.4). Towards the south, along northern Cyprus the seafloor becomes notably shallower. The sea-floor depth also increases from the Inner to the Outer Cilicia Basin (Fig. 1.4). Stratigraphic and structural relationships demonstrate that the late Pliocene-Quaternary Cilicia Basin evolved as an asymmetric piggy-back basin on the hanging wall of the large, south verging Misis-Kyrenia thrust culmination (Aksu et al., 2005). The Cilicia Basin is sub-divided into a NE-SW trending shallower segment referred to as the Inner Cilicia Basin and an E-W trending deeper segment known as the

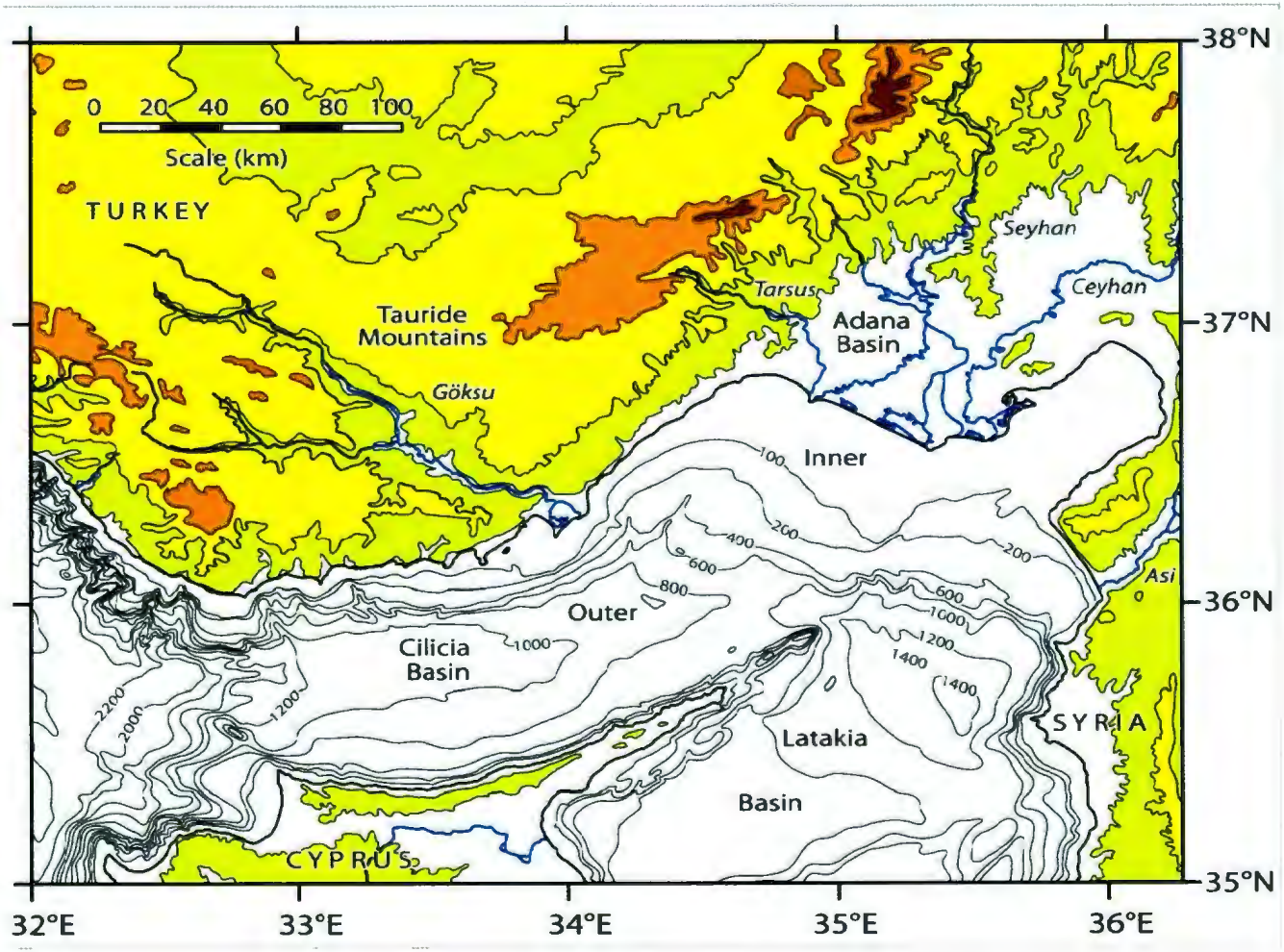

Figure 1.4: Bathymetry map of the Cilicia Basin and surroundings (Aksu et al., 2005b).

Outer Cilicia Basin (Fig. 1.4; Aksu et al., 2005). The study area for this thesis is the Outer Cilicia Basin and its transition to the Inner Cilicia Basin.

1.3. Previous Studies

Mulder (1973) and Mulder et al. (1975) suggested that the onset of the Neogene basins of the Mediterranean region occurred after the major Oligocene orogenic phase of the Alpine system. They distinguished several elongated salt basins which are separated by narrow thrust belts which were folded and uplifted in the late Miocene-early Pliocene, quoting the Kyrenia-Misis tectonic zone as an example. These publications were the first to note several kilometres of Pliocene-Quaternary subsidence and pointed to the presence of salt structures, including pillows and domes in the up to 1.5 km-thick upper Miocene evaporite succession.

Evans et al. (1978) denoted the asymmetrical infilling of the Cilicia Basin from north and northeast, and the flowage of the Messinian evaporites as a result of this asymmetrical infilling. They further concluded that the flowage of evaporites resulted in east-trending morphologic zones, and compression has not had a big role in this tectonism. They supported Woodside (1977) and Smith (1977) concerning the recently continuing basin subsidence and sediment deposition from the northeast. Evans et al. (1978) further suggested that the bathymetry of the shelf region of the outer Cilicia Basin is related to the surficial expressions of extensional faults in the upper portion of the Pliocene-Quaternary succession. Aksu et al. (1992) showed that the Pliocene-Quaternary depocentres are formed in extensional basins, bounded by splays of the East Anatolian Transform Fault.

Şengör et al. (1985) and Dewey et al. (1986) suggested that the Adana-Cilicia basin complex could be a major pull-apart in a left-lateral transform fault or more probably developed as the result of a compatibility gap in the evolution of a FFF-type triple junction, giving rise to a NNW extension in the region. Şengör et al. (1985) further proposed that when strike slip faults meet within the continental lithosphere, incompatibility problems could arise due to the buoyancy and low shear strength of the lithosphere. Their kinematic analysis, which considered the rates and directions of plate movements in the area, suggested that oblique, north to northwest directed extension should result in the Adana-Cilicia basin complex.

Robertson and Woodcock (1986) noted the subduction south of Cyprus and an extensional fore-arc setting in late Eocene and Miocene time followed by a dramatic subsidence and turbidite accumulation from the erosion of Taurides Mountains. They also suggested that in the middle Pliocene, large scale southward thrusting and tilting occurred in a compressional deformation setting as a result of the uplift and faulting in late Miocene. Kelling et al. (1987) noted that besides the collisional overthrusting of the Misis complex there is also evidence of sinistral strike slip faulting in the Misis Mountain complex. They related this faulting to post-Miocene inception of motion along the East Anatolian Transform Fault system. They supported the southward thrust culmination in middle Pliocene and believed that it was initiated by an Oligocene-Miocene phase of extension that caused intracontinental sagging, forming the Adana and Cilicia basins. Karig and Kozlu (1990) emphasized the strong evidence of extensional tectonism in the lower Miocene, and supported the idea of strike slip motion dominating the evolution of

the region. They further believed that the thrust tectonics component of the region was exaggerated in previous studies.

Aksu et al. (1992 a,b) noted that glacio-eustatic sea level fluctuations and basin subsidence are the major controlling factors in the Cilicia and Iskenderun basins. Aksu et al. (1992 b) and Kempler and Garfunkel (1994) suggested that the Misis-Kyrenia thrust belt may also have acted as a strike slip fault. Kempler and Garfunkel (1994) noted the different structural settings in the east and west of the northeastern Mediterranean. They interpreted the Misis-Kyrenia fault zone as a large flower structure in the west, and Adana-Cilicia and the Iskenderun-Latakia-Mesaoria basins in an extensional origin on its flanks in the east. They believed that the subsidence of these basins has occurred since mid to late Miocene, and the strike slip motion of the Misis-Kyrenia fault zone has occurred in late Eocene to early Oligocene.

Williams et al. (1995) proposed that the Miocene successions of the onland Adana Basin were deposited in an underfilled foreland basin formed in response to load-induced flexure resulting from thrusting in the Taurides Mountains in the north. They noted a phase of middle to late Miocene extensional faulting, synchronous with the development of a positive flower structure along a N-S trending sinistral fault zone west of the Misis Mountains followed by a phase of uplift centered on the Misis structural high in the Pliocene.

Yetiş et al. (1995) noted a phase of uplift in the region following the middle Eocene regression, and terrestrial deposition in an intramontane setting during the late

Eocene to early Miocene. The later phase of Eocene compression was followed by a regional regression marked by shallow marine-fluvial and deltaic deposits during the late Serravallian to Tortonian. They indicated that continuing regression resulted with significant evaporite deposition in the Messinian. They recognized a phase of Messinian uplift in the Misis Mountains, whereas uplift in the Kyrenia Range first occurred in the late Pliocene.

Koçyiğit and Beyhan (1998) suggested that the northwestern margin of the Adana-Cilicia Basin is delineated by strike-slip faults in the eastern portion of the newly proposed Central Anatolian fault zone, which in the study area is the reactivation of the older Ecemiş Fault. They noted that the present day structural pattern of this fault zone indicates ENE-WSW directed extension with a complementary NNW-SSE directed shortening.

Robertson (1998) suggested that the eastern Mediterranean pre-Messinian marine basins, including the Cilicia Basin were formed as a result of extensional faulting. He related the subsidence in the Adana and Manavgat Basins in the Middle Miocene to this extensional faulting. He indicated that in the Tertiary a single subduction zone occupied the northern Neotethyan margin, and that in southeastern Turkey this subduction zone remained active until early-middle Eocene. He noted that continental collision began in the early Eocene and progressively consumed the remaining oceanic crust until the suturing of the Bitlis-Zagros zone in the late Miocene. Robertson (1998) further indicated that subduction and arc volcanism persisted into the early Miocene along the northern margin of the eastern Mediterranean basins, but subduction jumped to the present plate

boundary south of Cyprus in the early Miocene. He noted that continued subduction caused the Erathosthenes Seamount to collide with the Cyprus margin in the early Pliocene, initiating the rapid uplift of Cyprus from late Pliocene to mid-Pleistocene.

1.4. Strike-slip fault systems

Many previous studies showed evidence for strike-slip motion in the Cilicia Basin (Şengör et al., 1985; Dewey et al., 1986; Kelling et al., 1987; Karig and Kozlu 1990; Aksu et al., 1992b, 2005; Koçyiğit and Beyhan 1998). Therefore, it is important to understand the kinematics of a strike-slip fault system. Strike-slip fault systems are narrow and continuous zones where there is no net addition or subtraction to the crust. A typical strike slip system occurs in a triaxial stress field, where intermediate principal stress $\sigma 2$ is vertical, and maximum and minimum principal stresses $\sigma 1$ and $\sigma 3$ are in the horizontal plane (Fig. 1.5a). Strike-slip fault zones usually consist of an array of subsidiary deformations. Faults parallel to the main vertical strike slip fault are Y-shears or PDZ's (principal deformation zone). Strike-slip fault systems often contain many *en échelon* synthetic and antitethic faults that lie at low (~20°) and high angle to the main fault, respectively. These are called Riedel shears (R- and R'-shears). P-shears are another synthetic subsidiary deformation that lie symmetrically to R-shears with respect to the fault plane (Fig. 1.5b).

Restraining and releasing bends may develop along the course of continuous strike-slip fault systems (Fig. 1.5c, Crowell 1974, Rodgers 1980, Cunningham and Mann, 2007). Rodgers (1980) defined the two approximately parallel strike- slip faults that

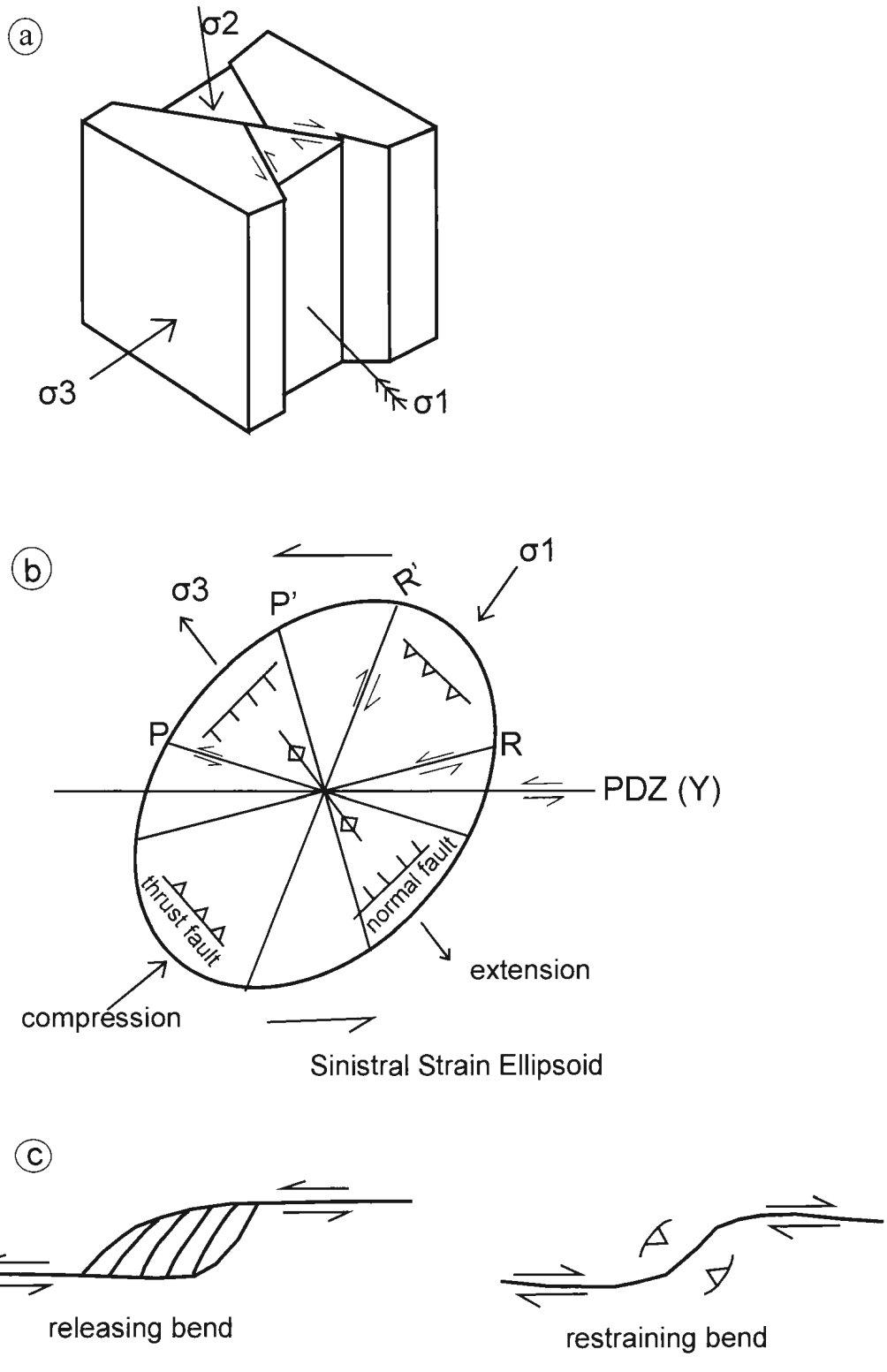

Figure 1.5: Strike-slip fault systems

delimit the restraining or releasing bends as master faults. Burchfiel and Stewart (1966) defined pull-apart basins as zones of depression generated by extension along strike-slip faults based on their interpretation of Death Valley Basin occurring at a releasing bend. Increase in the offset of the master faults of a sinistral strike-slip system generates "lazy-S" shaped pull-apart basins (Mann et al., 1983). Mann et al. (1983) further noted that pull-aparts most commonly originate on oblique fault segments which represent releasing fault bends, and increased extension of the basin generates topographic depression between oblique-slip faults defining the edges of the basin. Pull apart basins can be observed in any strike slip settings, such as, oblique subduction zones, escape tectonics, intracontinental strike-slip activity.

1.5. Outline of the Problem and Scientific Objectives

The incipient collision of the Aegean-Anatolian Microplate with the African and Eurasian plates offers a unique opportunity to study the switch from subduction to collision over a timeframe that is young enough to avoid the overprint of later events.

The scientific objectives of this project are mainly focused on the structural elements that are observed in the Outer Cilicia Basin and its transition to the Inner Cilicia Basin.

- The broad objective of this thesis is to establish the Miocene to Recent structural and stratigraphic framework of the study area based on the interpretation of the high resolution multichannel seismic reflection data that were acquired for this study, and other available data in the study area from the previous studies.

- A specific purpose of this research is to focus on the structures that developed near the Turkish continental shelf. This study will allow us to have a better understanding of the nature and the evolution of these structures and their place in a broader regional context in the Central Anatolian Plateau and surroundings.
- A specific problem that is addressed concerns the relationship of seemingly contemporaneous contractional to extensional deformation in the study area.

Many authors have commented on extensional or transtensional structures along the margins of the Cilicia Basin (Evans et al., 1978; Şengör et al., 1985; Karig and Kozlu 1990; Aksu et al., 1992a,b; Aksu et al., 2005b). Pliocene-Quaternary extension certainly occurs within the basin (Aksu et al., 2005). However this extension appears to be contemporaneous with the contractional or transpressional structures along the southern margin of the basin (the Misis-Kyrenia fold-thrust belt, Aksu et al., 2005).

In mapping the Cilicia Basin, a key issue will be to delineate the structures more precisely than in previous studies, not only in space, but also in time. The use of growth strata and progressive syn-tectonic unconformities, indicatives of the duration of faulting; is critical in the evaluation of the timing of the contractional and extensional structures that developed in the basin.

CHAPTER TWO

Scientific Methods

2.0. Data Acquisition

The data for this project were collected from the Cilicia Basin in a 30-day cruise in 2008 in collaboration of the research teams from Memorial University of Newfoundland and Dokuz Eylül University in Turkey. In addition, this project also ties to previous data from two of the four major research cruises collected by the research team from Memorial University of Newfoundland and Dokuz Eylül University in 1991, 1992 and from Turkish Petroleum Corporation (TPAO). Approximately 2500 km of high resolution marine seismic reflection data were acquired using the RV *Koca Piri Reis* of the Dokuz Eylül University during the 2008 cruise. The seismic profiles were positioned as a fan, spreading out from the present-day Göksu River mouth, and the seismic grid was tied to two offshore exploration wells: Seyhan-1(S1) and Karataş-1 (K1) (Fig. 2.1).

The equipment of this marine survey consisted of the following components: seismic source consisting of an air gun array, receiver consisting of a multichannel hydrophone streamer, and digital recording device (Fig. 2.2). The seismic source for this survey was an air-gun array consisting of 7 guns with a combined volume of 200 cubic inches (3277 cm^3). A set of 4x40 cubic inch (656 cm^3) guns; 1x20 cubic inch (328 cm^3) gun; 2x10 cubic inch (164 $cm^{3)}$ guns were combined to create the 200 cubic inch (3277 cm^3) volume. Two of the 40 cubic inch (656 cm^3) guns were placed adjacent to each other to imitate an 80 cubic inch (1312 cm^3) gun. The wavelet created by this air gun array

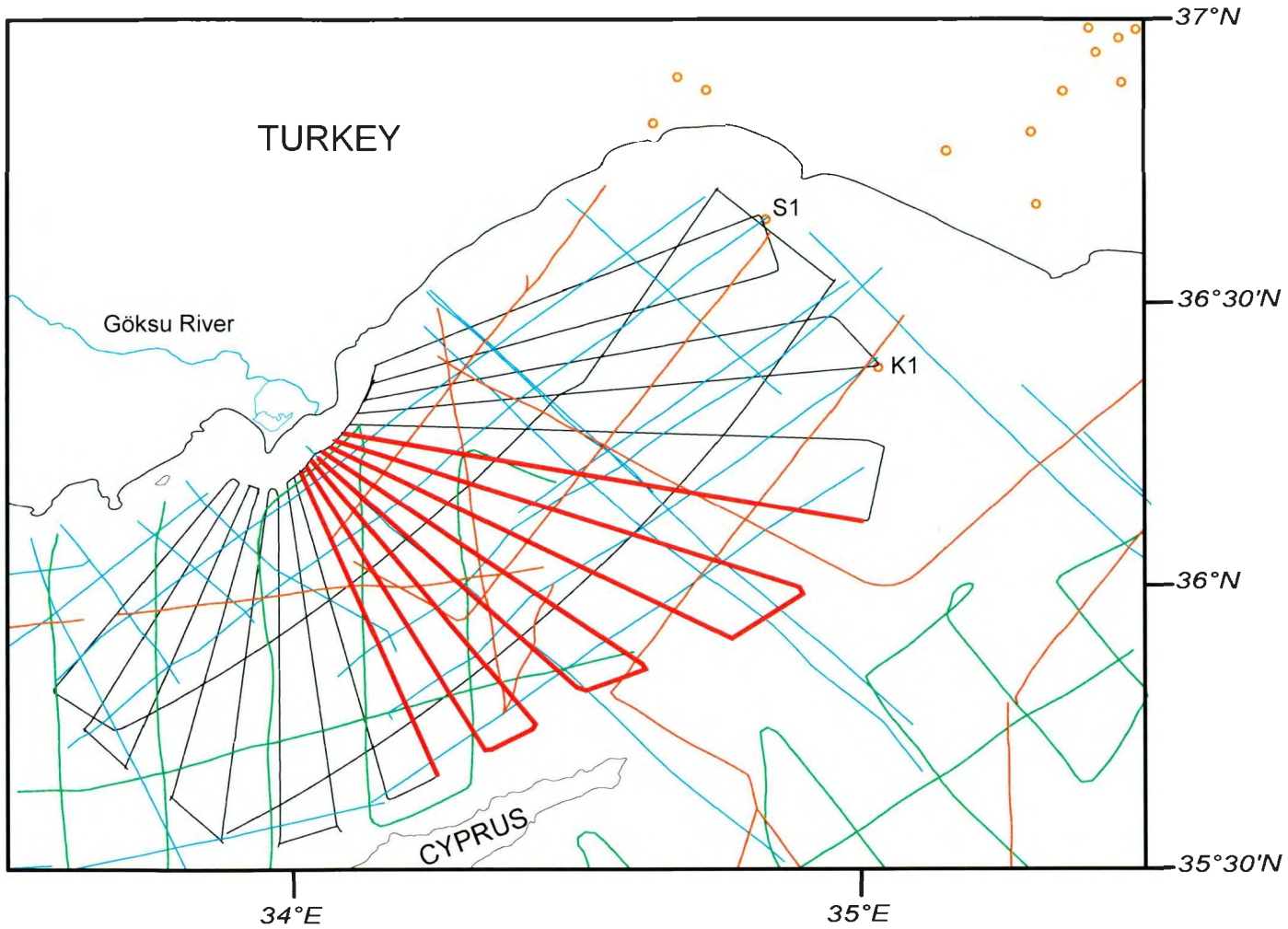

Figure 2.1: Location map showing all the available data in the Cilicia Basin. Black lines are 2008 data, orange lines are 1991 data, green lines are 1992 data and light blue lines are the industry seismic reflection profiles. Thick red lines are the seismic data from the 2008 dataset that is used in this thesis. S1 and K1 are the Seyhan-1 and Karataş-1 exploration wells in the Inner Cilicia Basin. Uninterpreted seismic sections and a map showing their locations and fix numbers are provided in the of the thesis

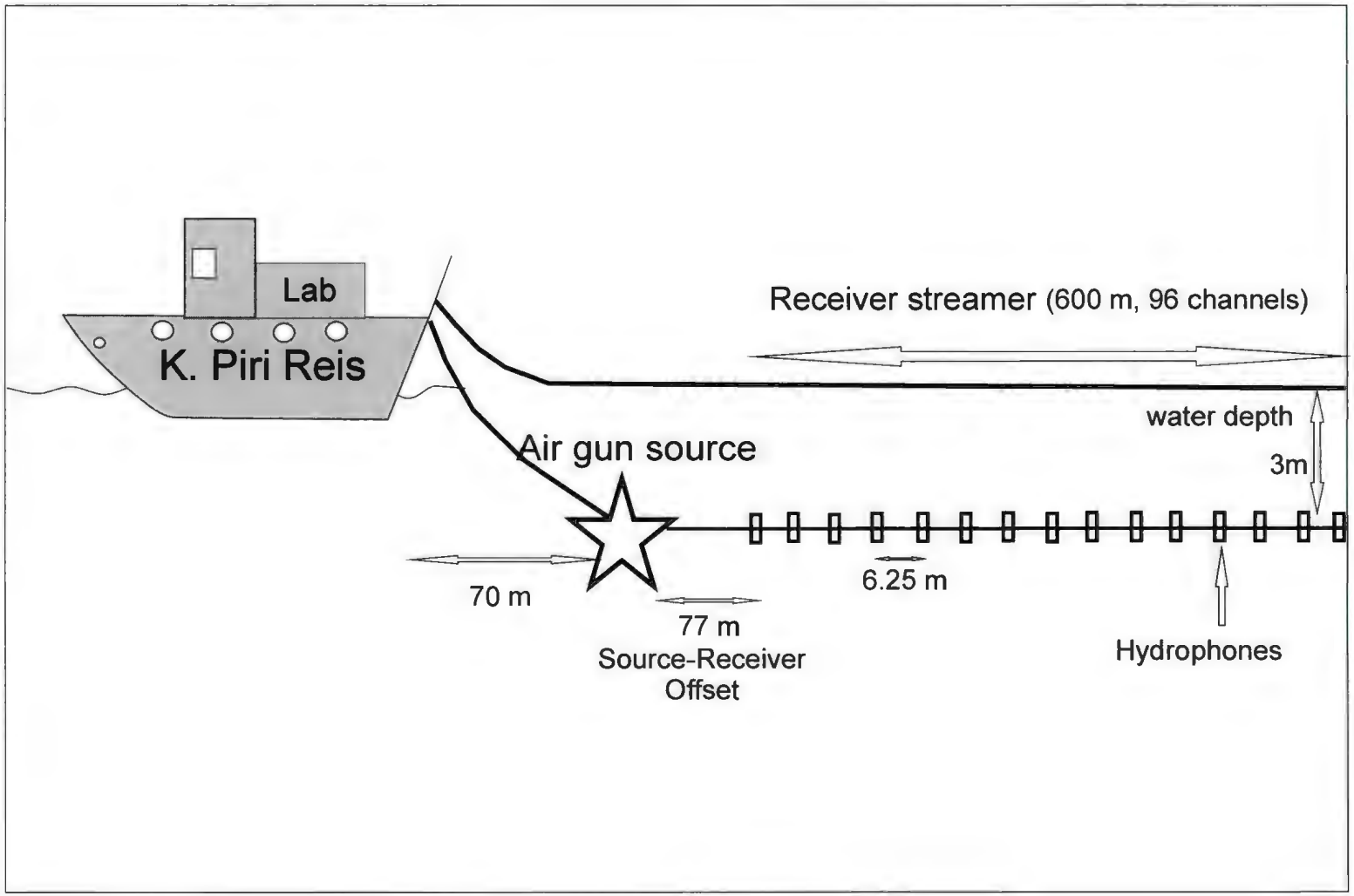

Figure 2.2: Schematic view of the survey set-up for 2008 cruise.

source has a signal bandwidth of 30-200 Hz. Compressed air for the guns was provided by a deck-mounted diesel compressor. The source was towed 70 m behind the ship at a 3 m depth below the sea surface to provide an optimal tuning of the primary pulse and the pulse of the reflection from the air-to-sea interface at a source frequency of 120 Hz. The trigger pulses were generated from the Global Positioning System (GPS) of the ship. Shots were fired at an adjusted time interval of every 10 seconds at the time of recording GPS navigation fixes for the shot spacing of 25 m.

The incoming reflections were detected and recorded using Dokuz Eylül University's 96 channel digital hydrophone streamer and an NTRS-2 seismograph. The streamer had a total length of 600 m with the channels spaced every 6.25 m (Fig. 2.2). The hydrophone streamer was towed at a constant depth which was approximately 3 m below the sea surface, and the depth of the streamer was controlled by nine streamer depth controllers, also known as streamer birds at 75 m intervals. The offset of the first channel from the source was 77 m.

2.1. Data Processing

To convert the raw data into interpretable seismic images some processing steps were applied. The main objective of the processing was to increase the signal quality by eliminating or decreasing the noise from the data, and creating better images for the interpretation. The data were processed by using Landmark's ProMax© software and the following processing flow:

- SEG-Y Data Import

- Spherical Divergence Correction
- Static Correction
- Geometry and Common Depth Point (CDP) Stacking
- Velocity Analysis and Normal Move Out (NMO) Correction
- Predictive Deconvolution (Pre- and Post-Stack)
- Migration (Stolt and Kirchhoff Time Migration)
- Display
- Archive SEG-Y
- Final Starpak Plotting and Corel Draw Plotting

2.1.1. SEG-Y Data Import

The primary step of the data processing was to import the data into the processing software and loading the raw data into ProMAX© by using the SEG-Y input function. Following the data import, visual inspection took place to check the shots, channels, and the noise distribution of the data. For the initial inspection, the data were displayed as a single channel or near-trace gathers which use the nearest shot groups. There was only one problematic channel within 96 channels which was the 13^{th} channel. This channel was the only noisy channel; however the noise was not a major issue, because an attempt to remove the high frequency noise from the data would remove the noise of this channel as well. The noise on the channel 13 can be seen in Figure 2.3 which is the raw data

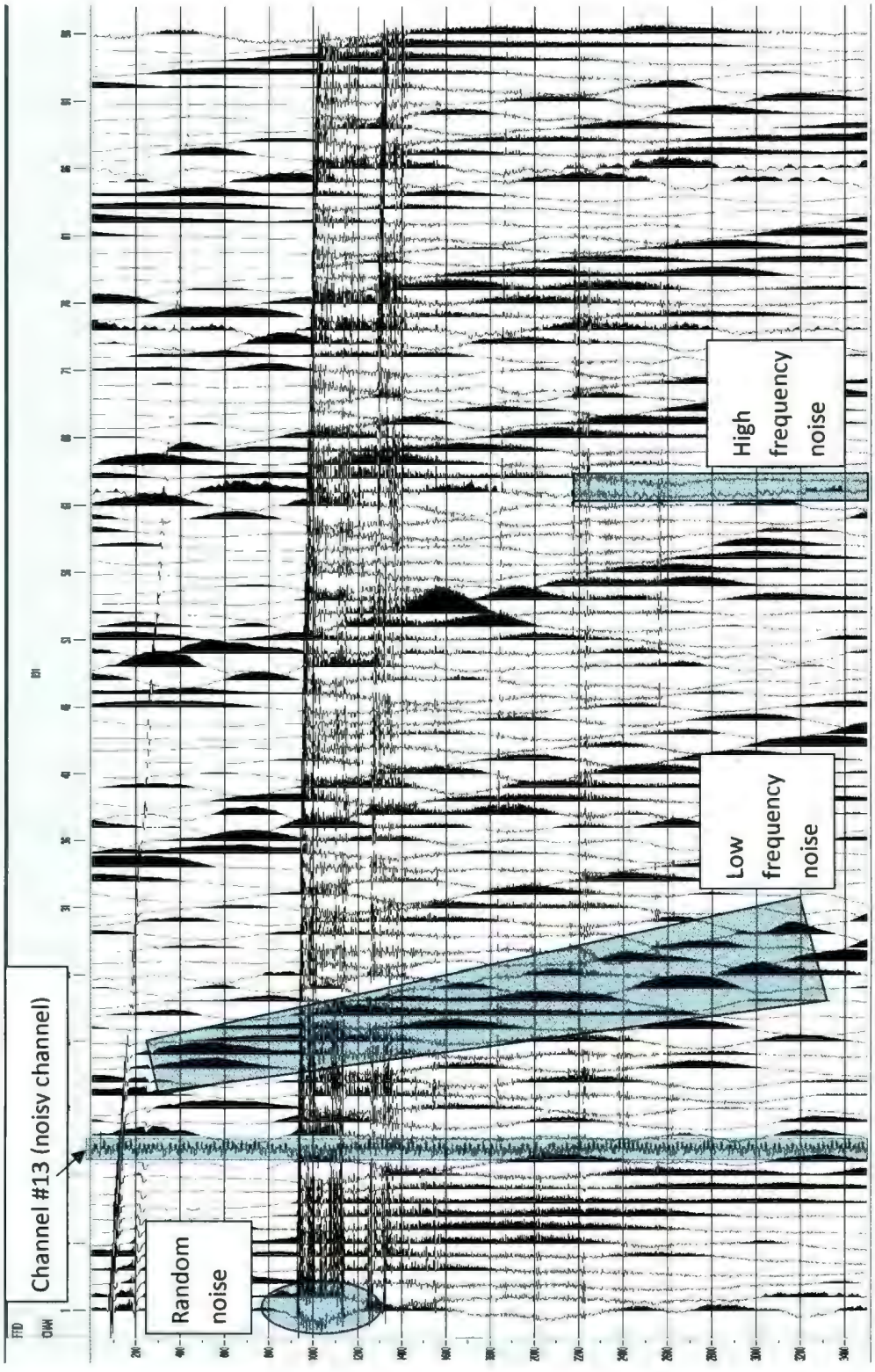

Figure 2.3: Raw data. All channels of the first shot.

showing all channels of the first shot. The figure also illustrates the low and high frequency noise, and some random noise. Figure 2.4 is also the raw data in a different display that illustrates only one channel of all shots: a near trace gather. This section is also very noisy, and the primary energy is not very strong. An automatic gain control (AGC) and a bandpass filter were applied for display to bring up the weak signals and eliminate some of the noise, respectively, but they were not applied permanently. Effects of the AGC and bandpass filter can be seen in Figure 2.5, which shows that the primary energy is more visible and most of the noise is eliminated.

The bandpass filter was applied to the data for better display purposes and it was not applied permanently until after the final migration. The filter type and the parameters were decided by the inspection of the raw data and also using the frequency spectrum. Raw shots and the near-trace gather display the noise which can be both high and low frequency (e.g. Fig. 2.4). The signal that our source generates has a bandwidth of 30-200 Hz, so in theory the frequencies below 30 Hz and above 200 Hz are considered to be noise. Eliminating the noise outside the signal bandwidth, the signal to noise ratio is significantly increased. For the 2008 data, a minimum phase, time Butterworth filter with the parameters of 40-12-240-48 Hz worked almost perfectly. The parameters of 40 and 240 here are the low and high cut frequencies respectively, while the 12 and 48 are their corresponding dB/octave slope. Comparison of the Figures 2.3 and 2.6, or 2.4 and 2.5 illustrates the effect of the bandpass filter on the data. Figure 2.7 is shows the percent power frequency spectrum which is also used to determine the filter parameters. The noise in the data that have very high or very low frequency can easily be determined by displaying this spectrum. The first panel in this display shows the seismic traces and the

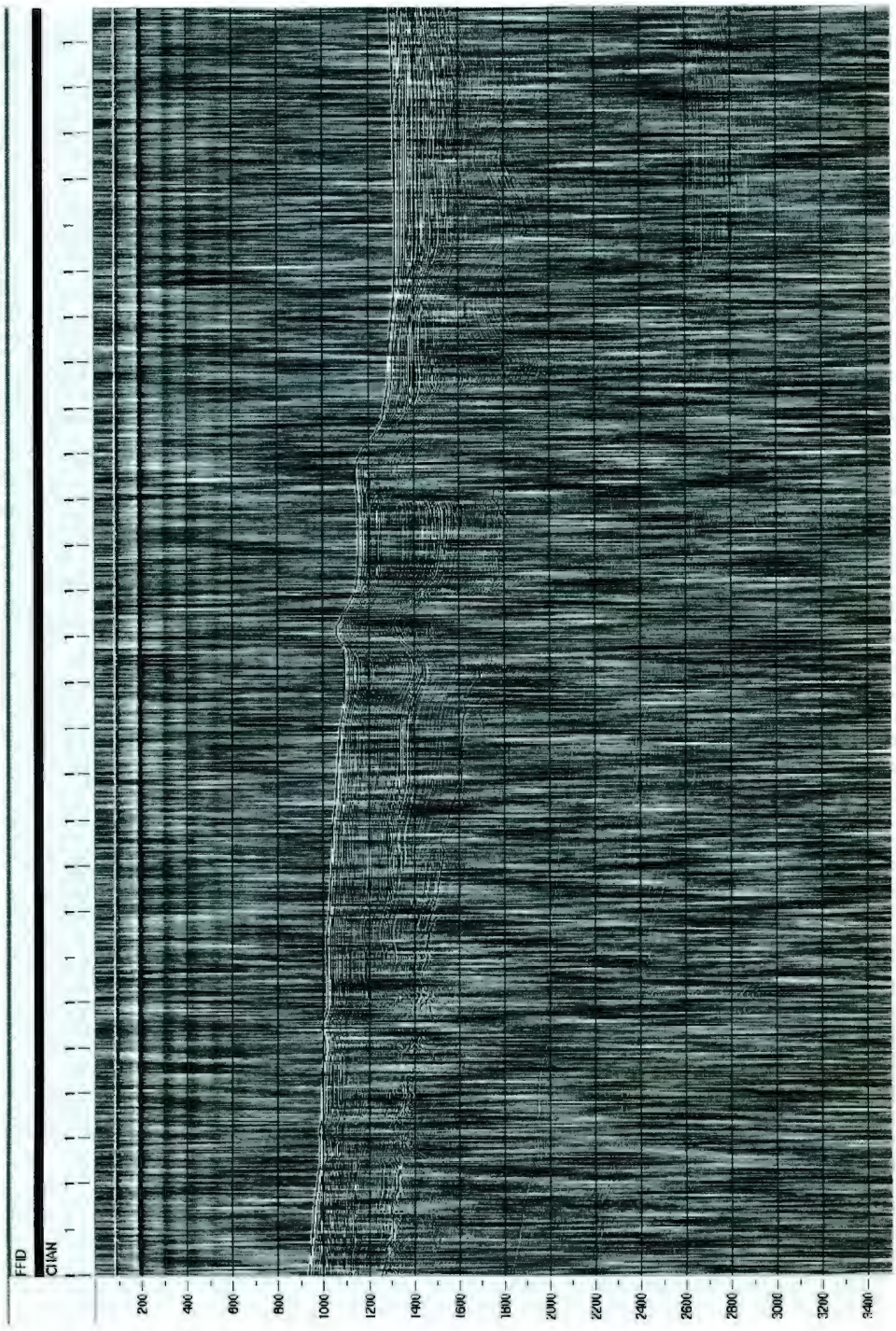

Figure 2.4: Raw data showing a single channel of all shots. The section is noisy and primary energy is not very strong.

Figure 2.5: The same display in Figure 2.4 after an Automatic Gain Control (AGC) and bandpass filter. The section is less noisy and the primary energy is more visible.

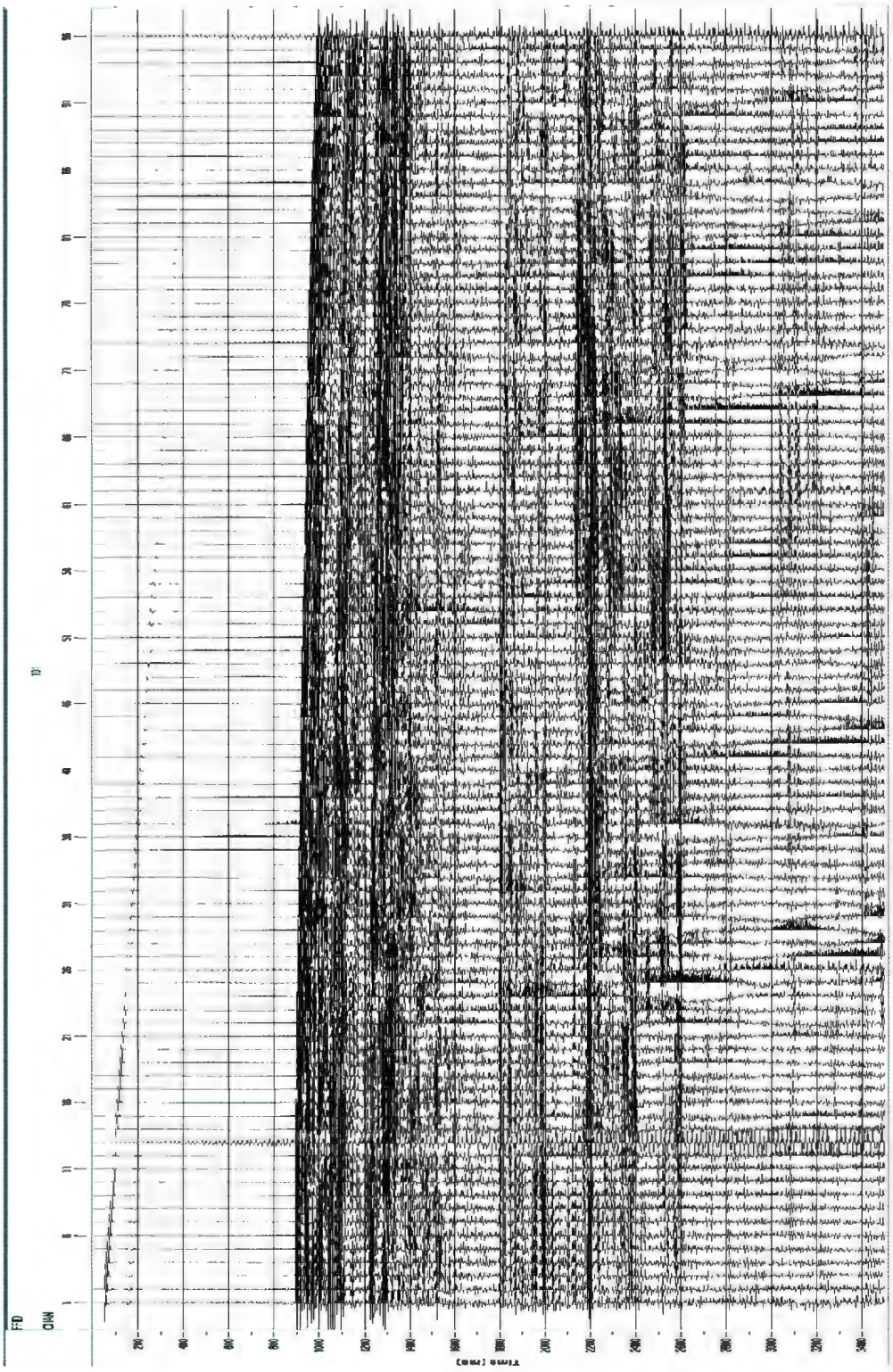

Figure 2.6: The same shot in figure 2.3 after true amplitude recovery (TAR) and bandpass filter.

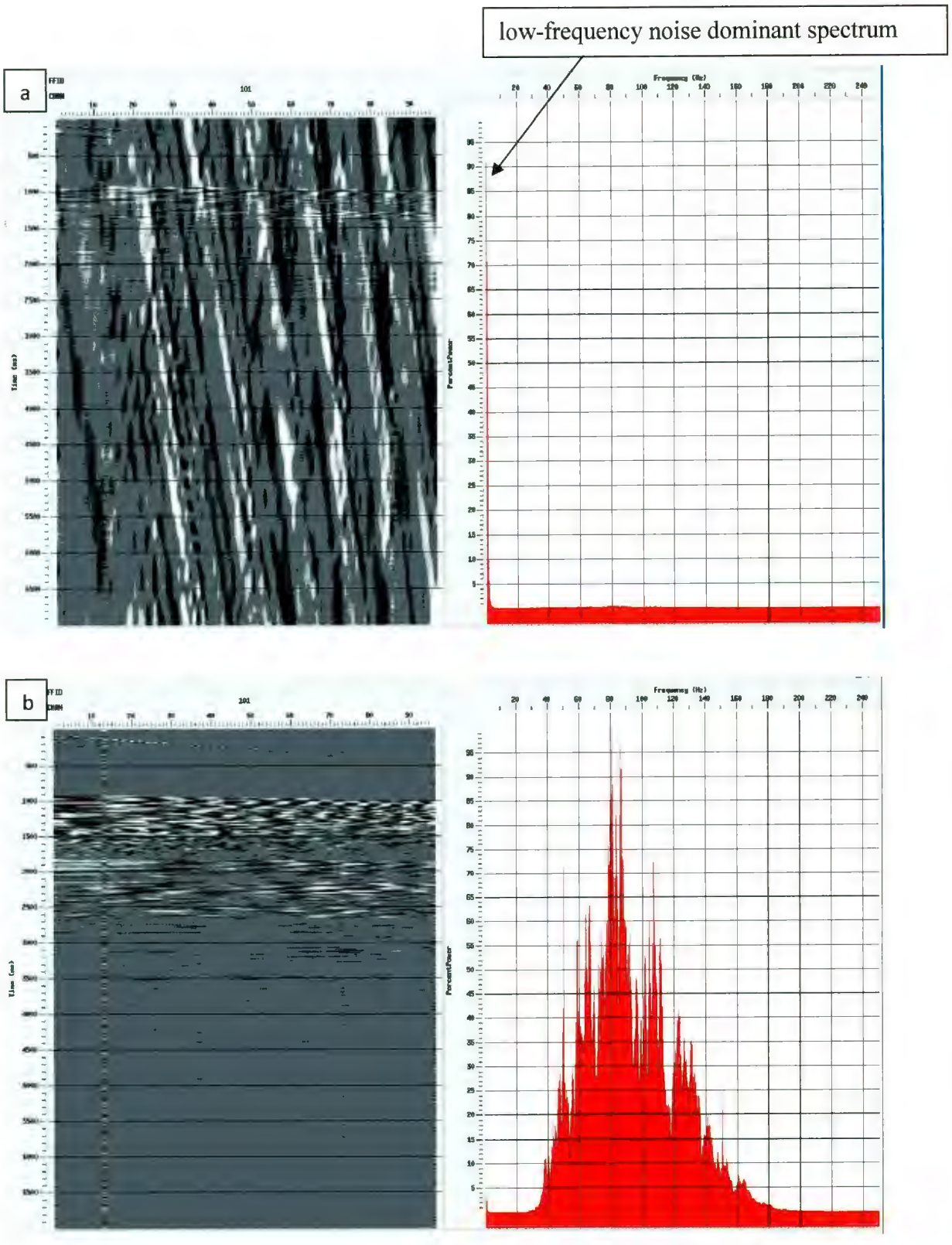

Figure 2.7: Percent power frequency spectrum (a) before and (b) after a band-pass filter.

second one shows the frequency distribution in percentage. Before the filter is applied the data mostly consists of very low frequency noise (Fig. 2.7a), and the target frequency range is in a low percentage. After a bandpass filter and AGC application the low frequencies are eliminated from the data and our target frequency range (30-200 Hz.) has a higher percentage in the data (Fig. 2.7b). The improvement in the signal-to-noise ratio can also be seen in the seismic traces in the left-hand panels (Fig. 2.7a and b)

2.1.2. Spherical Divergence Correction

Spherical divergence correction was applied to the data to compensate the seismic wave's geometrical spreading and inelastic attenuation effect on the wavelet. As P-waves travel through the Earth, the amplitude of the wavelet decreases with time due to geometrical spreading and inelastic attenuation of the energy (Yılmaz 2001). This effect causes an imprecise distribution of amplitudes: high amplitudes in short offsets and low travel times, and low amplitudes in long offsets and larger travel times. To correct this effect we applied the true amplitude recovery (TAR) function in ProMAX©. With TAR application we aimed to compensate for the spherical divergence of the wave energy. Effects of the TAR application can be seen in Figure 2.6 which shows the same shot in Figure 2.3 after TAR and bandpass filter. As seen in the figure most of the low and high frequency noise is eliminated with bandpass filter, and the amplitudes of the signals are improved with TAR (Fig. 2.6).

2.1.3. Static Correction

During the data acquisition in the 2008 survey the shot firing was not exactly synchronised with the recorder start and shots were fired 30 ms after the recorder started. During the data processing to synchronize the shooting time with the recording time we had to deduct 30 ms from the recorded times. Using the hand static option in ProMAX© -30 ms delay was applied to the data and signals were carried to 30 ms earlier.

2.1.4. Geometry Loading and CDP Sorting

Geometry loading and CDP sorting of traces need to be applied to the data before the stacking step. The geometry loading step was applied to the data to load the location information of sources and receivers into the trace headers. For my dataset manual geometry loading option was used instead of Auto-2D feature in ProMAX©. The importance of geometry loading is to determine the offset and CDP by loading the source and receiver locations; thus the data can be sorted into CDP ensembles in ProMAX©. A CDP is the common depth point which represents a point on a flat reflector. Various signals reflect from that point following different ray paths from successive shots (Fig. 2.8). Summing these traces from that point improves the signal quality by attenuating the uncorrelated noise, and enhances the reflectors.

2.1.5. Velocity Analysis, NMO Correction and Stacking

Velocity analysis is one of the most important steps in seismic data processing. We need precise velocity information for some essential processing steps such as NMO corrections, migration, and depth conversion. There are several velocity determining

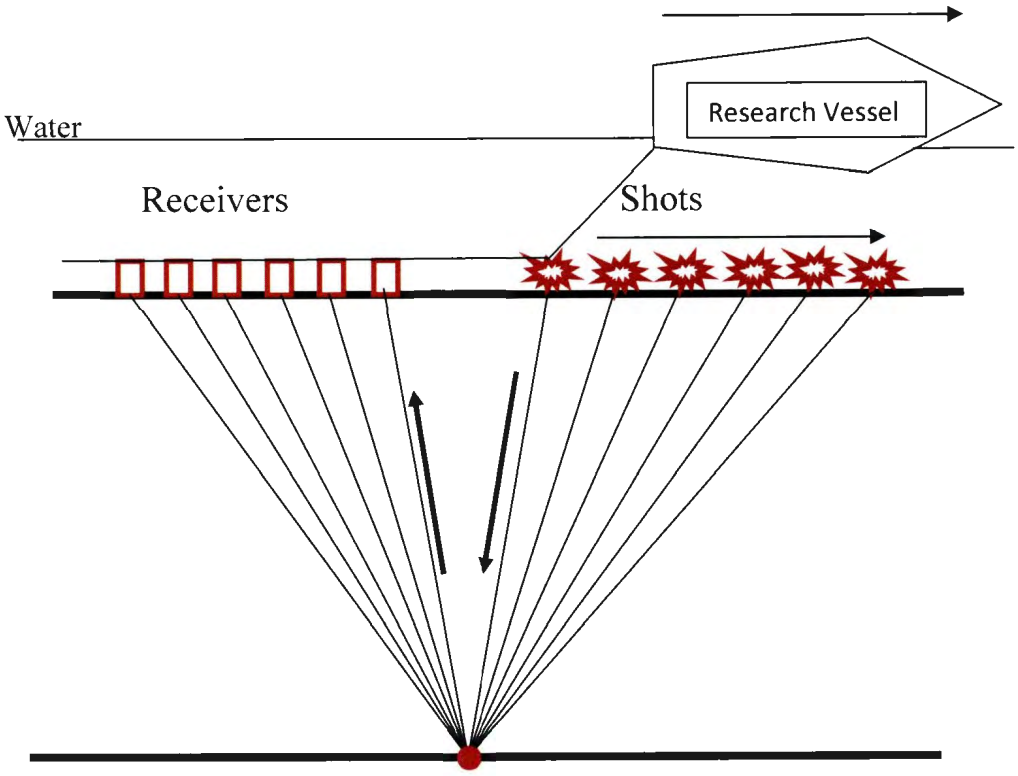

Figure 2.8: A schematic view of the CDP geometry

methods from the seismic data. $x^2 - t^2$, constant velocity scan, constant velocity stack, and velocity spectrum (semblance analysis) methods are some of them.

The reflection travel time curve as a function of offset is a hyperbola because of the time difference at different offsets. If we consider a reflection event on a CDP (Fig. 2.8) the time difference between the zero-offset and a given offset is normal move out (NMO). This difference in reflection travel times needs to be corrected prior to stacking the traces. The velocity that is used to correct NMO is called NMO velocity, and it is determined by the velocity analysis. The NMO correction is applied to the CDP gathers before stacking by using the primary velocity function. Velocity analysis defines the quality of the NMO correction and stack.

In this study, velocity spectra in ProMAX© were used to determine the NMO velocities. The velocity functions were selected based on three panels: semblance contour plots, a panel of constant velocity stacks, and a CDP gather for each location. These panels and velocity picks can be seen in Figure 2.9 and 2.10, which illustrates the data before the NMO correction. The semblance plot displays contours of semblance as a function of velocity and time. In practice, CDP supergathers are used for the semblance analysis. These supergathers are created by combining several adjacent CDP gathers; therefore they include more traces than CDP gathers. The CDP fold of 2008 data was 12, and 13 CDP gathers were combined to create the supergathers. Supergathers improve the quality of the semblance spectra by increasing the signal/noise ratio. The velocity that best flattens each event in the NMO corrected gather should be picked as the NMO velocity (Fig. 2.10). If the NMO velocities are selected too low, reflections will curve

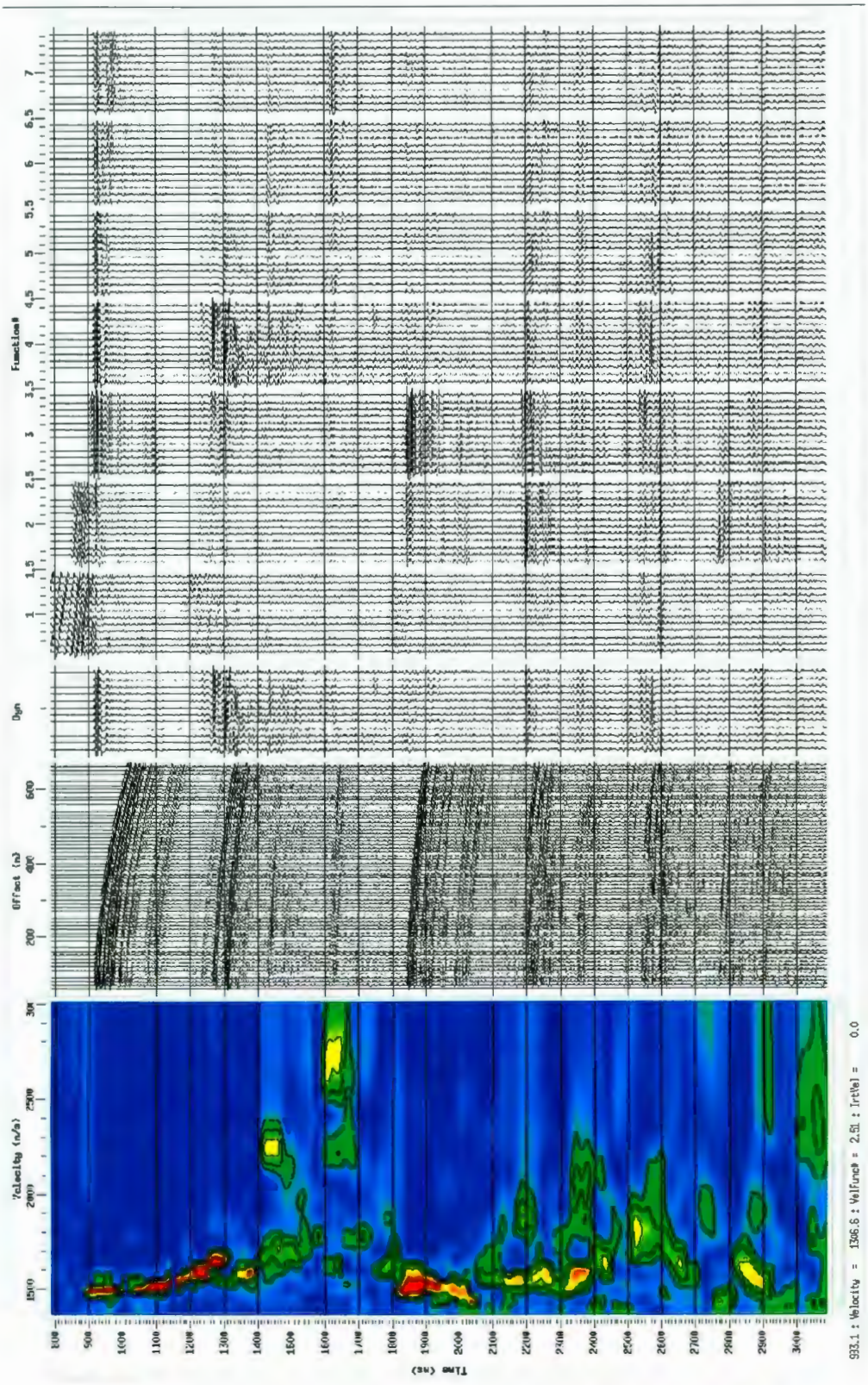

Figure 2.9: Velocity semblance analysis before the NMO correction.

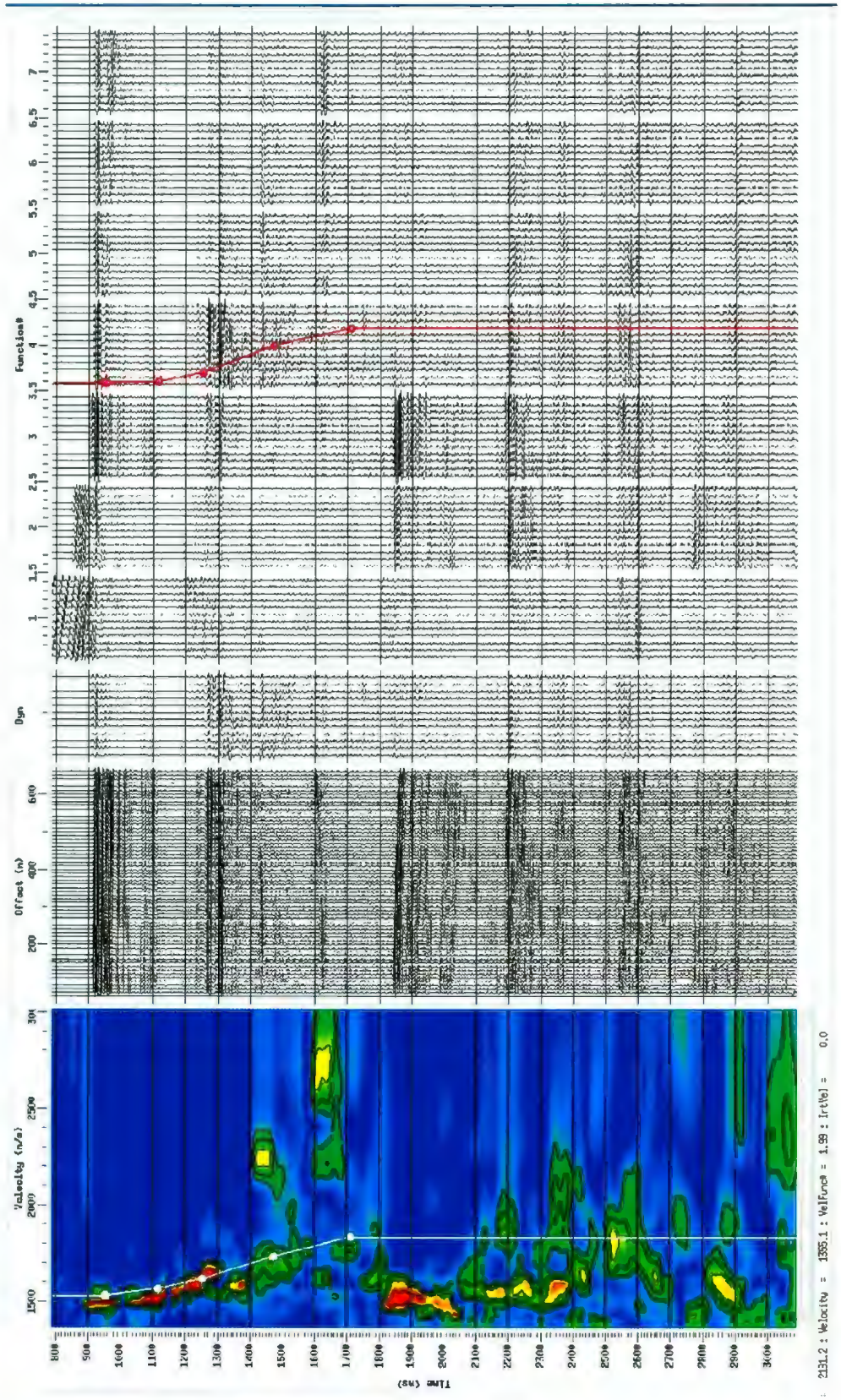

Figure 2.10: Velocity semblance analysis screen after the NMO correction.

upwards as a result of over-correction, and high velocities will curve the reflections downwards because of the under-correction.

The velocity functions which were selected for the NMO correction were applied to stack the data. The NMO correction has a side effect on the data called NMO stretching. This side effect is a frequency distortion which especially occurs at shallow events and large offsets. A 30% stretch mute was applied to discard the worst effects of the NMO stretching. As seen in Figure 2.11a, which illustrates the stacked data, stacking helps to remove a significant amount of noise and some part of the multiple energy which is the reverberation of the primary energy within the seafloor and sea surface (compared with the near-trace gather, Fig 2.4).

After the data is sorted to CDP and the offset effect has been removed from travel times by applying NMO correction the stacking is applied. The traces on each CDP gather are summed together in order to generate a stacked trace at each CDP location, and improve the signal-to-noise ratio. The number of traces in a CDP gather defines the fold of the data. In our survey, 6.25 meters group interval of 96 channels, 25 meters of shot spacing, and 3.125 meters of CDP spacing gave us a 12 fold stack.

2.1.6. Predictive Deconvolution (Pre- and Post-Stack)

Removing multiple energy from the seismic data is very important, because multiple energy can mask a significant amount of the primary energy which complicates geological interpretation of the data. Multiple removal is a great challenge, because it is crucial not to disturb the nature of the primary energy during the multiple removal

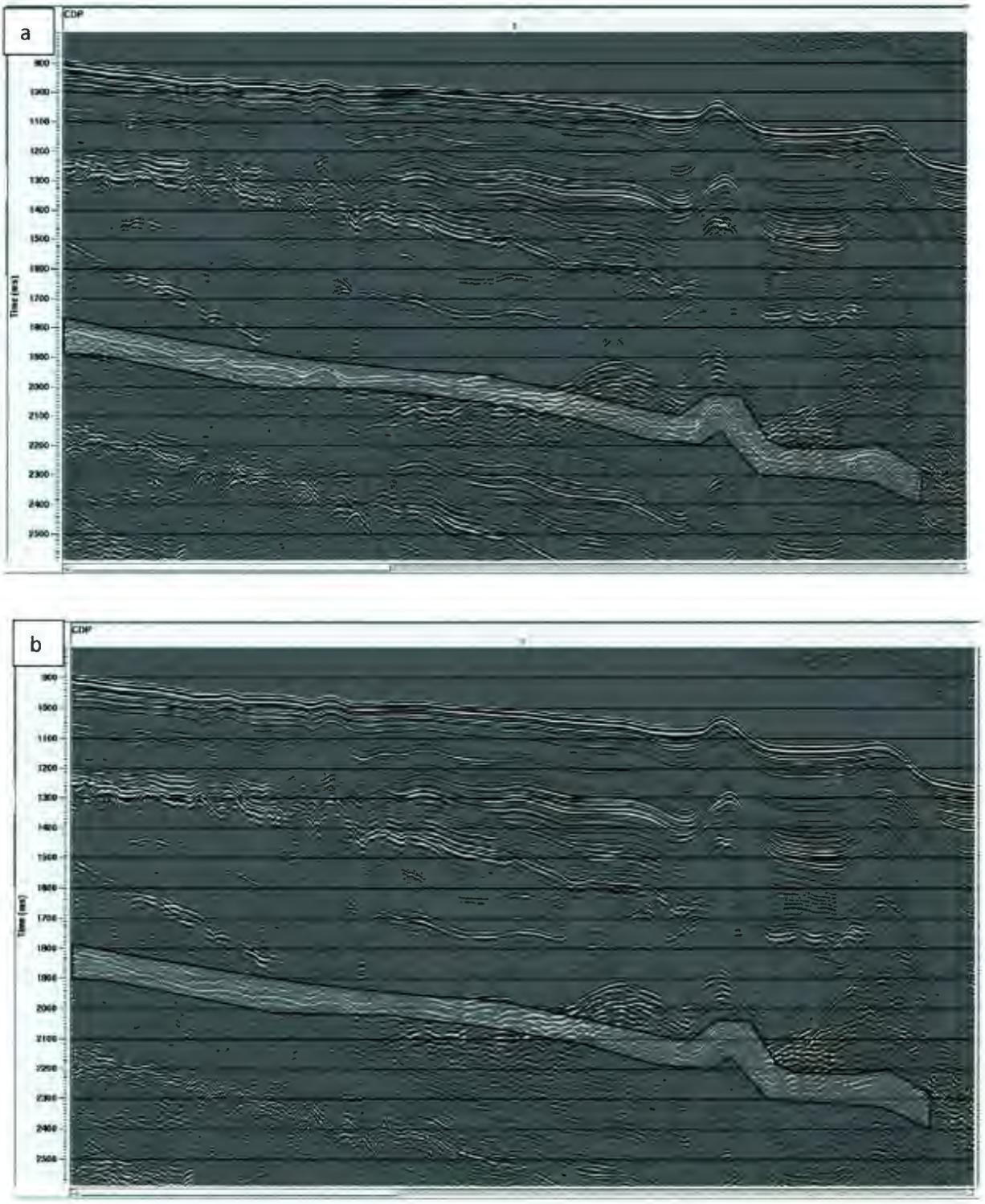

Figure 2.11: Demonstration of a multiple event on a stack section (a) without deconvolution and (b) with only pre-stack deconvolution. Seabed multiple is traced transparent.

process, and in some cases high amplitudes of the multiple energy makes it impossible for it to be removed completely. The success of multiple removal is not only based on the amount of the multiple energy removed from the data, but also related with the amount of the primary energy that is protected.

Some part of the multiple energy can be reduced during stacking, because the NMO corrections before stacking is made based on the primary velocity function, and the multiples have a larger moveout than primaries. This means that multiples are under-corrected, and they are attenuated by stacking. However, in most cases multiple energy exists even after stacking.

Deconvolution is applied to the seismic data to increase the resolution and the quality of the data by removing or reducing the multiple energy and attenuating reverberations. This process can be applied before or after stack. The main concept of deconvolution is to compress and restore the wavelet to the original form behaving like an inverse filter to reverse the effects of convolution and leave only the Earth's reflectivity in the seismic trace (Yılmaz 2001). Figures 2.11-2.15 demonstrate predictive deconvolution applications. Figures 2.11, 2.13, and 2.15 show stack sections and pre-stack predictive deconvolution applications. In these three figures it is clearly seen that the multiple energy is either removed from the data or weakened, and the primary energy became more dominant after the deconvolution. Figures 2.12, 2.14, and 2.16 show the post-stack deconvolution of the same sections illustrated in Figures 2.11, 2.13, and 2.15, respectively. After both pre- and post-stack deconvolution were applied multiple energy was almost completely removed from the data.

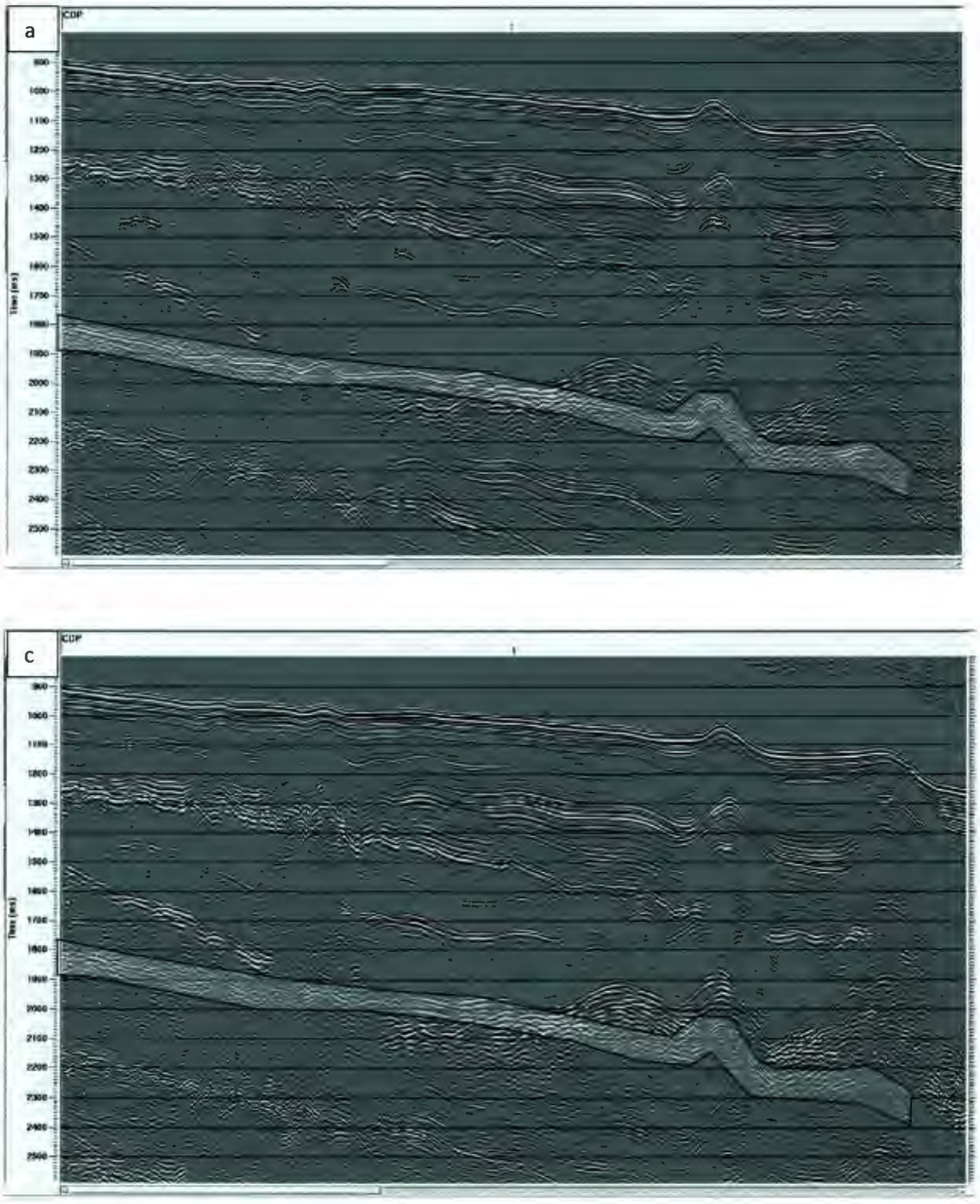

Figure 2.12: The same stack section in Figure 2.11 (a) with pre- and post-stack predictive deconvolution (c). Seabed multiple is traced transparent.

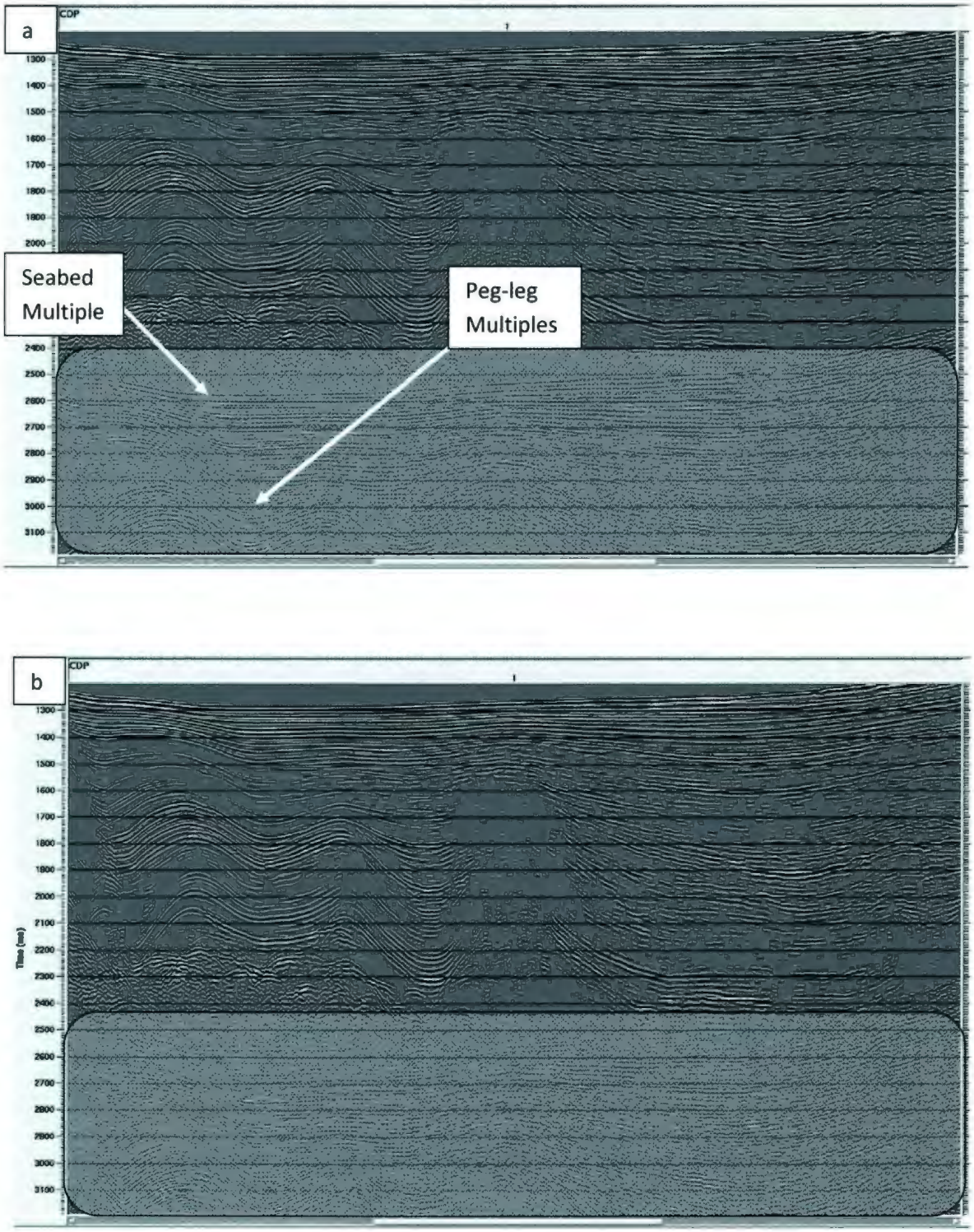

Figure 2.13: Demonstration of another multiple event on a stack section (a) without deconvolution and (b) with only pre-stack deconvolution. Seabed multiple and peg-leg multiples take place within the transparent box.

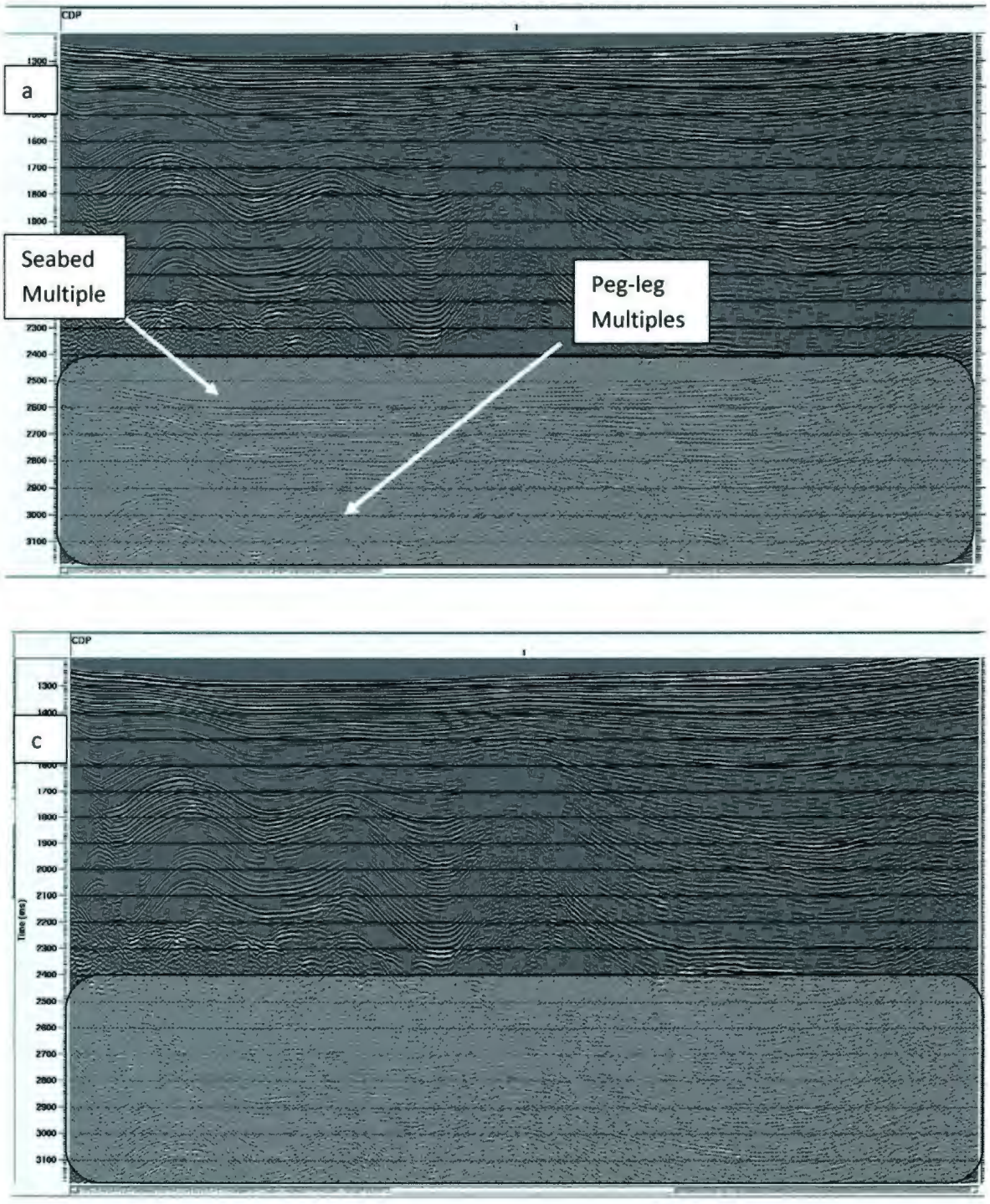

Figure 2.14: The same stack section (a) in Figure 2.13 with pre- and post-stack predictive deconvolution (c). Seabed multiple and peg-leg multiples take place within the transparent box.

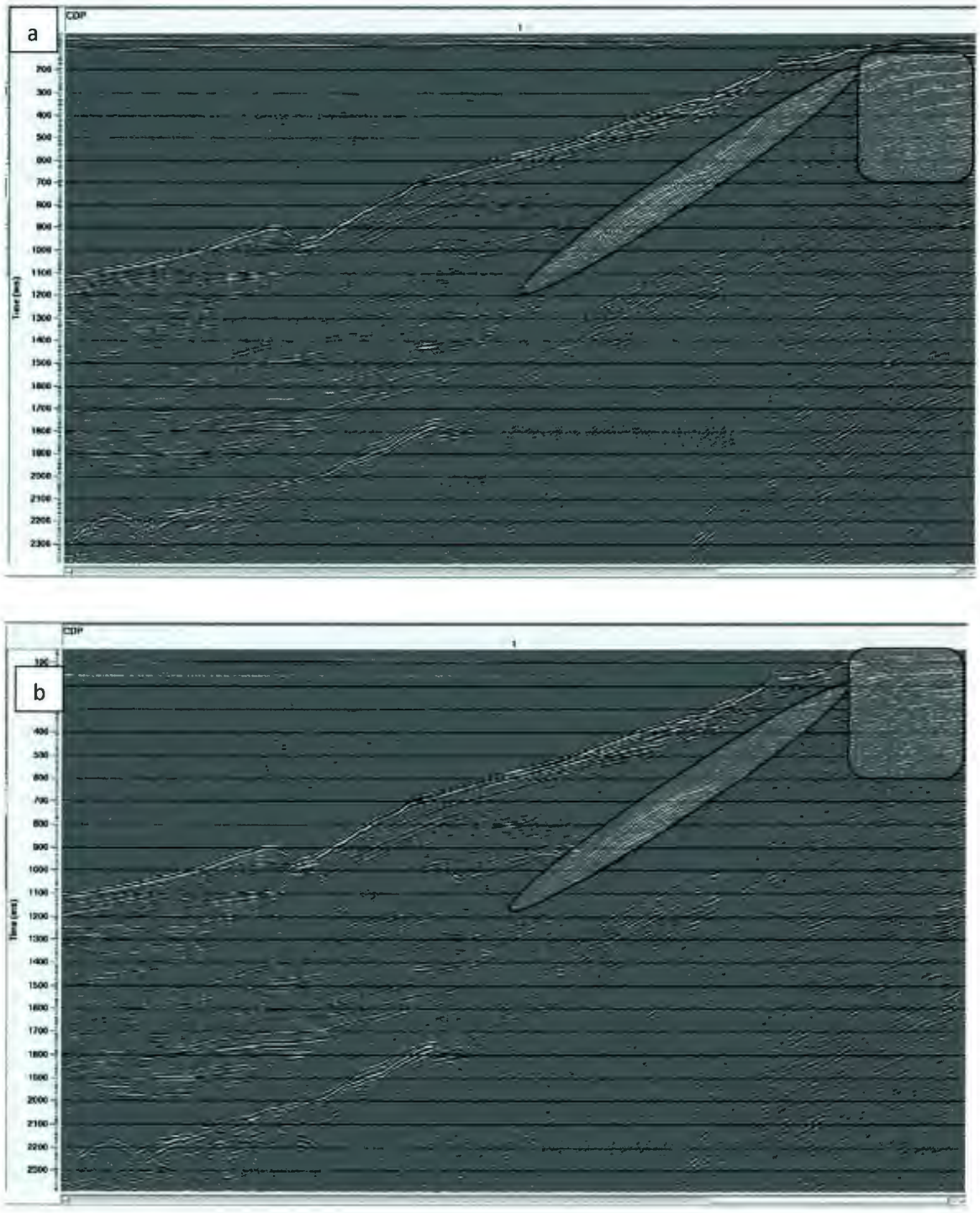

Figure 2.15: Demonstration of another multiple event on a stack section (a) without deconvolution and (b) with only pre-stack deconvolution. Seabed multiple is traced transparent.

Figure 2.16: The same stack section (a) in Figure 2.15 with pre- and post-stack predictive deconvolution (c). Seabed multiple is traced transparent.

Predictive deconvolution converts a repeating signal to a signal that is not repeating. It predicts and removes the repeating events from the data using the information from the earlier parts of the seismic record. For the 2008 data predictive deconvolution was applied relative water bottom, which makes the seabed the information to be used to predict and remove the seabed multiples. Pre- and post-stack predictive deconvolution helped us to remove most of the multiple energy from our data; however in some cases some additional processes were required such as time varying bandpass filter and adaptive deconvolution.

Predictive deconvolution was applied relative to seabed for an accurate prediction distance. The water bottom needed to be picked for this application, and selecting the picks above the seabed ensured that water bottom wavelet was included in the prediction process. 125 ms operator length and -5 ms prediction distance were selected after many iterations. Prediction distance was same for all lines, but there were some slight changes of the operator length in some lines.

Adaptive deconvolution can be used as an additional method to predictive deconvolution in some cases. For our data, adaptive deconvolution was not a successful method, because it was removing a significant amount of primary energy from the data with multiple energy. Although it was efficient on multiples, it was not preferable because of the primary energy loss. Figure 2.17 shows the effect of the adaptive deconvolution. In this figure the seabed multiple is removed from the data, but the primary energy is also removed with the multiple.

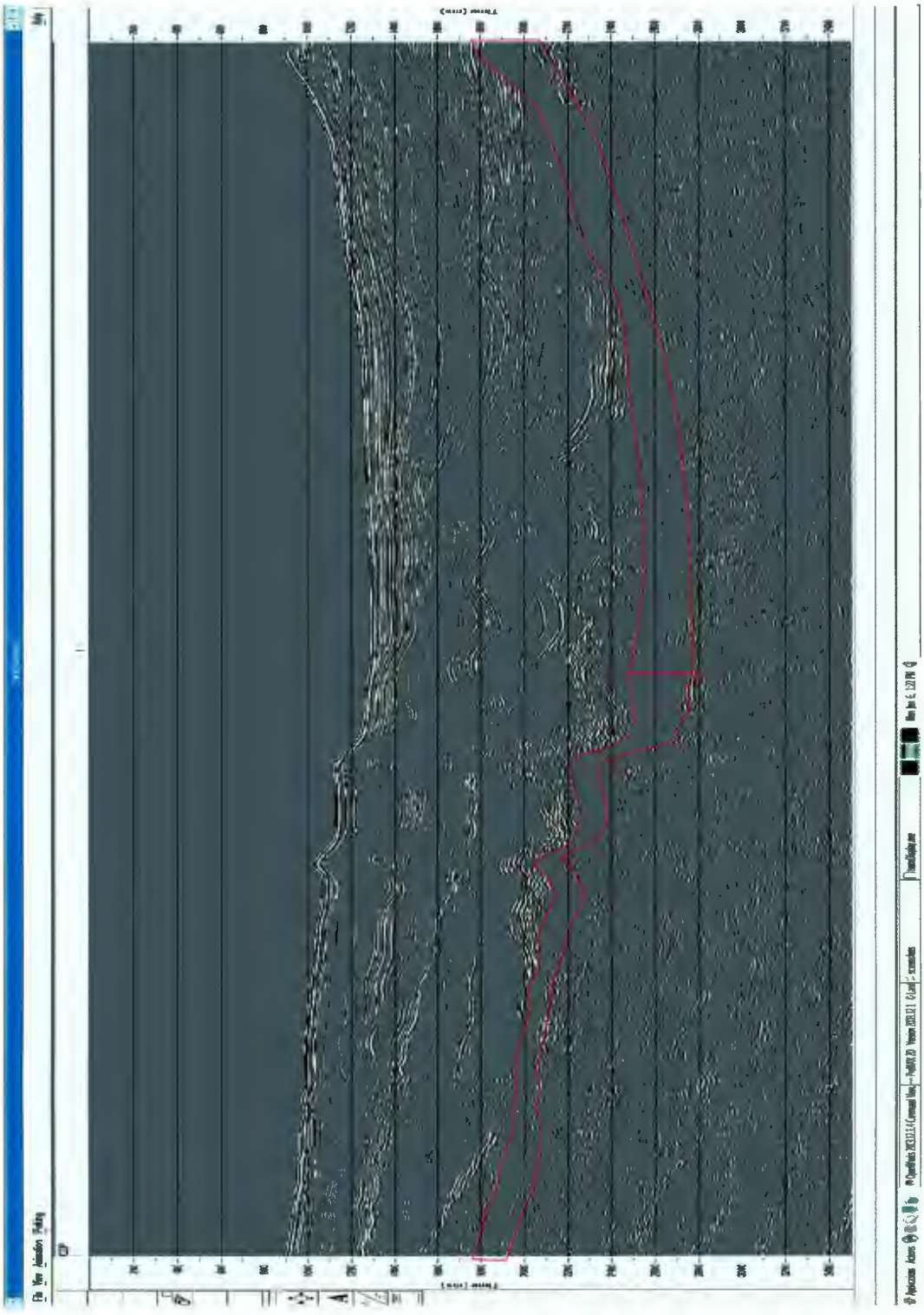

Figure 2.17: Adaptive deconvolution. Red outline is showing the effect of the adaptive deconvolution. Most of the primary energy removed from the data along with the multiple energy.

Time varying bandpass filter can also be used as an additional method to improve the effectiveness of the multiple removal process. Primary reflections quite possibly have lower frequencies than the multiple energy. We applied an Ormsby bandpass filter with 10-20-250-275 Hz bandwidth to the shallow part of the section to keep most of the energy in this part, and 10-20-150-200 Hz bandwidth to the deeper part to eliminate the higher frequencies associated with multiple energy. Figure 2.18 shows the effects of time varying bandpass filtering.

2.1.7. Migration (Stolt and Kirchhoff Time Variation)

Migration is the final step of seismic data processing flow. This process increases spatial resolution by collapsing diffractions and moving the dipping events to their true subsurface locations. Migration is a very important step especially in structurally complicated areas with varying seismic velocities. Migration velocities are different than stacking velocities, and to estimate accurate migration velocities, different types of migrations were applied to the post-stack data. Constant velocity Stolt migration and Kirchhoff time migration were used for this study.

Constant velocity Stolt migration was used to estimate the proper velocities for the migration step. We applied F-K Stolt constant velocity migration with the velocity values of 1500 m/s, 1700 m/s, 1900 m/s and 2100 m/s; and printed the generated constant velocity plots. After inspection of the constant velocity migrations variable-velocity Stolt migrations were completed. Working on paper copies made it easier to compare the sections and identify the best velocities for the Kirchhoff migration. Stolt migrations are

Figure 2.18: Time varying bandpass filter.

very quick in practice when compared to the Kirchhoff migration, but the latter is more accurate than the Stolt migration. Stolt migration was used as a step to assist the accuracy of the Kirchhoff time migration. Kirchhoff migration was applied as a final step after a velocity model was created by using the Stolt migration. Figures 2.19 and 2.20 illustrate the seismic data before and after Kirchhof migration was applied. After Kirchhoff migration reflectors became shorter and narrower, fault planes became more clear, dipping events are moved to their correct locations, and bow-ties were eliminated from the data.

2.2. Data Interpretation

After the processing step seismic reflection profiles were interpreted using both conventional hand interpretation and SeisWorks©, a seismic interpretation package. For the hand interpretation final images of all seismic lines were printed at the same scale. There were several important markers to be interpreted on the seismic sections, such as seismic horizons, faults, folds, diapirs and unconformities. As a first step these important markers were traced by hand on printed paper copies of original seismic reflection profiles. All the prominent structures within the Pliocene-Quaternary and Messinian Units including the thrusts, extensional faults, the top and the base of the Messinian evaporite unit, the reflectors that delineate the sub-units of the Pliocene-Quaternary succession were traced. The interpretations of the seismic reflection profiles later were correlated with the stratigraphic information from Seyhan-1 and Karataş-1 wells. Key horizons within Pliocene-Quaternary (i.e., the A- and P-markers), as well as the M- and N-markers were placed into a chronostratigraphic framework. Correlating the well data

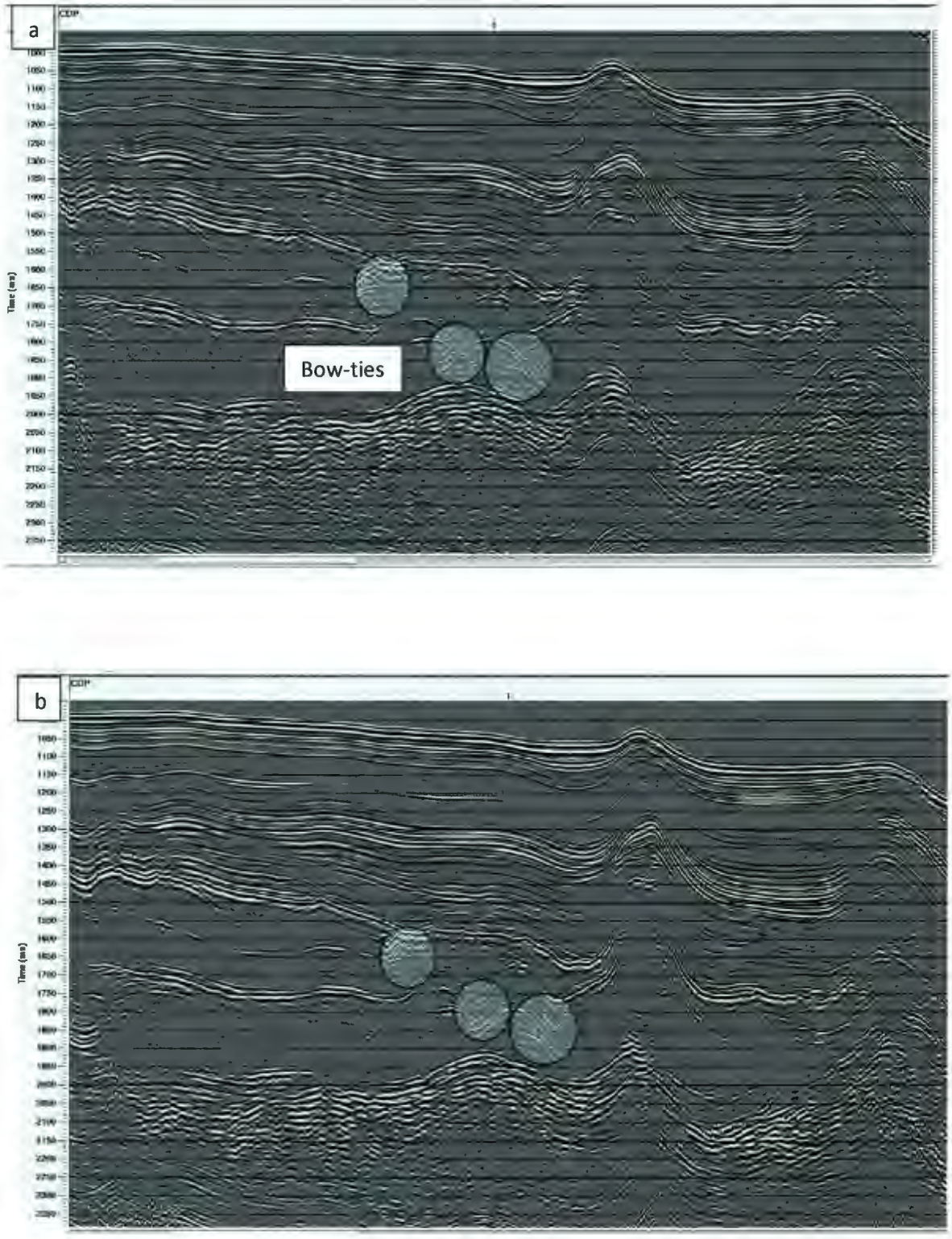

Figure 2.19: A stack section before (a) and after (b) Kirchhoff migration.

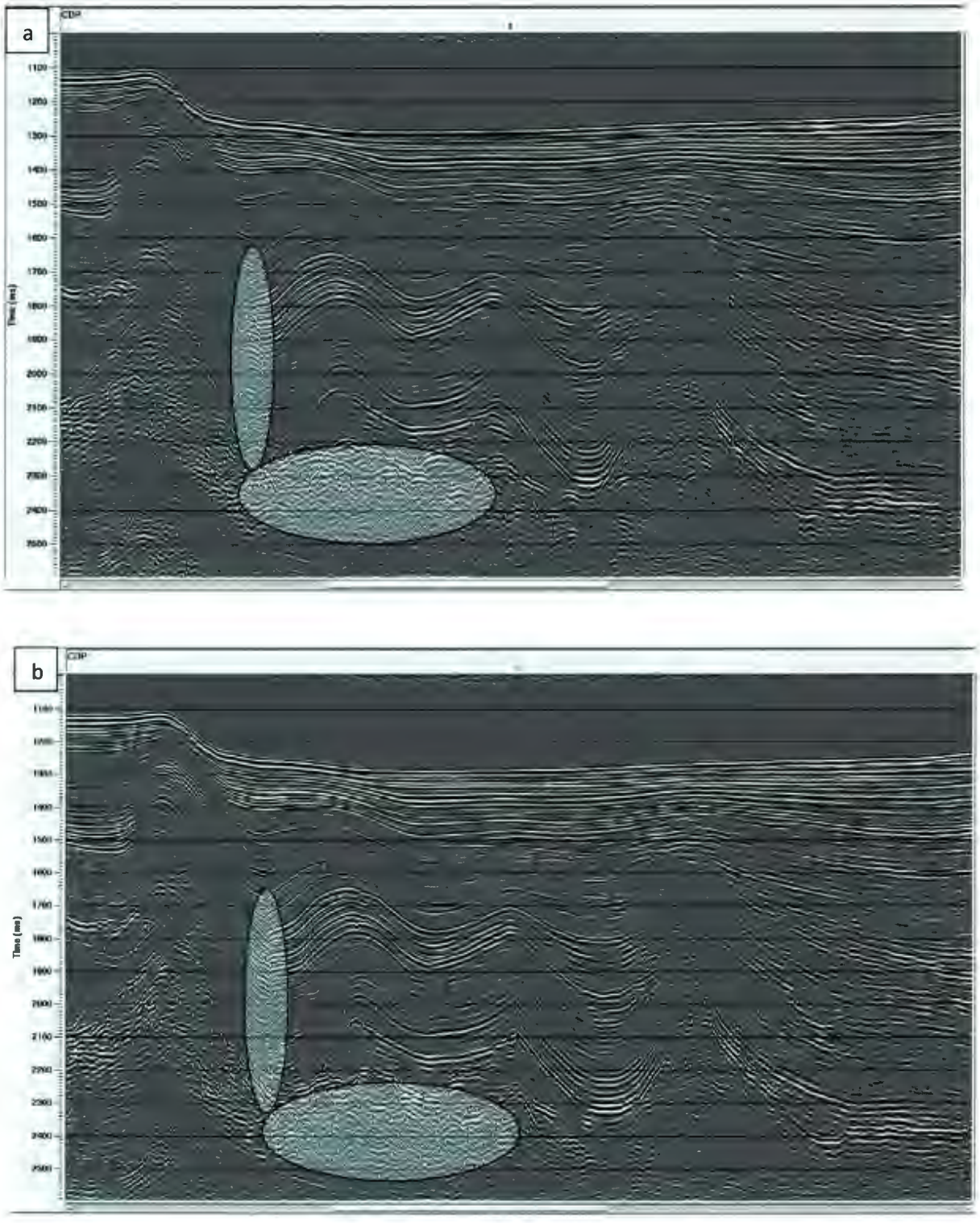

Figure 2.20: A stack section before (a) and after (b) Kirchhoff migration.

with the seismic successions provided a firm chronostratigraphic framework of the study area. After the structural interpretation isopach contour maps in two-way travel time thicknesses of the Pliocene-Quaternary and the Messinian evaporite deposits and the seabed bathymetry map were completed.

Unconformities and truncations are important parts of the seismic stratigraphic interpretation, because they indicate the missing strata in the depositional sequences. Truncations are the terminations of the reflectors within the depositional surfaces and they are traced in seismic reflection profiles as onlaps, downlaps, toplaps, pinch-outs. Several geological events can cause the truncation of reflectors such as erosion, deposition or faulting (Mitchum et al., 1977). Onlap is the termination of a reflection which laps onto a more steeply dipping surface at the base of a unit (Fig. 2.21). Downlap is the downwards angular termination of a steeply-dipping reflection onto a less steeply-dipping reflector (Fig. 2.21). Toplap is the reflection termination caused by the deposition of a horizontal strong reflector above a succession of downlapped or inclined packages of strata. Offlap is the termination of a reflector by the converge of upper and lower reflections.

Distinction of the normal and reverse faults in the seismic reflection profiles is another important step of the seismic interpretation. This definition can be made easily if the hanging walls and the footwalls of the faults are clearly imaged, and they create cut-offs on key reflectors. However; that is not always the case, and when the faults are not clearly imaged the growth in the sedimentary packages developed around them aids to the

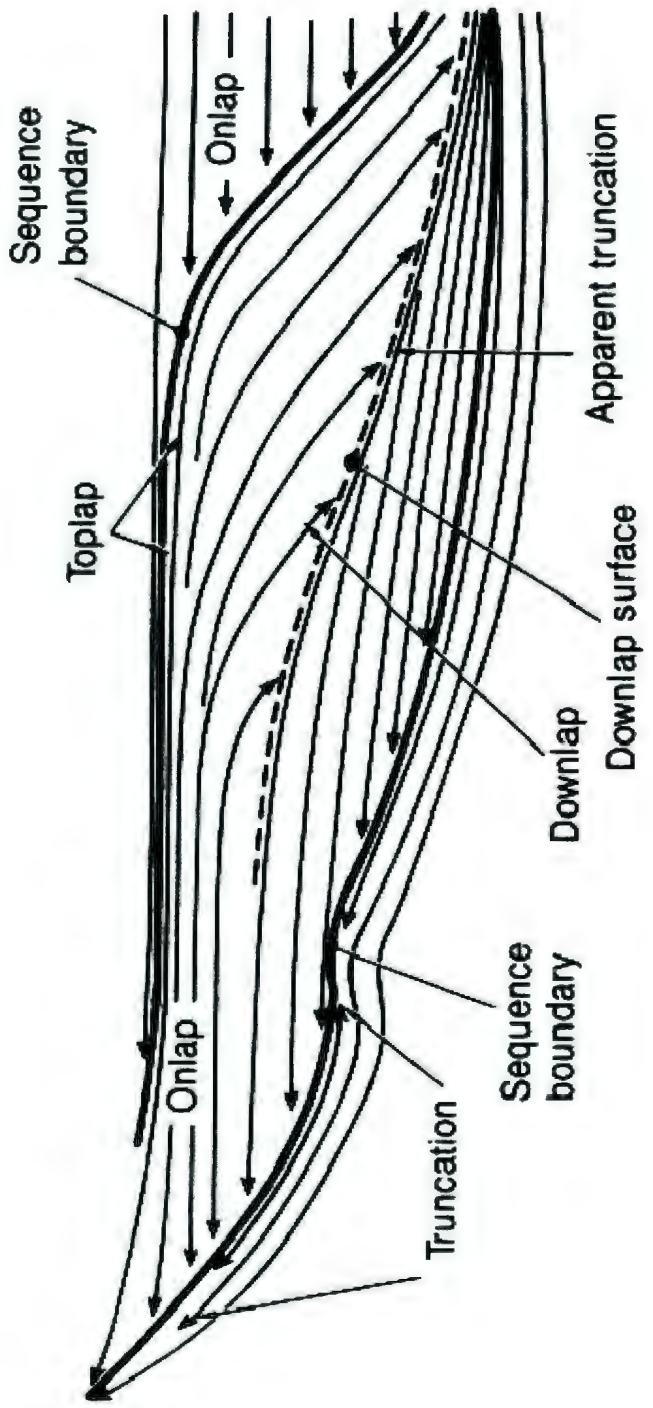

Figure 2.21: Schematic demonstration of reflection terminations.

interpretation of these faults. Interpretation of these faults requires the geometrical analysis of the growth strata wedges or progressive unconformities. Growth strata wedges associated with listric normal faults are observed on the hanging wall of the fault plane (Fig. 2.22). Thrust faults develop growth strata wedges at the hanging wall where the anticlines are not symmetrical. The strata on the limbs of the anticlines thin toward the crest of the ramp and thicken toward the troughs of the ramp (Fig. 2.22). Strike-slip faulting is commonly observed with clear footwall and hanging wall cut-offs of steeply-dipping bi-vergent faults (Fig. 2.22). These faults may be associated with negative or positive flower structures.

There are several examples in the interpretation of the seismic reflection profiles where faults are not explicitly visible from abrupt stratal terminations and offsets. This also occurs frequently in mapping of geology on land, where faults often occupy erosion hollows buried below un-deformed young sediment. On land, such 'hidden' faults are identified by extrapolated offset of geological features and by associated secondary structures. In this thesis the same rationalization is used in interpreting the seismic reflection profiles (Fig. 2.22), in which faults are indicated with explicit evidence of offset by full lines, and those shown as dashed lines identify faults where the evidence is only from secondary sedimentary structures. For example, in the southeastern segment of the Outer Cilicia Basin the fold-thrust structures of the Kyrenia Fault zone are poorly imaged in the seismic reflection profiles (see Chapter 4). However, the ramp anticlines associated with major thrusts are clearly visible as distinctly asymmetric structures defining the position of a blind thrust and a vergence direction (also see Chapter 4).

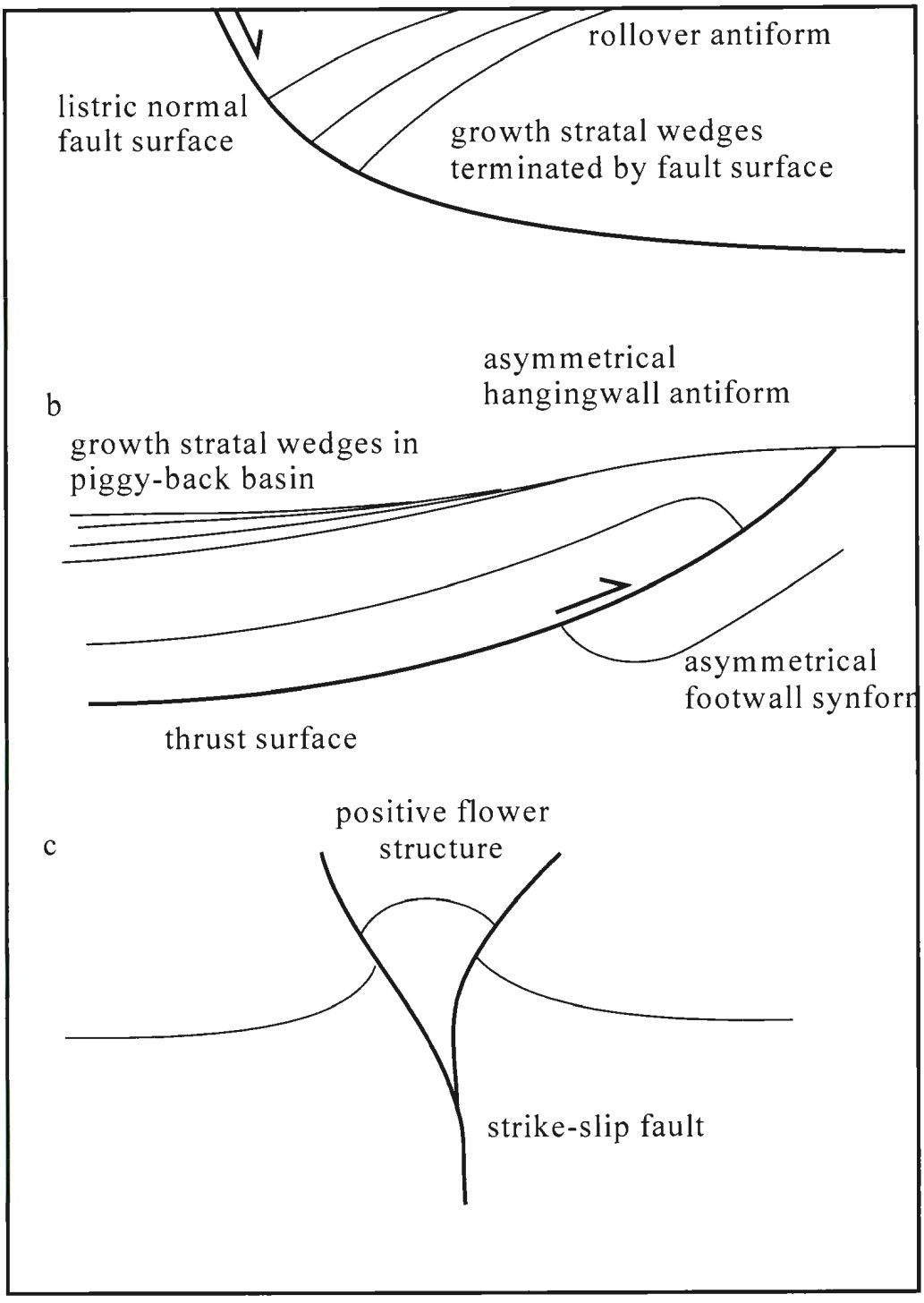

Figure 2.22: Schematic demonstration of a variety of reflection offset configurations with respect to different faulting motion often seen in reflection profiles.

In the following chapters, maps are constructed illustrating the spatial distributions of various faults that cut the Miocene successions of Units 3 and 2 and the Pliocene-Quaternary succession of Unit 1 (see Chapter 3). The fault maps are compiled to show all faults that affected the stratigraphic units involved, therefore invariably show the projections of tip points of faults onto the seafloor. The faults that extend to the depositional surface are always highlighted in the text. For example, such and such faults extend to the depositional surface where they create distinctive steps on the seafloor.

CHAPTER THREE

Seismic Stratigraphy and Chronology

The stratigraphic framework of the Cilicia Basin can be described using the principles of seismic stratigraphy, and correlation with well data from the Inner Cilicia and Adana Basins. A seismic sequence is defined as 'a stratigraphic unit composed of a relatively conformable succession of genetically related strata bounded at its top and base by unconformities or their correlative conformities' (Mitchum et al., 1977). Prominent reflectors are used to define the unconformities (or their correlative conformities) that determine the sequence boundaries. An unconformity is a surface along which there is a clear evidence for either erosion or non–deposition. In seismic reflection profiles unconformities are identified on the basis of angular discordances of reflectors above and/or below the boundary such as onlap, downlap, and toplaps. However, there may not be clear evidence of erosion or non–deposition everywhere. Angular unconformities are delineated on the seismic reflection profiles by the discordance between the underlying truncated reflections and the overlying onlapping or downlapping reflections (Figs. 3.1, 3.2, 3.3; Mitchum et al., 1977).

Seismic reflection profiles show the presence of three stratigraphic units in the Cilicia Basin: Units 1, 2, and 3. The chronology of these seismic units is established through correlations with two exploration wells drilled in the innermost Cilicia Basin by the Turkish Petroleum Corporation: Seyhan-1 and Karataş-1 (Fig. 3.4). The depths of the sedimentary successions observed in the exploration wells are correlated with the two-

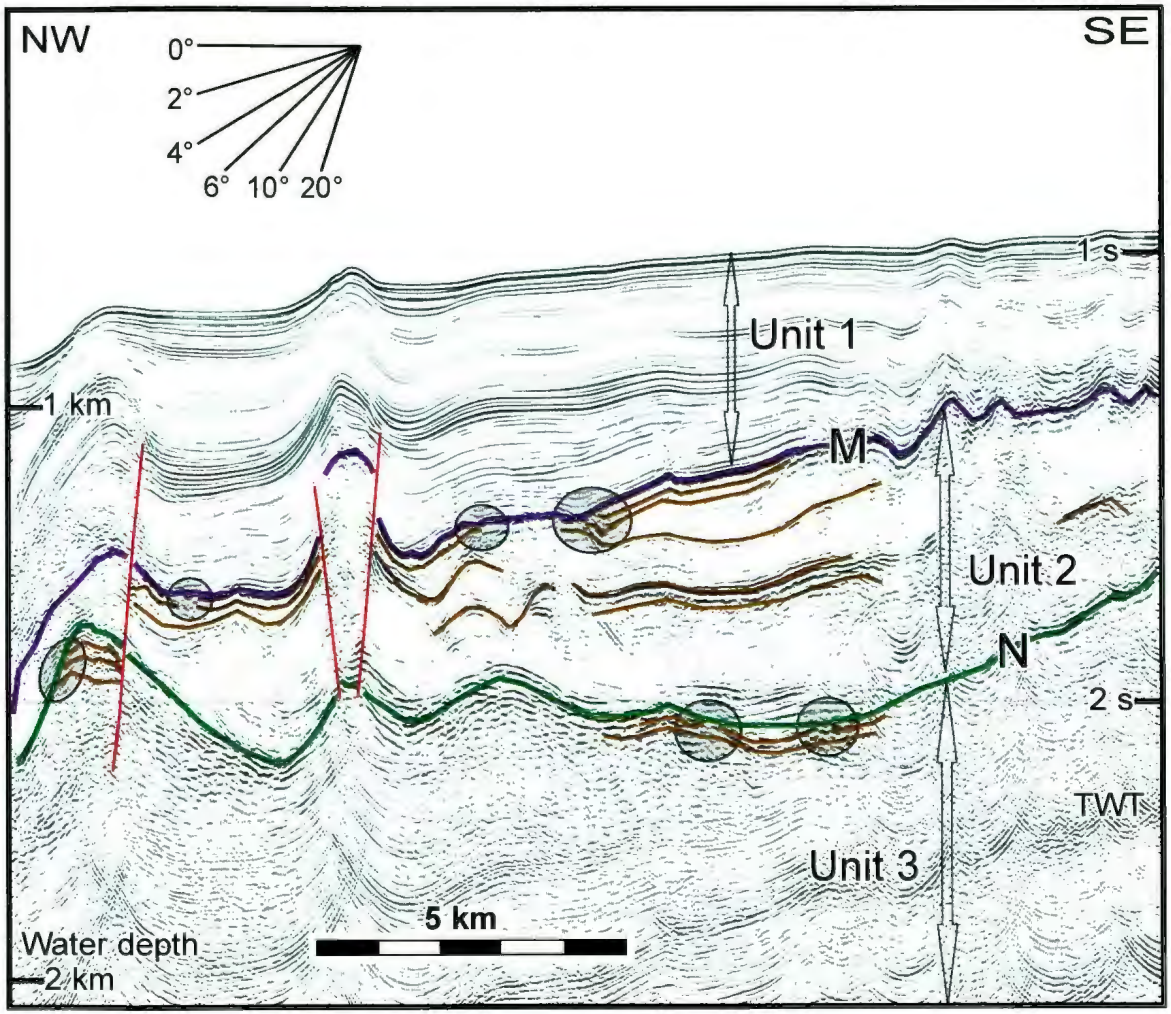

Figure 3.1: Seismic reflection profile from the central Cilicia Basin illustrating an angular unconformity (erosional truncation) in the study area (PLATE 1, Fixes 1654-1667). Brown reflectors are layers truncated by the base of Unit 1 and Unit 2; the M- and the N-reflectors, respectively.

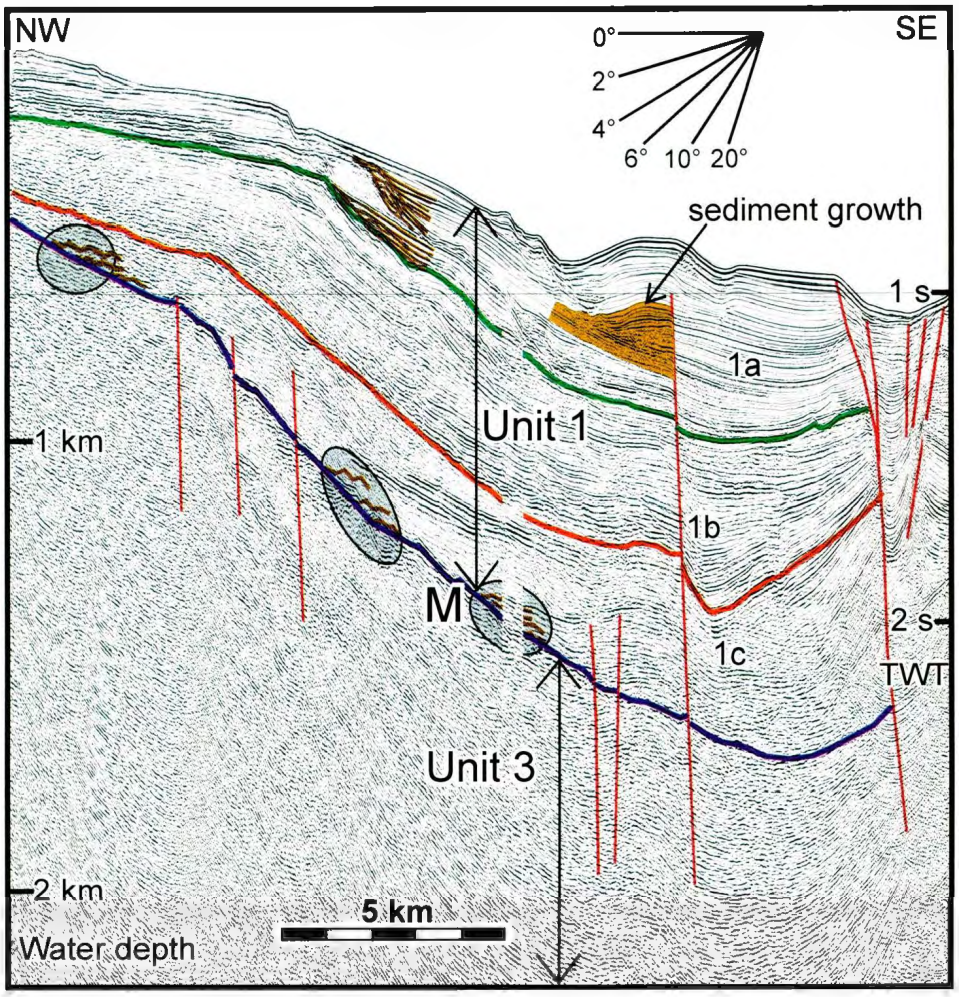

Figure 3.2: Multichannel seismic reflection profile from the shallow part of the study area (PLATE 6, Fixes 1383-1400). Circled brown reflectors are showing onlap structures above the M-reflector.

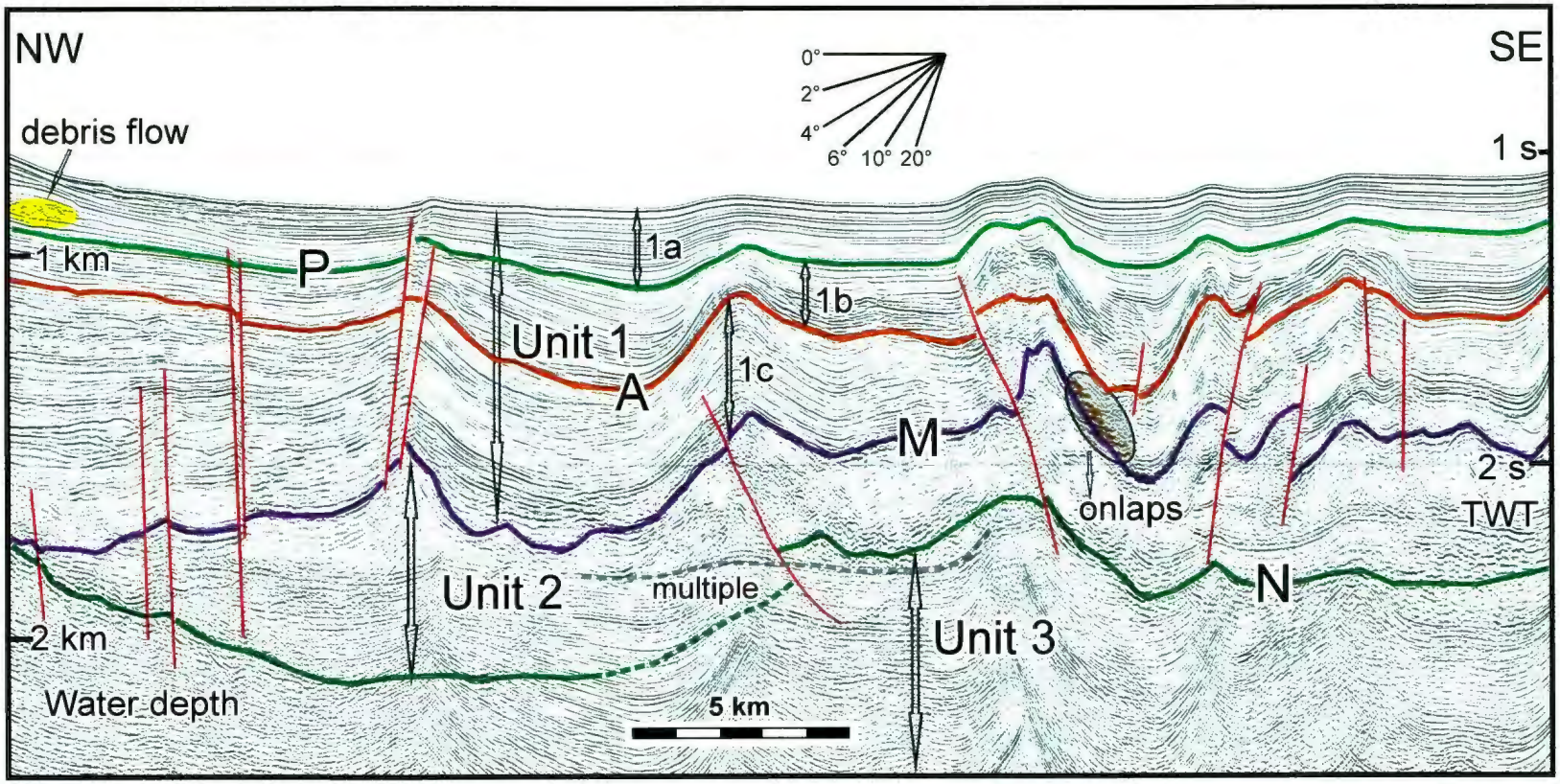

Figure 3.3: A seismic reflection profile from the study area (PLATE 3, Fixes 1564-1588) showing major reflectors P, A, M, and N; Units 1, 2, and 3, and subunits 1a, 1b, and 1c. Circled brown reflectors are showing onlap structures above the M-reflector.

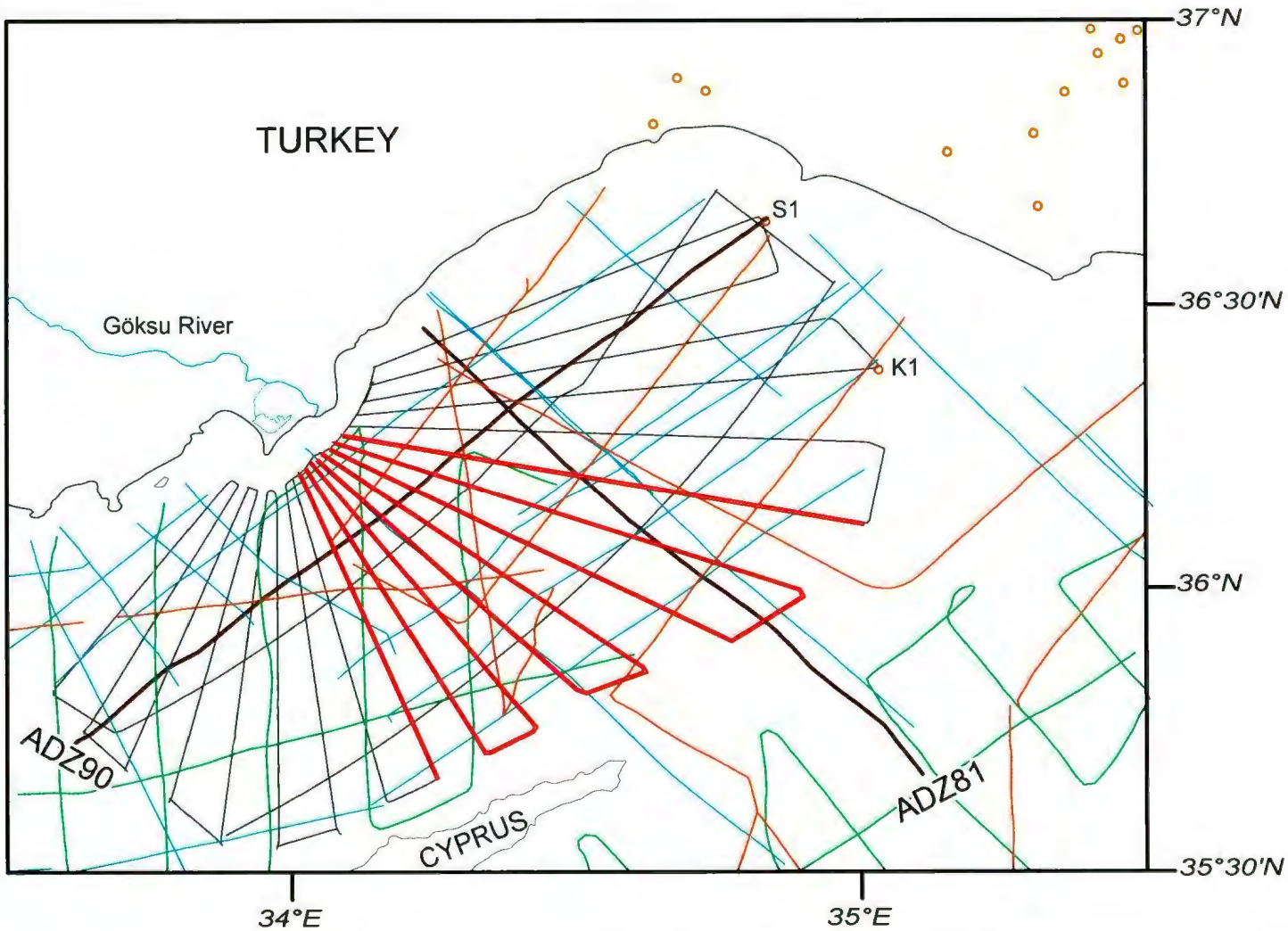

Figure 3.4: Location map showing all the available data in the Cilicia Basin. Black lines are 2008 data, orange lines are 1991 data, green lines are 1992 data and light blue lines are the industry seismic reflection profiles. Thick red lines are the seismic data from the 2008 dataset that is used in this thesis. S1-Seyhan1 and K1-Karatas1 are the exploration wells in the Inner Cilicia Basin. ADZ 81 and 90 are the Turkish Petroleum lines that are used to corelate wells to seismic sections.

way-time industry seismic reflection profiles using the velocity information provided by the Turkish Petroleum Corporation (Fig. 3.5). The Seyhan-1 well was drilled in the western and shallower portion (~40 m water depth) of the Inner Cilicia Basin. It recovered ~2158 m of Pliocene-Quaternary deltaic and pro-deltaic successions (Turkish Petroleum Corporation, unpublished data, Fig. 3.5). On the basis of lithostratigraphic data from the well, the Pliocene-Quaternary succession was further divided into a 453 m-thick upper subunit (Unit 1a), a 854 m-thick middle subunit (Unit 1b) and an 851 m-thick lower subunit (Unit 1c) (Fig. 3.3), separated by the A- and P- reflectors. The base of the Pliocene-Quaternary successions was marked by a major erosional unconformity, which is correlated with the regional M-reflector. Below this unconformity an 878 m-thick, predominantly evaporite unit is identified consisting of halite, anhydrite, and gypsum with frequent interbeds of minor siliciclastic and carbonate debris. This unit is correlated with the Messinian evaporite succession (Fig. 3.5). The base of the evaporitic unit is also delineated by another major unconformity (i.e., marked by the N-reflector). The well further recovered ~977 m of Tortonian age siliciclastic and carbonate-bearing clastic successions and terminated within the upper Miocene at a depth of 4053 m.

The Karataş-1 well was drilled southeast of the Seyhan-1 well in 74 m water depth (Fig. 3.4), near the Misis-Kyrenia fold-thrust belt which extends from the Kyrenia Mountains of northern Cyprus to the Misis Mountains of southern Turkey (Aksu et al., 1992a,b). The well recovered a sequence of sedimentary successions similar to those observed in the Seyhan-1 well, including ~2042 m-thick Pliocene-Quaternary siliciclastics, 393 m-thick Messinian evaporites, ~1633 m-thick Tortonian and middle

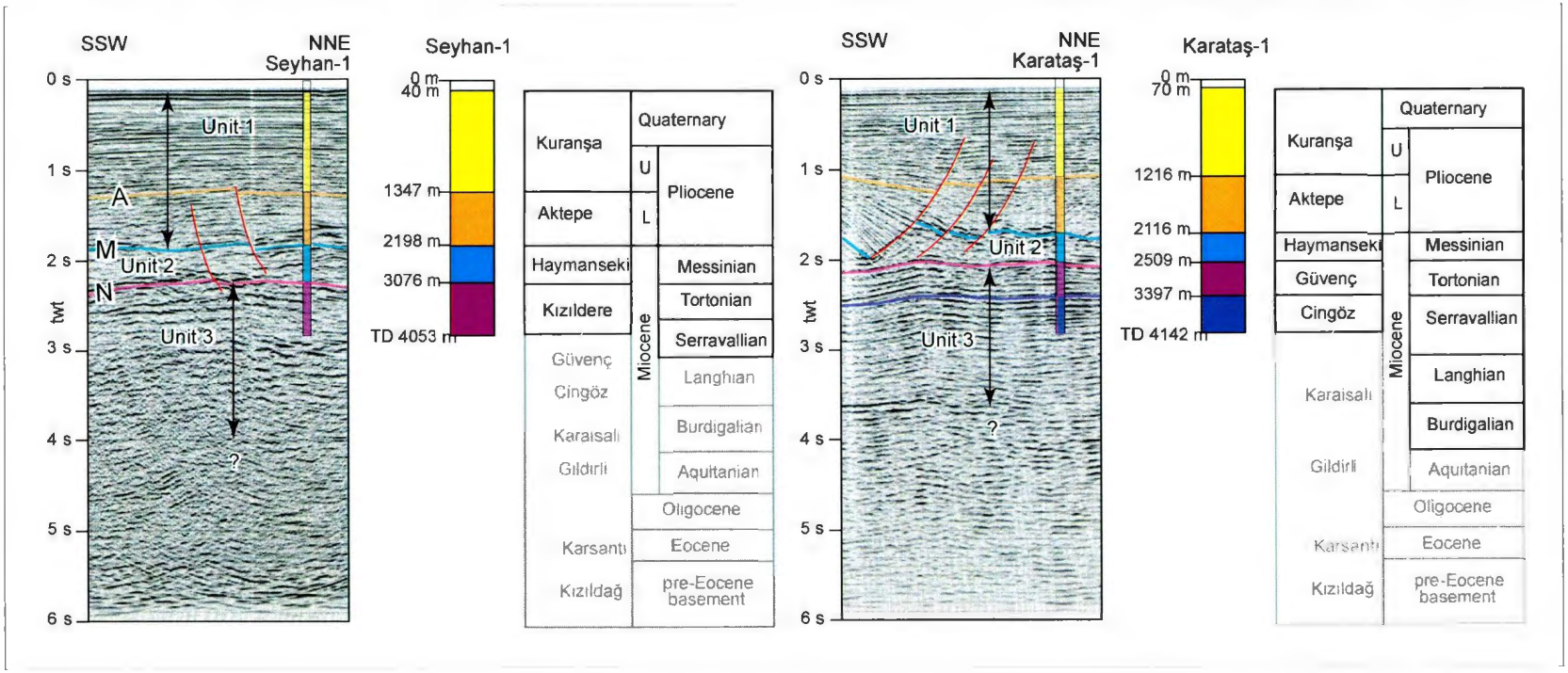

Figure 3.5: Lithostratigraphy of the Seyhan-1 and Karataş-1 exploration wells correlated with the seismic reflection profiles across the boreholes (Aksu et al., 2005). Data kindly provided by the Turkish Petroleum Corporation.

Miocene (?Langhian-Serravallian) successions penetrating a total depth of 4142 meters (Fig. 3.5; Turkish Petroleum Corporation, unpublished data).

In this study the depth in seismic reflection profiles are described in milliseconds as it is recorded in two-way travel time. For the time to depth conversions the following interval velocities are estimated through velocity anaysis: 1700 m/s in Pliocene-Quaternary Unit 1, 4000 m/s in Messinian evaporites of Unit 2, and 3000 m/s in pre-Messinian siliciclastics of Unit 3. Depth conversions showed that all major lithostratigraphic markers identified in the exploration wells by the Turkish Petroleum Corporation corresponded within ±30 ms with acoustically strong and laterally continuous reflections in the seismic reflection profiles except for the P-reflector. For example, the top and the base of the Messinian evaporite successions (i.e., Unit 2) correlated with strong seismic markers, referred to in the eastern Mediterranean region as the M- and N-reflectors, respectively (Ryan, 1969; Aksu et al., 2005, Figs 3.1, 3.3).

The chronostratigraphy of the Pliocene-Quaternary successions of the Cilicia Basin is studied in detail by Kennedy (2012), who kindly provided these data to the author. Because Kennedy (2012) is not yet published, a summary of the Pliocene-Quaternary chronostratigraphy is further provided here. Correlations of the Seyhan-1 and Karataş-1 wells with the industry seismic reflection profiles suggest that the prominent A-reflector marks the boundary between the lower Pliocene Aktepe Formation and the upper Pliocene Kuranşa Formation (Fig. 3.5). Because the chronostratigraphic charts of the Seyhan-1 and Karataş-1 wells indicate that the Aktepe to Kuranşa formation transition occurs at the lower-upper Pliocene boundary, the A-reflector is concluded to denote this

boundary (Figs. 3.3, 3.5). Geological time tables show that the lower-upper Pliocene boundary occurs at 3.6 Ma. Another prominent reflector in Unit 1 is the P-reflector (e.g., Figs. 3.2, 3.3). This marker often occurs near the top of prominent delta packages that exhibit east-directed clinoform progradation. Unfortunately there is no chronological information in the exploration wells above the Aktepe to Kuranşa formation transition, thus the age of the P-reflector cannot be extrapolated from the well data. However, the age of the P-reflector can be estimated using the assumptions that (i) the rate of sedimentation within the deepest portion of the Cilicia Basin during the upper Pliocene-Quaternary remained constant and (ii) the sediment-water interface represents the contemporaneous sedimentation surface. The thicknesses of sediments contained between the A- and P-reflectors are determined at several localities. On the basis of the above assumptions the age of the P-reflector is interpolated as 1.7 Ma. This age is slightly younger that the age of the upper Pliocene-Quaternary boundary at 1.8 Ma.

Correlations with global geological time scale suggest that the M-reflector separates the lowermost Pliocene sediments from the uppermost Miocene evaporite deposits. Recent studies show that in at least some regions of the Adana Basin, the latest Messinian event, also known as "lago-mare event" (5.45-5.33 Ma), extends into the lowermost Pliocene (e.g., Cosentino et al., 2010; Cipollari et al., 2010). This interpretation differs from the previous concept in which the M-reflector is said to occur at the Miocene-Pliocene boundary at 5.3 Ma (e.g., Yalçın and Görür 1984). The well data are mute regarding how much of the Messinian strata are missing, as well as when exactly the sedimentation resumed in Cilicia Basin during the early Pliocene following the

Messinian Salinity Crisis (e.g., Hsü et al., 1978; Bridge et al., 2005). Because the M-reflector is a major erosional unconformity and the Turkish Petroleum Corporation well data lack the biostratigraphic details about the Messinian evaporite successions, the exact ages of the underlying Messinian sediments are not known. However, it is known that within the Inner Cilicia Basin the Pliocene-Quaternary Unit 1 unconformably overlies the M-reflector and is characterized by a 2-3 seconds-thick delta succession (Figs 3.2, 3.3, also see Aksu et al., 2005). Seismic reflection profiles studied in this dissertation show no evidence for major interruptions in sedimentation within the Pliocene-Quaternary Unit 1. Because the post-Messinian refilling of the Mediterranean was rapid and said to have occurred at 5.3 Ma, combined with the fact that the deep Cilicia Basin shows a clearly conformable succession readily onlapping the M-reflector, the base of Pliocene immediately above the M- reflector is assumed to be 5.3 Ma. Please note that the age of the M-reflector is broadly taken to correspond with the Pliocene-Miocene boundary at 5.3 Ma; however this age is probably overestimated on the basis of recent studies showing that the lago-mare may extend into the lowermost Pliocene.

The four strong marker horizons (i.e., the P-, A-, M-, and N- reflectors), are correlated across the study area using two key industry seismic reflection profiles, ADZ 90 and ADZ 81 (Figs 3.4, 3.6 and 3.7). The strongest markers, the M- and the N-reflectors were easily correlated from line-to-line across the study area. The delineation of the N-reflector was challenging in regions of thick Unit 1. Although the N- reflector

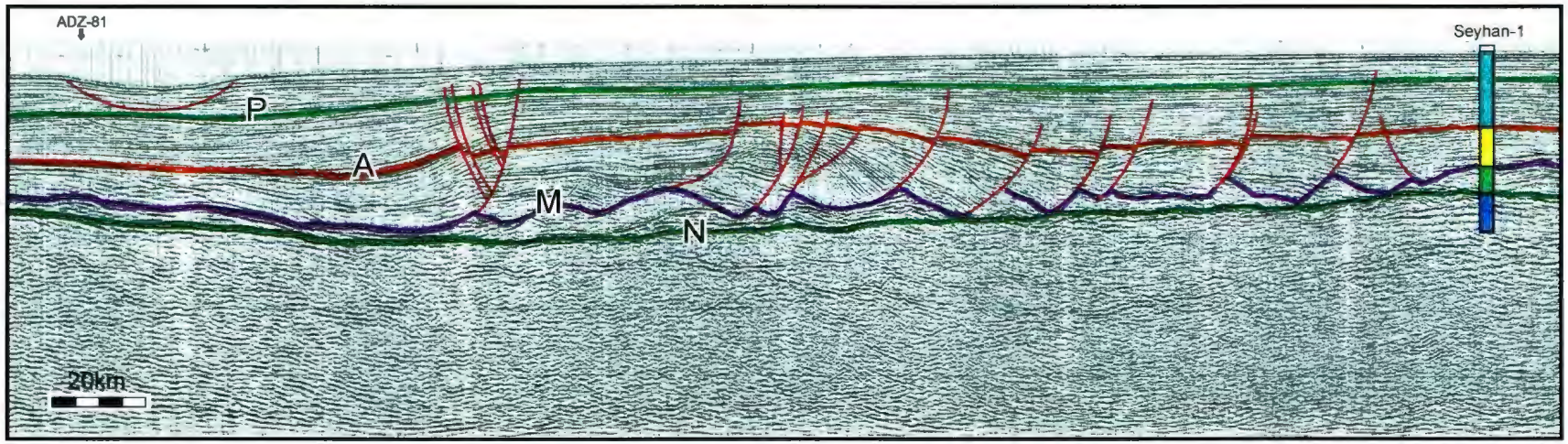

Figure 3.6: Industry multi-channel seismic reflection profile ADZ90 showing the lateral continuity of the A- P- M-and N-reflectors (Modified from Kennedy, 2012). This particular profile was also used to correlate these reflectors across the study area in the establishment of the chronology. Location is given in Figure 3.4.

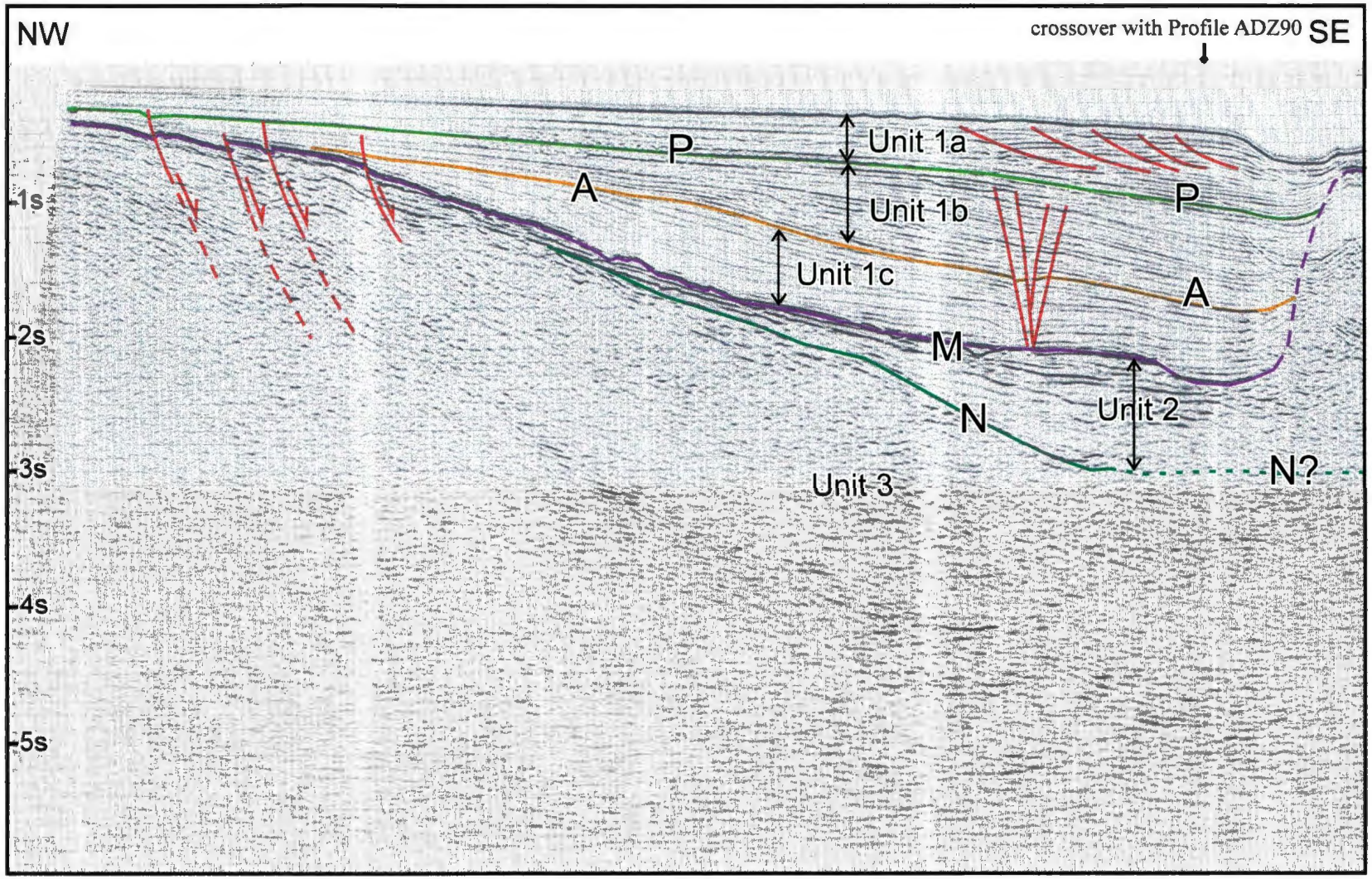

Figure 3.7: Industry multi-channel seismic reflection profile ADZ81 displaying the crossover with the industry profile shown in Figure 3.6 and the correlation of P-, A-, M- and N-reflectors used to establish the chronology in the study area. Location is shown in Figure 3.4. Red lines are faults.

was not observed well in these regions, the general trend of it was estimated using the line-to-line correlations.

3.1 Central Cilicia Basin Unconformities

M- and N-reflectors are prominent seismic markers in the eastern Mediterranean Sea (Ryan et al., 1973; Aksu et al., 2005; Hall et al., 2005; İşler et al., 2005). In the central Cilicia Basin, the M- reflector is characterised by continuous and high amplitude strong reflectivity (Figs. 3.1, 3.2, 3.3, 3.6, 3.7, 3.8). This basin-wide reflector marks the unconformity at the base of Unit 1, a continuous sedimentary package with strong reflectivity, across the entire study area. The unit underlying the M- reflector varies across the study area. In the deeper regions of the study area, the M reflector marks the top of the Messinian evaporites of Unit 2, and separates Messinian successions from the Pliocene Quaternary (Fig. 3.8). In the shallower shelf region along the Turkish coast, Messinian evaporites of Unit 2 are absent. In this part of the study area the M- reflector marks the top of Unit 3, and it separates pre-Messinian Miocene and Pliocene successions (Fig. 3.2).

The N- reflector has a lower reflectivity and notably more discontinuity than the M- reflector. It marks the base of the Messinian succession where the Messinian evaporites of Unit 2 are present (Figs. 3.1, 3.3, 3.6, 3.7, 3.8). The N- reflector is truncated by the M- reflector in the shallower part of the study area where the Messinian evaporites are absent (Fig. 3.2). The N- reflector is poorly imaged in some parts of the study area, especially where the salt layer is thicker (Fig. 3.9).

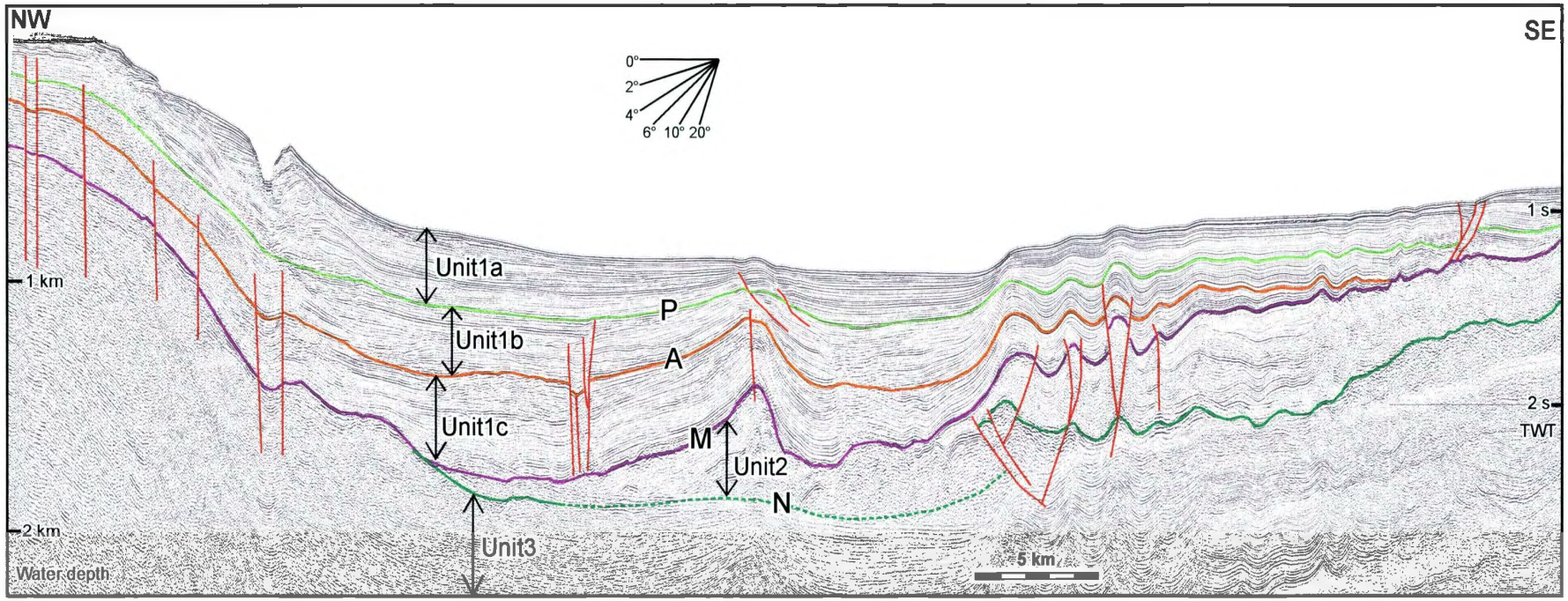

Figure 3.8: Multichannel seismic reflection profile illustrating the basin-wide M (purple), N (green), A (orange), and P (light green). Location is shown in Figure 3.5.

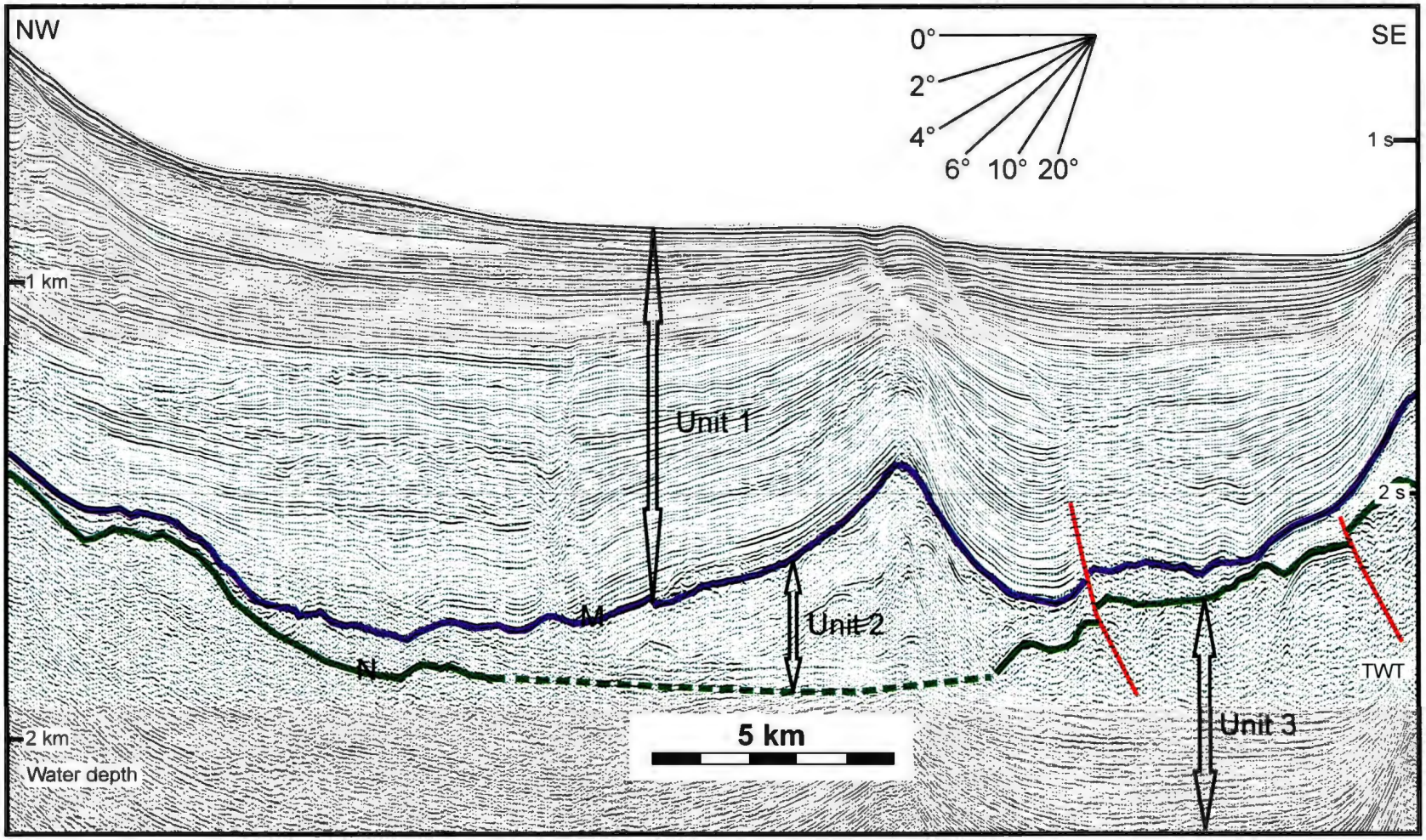

Figure 3.9: Poorly imaged N-reflector in the study area where the salt layer is thick.

3.2 Central Cilicia Basin Stratigraphic Units

3.2.1 Unit 1: Pliocene – Quaternary

Unit 1 is a highly-reflective sedimentary package which represents the youngest stratigraphic unit in the central Cilicia Basin. It is characterized by high frequency, strong and continuous reflectors. The M-reflector defines the base of this unit (Figs. 3.1, 3.2, 3.3, 3.6, 3.7, 3.8, 3.9). This unit is easily traced throughout the entire study area. Based on the correlations of exploration well data with seismic sections from the study area, this unit is determined to be the Pliocene-Quaternary age. Unit 1 is predominantly composed of siliciclastic successions mainly fed by major rivers draining into the Cilicia Basin (Aksu et al., 2005). Unit 1 is correlated with the Kuranşa and Handere formations of the Adana Basin, and the Erzin and Aktepe formations of the Iskenderun and Latakia Basins (Fig. 3.10). This unit is also correlated with the Fanglomerate and Nicosia formations of the Mesaoria Basin, and the Mirtou Formation of the Kyrenia Mountains, northern Cyprus (Aksu et al., 2005).

Unit 1 reaches its maximum thickness along the central axes of both the Inner and the Outer Cilicia Basins, and Latakia-Iskenderun Basins. Seyhan, Ceyhan, Tarsus, Göksu and Asi Rivers are considered to be the major sources of the sediments of Unit 1 into the Adana, Cilicia, Latakia and Iskenderun Basins (Fig. 3.11). This unit is characterized by a prograding wedge of deltaic sediments in the southern Adana and Inner Cilicia Basins, and it reaches its maximum thickness of ~2500 ms immediately seaward of the present

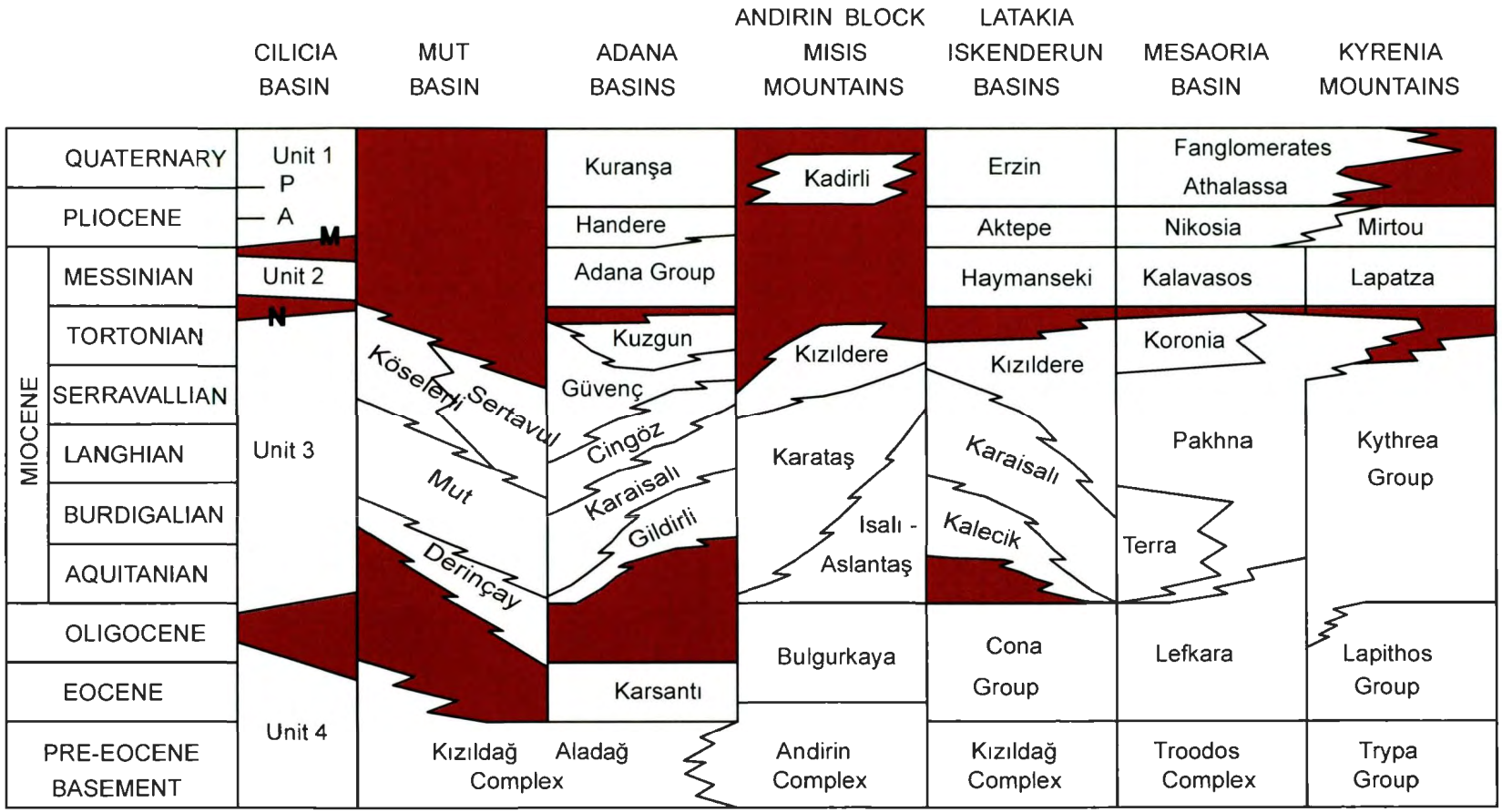

Figure 3.10: Chronostratigraphy of the northeastern Mediterranean basins showing correlations between seismic stratigraphic units and the sedimentary successions on land, compiled using Yalçın and Görür (1984), Kozlu (1987); Yılmaz et al (1988) and Gökçen et al. (1988). Stratigraphy of the Seyhan well courtesy of Turkish Petroleum Corporation. Series and stage chronology and ages from International Commission on Stratigraphy (2009).

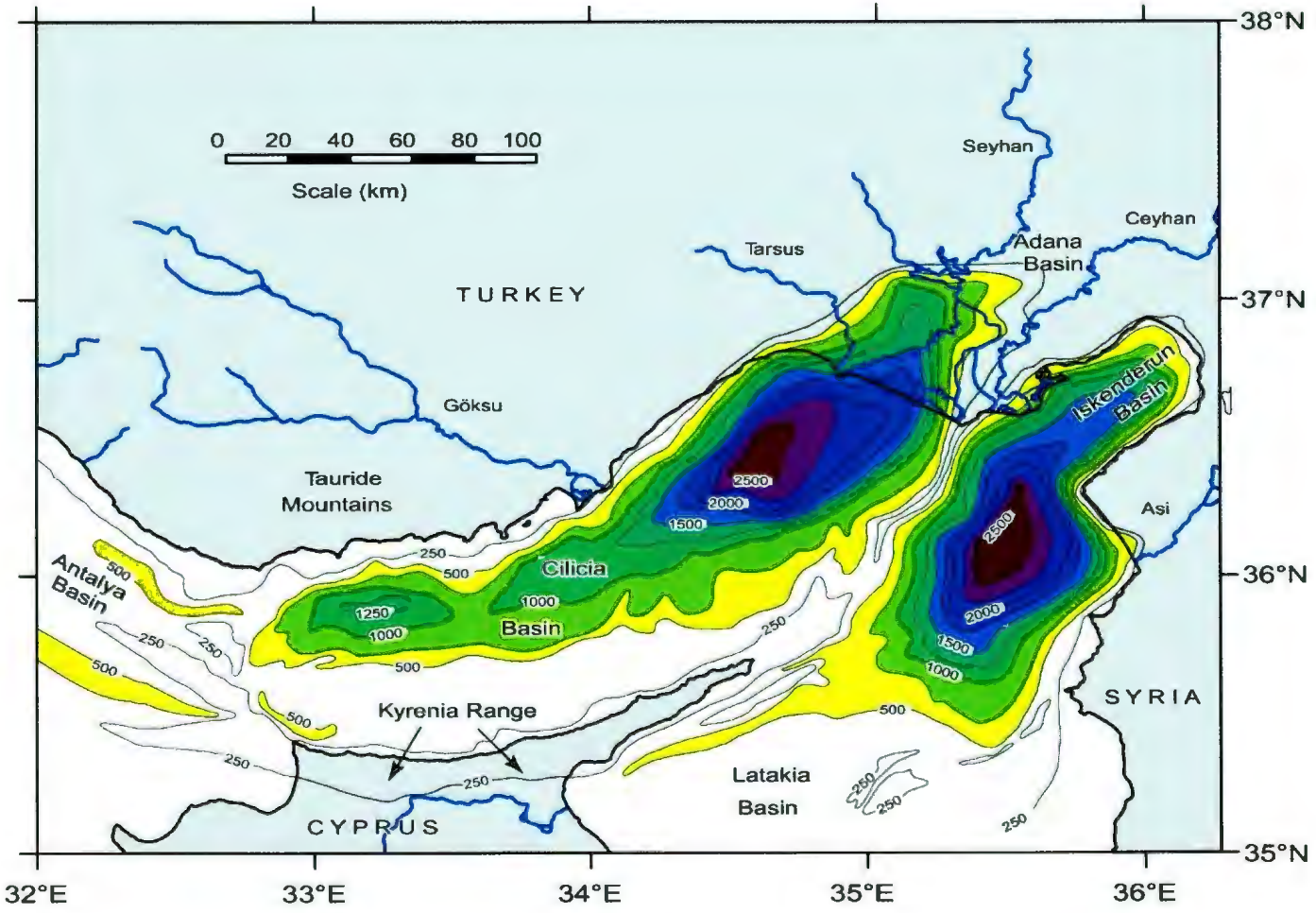

Figure 3.11: Isopach map of the Pliocene-Quaternary succession in the broader Cilicia Basin. Contours are in milliseconds, and 100 ms is approximately equivalent of 85 meters (Aksu et al., 2005).

day mouths of Seyhan and Tarsus Rivers (Aksu et al., 2005). Unit 1 sharply thins towards the Kyrenia Range and the southwestern Turkish coast.

The thickness of the Pliocene-Quaternary sediments is mapped in the study area (Fig. 3.12). Similarly to the broader isopach map (Fig. 3.11), Unit 1 thickens in the northeast portion of the study area through the Inner Cilicia and Iskenderun Basins, where it reaches a maximum thickness of 1900 ms. The thickness of Unit 1 decreases in the northwestern and southern portion of the study area toward the Turkish and Cyprus continental margins. This unit thins towards the Kyrenia range of northern Cyprus, and southern Turkey. The thinning of Unit 1 towards the continental shelves explains the absence of the unit over the Misis-Kyrenia Range of northern Cyprus and Tauride Mountains of southern Turkey (Fig.3.11).

Unit 1 shows several vertically stacked east-prograded clinoform successions that define discrete delta wedges in seismic reflection profiles (Fig. 3.2). The sediment load reaches its maximum thickness in the river-delta system of the Inner Cilicia Basin seaward of Tarsus and Seyhan Rivers (Figure 3.11). This unit also includes some stacked units of acoustically transparent weak internal reflections. These units are easily delineated in the seismic reflection profiles because of the contrast with the surrounding strong reflections of Unit 1 (Figs. 3.2, 3.13).

Unit 1 is further divided into three sub-units; Units 1a, 1b, and 1c. Unit 1c is early Pliocene and Unit 1b is late Pliocene age. M- and A-reflectors define the borders of Unit 1c, separating it from Messinian Unit 2, and upper Pliocene Unit 1b, respectively. Unit

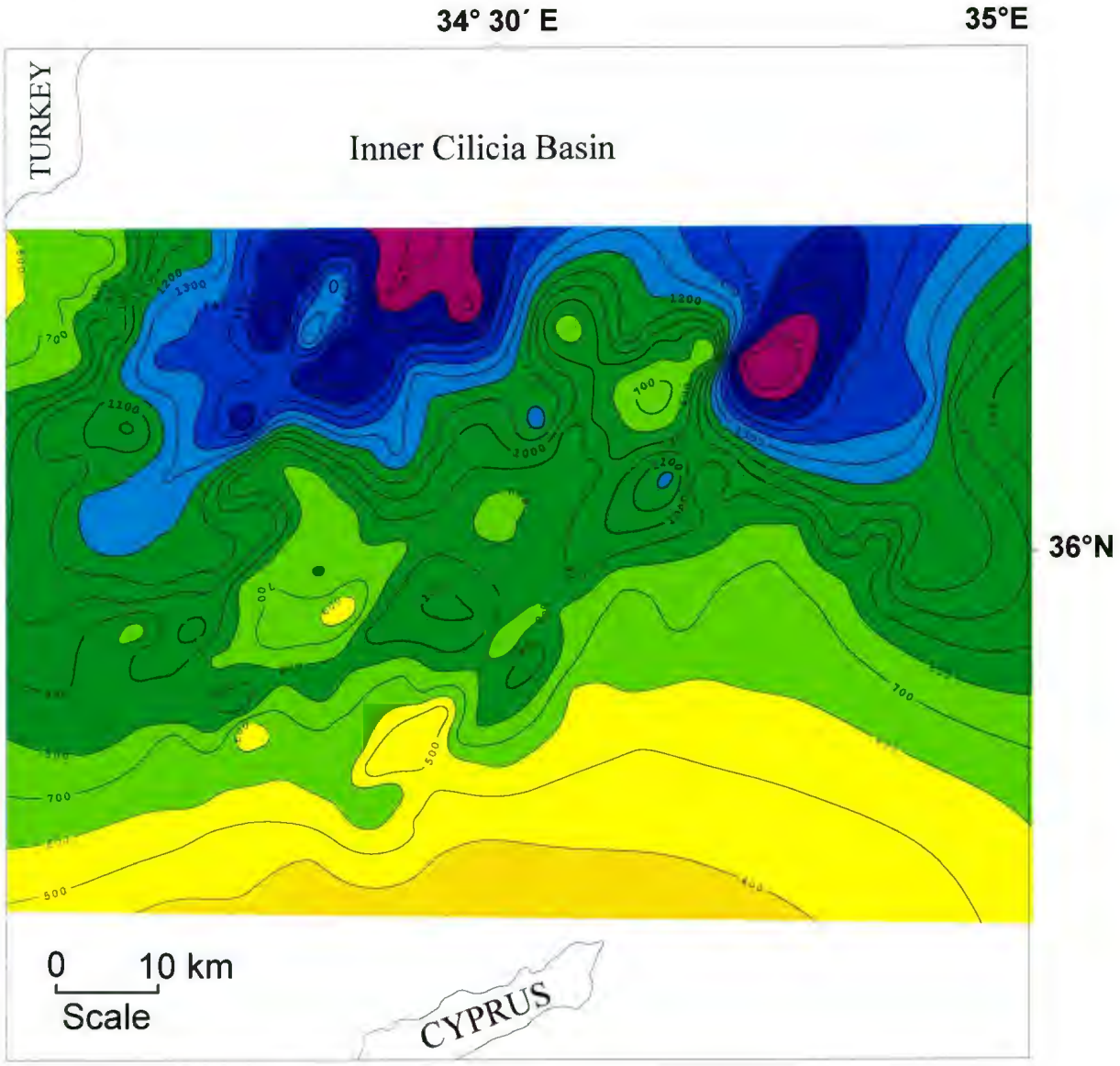

Figure 3.12: Isopach map of the Pliocene-Quaternary succession in the central Cilicia Basin. Contours are in milliseconds in two-way travel time. 100 ms is approximately equivalent of 85 metres.

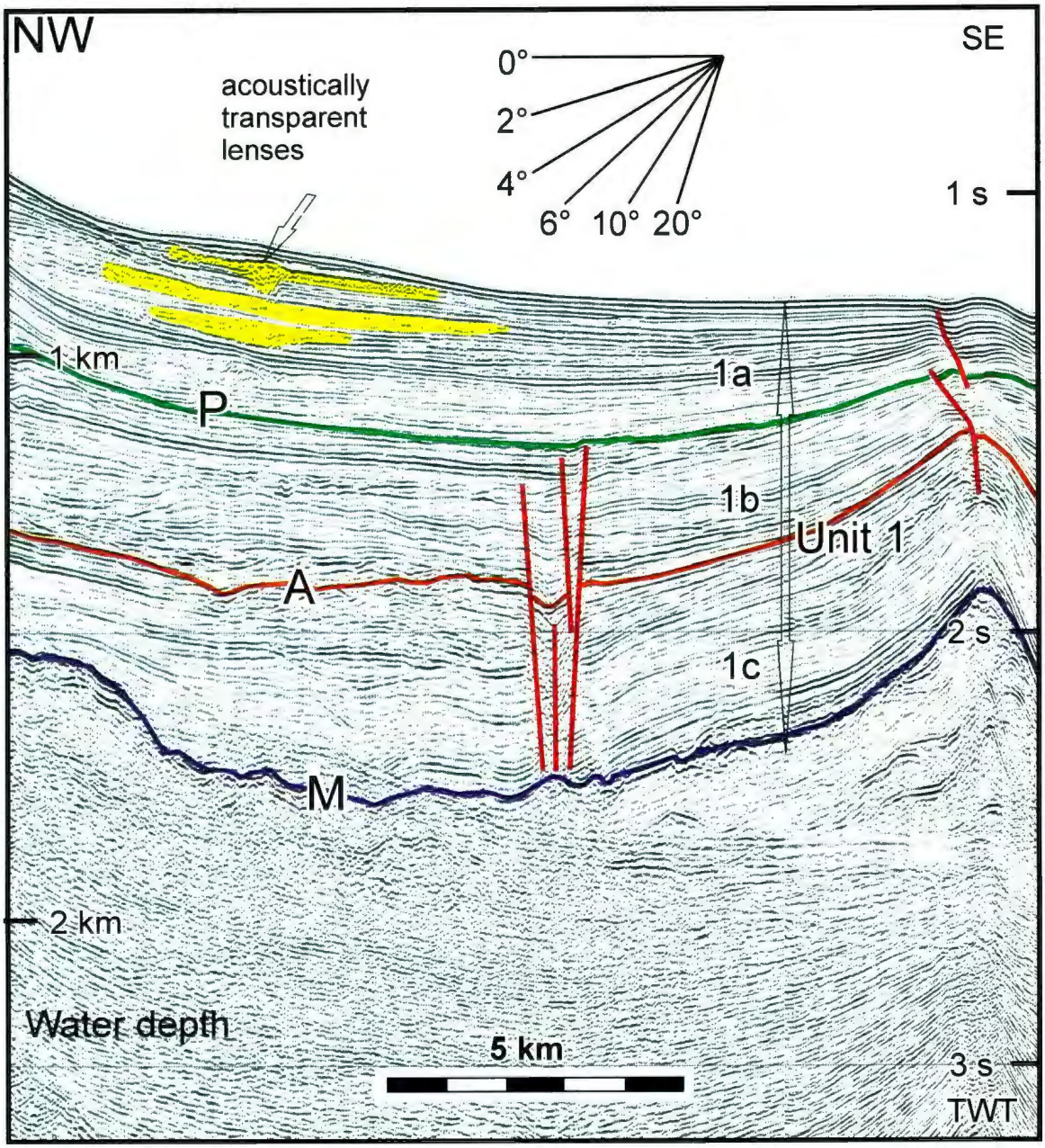

Figure 3.13: Multichannel seismic reflection profile showing the accoustically transparent units in the Unit 1 of the study area.

1a is predominantly Quaternary age, including mostly Quaternary and a very little portion of the uppermost Pliocene sediments. The P-reflector separates Unit 1a from the upper Pliocene Unit 1b.

3.2.2 Unit 2: Miocene (Messinian)

Unit 2 is generally characterized by a low reflectivity package with weak and often discontinuous reflections (Figs 3.1, 3.3, 3.8), although in the Outer Cilicia Basin, the succession has a stratified appearance delineated by a small number of discrete, strong, and continuous reflectors with a corrugated geometry (Figure 3.1, Aksu et al., 2005). The top of Unit 2 is distinguished by the M-reflector. The base of this unit is the N-reflector which has a lower reflectivity and more discontinuity. Exploration wells in the Inner Cilicia Basin show that Unit 2 is predominantly composed of halite alternating with lesser quantities of anhydrite and limestone, and is correlated with the Messinian evaporites (Fig. 3.10). Unit 2 is either very thin or not present near the Misis–Kyrenia horst block, the southern flanks of the Kyrenia Range, and the Turkish Margin of the basin (Fig. 3.8, Aksu et al., 2005). In the central Cilicia Basin this unit is only present below ~1250 ms depth.

In the Outer Cilicia Basin, Unit 2 shows some strong internal reflectors. These reflectors are mostly truncated at the M-reflector and discordant with the overlying and underlying strata, M- and N-reflectors, respectively (Figs. 3.1, 3.3, 3.8). These strong internal reflectors in Unit 2 are suggested to be thin siliciclastic layers between cycles from the several cycles of the evaporite history of the Mediterranean Sea (Hsü et al, 1973,

1978). Unit 2 reaches its maximum thickness ~900 ms in the transition from the Outer to the Inner Cilicia Basin. Also in the southern portion of the study area there are two prominent thick packages of Unit 2 (~500-600 ms); however it is absent in the southernmost portion of the study area over the Misis–Kyrenia horst block, and the northern portion of the study area in the southern Turkish margin (Fig. 3.14, Aksu et al., 2005). From the center of the study area through the Inner Cilicia Basin, the base of Unit 2 is poorly imaged due to complexly folded and faulted zone (further discussed in Chapter 4).

3.2.3 Unit 3: Miocene (pre-Messinian)

Unit 3 underlies the M- reflector where the Messsinian evaporites of Unit 2 is absent, and underlies the N- reflector where Unit 2 is present. The seismic character of the Unit 3 varies with depth. The upper portion of this unit, immediately below the M- or N-reflectors, is characterized by lower frequency rhythmic reflections, showing good lateral continuity (Figs 3.1, 3.2, 3.3, 3.7, 3.8). In the lower part of the unit high frequency, continuous, and rhythmic reflectors are present. The base of this unit is not clearly observed in the seismic reflection profiles in the study area. Data from the exploration wells show that Unit 3 is composed of fluvio-deltaic successions of mainly Tortonian age (Uffenorde et al., 1990), and the middle Miocene turbiditic successions of Serravallian and Langhian ages. It may include the lower Miocene Burdigalian and Aquitanian age successions at its base (Yalçın and Görür, 1984). Unit 3 is correlated with the Kuzgun, Güvenç, Cingöz, and Karaisalı (might include at its base) formations of the Adana and Inner Cilicia Basins and the Pakhna Formation of the Mesaoria Basin (Yalçın

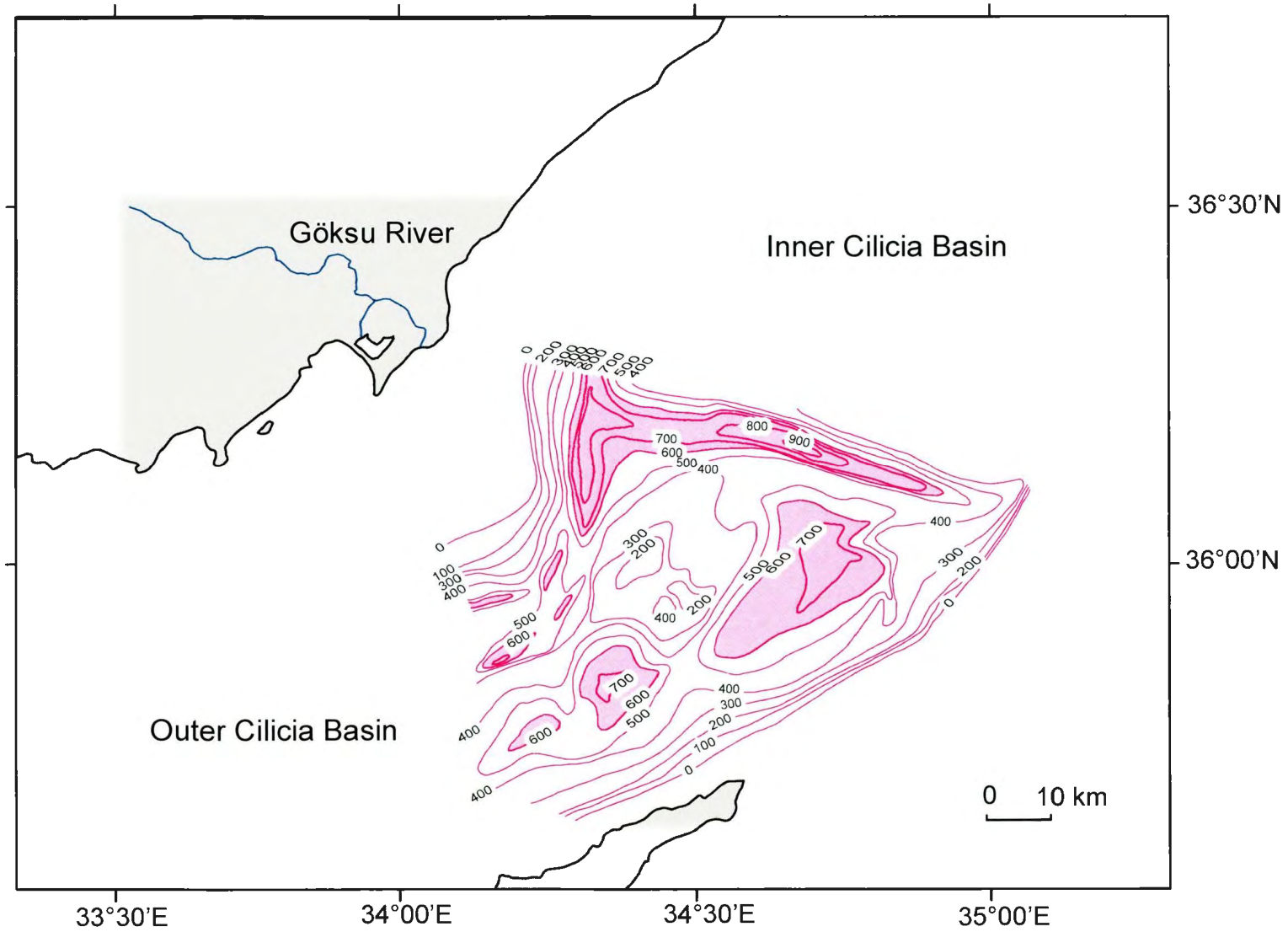

Figure 3.14: Isopach map of the Messinian evaporite Unit 2 in the study area. Thicknesses are in milliseconds two-way time, where 100 ms represents about 150 metres.

and Görür, 1984; Kozlu, 1987; Figure 3.10). The unit further correlated with Karataş/Isalı-Aslantaş formations of the Misis Mountains (Kelling et al., 1987) and the Kythrea Group of the Kyrenia Range (Figure 3.10; Aksu et al., 2005; Robertson and Woodcock, 1986; Weiler 1969).

CHAPTER FOUR

Structural Architecture of the Cilicia Basin

The Cilicia Basin is an ENE-WSW-trending arc-shaped depocentre in the eastern Mediterranean Sea, situated between the Island of Cyprus in the south and the central Anatolia in the north (Fig. 4.1). In the northeast, the basin merges with the onland Adana Basin and in the west it is separated from the Antalya Basin by the broadly north-south trending Anamur-Kormakiti zone (Fig. 4.1). The basin is naturally divided into two morphological regions: (*i*) the NE-SW trending shallow Inner Cilicia Basin, and (*ii*) the broadly E-W trending deeper Outer Cilicia Basin. The study area is situated in the eastern segment of the Outer Cilicia Basin, immediately southwest of the transitional zone between the Inner and Outer Cilicia Basins (Fig.4.1). This region exhibits considerable structural complexity as a transition zone between the Outer and Inner Cilicia Basins, as discussed below.

In this chapter the structural framework of the study area is described in detail, using major fault architectures, salt-related fold and thrust structures and sedimentary growth associated with these structures observed in high-resolution seismic reflection profiles. The study area is divided into three main morpho-tectonic domains (Fig. 4.2): (*i*) the southern basin margin, including the Misis-Kyrenia fold-thrust belt, and its re-activated normal and strike-slip faults and their southwest extension toward the Karpas Peninsula of the Island of Cyprus and its northeast extension toward the Misis Mountains of southern Turkey, (*ii*) the central basin floor which includes the complexly faulted-folded transition zone between the Inner and Outer Cilicia Basins, and (*iii*) the broadly

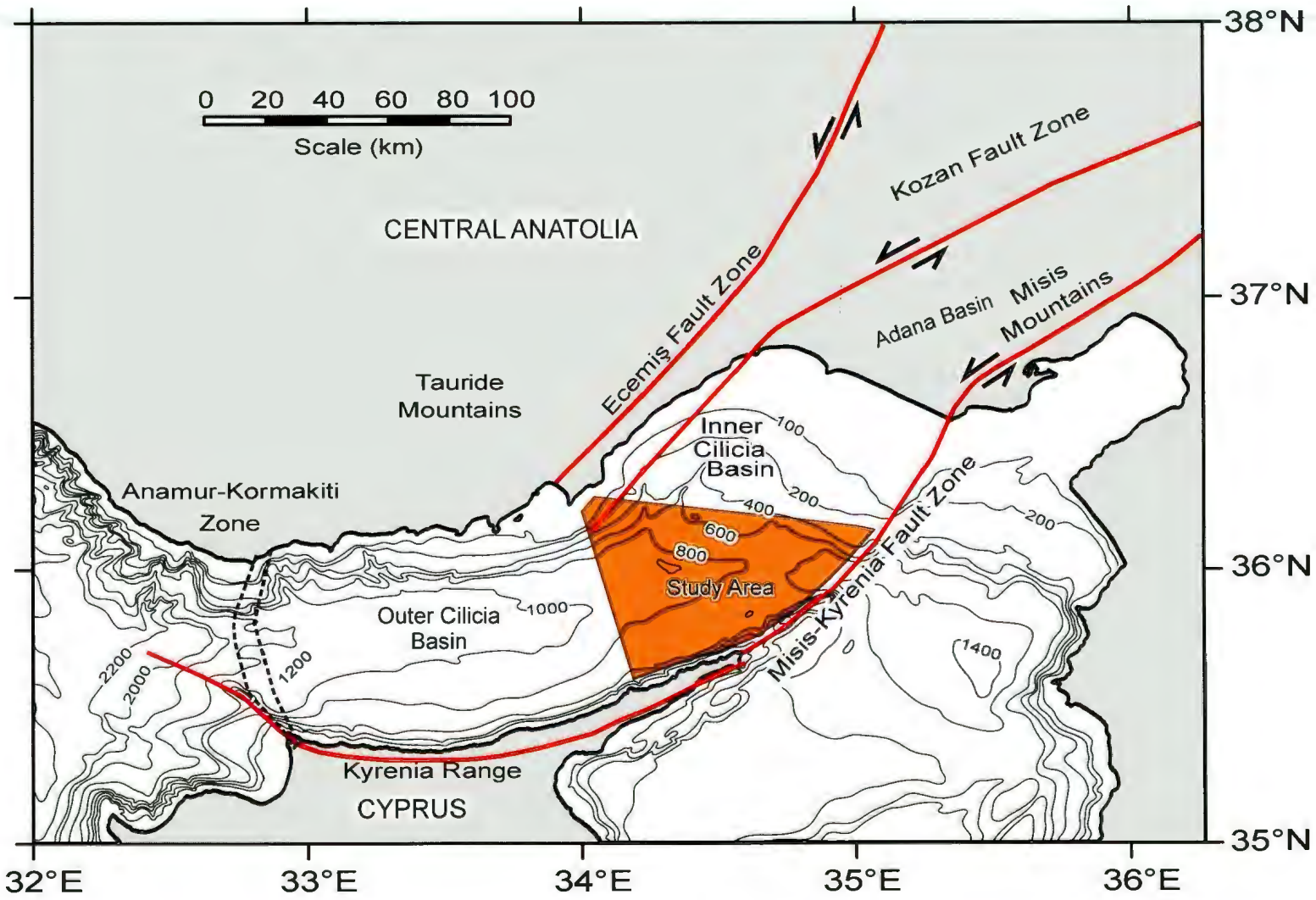

Figure 4.1: Simplified map of the Cilicia Basin showing the bathymetry and the important tectonic elements in the Cilicia Basin. The orange curve is showing the study area.

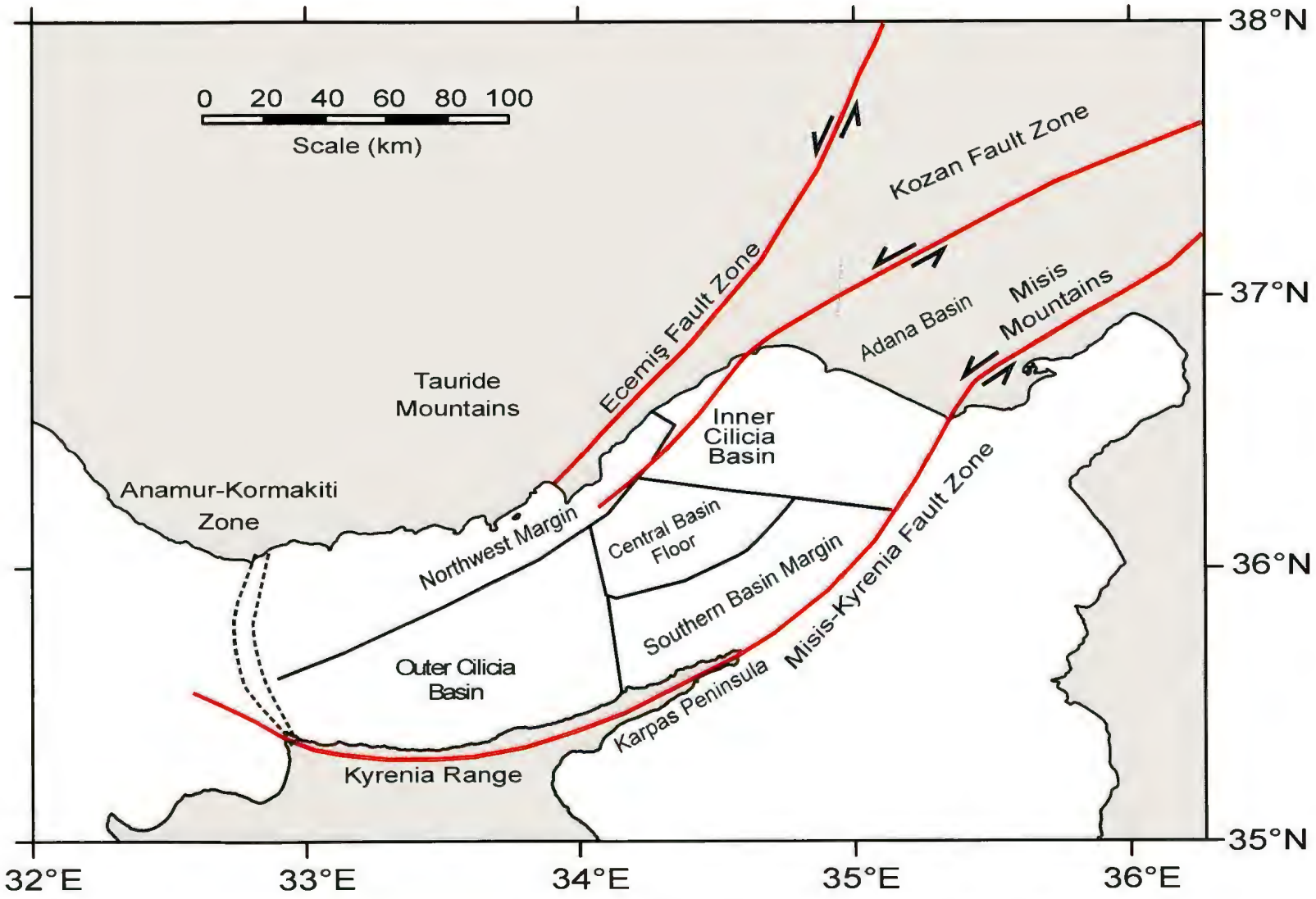

Figure 4.2: Map of the Cilicia Basin showing the three main morpho-tectonic domains in the study area.

northwest-concave shallow continental margin seaward of the present-day Göksu delta, which also includes a 30-40 km wide tectonically complex zone corresponding with the marine extension of the Kozan Fault zone. The location of the data used to describe the structural architecture of the Outer Cilicia Basin is given in Figure 4.3.

4.1. Southern basin margin: the Misis-Kyrenia fault zone

The Misis-Kyrenia Fault Zone is defined as an approximately 30 km-wide SE-convex zone which links the Misis Mountains of southern Turkey to the Kyrenia Range of northern Cyprus (Fig. 4.2). The southern basin margin is characterised by two prominent structures associated with the Misis-Kyrenia Fault Zone. These structures are temporally superimposed on one another and include *(i)* a NE-SW trending and SE-verging fold thrust belt which defines the architecture of the Miocene succession of Unit 3 and *(ii)* a prominent NE-SW trending and both NW-and SE-dipping extensional fault system which defines the architecture of the Pliocene-Quaternary succession of Unit 1 (Fig. 4.4). The NE-SW trending and SE-verging fold thrust belt defines the trailing panels of the Misis-Kyrenia fold-thrust belt, whereas the Pliocene-Quaternary fault system with high angle extensional faults creates a well defined horst structure centered over the Miocene Misis-Kyrenia fold-thrust belt (Fig. 4.5). In this context, the southern basin margin exhibits a duplex structure: a contractional belt and an extensional belt, separated by the prominent M-reflector.

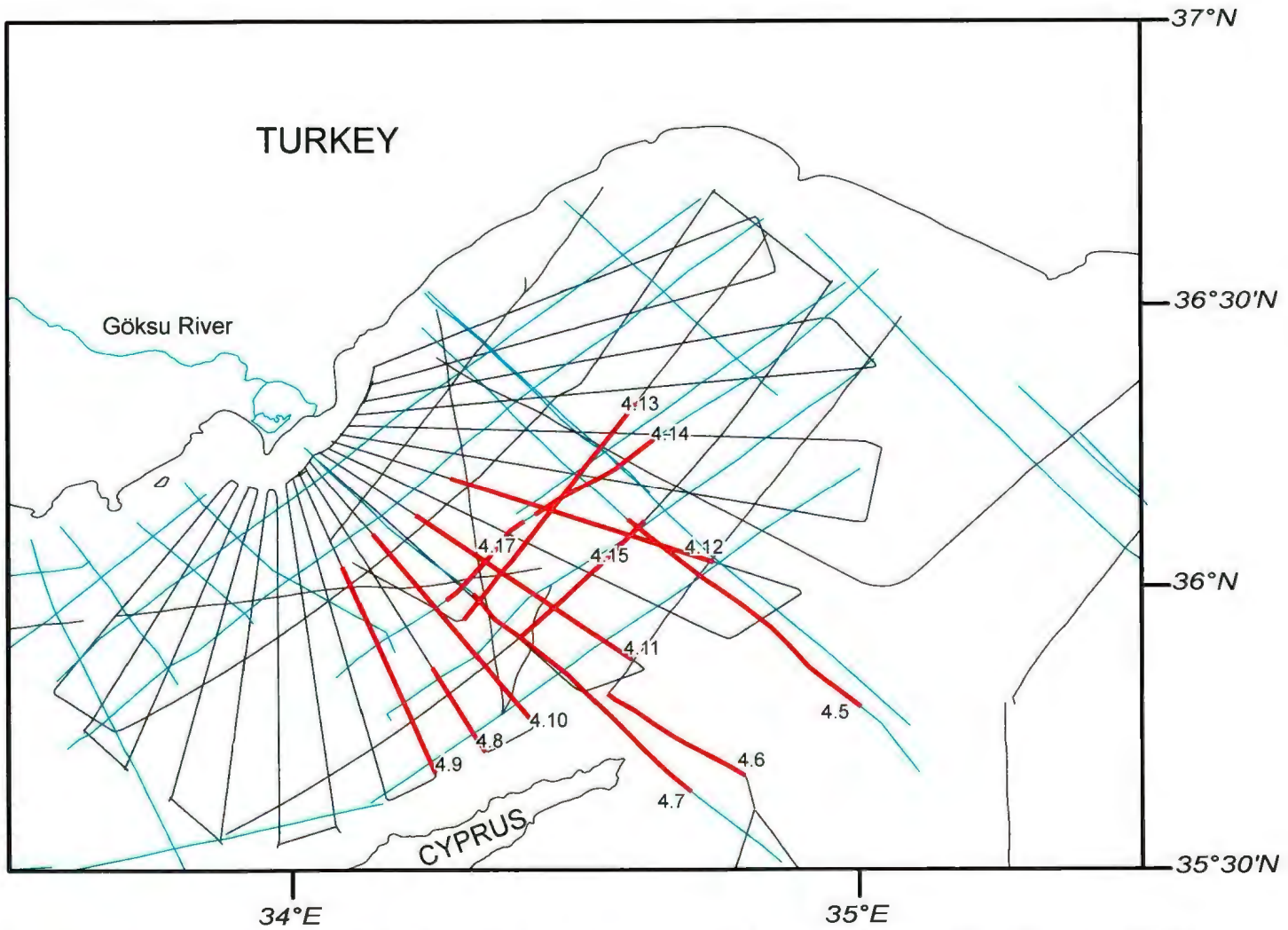

Figure 4.3: Location map showing the seismic reflection profiles in the study area . Black lines are 2008 data, brown lines are 1991 data, and light blue lines are the industry seismic reflection profiles. Thick red lines are the seismic sections that are used to describe the structures of the central basin floor and the southern margin.

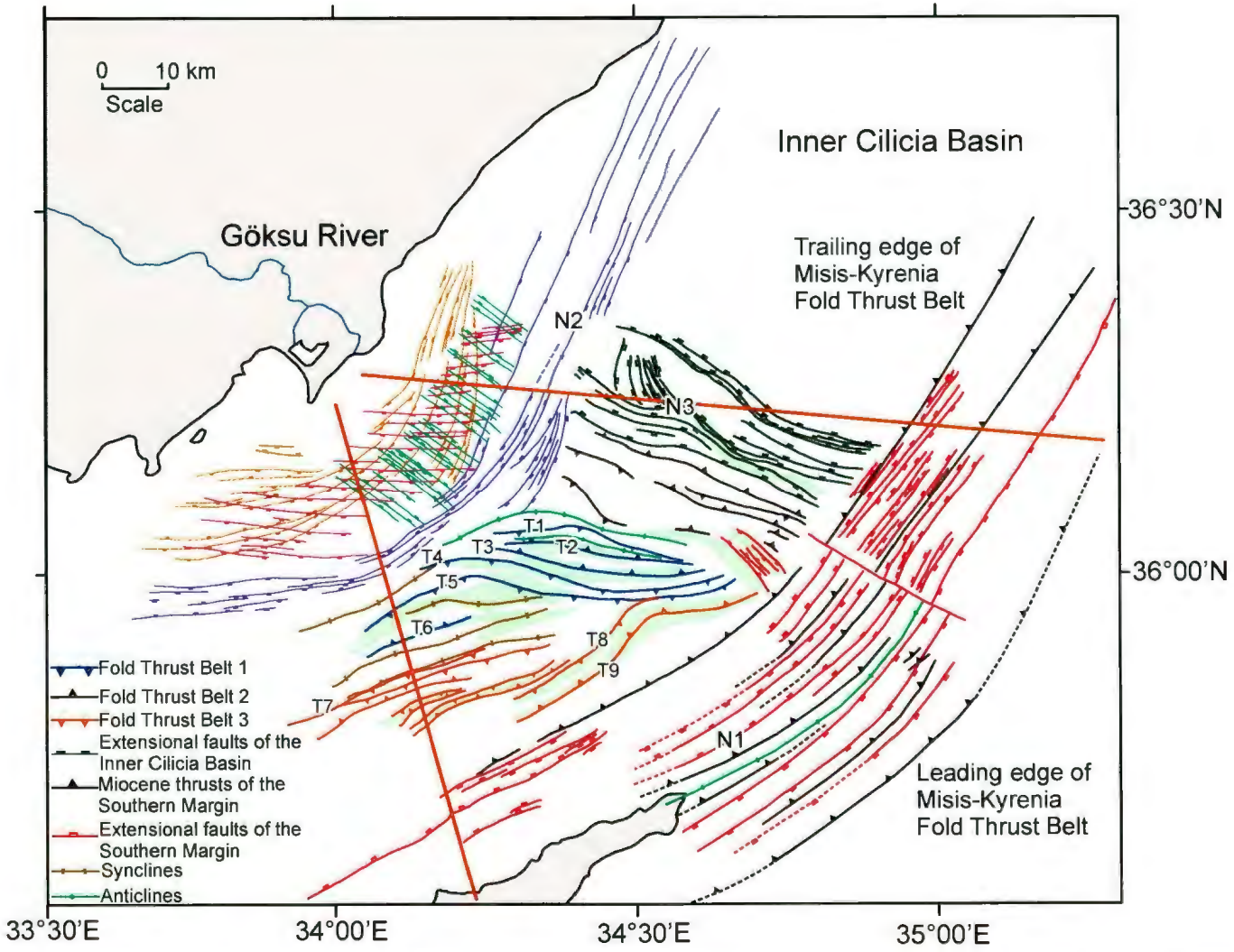

Figure 4.4: Tectonic map of the study area showing the important structural elements in the Cilicia Basin. Ticks are showing the hanging walls of the faults. Faults are mapped as a projection of tip points on the depositional surface. Green structures are salt walls. The orange, purple, red, and green faults on the NW portion of the study area are extensional faults further explained in Figure 4.18.

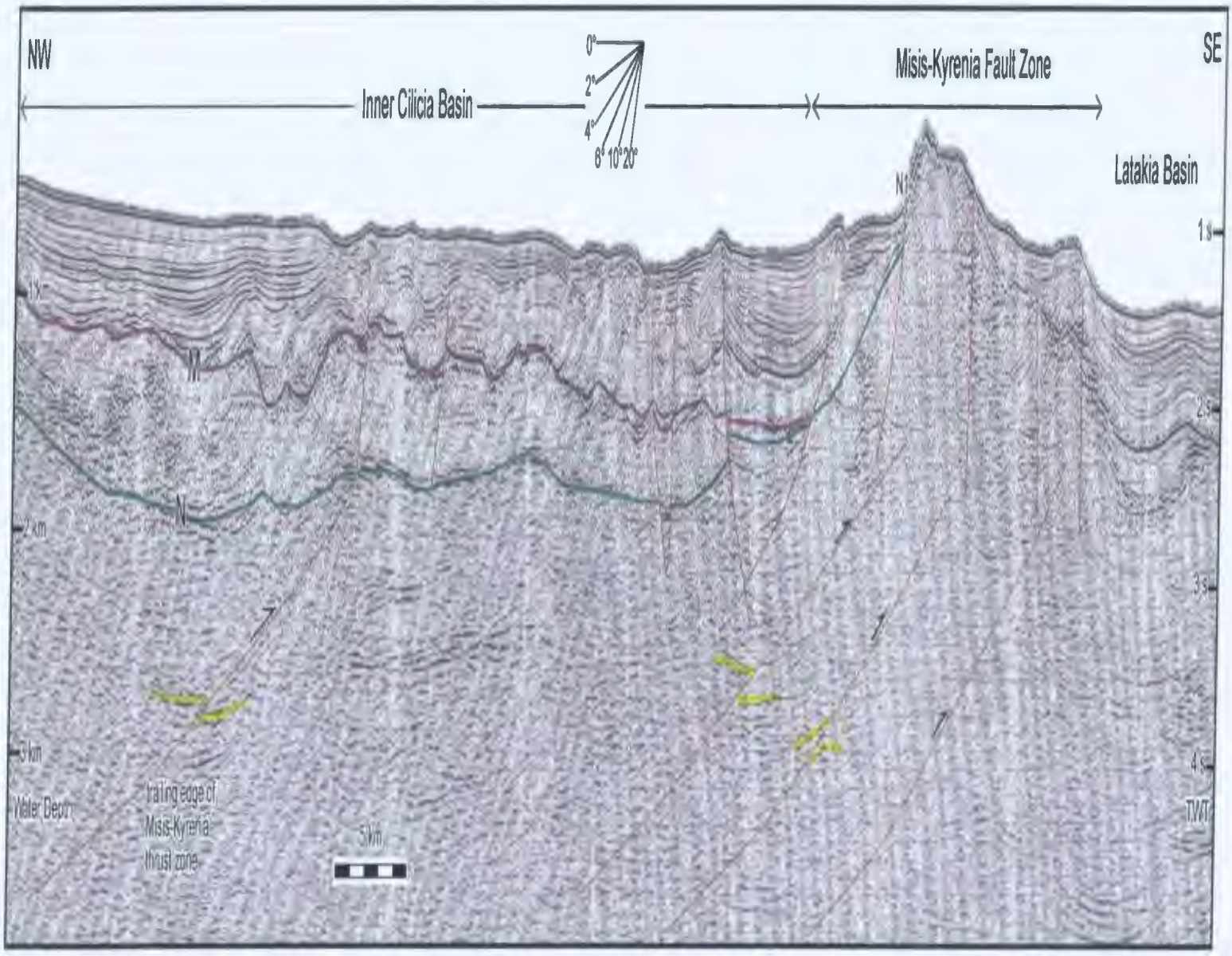

Figure 4.5: Industry seismic reflection profile showing the major structures of the southern margin

4.1.1. Misis-Kyrenia fold-thrust belt

Misis-Kyrenia fold-thrust belt links the Kyrenia Range of northern Cyprus to the Misis Mountains of the southwestern Turkey where the belt exhibits considerable terrestrial relief (e.g., Robertson and Woodcock, 1986; Kelling et al., 1987). In the marine seismic reflection profiles across the northeastern Mediterranean Sea, the fold-thrust belt is characterized by elevated seafloor morphology which is the expression of the erosional remnant of a late Miocene fold-thrust belt, superimposed by the extensional faults and the prominent horst block which is developed over the crestal region of the fold-thrust belt (Hall et al., 2005, Calon et al., 2005, Aksu et al., 2005)

The Misis-Kyrenia fold-thrust belt consists of 6-7 gently curved, broadly NE-SW trending and SE-verging thrusts that delineate the pre-Messinian successions of Unit 3 (Figs. 4.4, 4.5, 4.6, 4.7). These thrusts are often difficult to identify in the seismic reflection profiles, mainly because of the deep incision and decapitation by the overlying M-reflector, which eradicated most of the structural morphology. However, these thrusts have large ramp anticlines associated with thrust culminations that are centrally located across the Misis-Kyrenia fold-thrust belt (Fig. 4.4, 4.6). Although, the thrust trajectory cannot be clearly imaged in the seismic reflection profiles, the secondary structures associated with thrusting, such as the ramp anticline of the thrust culmination provide a clear indication of the location of the thrusts, as well as thrust vergence (see Chapter 2). The M-reflector is a prominent erosional unconformity across the crestal regions of these prominent thrust culminations across this zone (Figs. 4.5, 4.7). The Pliocene-Quaternary succession of Unit 1 dramatically thins toward the Misis-Kyrenia fold-thrust belt,

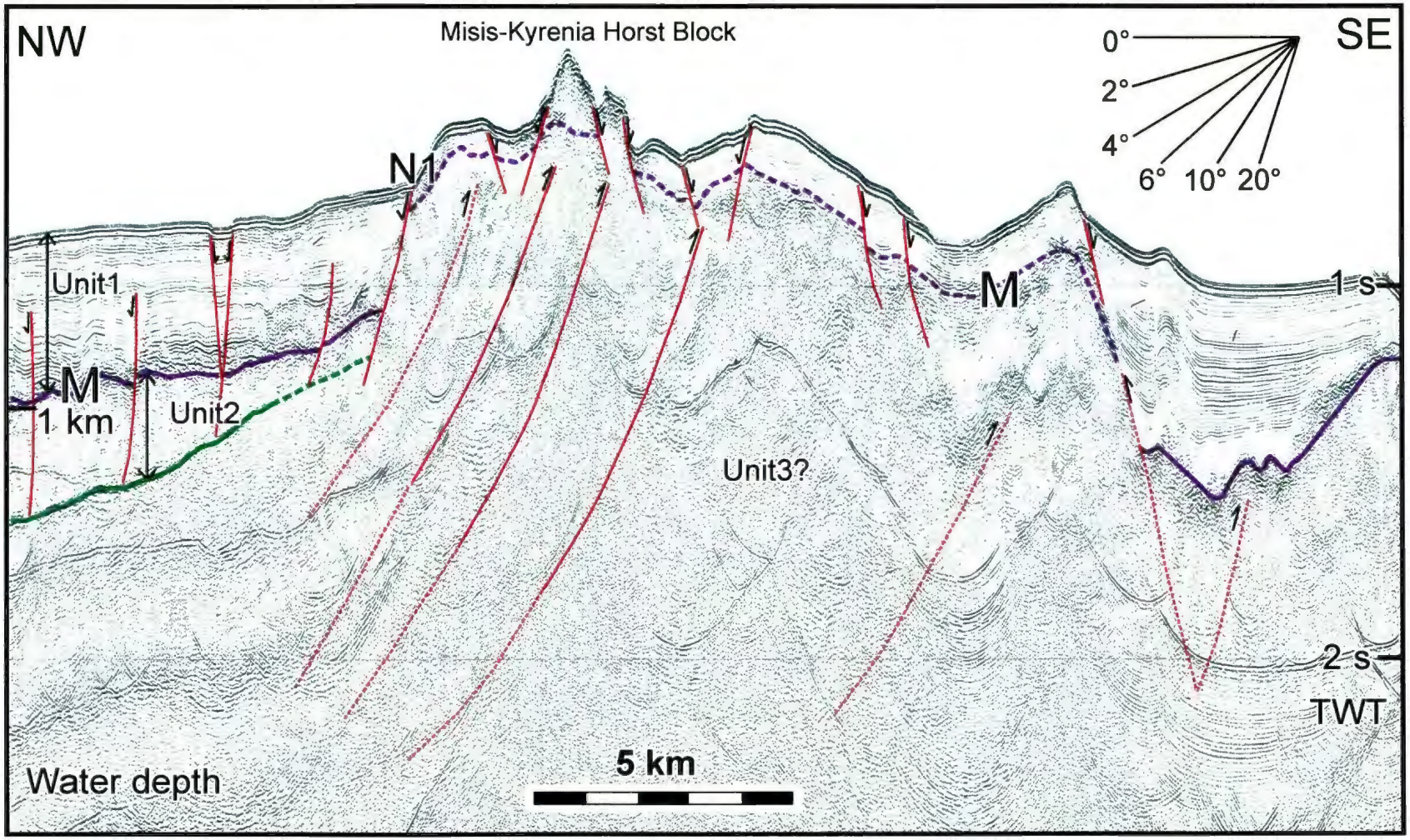

Figure 4.6: Seismic reflection profile showing the major structures of the southern margin. Location is shown in Figure 4.3.

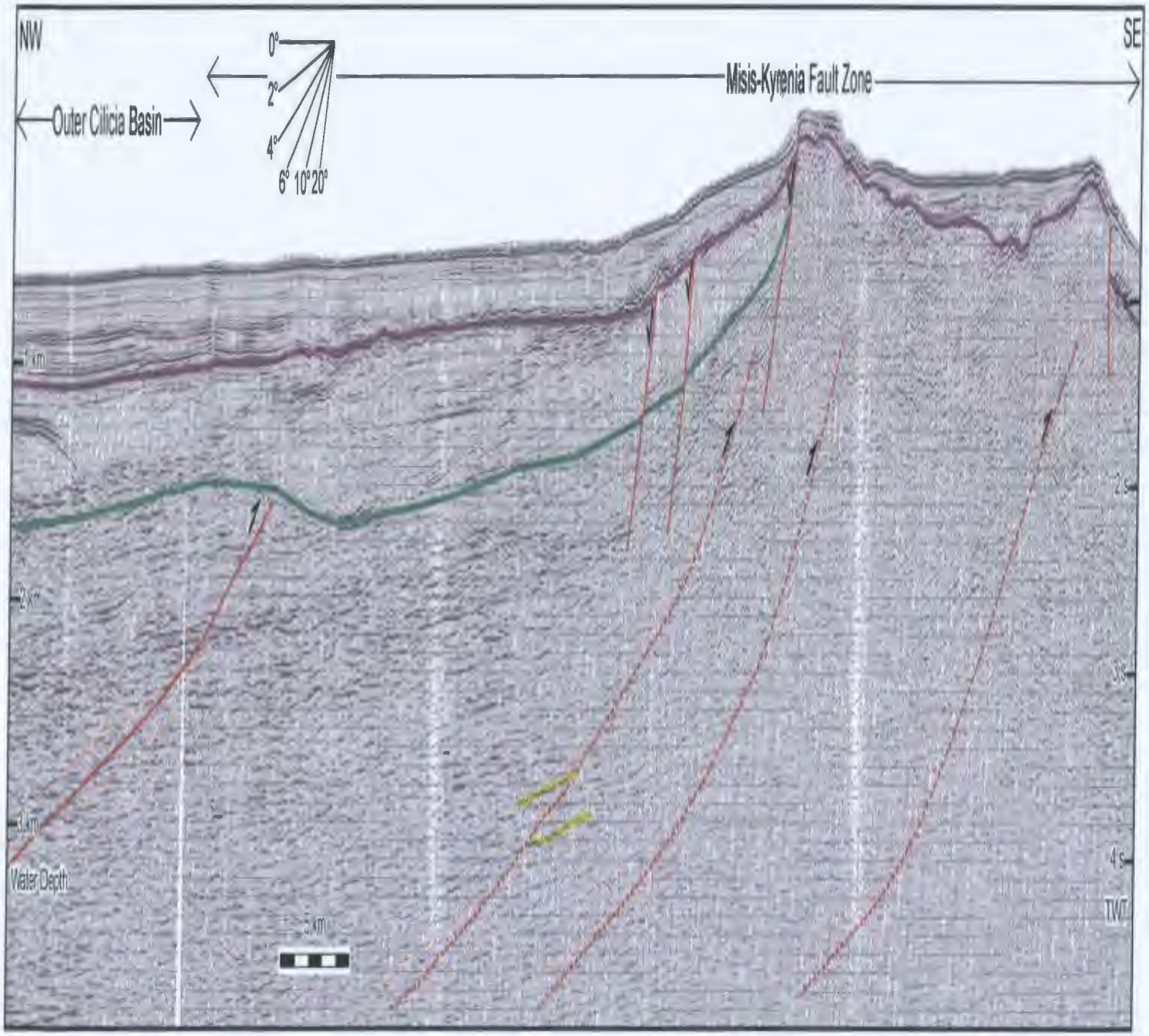

Figure 4.7: Industry seismic reflection profile showing the major structures of the southern margin

onlapping and eventually overstepping the crest of the structure (Figs. 4.6, 4.7). The southeastern edge of the Messinian evaporite Unit 2 is located near the southeastern margin of the Central Basin Floor (discussed below). Unit 2 is absent over the horst block (Figs. 4.5, 4.6, Aksu et al., 2005, Calon et al., 2005).

4.1.2. Misis-Kyrenia horst block

The Misis-Kyrenia horst block is situated over the crest of the Misis-Kyrenia fold-thrust belt (Fig. 4.4). It is bounded on both the northwestern and southeastern margins by relatively steeply (>20°) dipping normal faults that cut most of the Pliocene-Quaternary strata (Figs. 4.5, 4.6, Aksu et al., 1992, 2005). Some of these faults create pronounced steps on the sea floor (e.g., Fig. 4.6). This NE-SW trending and NW- and SE-dipping extensional fault system delineates the Pliocene-Quaternary structures of the southern margins of the Inner Cilicia and Outer Cilicia Basins (Fig. 4.4). The system consists of 6-8 extensional faults. The tip points of these faults are located at or near the depositional surface, and the faults extend well into the Pliocene Quaternary Unit 1 (Fig.4.6). The master fault of this system creates ~700 m dip separation on the M reflector, and defines one of the prominent faults of the Misis-Kyrenia horst block (i.e., fault N1; Figs. 4.4, 4.5, 4.6).

In the western part of the southern margin an ENE-WSW trending listric extensional fault system extends along the northern Cyprus, paralleling the coast with a cross-sectional width of 10-15 km (Fig. 4.4). The system can be readily traced toward the west where it defines a prominent imbricate fan of extensional fault system within the

Pliocene-Quaternary succession (Fig. 4.4; Aksu et al., 2005). Tip points of these faults are in the uppermost Pliocene or Quaternary, and they sole in the Messinian evaporite Unit 2 (Figs. 4.8). The individual faults of this system create small dip separations on the M-reflector, but notably larger separations in the Pliocene-Quaternary reflectors. At first glance, this relationship of the younger sediments showing larger stratigraphic offset than the older sediments may appear counterintuitive. However, in succession where the older sediments is evaporite deposits, including salt, these sediments readily become mobilized and may be injected into the footwall as well as the hanging wall of the fault, creating the observed stratigraphic relationship. Many such examples from the Outer Cilicia Basin are given by Bridge et al. (2005) and Aksu et al. (2005).

4.2. Central Basin Floor

The central basin floor is delimited by two extensional fault zones in its northwestern and northeastern margins, and a zone of basin-wide thrust faults in its southern margin (Fig. 4.4). A set of NE-SW trending extensional fault zone in the northwest, a NW-SE trending extensional fault zone in the northeast, and the trailing thrust of the Misis-Kyrenia fault zone in the south bound the central basin floor (Fig 4.4). The salt-related contractional fold-thrust zone confined to the central and southern portions of the central basin floor defines the Pliocene-Quaternary of the Outer Cilicia Basin. This zone is juxtaposed to the extensional fault system that characterizes the Pliocene-Quaternary structural architecture of the Inner Cilicia Basin (Fig.4.4).

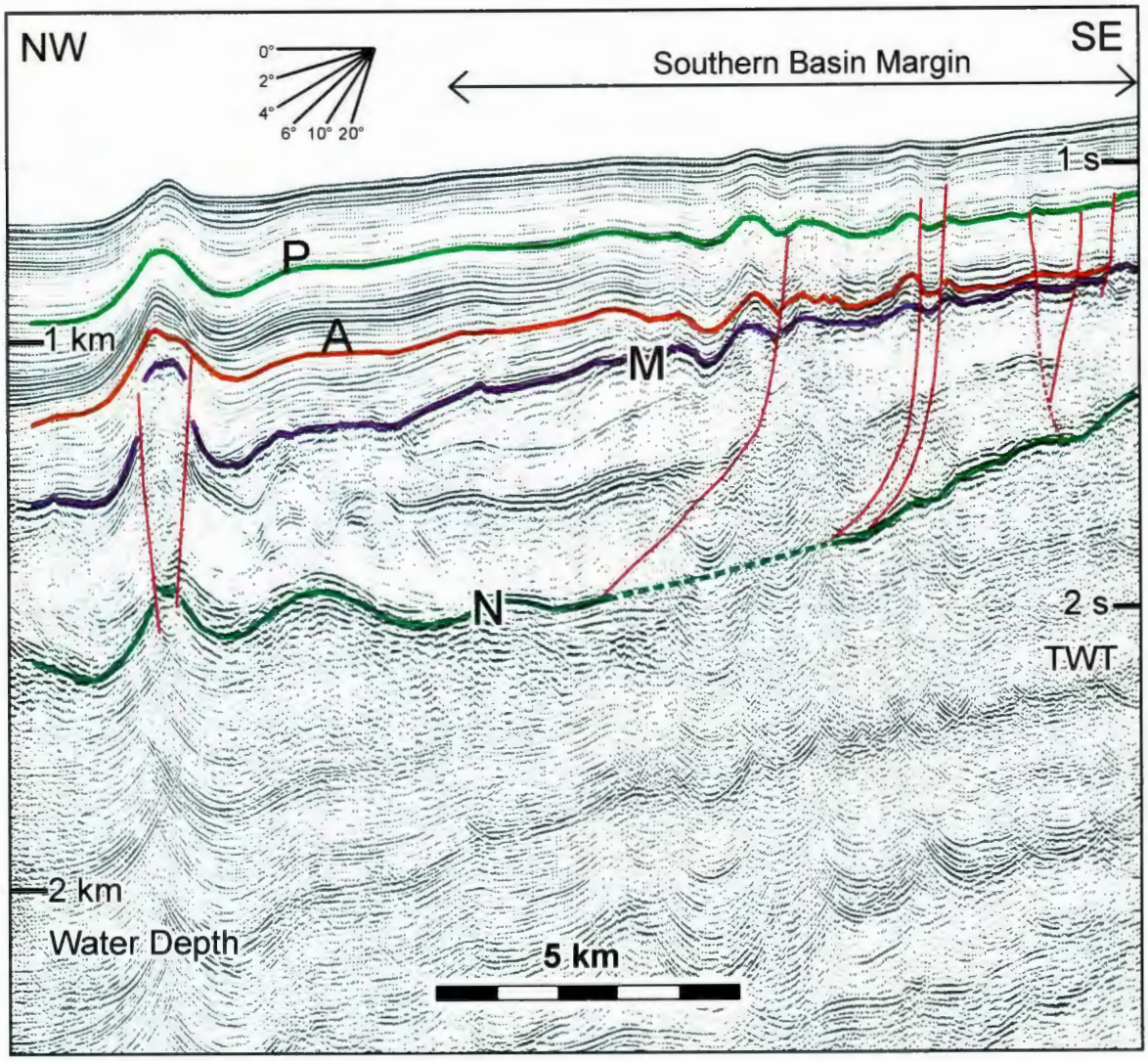

Figure 4.8: Multichannel seismic reflection profile illustrating the extensional faults of the Southern Basin Margin.

4.2.1. Basin Bounding Elements

The northwestern margin of the central basin floor is delineated by a NE-SW trending SE- and NW-dipping extensional fault system which is developed near the base of slope across the Outer and Inner Cilicia Basins (Fig. 4.4). Traced toward the west, the fault system progressively curves and assumes a broadly E-W trend. The NE-SW trending faults interfere with the NE-SW trending salt wall in the transition from the Outer to Inner Cilicia Basin (Fig. 4.4). The master fault of this fault zone (N2) is traced across the entire basin (Fig. 4.4). In the seismic reflection profiles these faults have clear trajectories where they cut the two prominent reflectors of the Pliocene-Quaternary Unit 1 (i.e., the A- and P-reflectors, Figs. 4.10, 4.11). The faults create dip separations of 65-450 ms on the A-reflector, and 0-200 ms on the P-reflector (Figs. 4.9, 4.10, 4.11). These faults do not appear to cut the M-reflector in the Outer Cilicia Basin (Figs. 4.9, 4.10); however, in the transition zone from Outer to the Inner Cilicia Basin they cut the M-reflector penetrating deeper in Messinian Unit 2 (Figs. 4.11, 4.12). In the northeastern portion of the Outer Cilicia Basin tip points of these faults are located in the upper Pliocene succession (Fig. 4.9). The faults descend into the lower Pliocene (Fig. 4.9, 4.10). Tracing the faults toward the northeast into the Inner Cilicia Basin, tip points move upwards into the Quaternary succession as the faults cut progressively younger successions. Here, they descend into the lowermost Pliocene or the Messinian evaporite unit (Figs. 4.11, 4.12). In the Inner Cilicia Basin, the tip points are at the depositional surface, and they create distinct graben structures on the sea-floor (Fig. 4.12). These

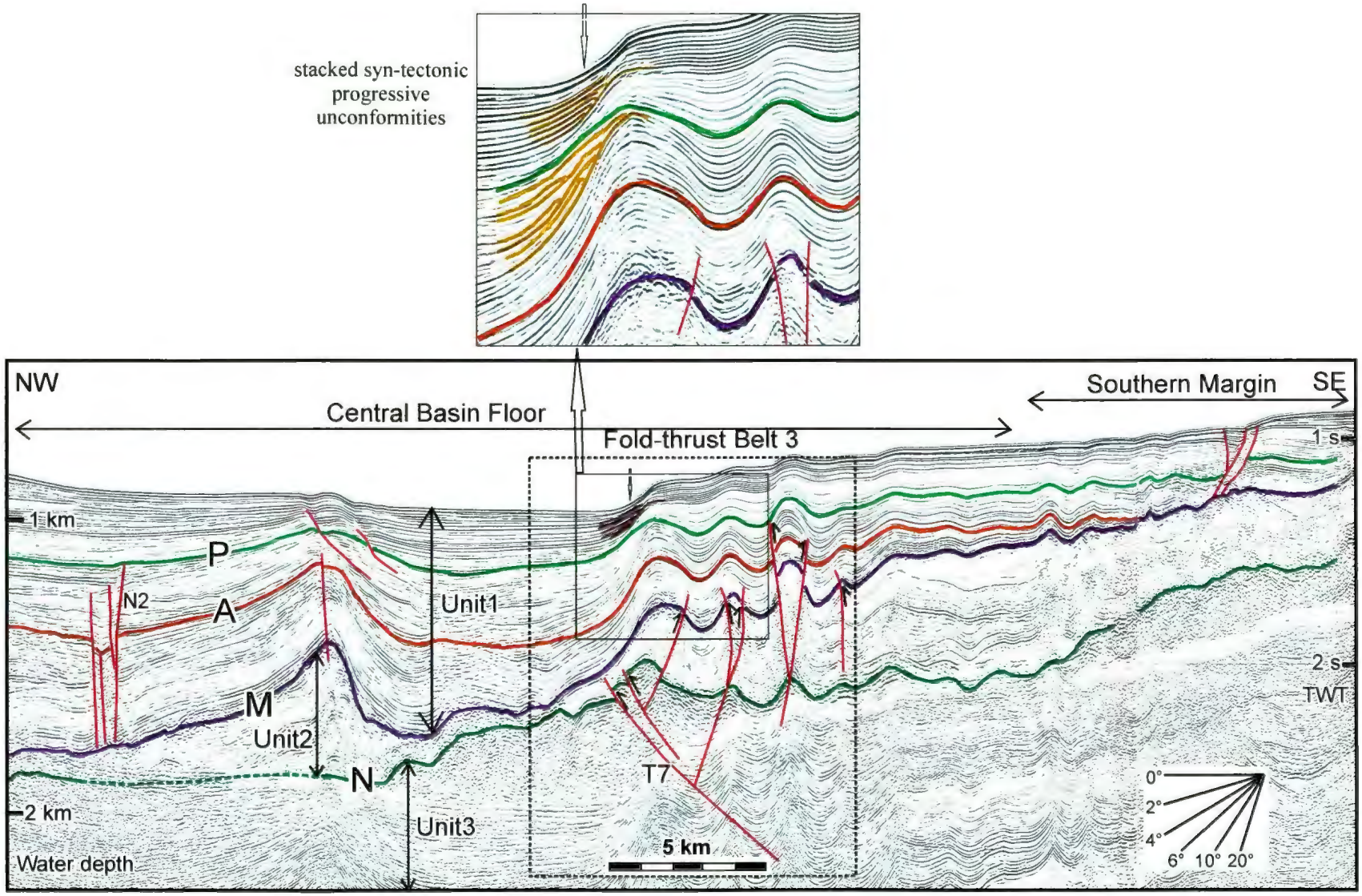

Figure 4.9: Seismic reflection profile showing the major structures of the central basin floor. Location is shown in Figure 4.3

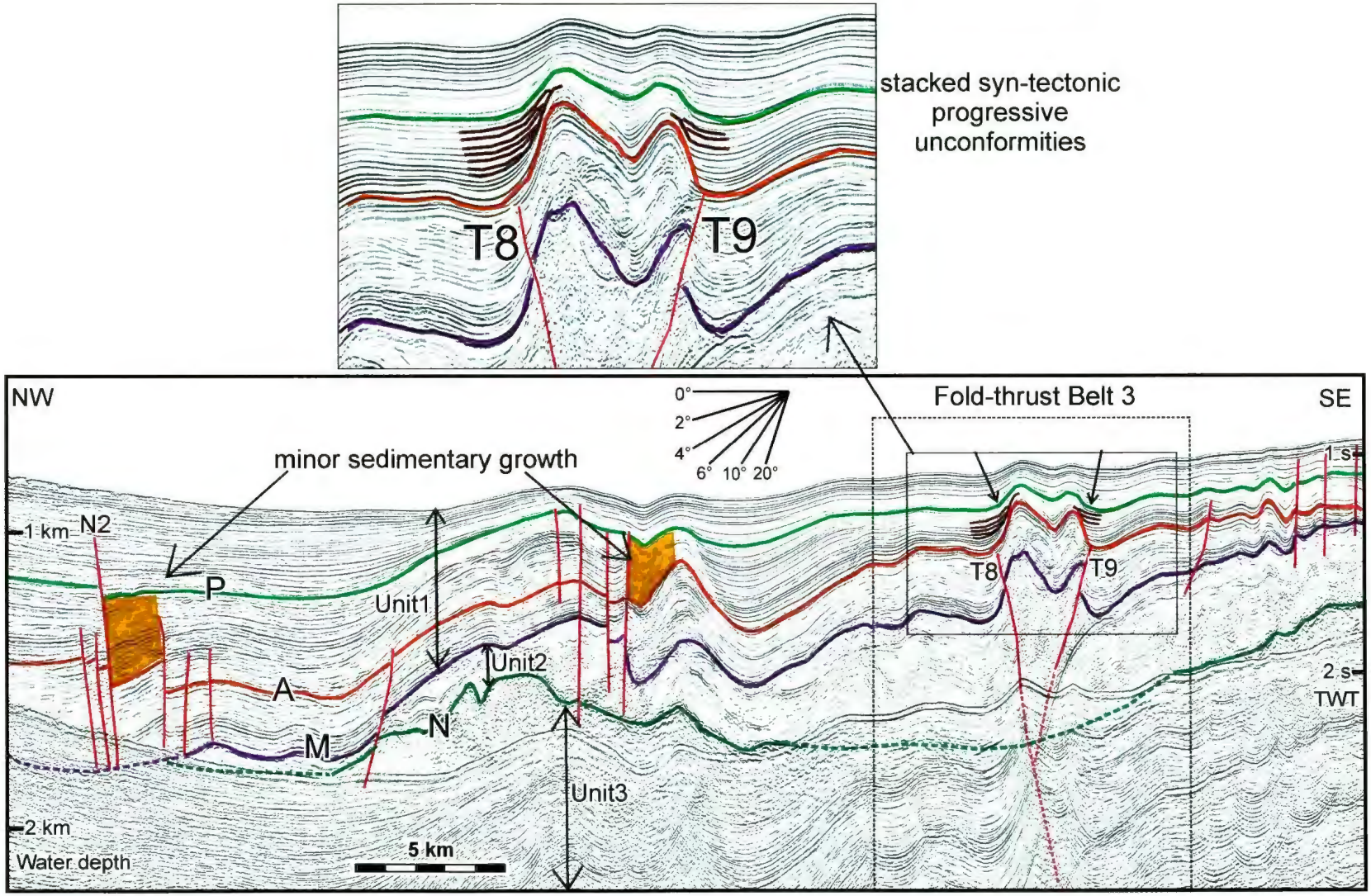

Figure 4.10: Seismic reflection profile showing the structural elements of the central basin floor. Location is shown in Figure 4.3.

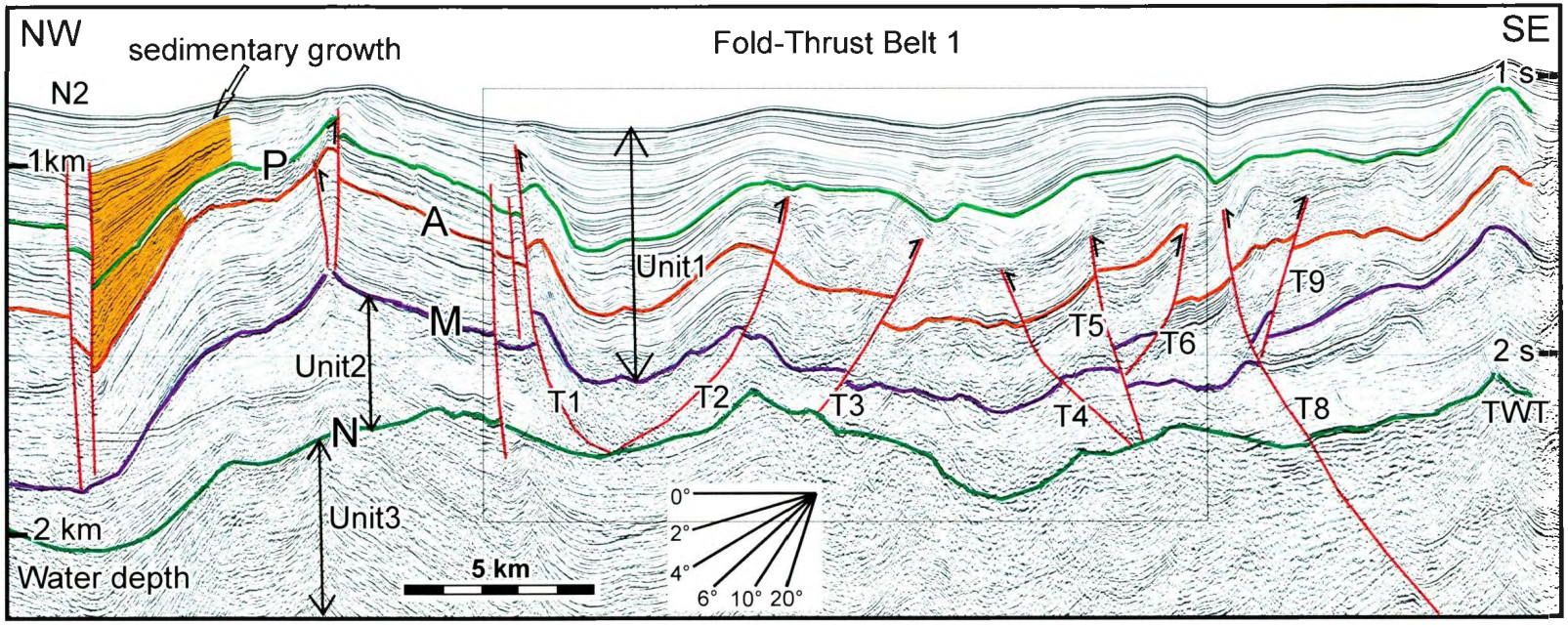

Figure 4.11: Seismic reflection profile showing the structural elements of the central basin floor. Location is shown in Figure 4.3.

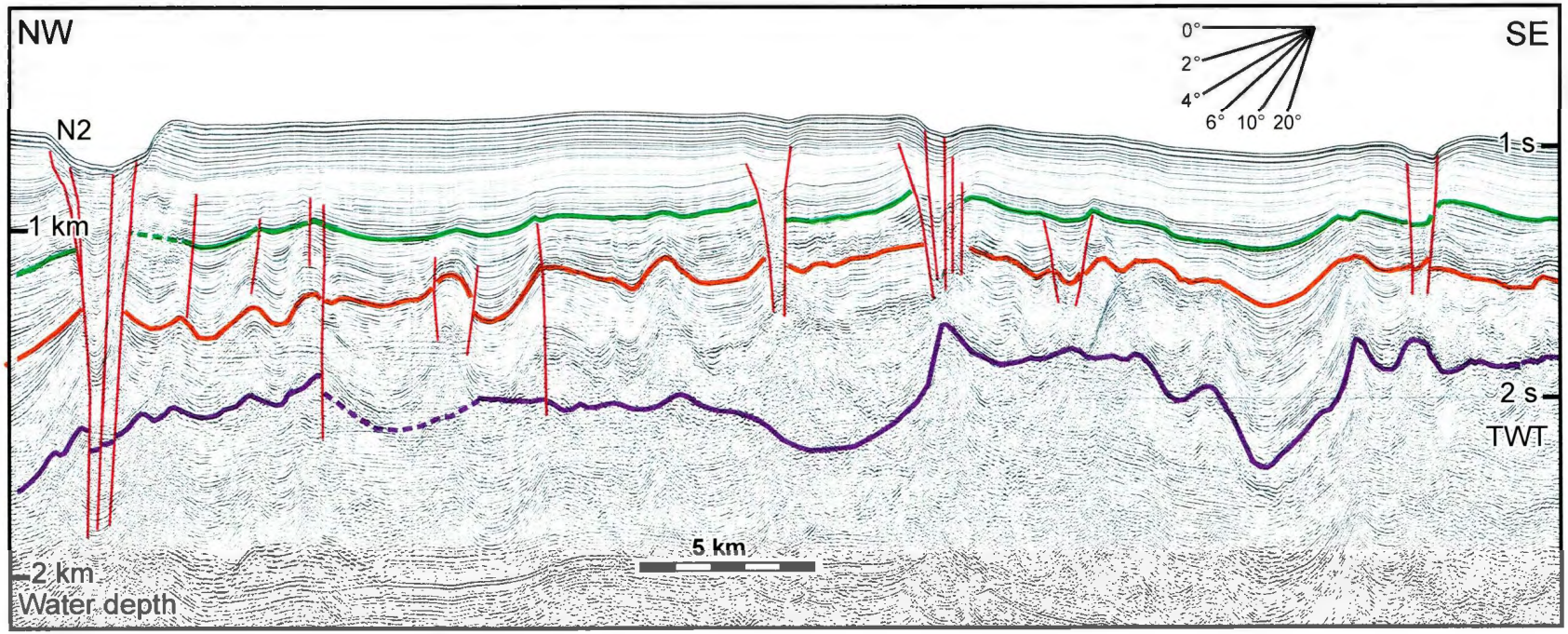

Figure 4.12: Seismic reflection profile showing the structural elements of the central basin floor. Location is shown in Figure 4.3.

faults exhibit notable sedimentary growth especially in the upper Pliocene and Quaternary successions (Figs. 4.10, 4.11).

The northeastern margin of the Central Basin Floor is delineated by a prominent broadly NW-SE trending zone of predominantly NE-dipping listric normal faults (Fig. 4.4, 4.13). The master fault of this fault fan (i.e. N3, Fig. 4.4) defines the southwestern-most panel of a very large NW-SE trending and predominantly NE-dipping fault fan that occurs in Inner Cilicia Basin (Aksu et al., 2005). This master fault (N3) exhibits a notably listric fault trajectory, extending from the depositional surface into the underlying Messinian evaporite succession of Unit 2 (Fig. 4.13). Deeper penetrating industry seismic reflection profiles show that this fault as well as its subsidiary synthetic and antithetic faults all sole into Unit 2 (Fig. 4.14). The hanging wall of the master fault exhibits considerable throw on the key markers, such as the A- and P-reflectors and syn-sedimentary growth. This stratigraphic architecture is also seen in many previous studies (e.g., Aksu et al., 1992a,b, 2005, Bridge et al., 2005).

A number of smaller similarly trending and NE- and SW-dipping extensional faults also occur in the northeastern portion of the central basin floor immediately southwest of the master fault N3 described above (Fig. 4.4). These faults have tip points at or near the depositional surface, and they sole in the M-reflector, or the Messinian evaporite unit (Fig 4.13).

On the map view, the master fault N3 extends from the NE-SW trending and predominantly NW-dipping high angle extensional fault zone which defines the

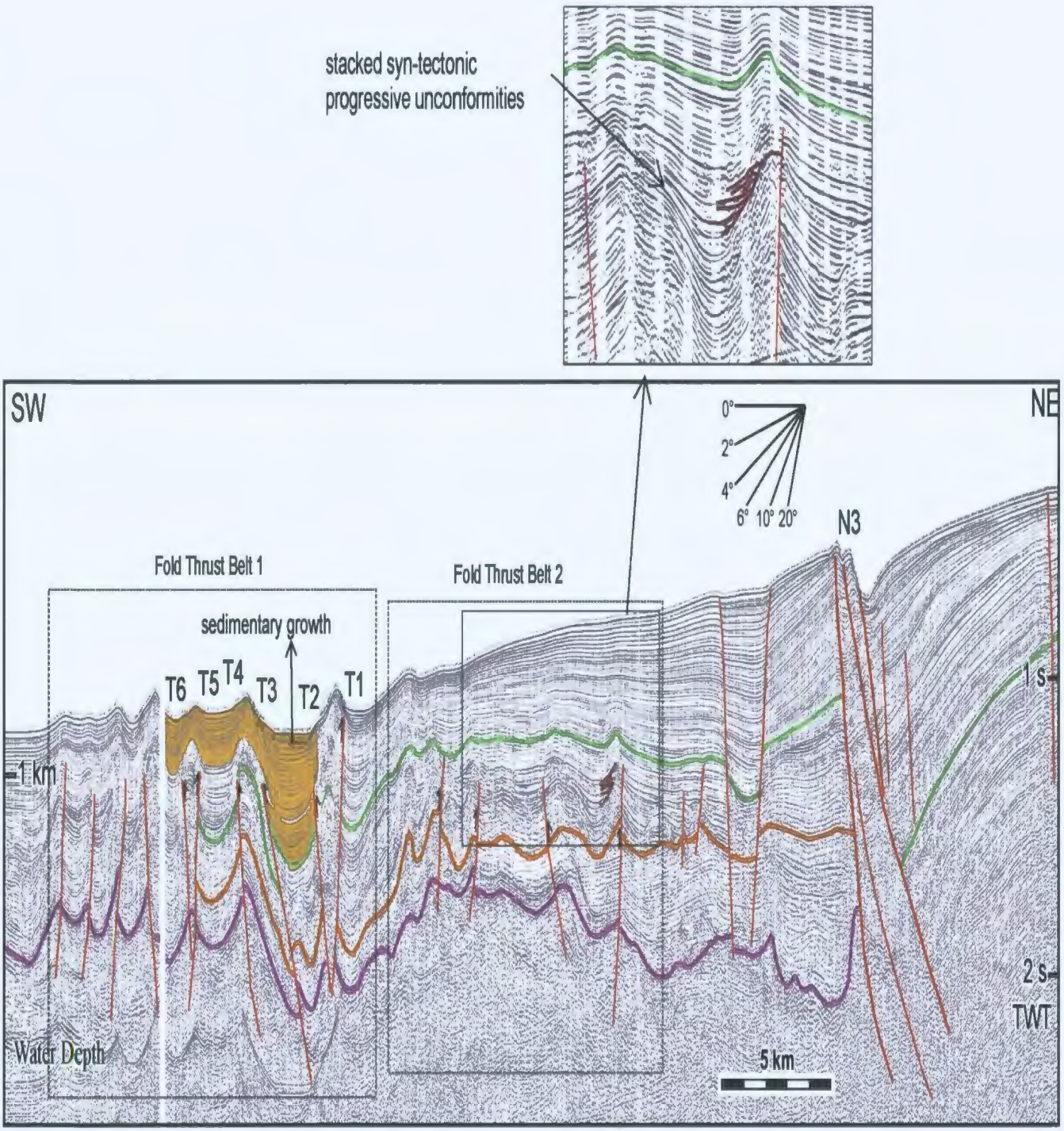

Figure 4.13: Seismic reflection profile showing the structural elements of the central basin floor. Location is shown in Figure 4.3.

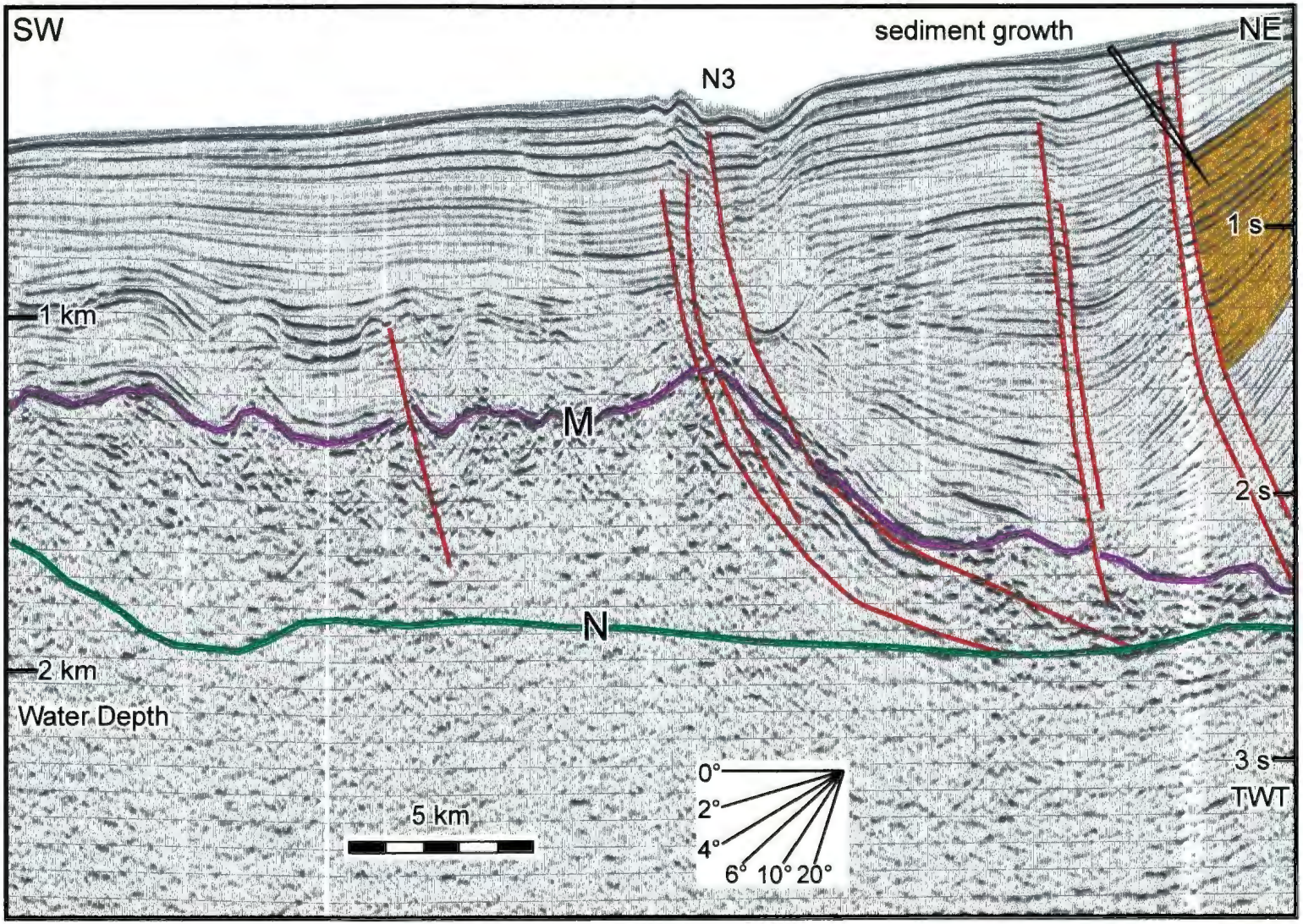

Figure 4.14: Industry seismic reflection profile showing the NW-SE trending extensional fault system of the Inner Cilicia Basin and the master fault of this system (N3).

northwestern margin of the Misis-Kyrenia horst block in the southeast to the NE-SW trending salt wall that occupies the southern fringes of the Göksu delta margin in the northwest (Fig. 4.4). There is a clearly orthogonal relationship between the basin bounding elements in the southeast and northwest and the master fault and the associated extensional fault fan to the northeast.

The southern margin of the central basin floor is delineated by the trailing thrust of the Misis-Kyrenia fault zone that defines the structural architecture of the Miocene succession of Unit 3, and an extensional fault system that defines the architecture of the Pliocene-Quaternary succession of Unit 1 (Figs. 4.4). This portion of the study area was described in detail in the southern margin above.

4.2.2. Central Fold-Thrust Systems

The structural architecture of the broadly triangular shaped central basin floor immediately south of the listric master fault N3 is characterized by thrust faulting and salt tectonism delimited by the basin bounding structural elements described above. When the structure map of the region is examined, the central basin floor is divided into three prominent morpho-tectonic sub-domains: (*i*) a complicated region of broadly WNW-ESE trending and SSW- and NNE-verging centrally located thrust belt, herein referred to as fold-thrust belt 1, (*ii*) a predominantly NW-SE trending and both NE- and SE-verging thrust belt in the northeast, herein referred to as fold-thrust belt 2, and (*iii*) a generally NE-SW trending and SE- and NW-verging thrust belt is the south referred as fold-thrust belt 3 (Fig. 4.4).

The fold thrust structures of fold thrust belt 1 gently curve toward the west in their northwestern extensions, whereas they curve toward the northeast in their eastern extensions, creating curvi-linear map traces resembling a 'lazy S' pattern. Both fold-thrust belts 1 and 3 can be readily traced toward the west where they progressively swing to assume a more or less E-W trend, paralleling the general shape of the Outer Cilicia Basin and its margin (Fig. 4.4).

4.2.2.1. Fold-thrust belt 1

The central portion of the Outer Cilicia Basin is dominated by E-W and ENE-WSW trending salt-related fold-thrust structures which are most readily imaged in the Pliocene-Quaternary succession (Figs. 4.4, 4.13, Aksu et al., 2005; Piercey, 2011). A wide zone of E-W trending fold belt extends across the entire Outer Cilicia Basin. The zone is characterized by a corrugated sea-floor morphology in the southwestern portion of the Outer Cilicia Basin. Seismic reflection profiles show that this surface morphology is the expression of underlying, larger fold structures that are mostly developed in the Pliocene-Quaternary succession (Fig. 4.13). Most of these folds are cut by thrusts that have their tip points in upper portion of the Pliocene succession (Fig. 4.15; Aksu et al., 2005).

In the central Cilicia Basin, the ENE-WSW trending salt-cored fold-thrust belt 1 turns to an ESE-WNW trend and terminates against the trailing edge of Misis-Kyrenia fault zone (Fig 4.4). In the seismic reflection profiles fold-thrust belt 1 is characterized by anticlines and synclines that create ~25-125 ms elevation on the sea-floor between the

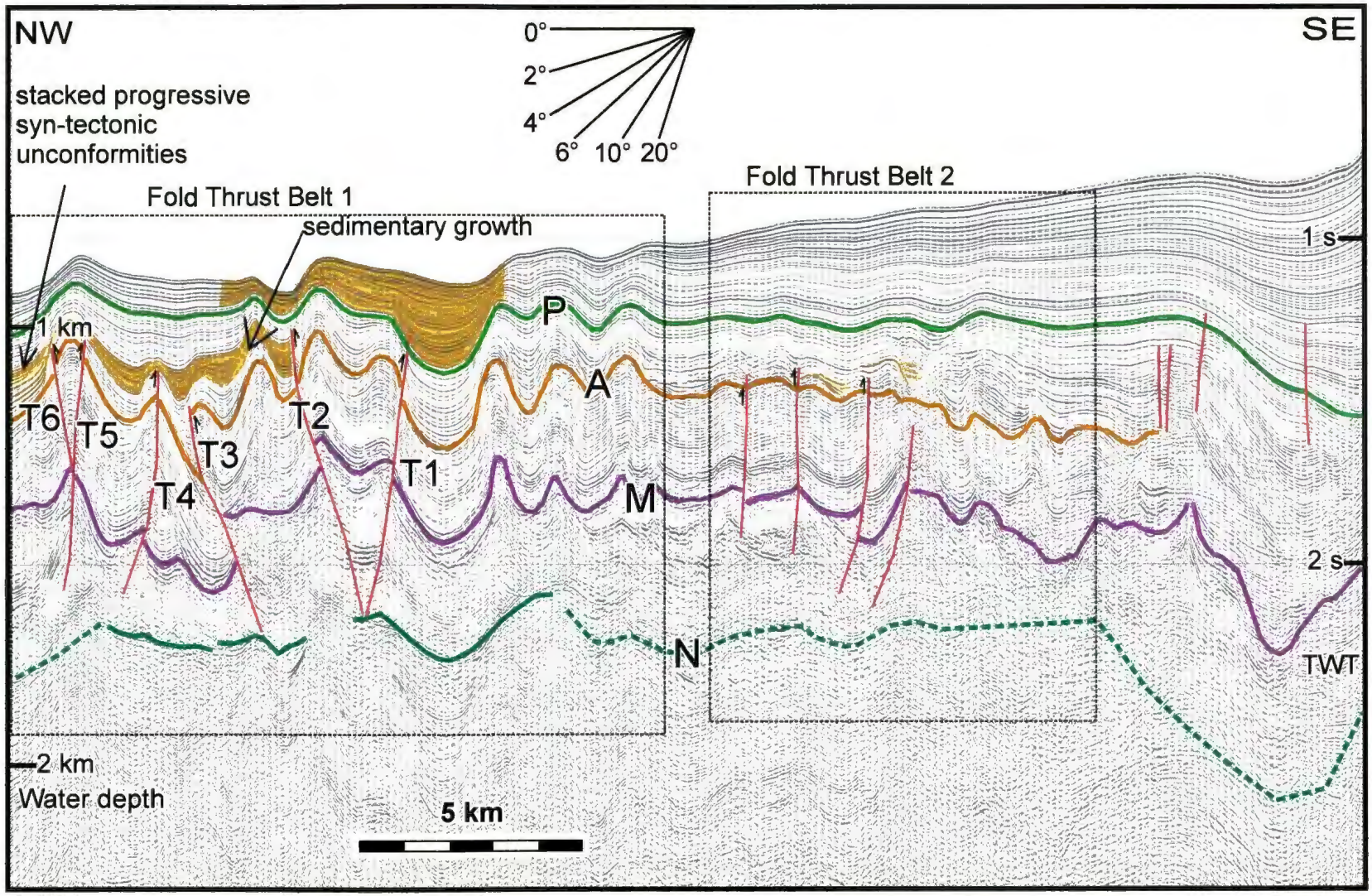

Figure 4.15: Seismic reflection profile showing the structural elements of the central basin floor. Location is shown in Figure 4.3.

adjacent crests and troughs (Fig. 4.13). The anticlines of the fold structures are cored by the Messinian evaporites (Figs. 4.13, 4.15; Aksu et al., 2005). The Pliocene-Quaternary Unit 1 thickens through the synclines and thins over the anticlines. Growth strata wedges are observed in the upper Pliocene and Quaternary successions, but there is not an obvious thickness variation in the lower Pliocene (Figs. 4.15). Progressive syn-tectonic unconformities are developed in the upper Pliocene and Quaternary successions over the crestal regions of the anticlinal structures (Figs. 4.15, 4.16). Most of the anticlines are asymmetrical and broken by thrusts faults that have tip points in the upper Pliocene or Quaternary succession (Fig. 4.15). Only one of these thrusts has tip point immediately below the depositional surface (T1, Figs. 4.11, 4.13). These thrusts sole in the Messinian evaporite Unit 2 or at the N-reflector (Fig 4.17). They create ~10-150 ms dip separations on the M-reflector, and 0-80 ms dip separations on the A-reflector (Figs. 4.13, 4.15). All of these thrusts penetrate into the Messinian Unit 2 where they are cored by salt in their footwalls and hanging walls (Figs. 4.13, 4.15, 4.17).

4.2.2.2 Fold thrust belt 2

Fold thrust belt 2 occurs across the transition zone from the Outer to the Inner Cilicia Basin and represents the northeastern most structures of the contractional domain. This belt consists of several NW-SE trending, and both NE- and SW-verging thrust faults occurring immediately south of the master fault (N3) of the northeastern margin. On the map view, this belt extends from the NE-SW trending extensional faults that delimit the northwestern margin of the central basin floor to the NE-SW trending extensional fault zone which defines the southern margin of the central basin floor (Fig. 4.4). In the

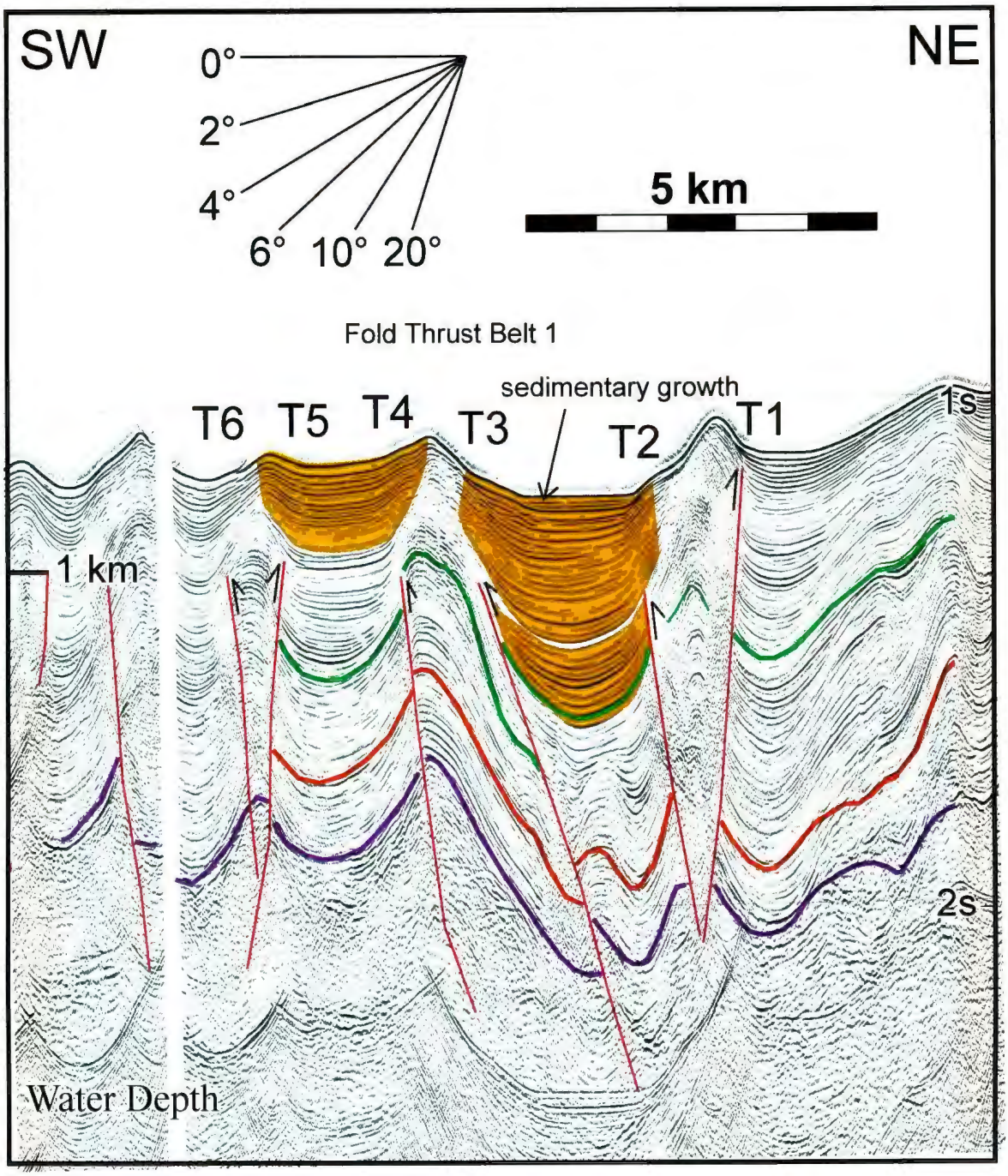

Figure 4.16: Seismic reflection profile showing the sediment growth and stacked syn-tectonic progressive unconformities over the anticlines of fold thrust belt 1. Fold thrust belt is zoomed from the seismic reflection profile in Figure 4.13.

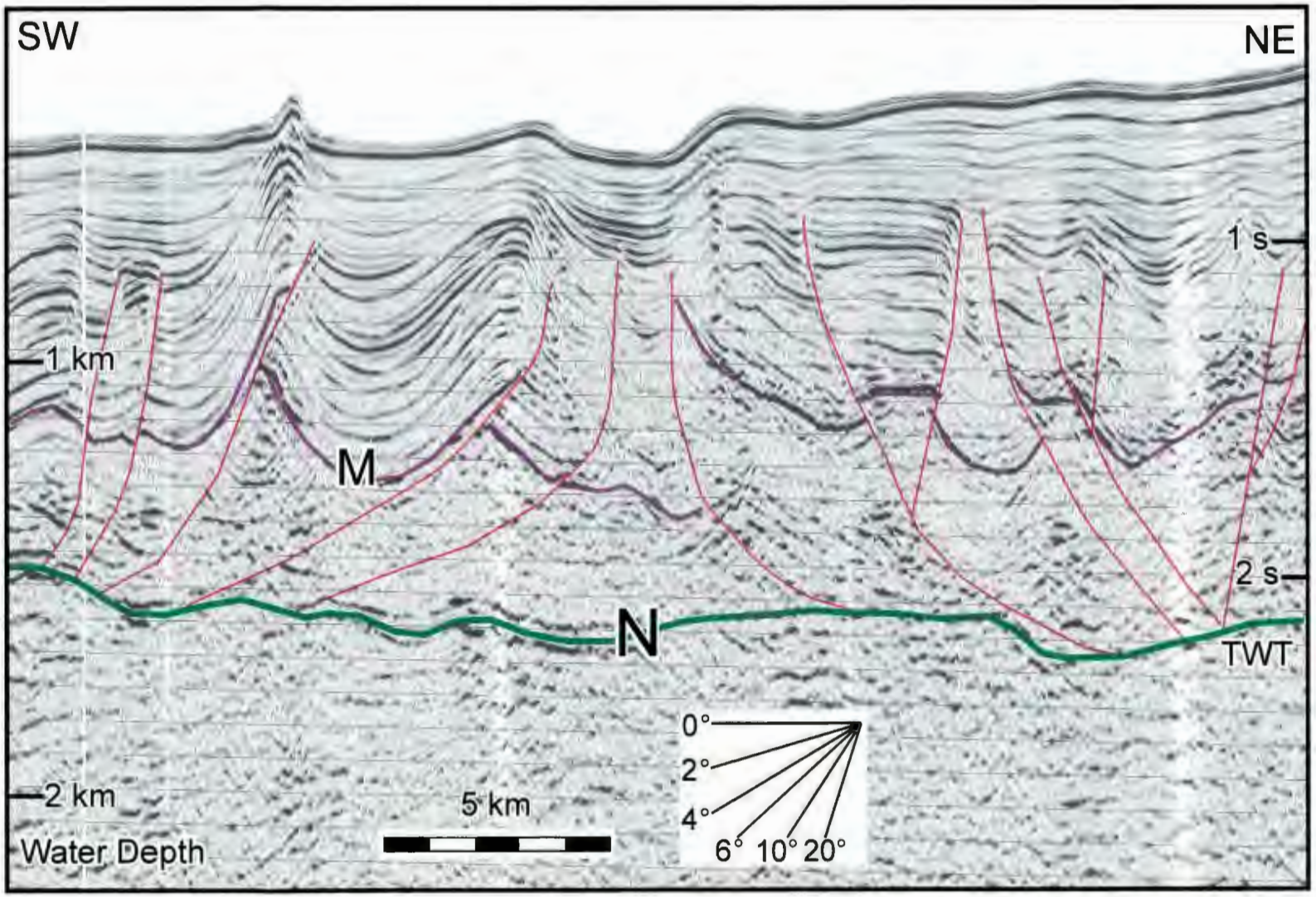

Figure 4.17: Industry seismic reflection profile showing the thrust faults of central basin floor that sole in the N reflector.

seismic reflection profiles the thrust faults of the fold thrust belt 2 have their tip points in the Pliocene successions, and these faults sole in the M-reflector or Messinian Unit 2 (Figs. 4.13, 4.15). They create small dip separations on M- (~10-50 ms) and A- (5-30 ms) reflectors, but they do not cut the P-reflector. They are associated with smaller scale fold structures that have minor or no influence in the sea-floor (Figs. 4.13, 4.15). This zone represents the last stage of the contraction and is a complexly faulted-folded transition zone between Outer and Inner Cilicia Basins. Progressive syn-tectonic unconformities occur over the crests of the small anticlines that the thrusts of the fold thrust belt 2 creates in the upper Pliocene succession (Figs. 4.13, 4.15).

4.2.2.3. Fold thrust belt 3

In the southern portion of the Outer Cilicia Basin a deeply seated NE-SW trending and both N- and S-verging fold-thrust belt extends toward the northeast, paralleling the northern Cyprus coastline (Fig. 4.4, Piercey, 2011). This belt affects the Miocene successions of Units 2 and 3, and characterises the pre-M-reflector structural architecture of the sub-domain in the Outer Cilicia Basin (Piercey, 2011). The major thrust of this belt extends across the entire Outer Cilicia Basin and it branches into two thrusts in the Central Basin Floor (T7, Fig. 4.4). Many smaller thrust faults merge with this NE-SW trending and N-verging major thrust (T7). In the seismic reflection profiles thrust T7 has tip point in the Messinian evaporite Unit 2, and it creates ~125 ms offset on the N-reflector (Fig. 4.9). The sole of the fault cannot be clearly delineated in the seismic reflection profiles, but it penetrates deep in the pre-Messinian succession (Fig. 4.9). Thrust T7 is associated with an asymmetrical fold structure in the Pliocene-Quaternary

succession. In the upper Pliocene and Quaternary, stacked syn-tectonic progressive unconformities are observed over the anticline of this fold structure (Fig. 4.9). In this region there are many relatively superficial thrusts that sole into the deeply seated thrust T7. On the map view these superficial thrusts are NE-SW trending and both N- and S-verging (Fig. 4.4). In the seismic reflection profiles they have their tip points in the Pliocene successions, and they create ~100 ms offsets on the M-reflector, and very little offsets on the N-reflector (Fig 4.9). They penetrate into the pre-Messinian Unit 3 where they sole in the deeply seated thrust T7. Both deeper and superficial faults described above terminate at the southeastern Outer Cilicia Basin (Fig. 4.4). There is another deep seated thrust (T8) and its associated antithetic thrust (T9, Fig 4.4). This pair occurs where the T7 and related superficial faults terminate (Fig. 4.4). Thrusts T8 and T9 have their tip points in the Pliocene, and they create ~200-250 ms offsets on the M-reflector (Fig. 4.10). Thrust T8 penetrates deep in the pre-Messinian Unit 3, but the sole of this thrust is not clearly imaged in the seismic reflection profiles. Thrusts T8 and T9 are associated with an asymmetrical fold structure in the Pliocene-Quaternary succession, and there is a significant thinning of the Pliocene-Quaternary successions over the anticline, and thickening over the syncline (Fig. 4.10). Thrust T8 merges with the WNW-ESE trending and NE-verging thrust T5 of fold thrust belt 1 and terminates together against the trailing edge of Misis-Kyrenia fault zone (Fig. 4.4).

4.3. Northwest Continental Margin: Göksu Delta Region

The northwest margin of the Cilicia Basin includes the shelf region immediately seaward of the Göksu delta, and the steeper continental slopes that lead into the deeper

basinal setting of the northeastern Outer Cilicia Basin (Fig.4.2). The region includes a complex fault architecture dominated by three extensional fault zones (i.e., fault zones 1-3): (*i*) A zone of NE-SW trending, NW- and SE-dipping normal faults in the northeast which progressively swing and merge with a broadly E-W trending, S- and N-dipping fault zone (orange faults, Fig. 4.18). This fault zone closely parallels the morphology of the continental slope and, to the northeast, links with the onland Kozan Fault Zone (discussed later). (*ii*) A broadly E-W trending and exclusively S- dipping normal fault zone which occurs across the continental slope (red faults, Fig.4.18), and (*iii*) a NW-SE trending fault zone of predominantly NE-dipping normal faults with occasional SW-dipping faults which are confined to the continental slope (green faults, Fig. 4.18). These three extensional fault zones create a complicated interference in the continental slope region (Fig 4.18, e.g. Aksu et al., 2005). Locations of the seismic reflection profiles that are used to describe the structures of the Northwest Continental Margin are given in Figure 4.19.

4.3.1. Extensional fault zone 1

The nearshore portion of the Outer Cilicia Basin is characterized by a set of E-W trending and broadly N- and S-dipping extensional faults (Figs. 4.18). These faults progressively swing to assume a northeast trend near the transition zone between the Inner and Outer Cilicia Basins. This fault system has the same orientation as the NE-SW trending basin bounding extensional fault set of the Central Basin Floor through the Outer Cilicia Basin. Proceeding towards the Inner Cilicia Basin the extensional fault zone 1

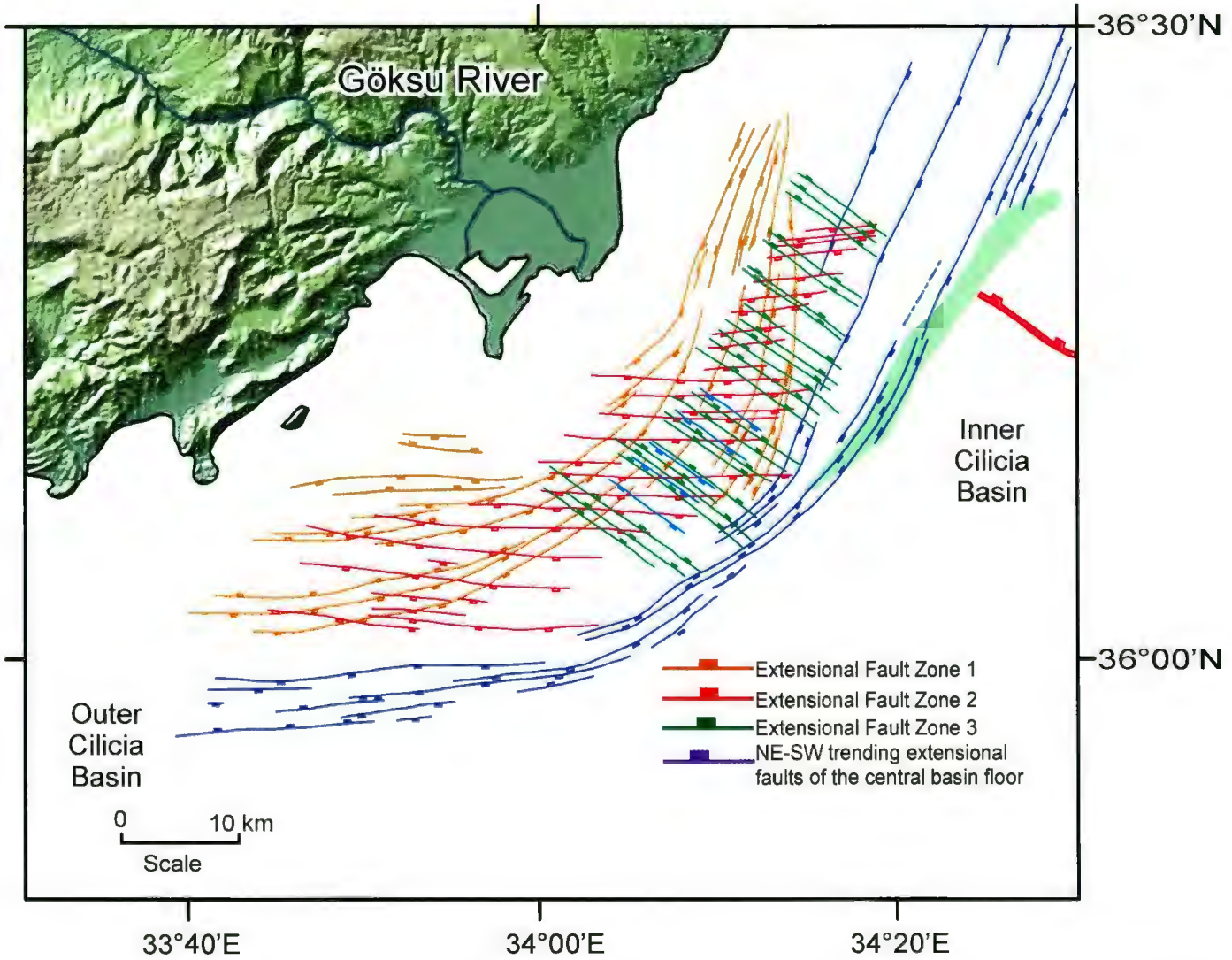

Figure 4.18: Tectonic map of the Northwest margin of the Cilicia Basin showing the three sets of extensional faults. Ticks are showing the hanging walls of the faults.

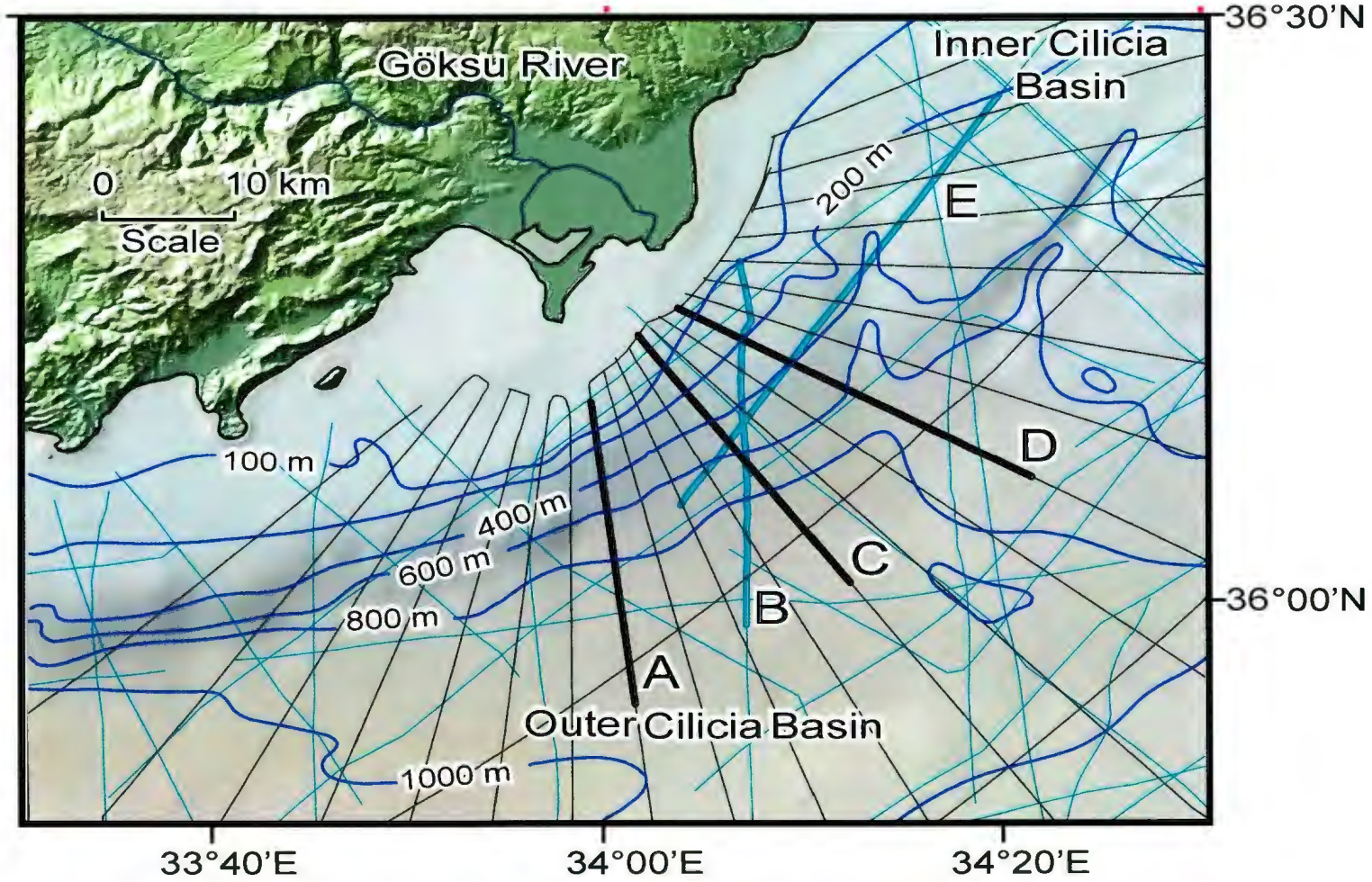

Figure 4.19: Locations of the seismic reflection profiles collected from the Cilicia Basin. A, B, C, D, and E are the profiles used to describe the structures in the northwest margin of the study area. Black lines show the seismic data from 2008 data set, and the blue lines are from the previous data sets.

turns to a NNE-SSW trend, while the other system remains at the NE-SW trend, and those two systems are separated. These two fault systems together delimit the northwestern margins of both the Inner and Outer Cilicia Basins. The NE-SW trending portion of the extensional fault zone 1 consists of narrowly-spaced N- and S-dipping high-angle extensional faults which have their main expression along the southern Turkish shelf (Fig.4.20). These faults define a 20-25 km wide zone across the Outer Cilicia Basin, a 15-20 km wide zone through the central Cilicia Basin, and a 5-10 km wide zone in the Inner Cilicia Basin (Fig 4.18). In the Outer Cilicia Basin occasional NE-trending, and NW-dipping antithetic sets are also observed (Fig. 4.18), where these faults create small horst and graben structures (Fig. 4.20). Similar structures are also described in central Outer Cilicia Basin (Aksu et al., 2005; Piercey, 2011). In the seismic reflection profiles the faults bounding these horst and graben structures are delineated as high-angle (25-30°) normal faults (Fig. 4.20). Many of these faults show obvious footwall and hanging wall cut-offs where they cut prominent reflectors in Unit 1 (Figs. 4.20, 4.21). In the upper slope and shelf regions, these faults also cut the prominent M- reflector and show 10-120 ms offsets on the M-reflector, again defining horst and graben structures (Fig. 4.20).

In the shallow portion of the study area near the present-day Turkish continental margin, the tip points of the E-W and NE-SW trending faults are situated in the uppermost Pliocene or Quaternary succession (Figs. 4.20). But traced toward the deeper portions of the Outer and Inner Cilicia Basins, the tip points become progressively deeper in the Pliocene successions. The roots of these faults are situated in the Miocene

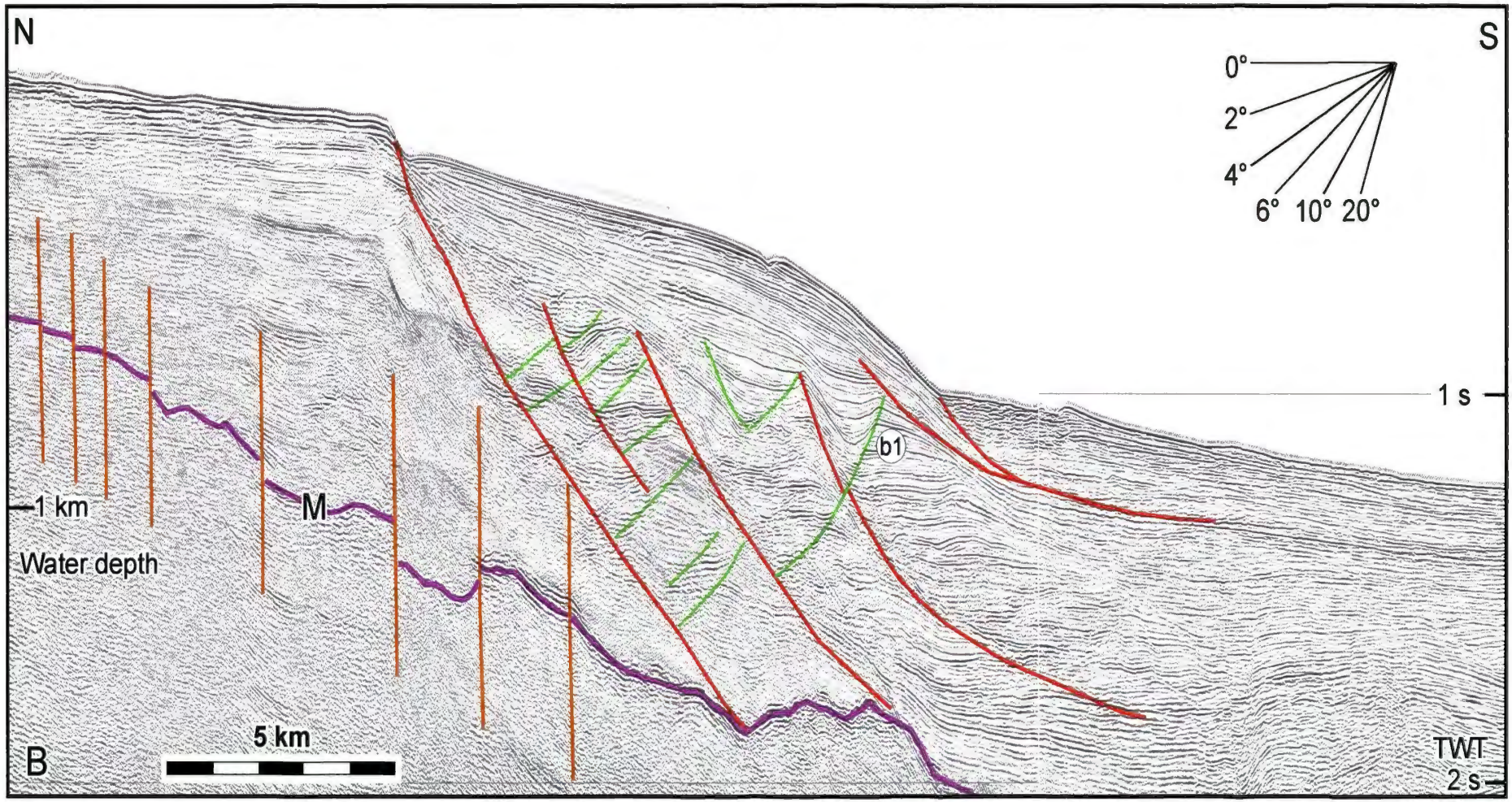

Figure 4.21: High resolution seismic reflection profile B showing the extensional faults of the northwest margin. Location is shown in Figure 4.19. orange=Extensional fault zone 1, red=Extensional fault zone 2, green=Extensional fault zone 3.

successions of Unit 3 (Figs. 4.20, 4.21, 4.22). In the northeastern shallow portion of the Göksu delta margin, the individual faults of this zone progressively converge to assume a NNE-SSW orientation (Fig 4.18).

4.3.2. Extensional fault zone 2

The second fault zone in the northwest margin of the Cilicia Basin is an E-W trending and solely S-dipping imbricate extensional fault fan (Figs. 4.18, 4.21-4.24). This set is also identified by Aksu et al. (2005) and prominently occurs in the region between the shelf break and the base of slope. The E-W trending fault system intersects with the extensional fault zone 1 in a complicated manner in the Outer and Inner Cilicia Basins. The extensional fault zone 1 progressively turns to assume a NE-SW trend through the central portion of the study area, whereas the extensional fault zone 2 maintains its E-W trend. Therefore, in the study area these two extensional fault systems are clearly separated (Fig 4.18).

The individual faults of the extensional fault zone 2 exhibit listric fault trajectories which are at very low angles (2-5°) in the Pliocene succession, but progressively steepen to ~10° in the Quaternary (Figs. 4.20). In the multichannel seismic reflection profiles these faults define a set of internally parallel fault traces delineating an imbricate extensional fault system (Figs. 4.21, 4.23, 4.24). The faults extend well into the lower Pliocene successions and sole either on the M-reflector (e.g., Fig. 4.24) or in bedding-parallel detachments within various levels of the Pliocene-Quaternary Unit 1 (e.g., Figs.

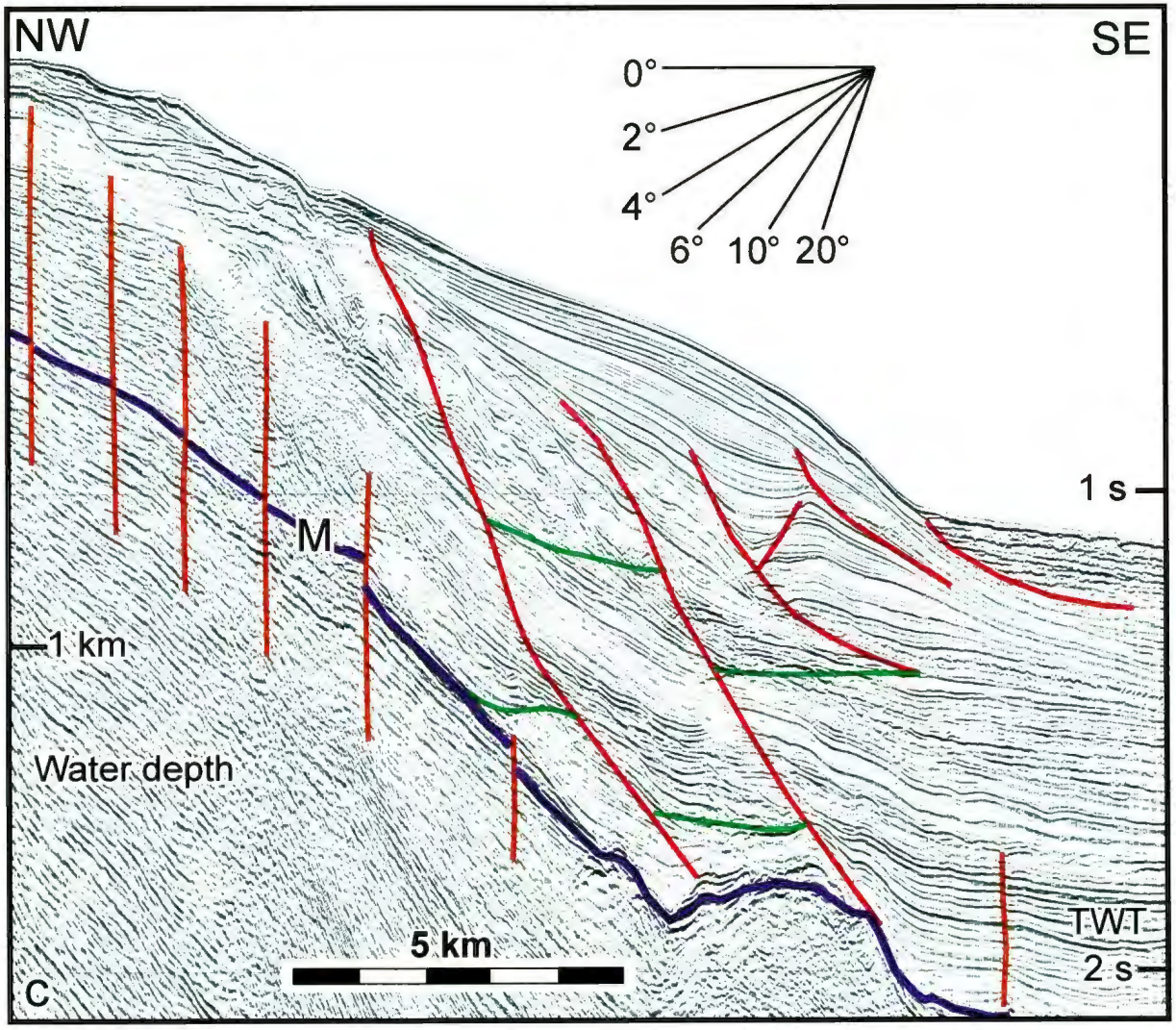

Figure 4.22: High resolution seismic reflection profile C showing the extensional faults of the northwest margin. Location is shown in Figure 4.19. orange=Extensional fault zone 1, red=Extensional fault zone 2, green=Extensional fault zone 3.

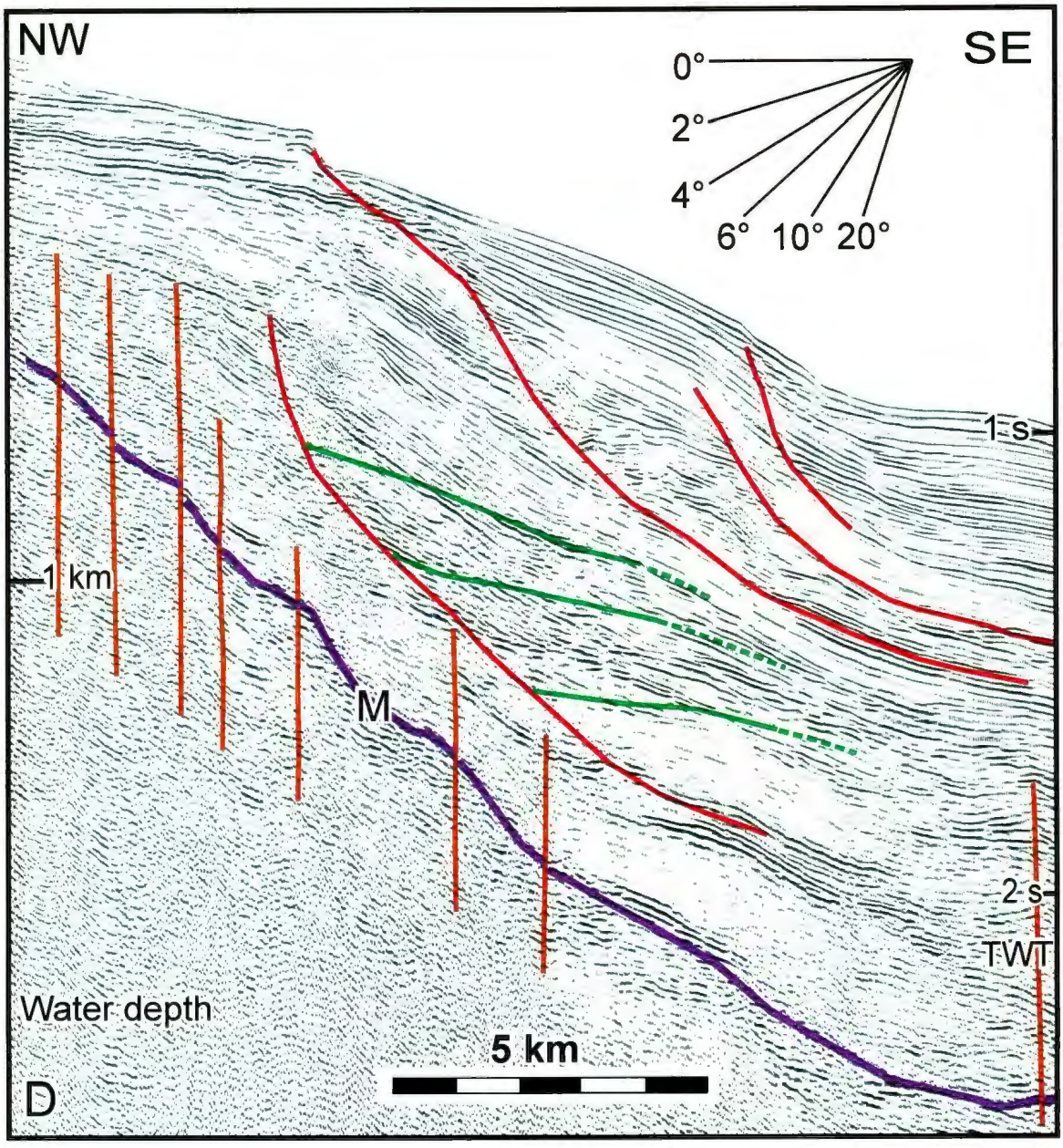

Figure 4.23: High resolution seismic reflection profile D showing the extensional faults of the northwest margin. Location is shown in Figure 4.19. orange=Extensional fault zone 1, red=Extensional fault zone 2, green=Extensional fault zone 3.

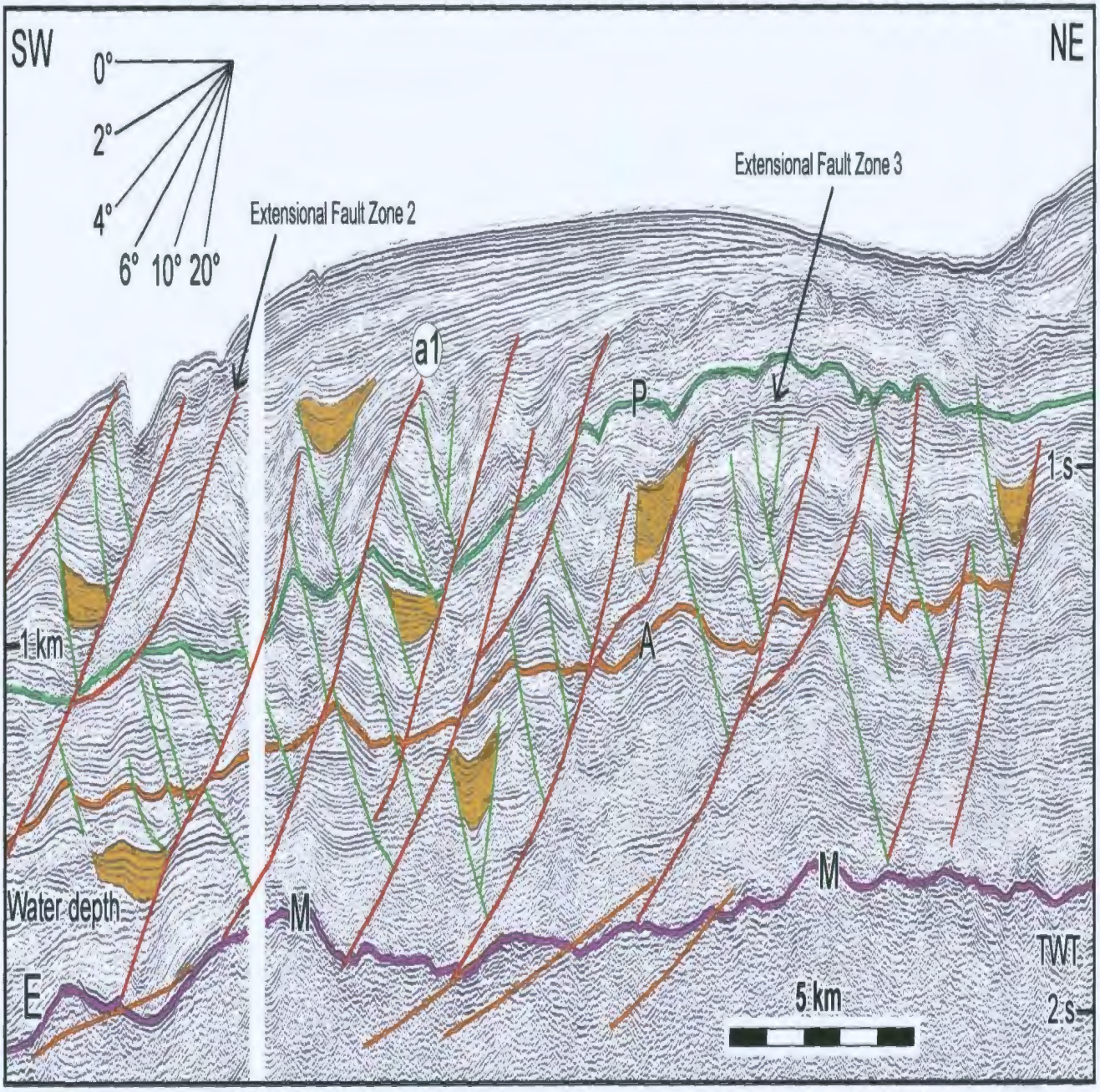

Figure 4.24: High resolution seismic reflection profile E showing the extensional faults of the northwest margin.

4.20, 4.21, 4.23). Along the region near the base of slope, a number of these faults have tip points at the depositional surface where they create bench marks on the sea floor (e.g., Fig. 4.20-4.23). Further onshore, the majority of the faults have tip points situated within the Quaternary successions (Fig. 4.24). Only a few of these faults show tip points in the Pliocene successions (Fig. 4.24). Sediment growth is observed in both Pliocene and Quaternary units associated with this fault zone (Fig. 4.24).

4.3.3. Extensional fault zone 3

The third fault zone observed in the NW margin of the study area is the set consisting of NW-SE trending and predominantly NE-dipping (with minor SW-dips) extensional faults (Fig. 4.18). These faults interact with the NE-SW and E-W trending fault systems in a complex manner, as discussed below (Fig. 4.18, Aksu et al., 2005). This fault system is only present in the Inner and the northeastern Outer Cilicia Basins, and does not extend into the central portion of the Outer Cilicia Basin. In some seismic reflection profiles, especially the profiles from the 1991 and 1992 dataset, these faults give the impression that they may be the antithetic faults of the extensional fault zone 2 (Figs. 4.21, 4.24). However, careful and detailed mapping of these faults in the 2008 data clearly shows that this set is a separate extensional fault system (Figs. 4.18, 4.20, 4.22, 4.23). This fault set is also described as a separate extensional set by Aksu et al. (2005). In Figures 4.22 and 4.23 these extensional faults are traced at a very low angle, almost as horizontal reflectors. The horizontal nature of these faults is caused by the orientation of the seismic profiles. Because the seismic profiles are oriented approximately parallel to trend of the extensional fault zone 3, the reflections emanating from the fault planes are

imaged as horizontal reflectors (compare Figures 4.18 and 4.19). Careful analysis and cross correlations of the vertically and horizontally exaggerated seismic reflection profiles reveal that these reflectors are indeed reflections emanating from the planes of the extensional faults.

In dip profiles individual faults of this zone have tip points ranging from Quaternary to lower Pliocene successions (Figs. 4.20, 4.21, 4.24). These faults have relatively straight to low-angle listric trajectories which extend into the Pliocene-Quaternary succession and interact with the faults of the extensional fault zone 2 (e.g., Fig. 4.24). These faults demonstrate minor growth strata in the Quaternary and Pliocene succession (Fig. 4.24). In the northeastern Outer Cilicia Basin there are several antithetic faults associated with the NW-SE trending faults, where the synthetic-antithetic pairs create small graben structures (Figs. 4.18, 4.20, 4.21, 4.24).

4.4. Fault interactions

A NE-SW oriented seismic reflection profile provides an exceptional image of the complex interactions between the three extensional fault zones (Fig. 4.24). Here, the extensional fault zone 1 is imaged as very-low angle traces cutting the M-reflector. The extensional fault zones 2 and 3 interact with each other in a complex manner. In the majority of this interaction extensional fault zone 3 seems like the antithetic set of extensional fault zone 2 although these two systems are independent. However, in several occasions the faults of these two systems cut each other. It is not clear in the seismic reflection profiles the geometric relationships of the fault displacements. For

example, in the southwestern portion of the profile extensional fault labeled as a1 (red) clearly cuts and offsets the trajectories of several faults of the extensional fault zone 3 (Fig. 4.24). However, a fault belonging to the extensional fault zone 3 (i.e., labeled as b1 in Fig. 4.21) clearly cut and offset a major fault belonging to the extensional fault zone 2. This non-systematic and complex faults-cutting-faults relationship indicates that faulting was concurrent in extensional zones 2 and 3. It should be noted that the faults within the extensional fault zones 2 and 3 are shown on Figure 4.18 as straight and continuous lines, despite the fact that these faults clearly cut one another. The simple reason for this is as follows: the placement of a fault plane that exhibits listric trajectories that assume bedding parallel orientation at depth is not a simple task. Only the seabed projections of the tip points are shown on various seismic reflection profiles and these points of projections are connected on the map, thus creating straight and continuous lines on fault maps.

Careful examination of the seismic reflection profiles shows that in the shallower portion of the study area, the faults of the extensional fault zones 2 and 3 tip mostly within the Quaternary succession (Fig. 4.24). If the Quaternary strata are stripped from this region, the underlying surface would arise as a heavily corrugated morphology. The corrugations are the result of the deformation and sedimentation associated with the tip points of the red and green faults. Correlations with the data from the exploration boreholes show that this level is coincident with the P-reflector (i.e., 1.7 Ma). The lack of growth in the lower portion of the Pliocene succession and the minor growth in the upper

Pliocene succession immediately below the P-reflector suggest that the onset of the primary phase of faulting barely predates the P-reflector.

CHAPTER FIVE

Discussion

The major structural elements that were described in the previous chapter contribute significantly to understanding of the Neogene evolution of the Cilicia Basin. The timing of various phases of deformation is consolidated in a tectonostratigraphic chart (Fig. 5.1). This chapter documents the history of the area, based on details from Chapter 4, and described from southeast to northwest in domains: southern basin margin, central basin floor, and NW continental margin (Fig. 5.2). The implications of the tectonostratigraphic chart are discussed in terms of the regional structural evolution.

5.1. The southern basin margin

The southern basin margin is a wide SE-convex zone, bounded by the Kyrenia Range of northern Cyprus and its marine extension, the Misis-Kyrenia fault zone (Fig. 5.2). This fault zone is associated with two prominent structural elements that are temporally superimposed on each other. Miocene deformation is defined by a contractional belt of NE-SW trending and SE-verging fold thrusts (fault set A, Figs. 5.1, 5.2, 5.3, 5.4). The Pliocene-Quaternary deformation is characterised by reactivation of fault set A with some additional back thrusting and by a separate extensional zone of NE-SW and ENE-WSW trending and both NW-and SE-dipping faults (fault set B, Figs. 5.1, 5.2, 5.4).

5.1.1. Misis-Kyrenia fold-thrust belt

The Misis-Kyrenia fold-thrust belt consists of 6-7 NE-SW trending and SE-verging thrusts. These thrusts create elevations on the seafloor which are the expression of the erosional remnant of a late Miocene fold-thrust belt (fault set A, Figs. 5.1, 5.2, 5.4;

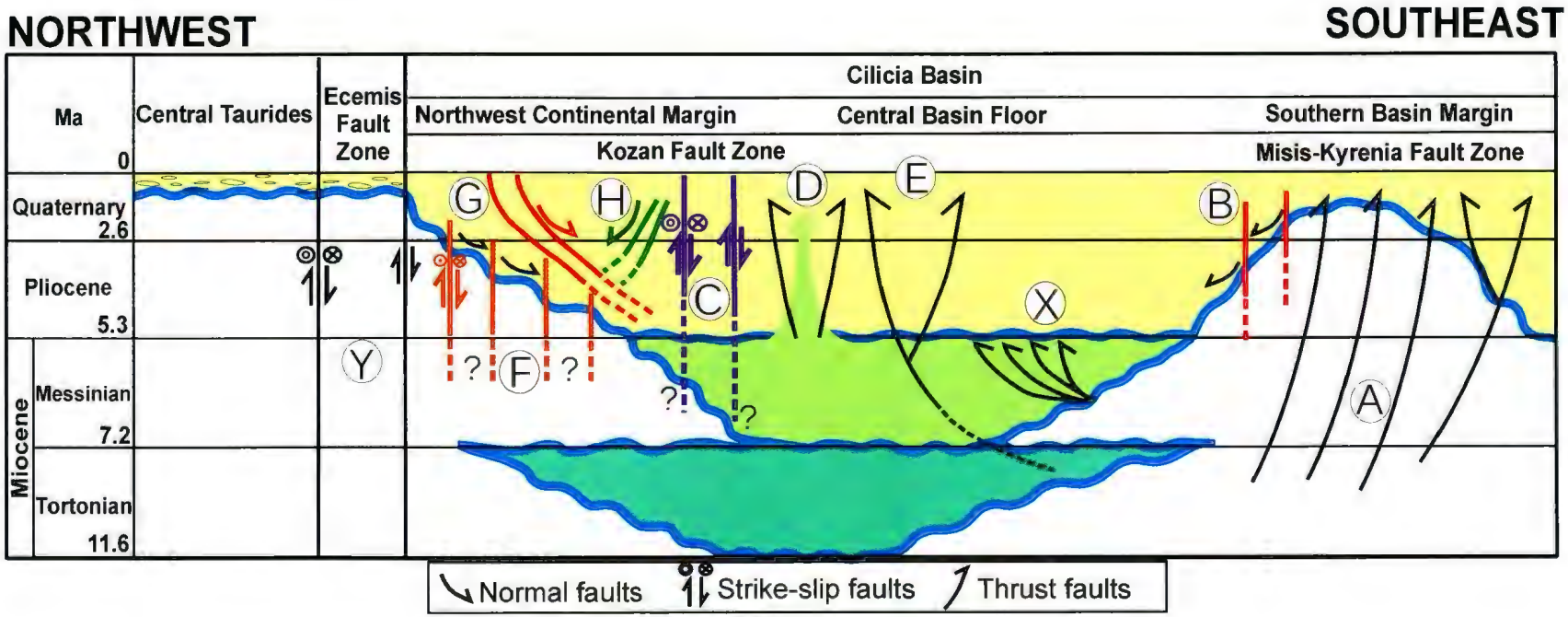

Figure 5.1: Tectonostratigraphic chart of the study area. The circles with letters are the fault sets that found in the study area. Different colours of the northwest continental margin's faults are compatible with the structure map and seismic sections.

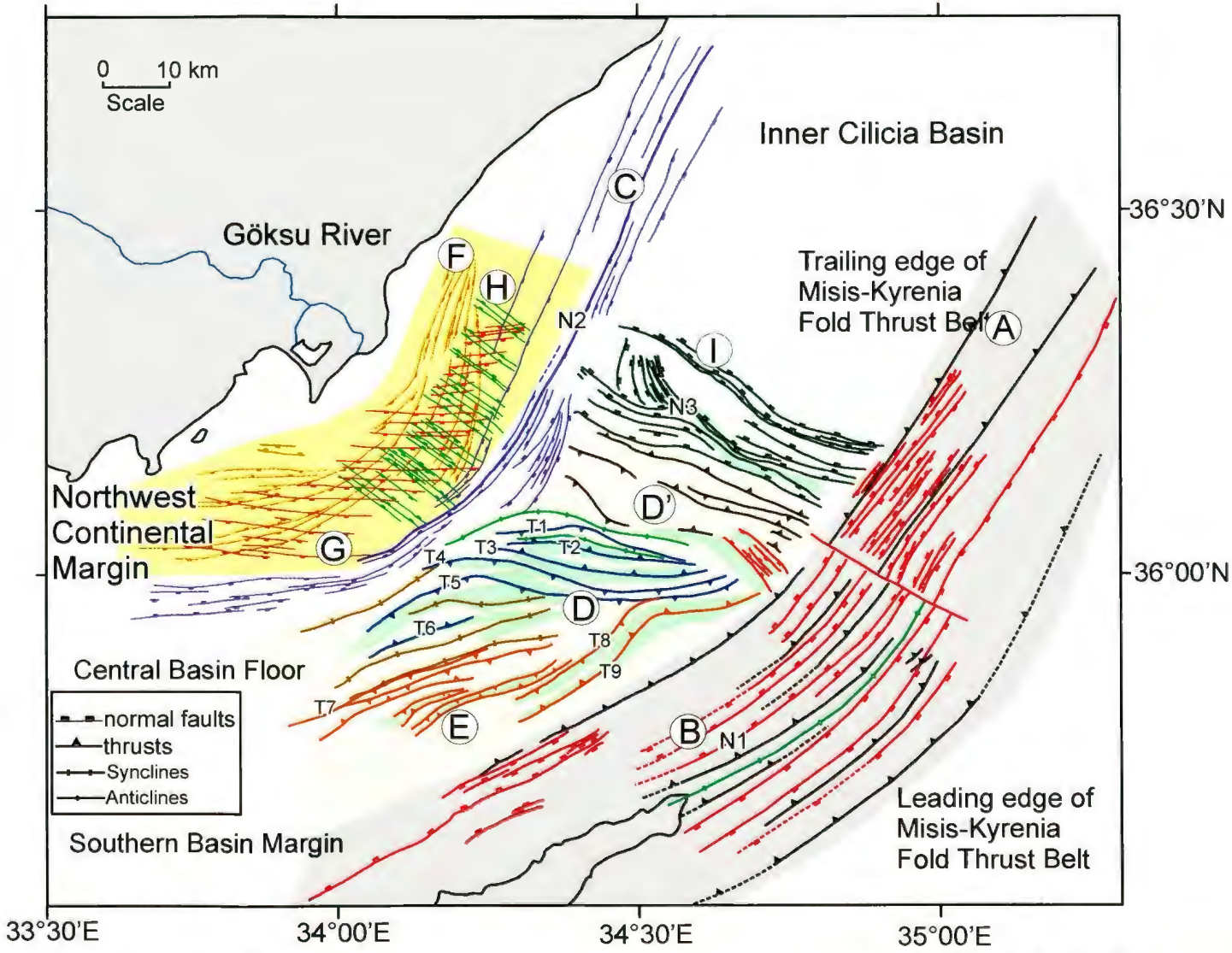

Figure 5.2: Tectonic map of the study area showing the important structural elements in the Cilicia Basin. Ticks are showing the hanging walls of the faults. Green structures are salt walls. Letters with circles are fault sets that are described in Chapter 5. Letters with numbers are individual faults of these fault sets.

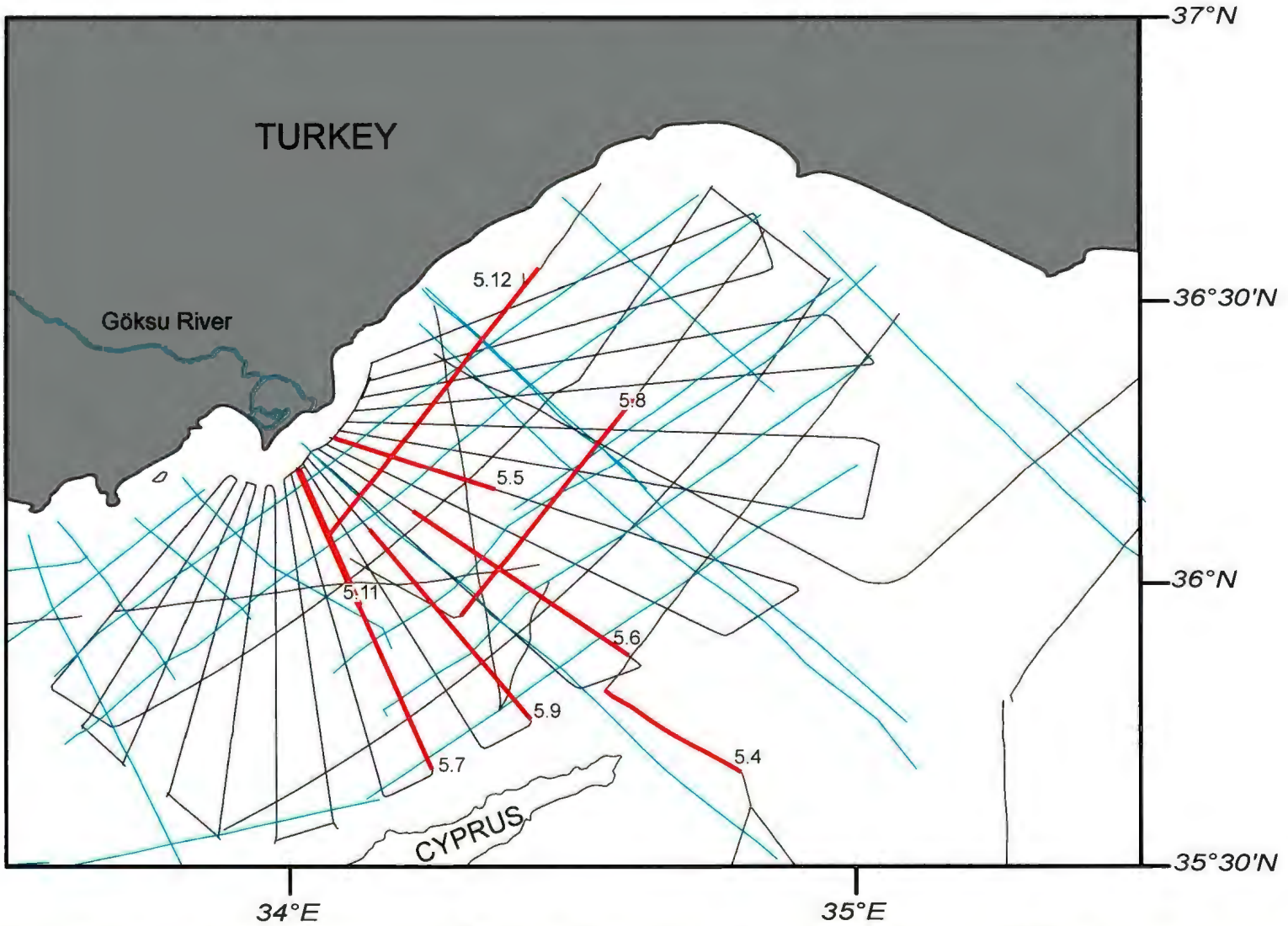

Figure 5.3: Location map showing the seismic reflection profiles in the study area . Black lines are 2008 data, brown lines are 1991 data, and light blue lines are the industry seismic reflection profiles. Thick red lines are the seismic sections that are used to describe the structures of the central basin floor and the southern margin.

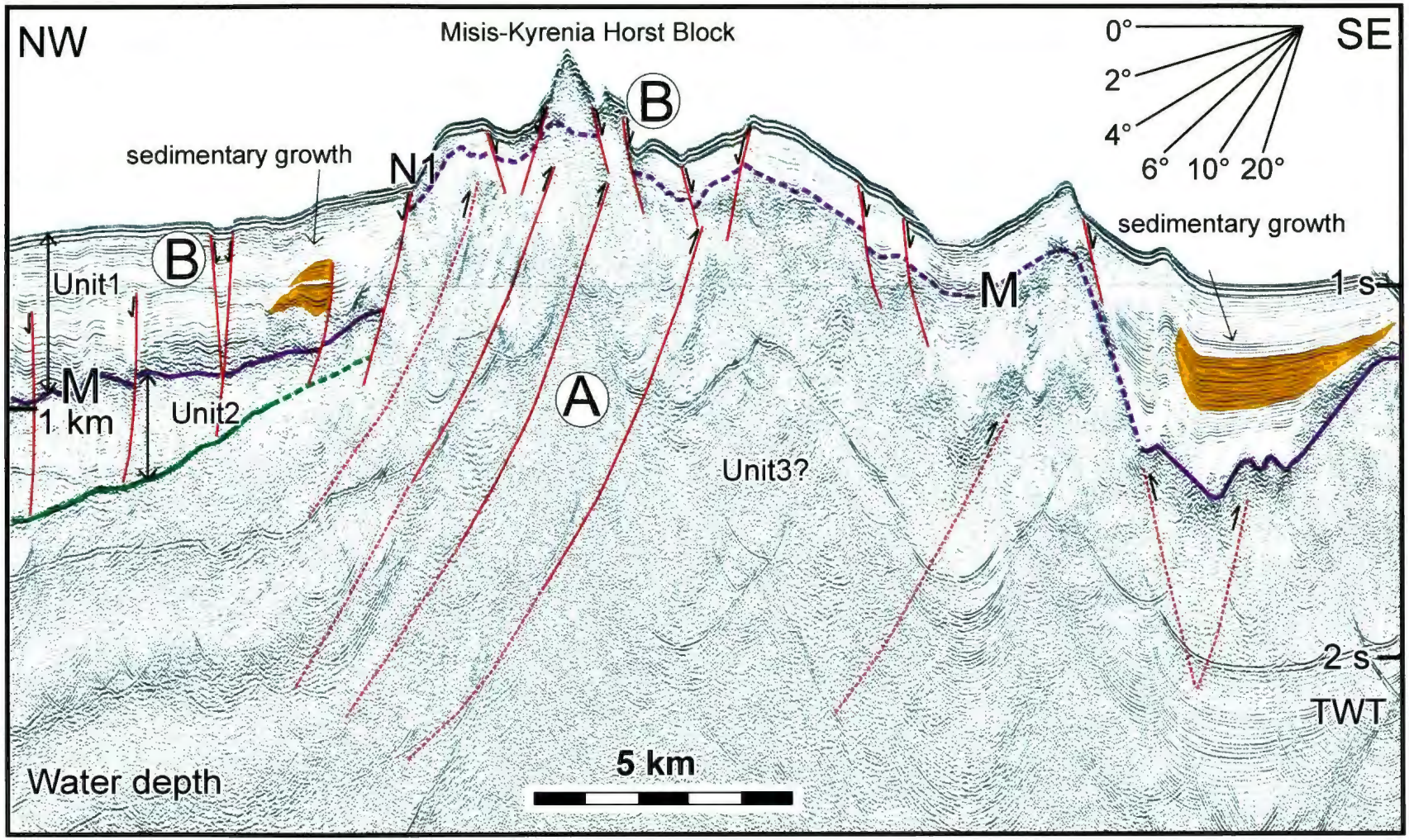

Figure 5.4: Seismic reflection profile showing the major structures of the southern margin. Location is shown in Figure 5.3.

Hall et al., 2005; Calon et al., 2005; Aksu et al., 2005). In the Outer Cilicia Basin these thrusts cut through the upper Miocene successions where Messinian salt unit is absent (fault set A, Fig 5.4). The Pliocene-Quaternary unit dramatically thins towards the crest of the fold-thrust belt and deformation is observed on the seafloor morphology (Fig. 5.4). This architecture suggests that the fold-thrust belt is active at least since the late Miocene, and that thrust activity continued to the present in the Outer Cilicia Basin (fault set A, Fig. 5.1). The growth strata architectures show that the thrusts are active during the Pliocene-Quaternary. The overprinting of the thrust stack by faults with normal-sense dip separations primarily structuring the Pliocene-Quaternary succession of Unit 1 suggest that the Miocene thrusts must have been re-activated in the Pliocene-Quaternary as a strike-slip zone.

Late Miocene contraction was followed by a phase of extension in the southern basin margin which created horst-graben structures in the Pliocene-Quaternary (fault set B, Figs. 5.1, 5.4). The Misis-Kyrenia horst block is bordered to the NW by NE-SW trending and NW-and SE-dipping extensional faults that developed over the northern margin of the fold-thrust belt (Fig. 5.2). The steeply dipping normal faults cut through most of the Pliocene-Quaternary unit and create pronounced steps on the seafloor and dip separations on the M-reflector (Fig. 5.4). Growth strata and the seabed deformation indicate that they were active throughout Pliocene-Quaternary time. Some may represent superficial sliding of the Pliocene-Quaternary succession over an underlying mobile Messinian evaporite succession (Aksu et al., 2005; Bridge et al., 2005).

5.2. The central basin floor

The central basin floor is bounded by a NE-SW trending extensional fault zone in the northwest (fault set C in Figs. 5.1, 5.2), a NW-SE trending extensional fault zone in the northeast (fault set I, Fig. 5.2), and the Misis-Kyrenia fault zone in the southeast. Delimited by these three zones, a central fold-thrust system (fault sets D, D' and E) extends through the entire Outer Cilicia Basin (Fig. 5.2).

5.2.1. Central basin bounding faults

The northwest margin of the central basin floor is bounded by NE-SW trending, SE-and NW-dipping extensional faults which are interpreted as the marine extension of the Kozan Fault zone (fault set C, Figs. 5.1, 5.2). The master fault of this fault zone is traced through the entire Cilicia Basin (N2, Figs. 5.2, 5.5, 5.6, 5.7). In the Inner Cilicia Basin tip points of the NE-SW trending faults are at or near the depositional surface. These faults extend across the entire Pliocene-Quaternary succession and cut the M-reflector, penetrating into the Messinian Unit 2 (Fig. 5.5). These faults are associated with seafloor deformation (Fig. 5.5) and sediment growth in the Quaternary and the upper Pliocene in the Inner Cilicia Basin (Figs. 5.5, 5.6). There is no clear evidence of growth strata in the lower Pliocene (Figs. 5.5, 5.6). Towards the Outer Cilicia Basin these faults lose their seafloor expression where they have tip points in the upper Pliocene and penetrate deep in the lower Pliocene, but do not cut the M-reflector (N2, Fig. 5.7). There is minor sedimentary growth in the upper Pliocene, but not in the Quaternary, suggesting that these faults are active in the late Pliocene, but not in the Quaternary. Aksu et al. (2005b) suggests that the development of these extensional faults is not compatible with the Miocene contraction, and is an expression of the shift in the kinematic framework.

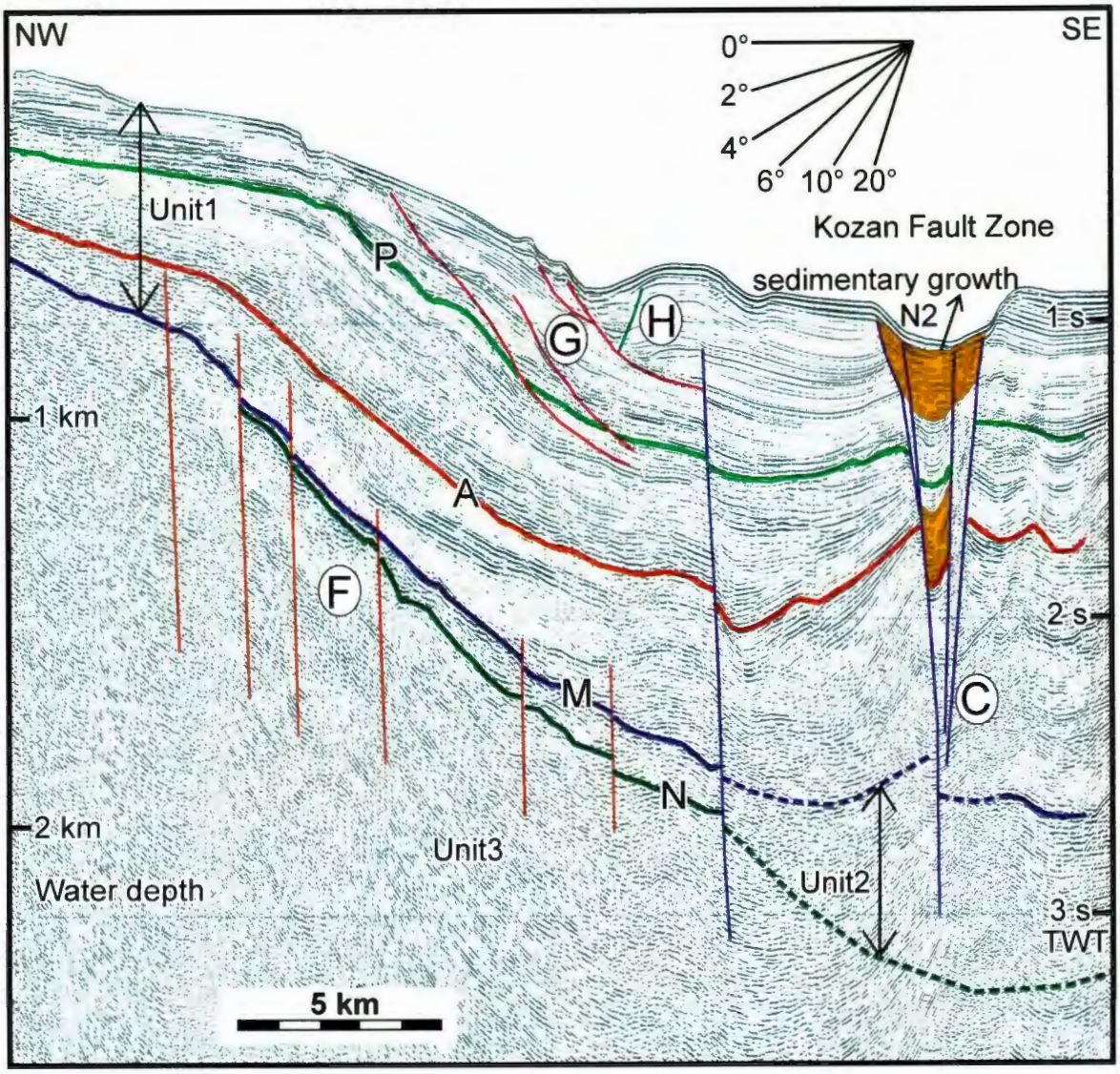

Figure 5.5: Seismic reflection profile showing the structural elements of the northwest continental margin in the Inner Cilicia Basin.Letters with circles are fault sets that are described in Chapter 5, and N2 is the master fault of the fault set C.

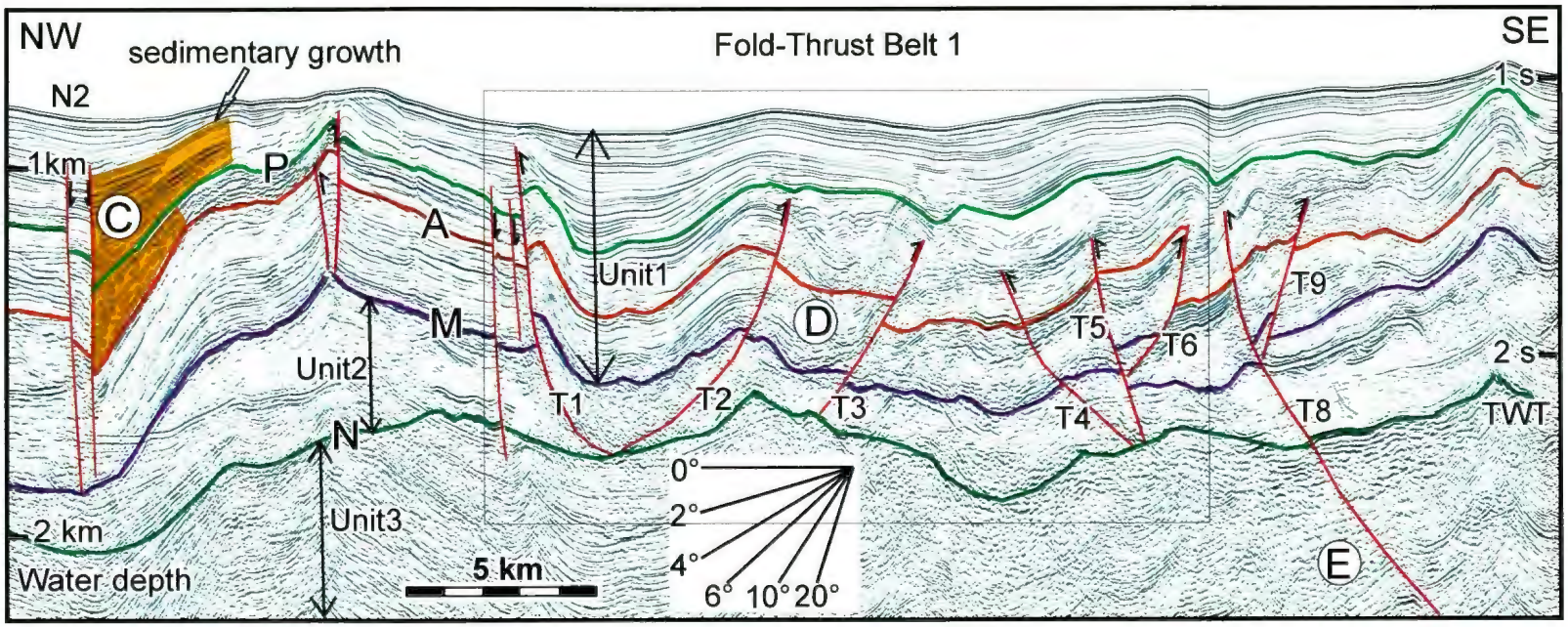

Figure 5.6: Seismic reflection profile showing the structural elements of the central basin floor. Location is shown in Figure 5.3. Letters with circles are fault sets that are described in Chapter 5. Letters with numbers are individual faults of these fault sets.

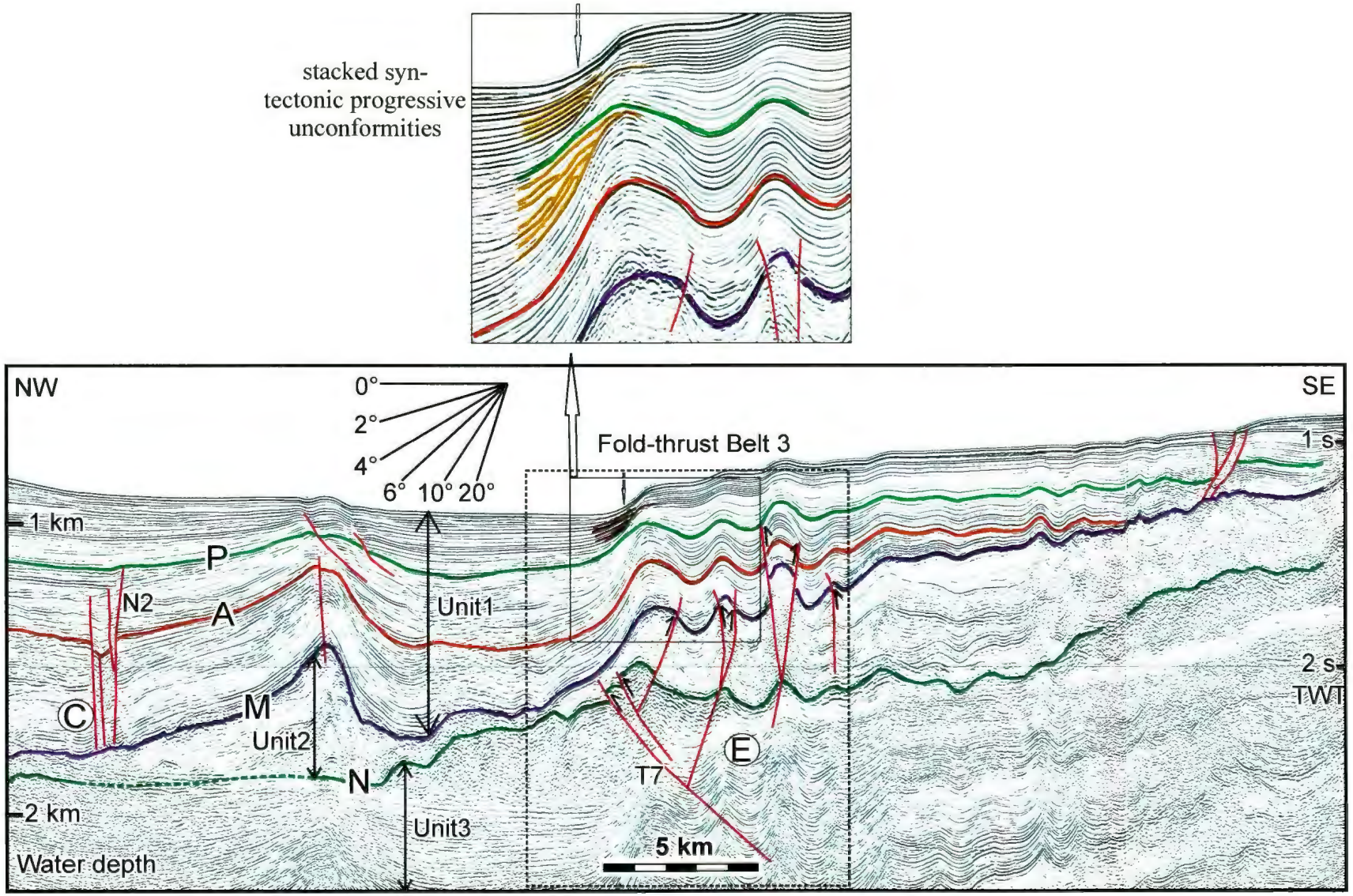

Figure 5.7: Seismic reflection profile showing the major structures of the central basin floor. Letters with circles are fault sets that are described in Chapter 5, and letters with numbers are the individual faults of these fault sets.

They further noted that the onset of the extensional fault activity in the Kozan Fault system is the latest Miocene (Messinian). Burton-Ferguson et al. (2005) also noted that Messinian deposition in the onland Adana Basin was probably controlled by the development of the Kozan Fault zone. The sedimentary growth indicates that these basement rooted faults are reactivated in an extensional setting in the late Pliocene, and are also active in the Quaternary. These faults are active until recent times in the Inner Cilicia Basin, but fault activity died earlier towards the Outer Cilicia Basin.

The northeastern margin of the central basin floor is delineated by the southwestern-most panel of a very large NW-SE-trending and predominantly NE-dipping listric normal fault fan that occurs in the Inner Cilicia Basin (fault set I, Fig. 5.2, Aksu et al., 2005). This fault fan has an orthogonal relationship with major basin bounding faults on the northwest and southeast ends (Fig. 5.2). The master fault of this fault set (N3, Fig. 5.2) demonstrates a notably listric fault trajectory, extending from the depositional surface to the Messinian salt unit (N3, see Chapter 4, section 4.2.1). These faults are associated with large sedimentary growth especially in upper Pliocene and Quaternary, suggesting that these faults are active in the late Pliocene, and Quaternary.

5.2.2. Fold-thrust belt 1

Fold-thrust belt 1 is a set of E-W and ENE-WSW trending, and broadly N-and S-verging salt related folds and thrusts that are observed in the Pliocene-Quaternary (fault set D, Figs. 5.1, 5.2, 5.8). These thrusts created a corrugated seafloor morphology and growth strata wedges in upper Pliocene and Quaternary (Fig. 5.8). Quaternary sediment fill is thicker within the synclines, but thins over the anticlines created by these thrusts (Fig. 5.8). Progressive syn-tectonic unconformities are also observed in the Quaternary

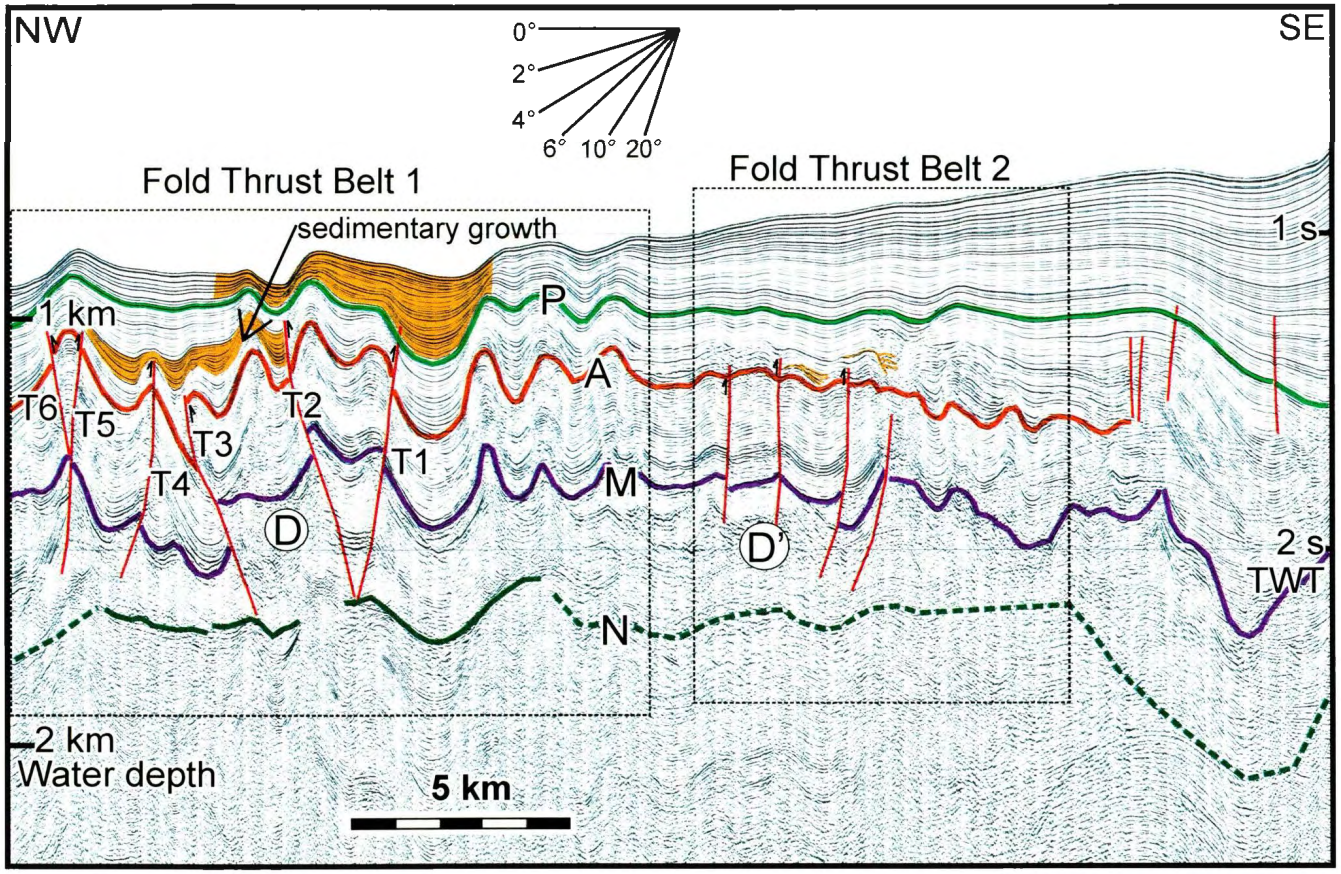

Figure 5.8: Seismic reflection profile showing the structural elements of the central basin floor. Location is shown in Figure 5.3. Letters with circles are fault sets that are described in Chapter 5, and letters with numbers are the individual faults of these fault sets.

sediments over the crestal regions of the anticlinal structures (see Fig. 4.16, Chapter 4). There is minor or no variation in the thickness of the lower Pliocene sediments.

Salt-related fold-thrust belt 1 characterises the architecture of the Pliocene-Quaternary succession in the central basin floor (fault set D, Fig. 5.1). The growth strata wedges and the progressive syn-tectonic unconformities indicate that these salt related thrusts were active through the Pliocene-Quaternary (fault set D, Fig. 5.1). Messinian salt deposits reach their maximum thickness in the central basin floor, and pinch out towards the southeast in the southern margin (Fig. 5.1).

5.2.3. Fold-thrust belt 2

Fold-thrust belt 2 consists of several NW-SE trending and both SW-and NE-verging salt-related thrusts that show progressive syn-tectonic unconformities over the crests of the anticlines in the upper Pliocene (fault set D', Figs. 5.2, see previous chapter Fig. 4.13). These thrusts create smaller anticlines and synclines in the upper Pliocene (Fig. 5.8). This thrust belt is interpreted as the continuation of the fold-thrust belt 1 in the transition zone from Outer to Inner Cilicia Basin where thrust activity loses its seafloor expression. There is no evidence for the fault activity in the Quaternary indicating that salt related fold-thrust activity ceased in the Quaternary towards the Inner Cilicia Basin.

5.2.4. Fold-thrust belt 3

Fold-thrust belt 3 is a deeply seated NE-SW trending, both N-and S-verging thrust system that affects the Pliocene-Quaternary and possibly the upper Miocene successions (fault set E, thrusts T7, T8, T9, Figs. 5.1, 5.2, 5.7, 5.9). The major structure of this belt is a N-verging thrust that affects the Miocene structures, and characterises pre-M reflector

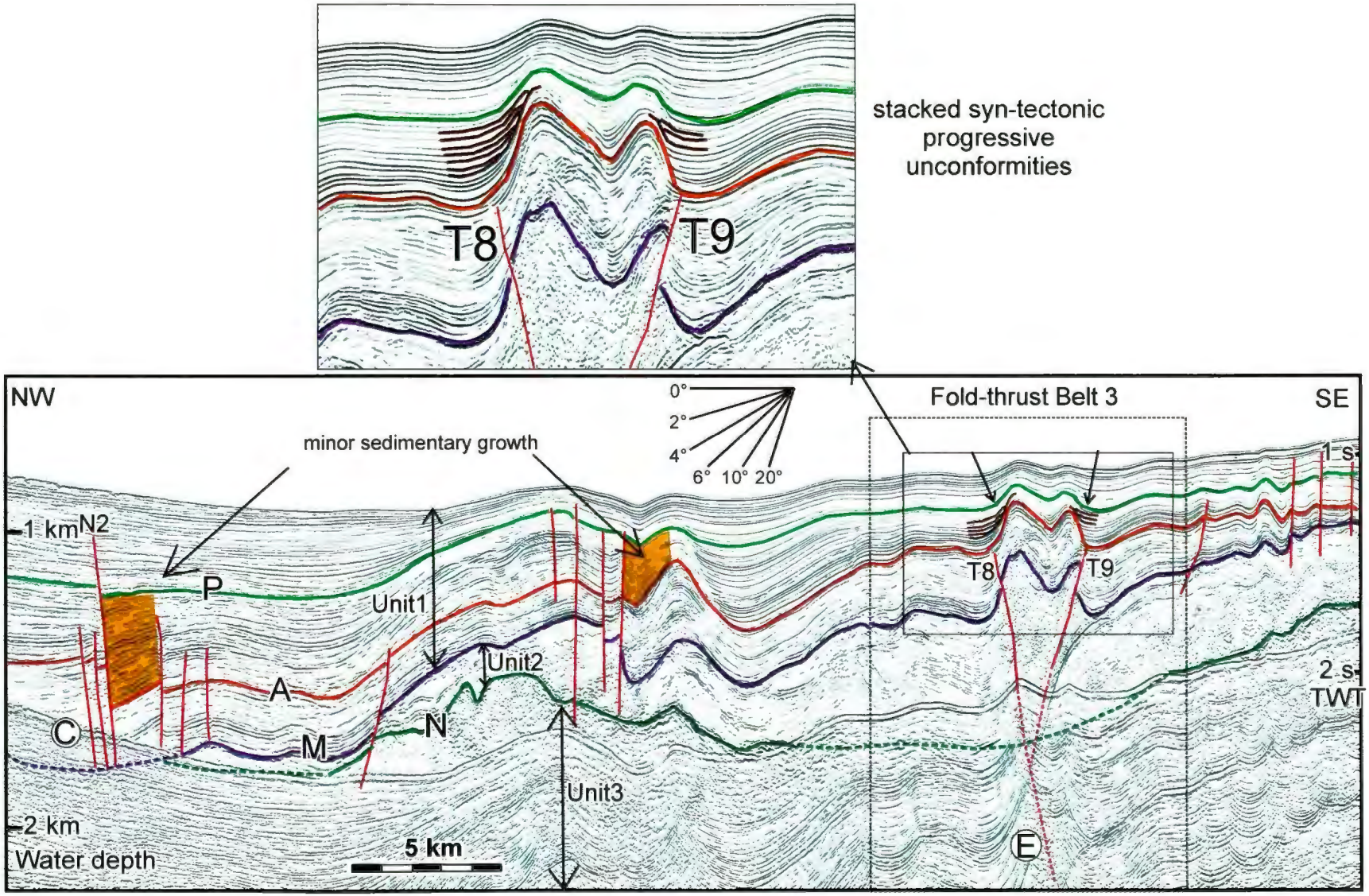

Figure 5.9: Seismic reflection profile showing the structural elements of the central basin floor. Location is shown in Figure 5.3. Letters with circles are fault sets that are described in Chapter 5, and letters with number are the individual faults of these fault sets.

structural architecture (T7, Figs. 5.2, 5.7). Some relatively superficial thrusts that affect the Pliocene-Quaternary sucession merge with the major thrust fault T7 (Fig. 5.7). This structural architecture suggests that there is a major crustal-scale N-verging thrust which controls the tectonic framework of the southern margin of the Outer Cilicia Basin. This thrust belt is also mapped by Aksu et al. (2005) who suggested that the fold-thrust belt defines shallow-rooted structures. However, recent work by Piercey (2011) unequirocally showed that the belt is a deeply rooted structure. There is evidence for the variation in the sediment thickness associated with thrust activity in the lower Pliocene sediments (faults T8 and T9, Fig 5.9), and stacked syn-tectonic progressive unconformities are observed in the upper Pliocene and Quaternary sediments associated with this fold-thrust belt (Figs. 5.7, and 5.9). These structures clearly demonstrate that some of these deeply-rooted thrusts are active in the Pliocene-Quaternary. The thickness variation in the Messinian associated with this fold-thrust set may suggest that these thrusts are active in the latest Miocene (fault set E, Fig. 5.1). These deeply seated thrusts show fault activity in the late Pliocene and Quaternary that may be the evidence for reactivation of these thrusts. The thrusts of the central basin floor were mapped by Bridge et al. (2005); however the existence of the new data set allowed us to map this system in more detail.

5.3. The Northwest continental margin

Northwest continental margin is bounded by two distinct strike-slip faults zones: the late Eocene Ecemiş Fault zone (Yetiş 1978; Jaffey and Robertson, 2001) separates the northwest continental margin from the Central Taurides, and the Kozan Fault zone defines the border with the central basin floor. The northwest continental margin is a

complexly faulted extensional zone that consists of three extensional fault systems that have a complex interaction with each other (fault sets F, G, H, Figs. 5.1, 5.10).

5.3.1. Extensional fault zone 1

Extensional fault zone 1 defines the northern and northwestern margins of the entire Cilicia Basin (fault set F, orange faults, Fig. 5.10). In the Outer Cilicia Basin individual faults of this set have tip points in the Quaternary, and create small dip separations in the Quaternary reflectors (Fig 5.11). In the Inner Cilicia Basin these faults lose their Quaternary expression where their tip points are in the lower Pliocene (Fig. 5.5). There is a little evidence of growth strata related to these faults in the lower Pliocene sediments in the Inner Cilicia Basin, but no evidence in the upper Pliocene or Quaternary sediments (Fig. 5.5). This suggests that in the Inner Cilicia Basin these faults were last active in the early Pliocene, but in the Outer Cilicia Basin they are active in the Quaternary. The faults of this set create small dip separations on the M-reflector and define the Miocene successions in the northwest continental margin where Messinian Unit 2 is absent (Figs. 5.5, 5.11). In the southwestern portion of the northwest continental margin there is no evaporite deposition observed. Proceeding from northwest to southeast there is a serious thickening in the Messinian deposits (Fig 5.1).

5.3.2. Extensional fault zone 2

Extensional fault zone 2 is an E-W trending and S-dipping imbricate extensional fault fan (fault set G, Figs. 5.1, 5.10). This zone consists of several low angle listric faults that extend from or near the depositional surface to well into lower portion of the Pliocene (fault set G, red faults, Figs. 5.10, 5.11). These faults show clear listric trajectories that are associated with sedimentary growth in the Pliocene-Quaternary (Figs.

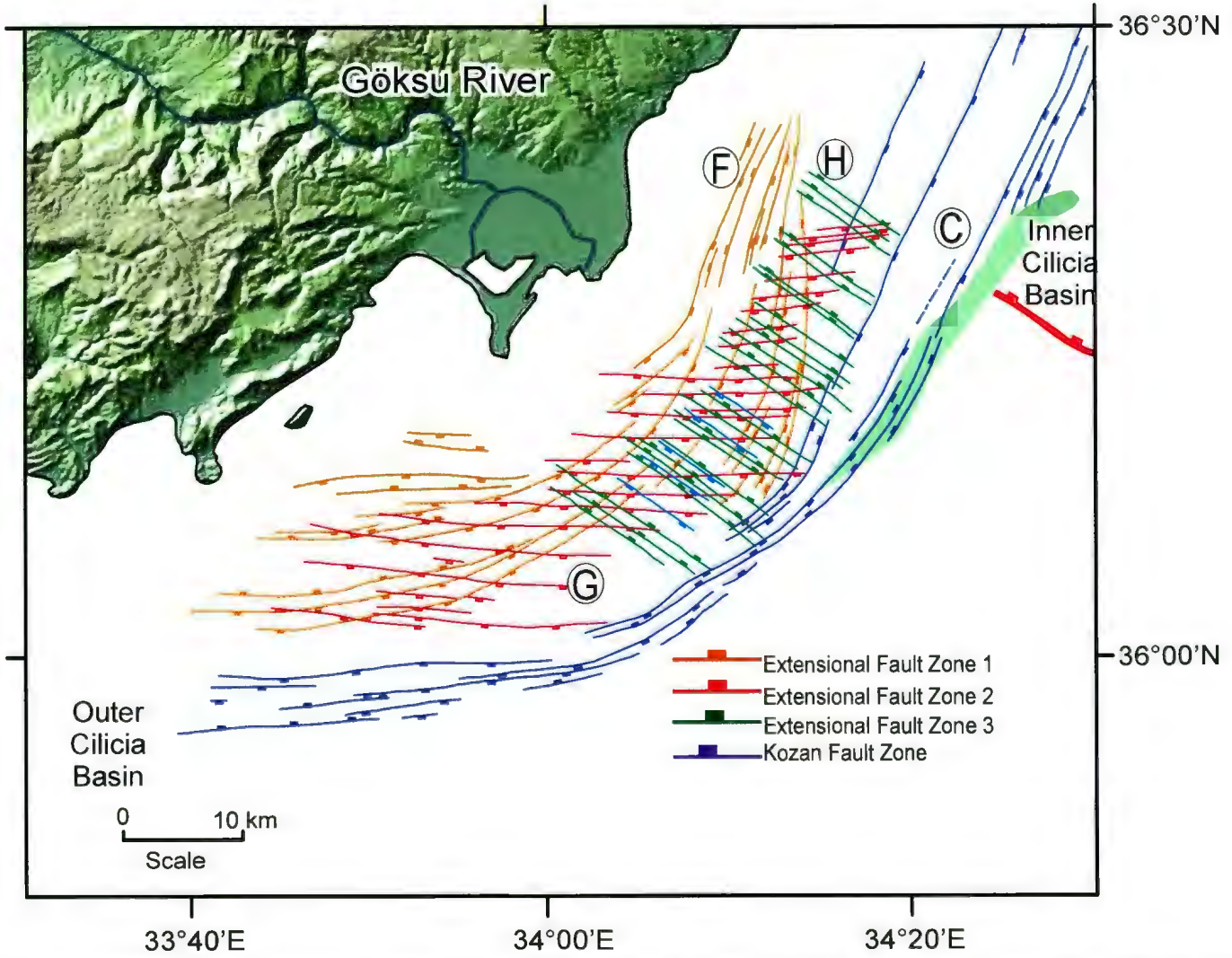

Figure 5.10: Tectonic map of the Northwest margin of the Cilicia Basin showing the three sets of extensional faults. Ticks are showing the hanging walls of the faults. Letters in circles are fault sets that are described in Chapter 5.

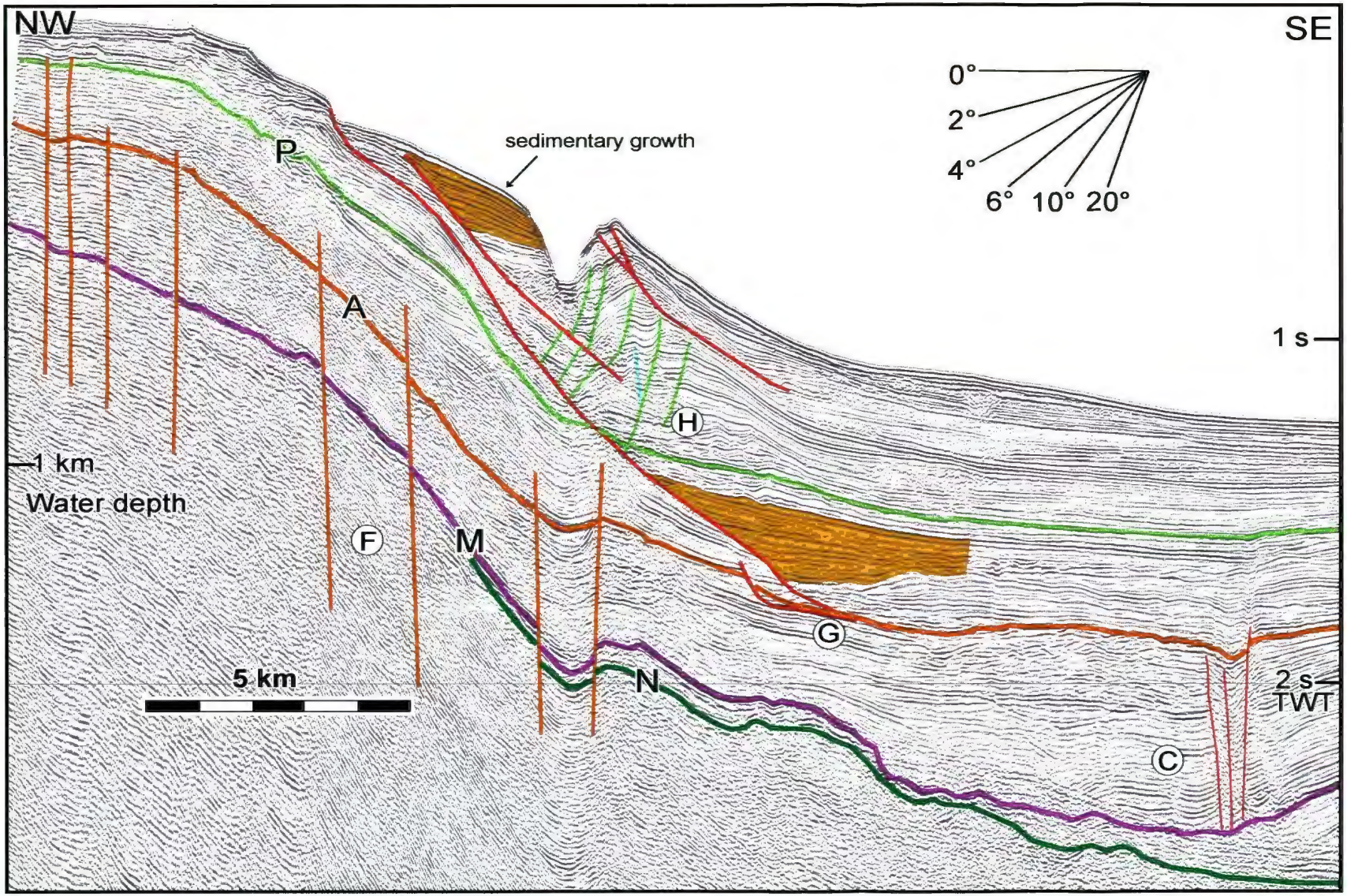

Figure 5.11: High resolution seismic reflection profile showing the extensional faults of the northwest margin. Location is shown in Figure 5.3. Letters with circles are fault sets that are described in Chapter 5.

5.11, 5.12). Some of these faults have tip points at the depositional surface where they create benches on the sea floor (Fig. 5.11). There is no clear evidence for growth in the lower Pliocene sediments (Figs. 5.11, 5.12). Fault architecture and growth strata evidence indicate that these faults are active from the late Pliocene to Quaternary and recent (fault set G, Fig. 5.1).

5.3.3. Extensional fault zone 3

Extensional fault zone 3 is a NW-SE trending and predominantly NE-dipping extensional fault set that interacts with the extensional fault zone 2 in a complex manner (fault set H, green faults, Figs. 5.1, 5.10). These faults are confined to the northeastern part of the Outer Cilicia Basin and the Inner Cilicia Basin. Tip points of these low angle listric faults vary from Quaternary to lower Pliocene. These faults show minor sedimentary growth in the Pliocene and Quaternary (Fig. 5.12). This indicates that these faults are also active in the Pliocene and Quaternary, and they overlap in time with the extensional fault zone 2 (fault set G, red faults).

These three fault zones of the Northwest Continental Margin were schematically mapped in the previous study of the Cilicia Basin by Aksu et al., (2005). The new high resolution seismic data allowed us to better understand the nature of this area by mapping these extensional faults in great detail also supported the schematic trends of the previous study.

5.4. Fault Sets X, and Y

Fault set X (Fig. 5.1) is an E-W trending and N-verging fold-thrust set that was observed in the Outer Cilicia Basin and documented in the previous studies (Aksu et al., 2005b, Calon et al., 2005a.b). These thrusts are truncated by the M-reflector (Aksu et al.,

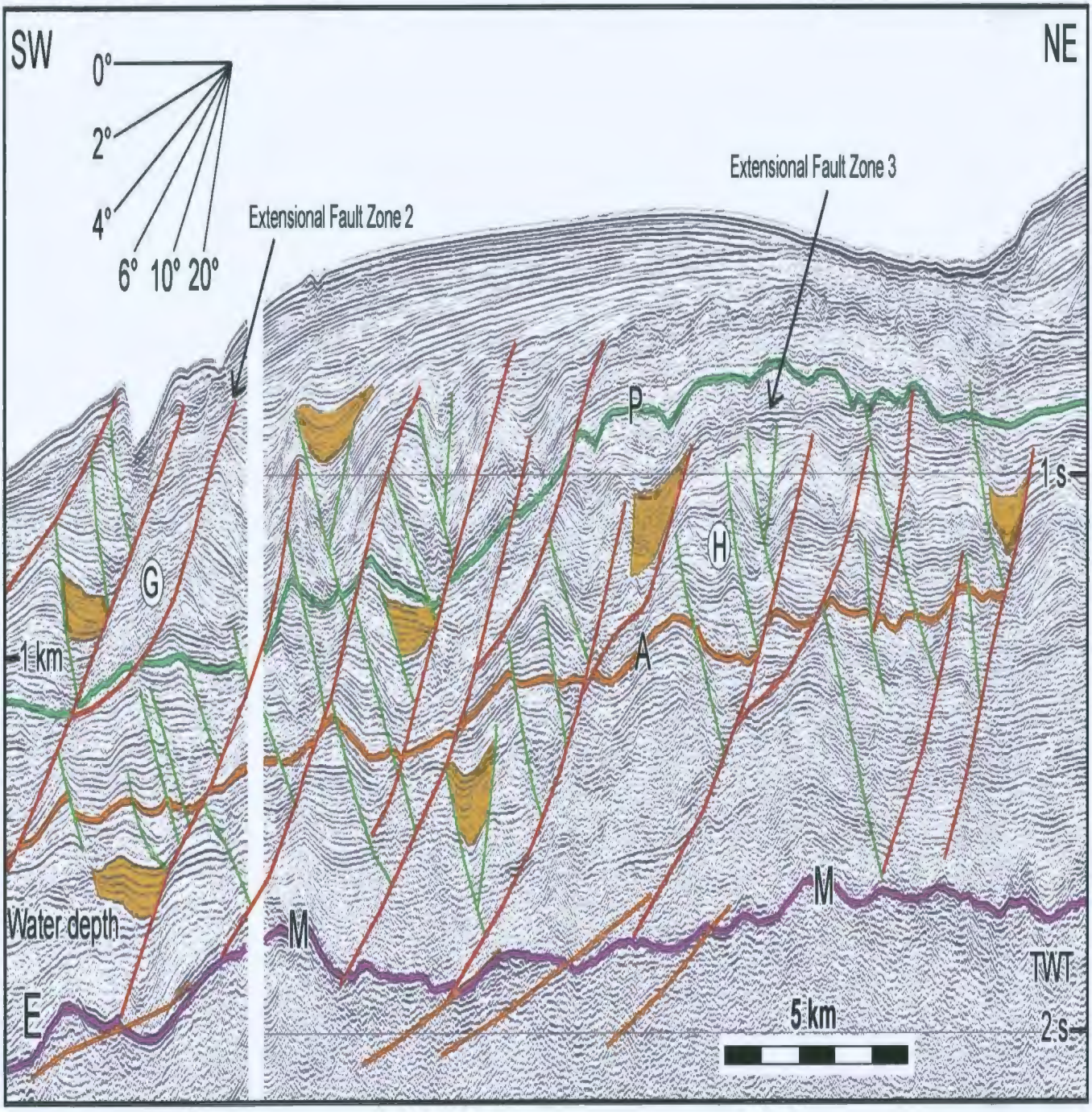

Figure 5.12: High resolution seismic reflection profile E showing the extensional faults of the northwest margin. Letters with circles are fault sets that are described in Chapter 5.

2005b). Aksu et al. (2005b) interpreted these thrusts as surficial gravity driven slide structures that developed in the late Miocene, and related them to the tilting of the late Miocene piggy back basin fill on the trailing flank of the rising Kyrenia culmination.

Ecemiş Fault zone (fault set Y, Fig 5.1) is a NE-SW trending extensional fault zone that is confined to onland Turkey, and does not have a marine extension. This is a sinistral strike slip fault zone that was interpreted as a major splay from the East Anatolian Transform Fault (Özer et al., 1974). Şengör and Yılmaz (1981) suggested that Eocene onset of this strike slip fault zone was developed as a trench-trench transform that separates extensional and contractional segments in the subduction zones. Jaffey and Robertson (2001) related this sinistral strike-slip activity to the internal deformation in the Aegean-Anatolian Microplate. They further suggested that Ecemiş fault is older than both East and North Anatolian Transform faults.

Fig. 5.1 clearly demonstrates that several kinds of deformation occur at the same time in the different parts of the Cilicia Basin. Some of this deformation is explicable as superficial deformation on a mobile substratum-the Messinian evaporites. Thus, thrust set A causes uplift of the Misis-Kyrenia Fault zone and normal fault set B may be the corresponding slumping of the Pliocene-Quaternary on the tilted Messinian of the southern basin margin. Also, normal faults I represent the downslope collapse of the Inner Cilicia Basin delta, complemented by the fold-thrust belts D, and D' of the Outer Cilicia Basin.

Other elements of the deformation are more probably basement controlled and are discussed in more detail in the following synthesis.

5.5. The Evolution of the Cilicia Basin

5.5.1. Early Tertiary to Miocene Development

The evolution of the Cilicia-Adana basin complex started in the Oligocene to early Miocene in a foredeep setting in front of the Tauride fold-thrust belt (Williams et al., 1995; Calon et al., 2005 a; Aksu et al., 2005). Williams et al. (1995) suggested that the early Miocene extension in the Adana Basin was caused by load-induced flexure resulting from renewed thrusting in the Taurides, whereas Şengör et al. (1985) related the extension to differential slip rates on three major faults that meet at a triple plate junction northeast of the area.

In the late Miocene the area was exposed to a phase of regional compression that caused the formation of an arcuate fold-thrust belt extending from the Taurides in the west, to the Troodos complex, and to the western fringe of the Arabian platform in the east (Kelling et al., 1987; Robertson and Woodcock, 1986; Aksu et al., 2005). This compressional phase resulted with the development of a major thrust culmination in two segments. The northeast trending Misis Mountains defines the eastern segment, whereas the Kyrenia Range represents the southern segment. The development of the Misis-Kyrenia culmination in the late Miocene separated the foredeep basin into two large piggyback basins: the Cilicia-Adana basin complex and the Iskenderun-Latakia-Mesaoria basins. The Cilicia Basin has evolved on the backlimb of this thrust culmination since the late Miocene (Aksu et al., 2005b; Hall et al., 2005; Calon et al., 2005a,b). The existence of the late Miocene fluvio-deltaic fill over the Misis Mountains showed that the Adana-

Cilicia basin complex became emergent and exposed to erosion along the northern fringes of the Misis-Kyrenia culmination (Kelling et al., 1987, Williams et al., 1995).

During the Messinian the entire Mediterranean Sea desiccated, and this event resulted in an immense evaporite deposit (Hsü. et al., 1973, 1978). Mulder et al. (1975) noted that the occurrence of the Misis-Kyrenia paleohigh in the Messinian separated the evaporite depocenters of the Adana-Cilicia and Iskenderun-Latakia basins. The Messinian evaporites reach a thickness of 500-800 ms in these basins (Bridge et al., 2005). In the Cilicia Basin the relatively stratified character of the Messinian evaporite succession is evidence of possible interbedded deposition of siliciclastic and carbonate debris (Aksu et al., 2005b). The Messinian salinity crisis was ended by the Pliocene flooding, and the evaporites were confined to isolated subbasins (Hsü et al., 1978; Bridge et al., 2005).

5.5.2. End of Miocene to Quaternary Development

5.5.2.1. Southern basin margin

Continued contraction across the Misis-Kyrenia fold-thrust belt caused northwestward tilting of the basin in the post Messinian suggesting that southerly-verging listric thrusts dominate the contraction. The prominent occurrence of east-northeast – west-southwest striking and north-northwest and south-southeast verging thrusts along the northern margin of the Kyrenia segment of the Misis-Kyrenia Fault zone (i.e., thrust set E in Fig. 5.2), and the geometry of these thrusts in the seismic reflection profiles delineating positive flower structures that originate from a large single stem collectively

suggest that the Kozan-Fault zone must have been re-activated in the Pliocene-Quaternary as a strike-slip system. The southern Kyrenia segment of this fault zone acted as transpressional zone whereas studies from the southern Adana Basin showed that northeastern segment of the fault zone was largely transtensional (e.g., Burton-Ferguson et al., 2005). Superficial extensional faulting along the southern basin margin is related to the gravity-driven slumping of Pliocene-Quaternary deposition on a mobile underlying Messinian evaporite unit.

5.5.2.2. Central basin floor

The northeastern portion of the Outer Cilicia Basin is characterized by active salt tectonism where the structural architecture is nearly orthogonal to the strike of the basin-bounding faults (Bridge et al., 2005). The zone has a cross-sectional length and width of 150 x 50 km in the Cilicia and Adana Basins. Based on the structural style of the Pliocene-Quaternary and Messinian successions and kinematic criteria each the northeastern portion of the Outer Cilicia Basin extending into the Inner Cilicia Basin can be evaluated as (i) an invariably extensional region in the Inner Cilicia Basin which is characterized by salt rollers and pillows developed on the footwalls and hanging walls of listric normal faults and (ii) a predominantly contractional region in the Outer Cilicia Basin which is characterized by active diapirs and salt-cored growth folds commonly associated with thrust faults, where salt forms intrusions into the footwalls and hanging walls of thrusts (Bridge et al., 2005). The boundary between the two regions lies at the edge of the continental slope in Cilicia Basin and is delineated by the master fault N3 and the presence of very large and irregular salt wall (Fig 5.2). The structures in both the

extensional and contractional regions are totally detached at a level that lies either within the salt or at the base of the salt (e.g., Bridge et al., 2005). Many previous studies documented that the pre-Messinian strata are not affected by the overlying extensional and contractional deformation (Hall et al., 2005; Aksu et al., 2005a), suggesting that the regions must be linked across the salt wall via the regional salt detachment (e.g., Bridge et al., 2005). The linked extensional-contractional systems are well understood both in the field studies as well as in analogue modelling of the effects of thin-skinned extension and sediment progradation (e.g. Vendeville and Jackson, 1992 a,b; Jackson et al., 1994; Ge et al., 1997).

Therefore, the collapse of the Adana-Inner Cilicia basin delta results in development of normal fault set I in the Inner Cilicia Basin. This extension in the central part of the Inner Cilicia Basin is complemented by the development of fold-thrust belts D and D' in the central part of the deeper-water Outer Cilicia Basin.

Fold-thrust set E is driven by a prominent strike slip system that developed over the remnants of the Misi-Kyrenia fold-thrust belt. This new system was also basement-controlled where the thrusts associated with the positive flower structures along the northern margin of the Kyrenia Range linked with deeply rooted primarily N-verging back-thrusts (Piercey 2011). The growth strata architecture observed in the thrusts suggested that the Miocene thrusts developed pop-up structures during the Pliocene-Quaternary (fault set E, also see Domain M1, Piercey 2011). Piercey (2011) related the arcuate basin morphology of the Cilicia-Adana basin complex to the development of the northerly verging fold thrust belt. She further related the development of these structures

to the collision and eventual suturing of the Hecataeus Ridge with the Island of Cyprus during the late Miocene.

5.5.2.3. The northwest continental margin

The focus of this study and its biggest contribution to the eastern Mediterranean project is the detailed mapping of the four extensional fault sets in the northwest continental margin (Fault sets C, F, G, and H, Fig. 5.10). The Neogene history of the Cilicia Basin in the northwest continental margin is mainly characterised by transtension in the Pliocene-Quaternary by strike-slip faults that are reactivations of the Miocene contraction (Fig. 5.1) and extensional faults that are confined to the northwest continental margin with fault activity in the Pliocene-Quaternary.

5.5.2.3.1. Fault Sets C and F

The Kozan Fault zone is one of the major splays emerging from the East Anatolian Transform Fault. The precise timing of the transtensional fault activity in the Kozan Fault system is latest Miocene to Pliocene (Aksu et al., 2005b). The marine extension of this zone (fault set C, Figs. 5.5, 5.10) is characterized by extensional separations incompatible with the Miocene contraction (Aksu et al., 2005b). In the previous chapter high-angle extensional faults of extensional fault zone 1 (fault set F, orange faults) and NE-SW trending basin-bounding extensional faults of the central basin floor (fault set C, purple faults) were described as two different fault sets (Fig. 5.10). This discrimination was based on the fact that in the map view these two fault sets are separated in the Inner Cilicia Basin, where they tend to merge in the Outer Cilicia Basin.

However the seismic characters of two systems are quite similar. In the cross sections both sets consist of high angle faults with some extensional separations that occupy narrow zones of 5-10 km width (Figs. 5.5, 5.11). The high-angle extensional faults of these two systems delineate the northern margin of the Cilicia Basin and extend towards the onland Adana Basin where they merge with the prominent Kozan Fault zone. Careful analysis of the individual faults of these two fault sets showed that they vary in age. In the Inner Cilicia Basin, fault set C is active in the late Pliocene, Quaternary, and Recent. In the Outer Cilicia Basin, fault activity is last observed in the late Pliocene. These Messinian-rooted faults have remained active until the Recent in the Inner Cilicia Basin, but the fault activity died out earlier in the late Pliocene towards the Outer Cilicia Basin. For the fault set F, the opposite occurs. In the Inner Cilicia Basin the fault activity is last observed in the early Pliocene, but in the Outer Cilicia Basin faults are active in the Quaternary. In the Inner Cilicia Basin, strain in the Pliocene-Quaternary is mainly on the fault set C, but in the Outer Cilicia Basin fault set F seems to take over the strain in that area where the fault activity on the fault set C ceases or is less prominent.

Until now, the faults within the northwestern margin of the Inner and Outer Cilicia Basins are described as extensional faults, which are probably associated with the Kozan Fault Zone (e.g., Aksu et al., 2005). The absence of an unequivocally clear "piercing point" in seismic reflection profiles precludes the use of seismic data in the confirmation of the strike slip motion along the Kozan Fault Zone. However, the strong geographic correspondence of the fault sets C and F (i.e., the orange and purple faults in various figures and maps) with the orientation of the marine extension of the Kozan Fault Zone as

well as the basin-bounding nature of the purple faults, collectively suggest that the extensional faults C and F must define the marine extension of the Kozan Fault zone. Therefore, these faults must also possess an undetermined amount of strike slip, and must be classified as structures showing normal-sense stratigraphic separations. The faults mapped as C and F are herein linked with the Kozan Fault Zone. Although the fault activity seems to terminate in the late Pliocene towards the southwest on the Kozan Fault zone, sinistral strike-slip motion seems to continue in the southwest along the fault set F. Fault set F can either be part of the same system that is reactivated in the early Pliocene in the Outer Cilicia Basin, or a subsidiary set generated from the main fault set C. However both of these two fault systems are likely to be the Pliocene-Quaternary reactivation of the Miocene faults but in a different stress system.

5.5.2.3.2. Kinematics of Fault Sets C and F

In a regional context the kinematics of the fault set F can be explained with respect to the fault set C. Individual faults of both sets are likely transtensional features that are the marine extension of deep splays coming from the major sinistral strike-slip Kozan Fault zone. Aksu et al. (2005a) noted a southwestward increase in extensional separation and shift in the timing of the fault activity on the individual faults of the fault set C, and related it to a scissor type motion.

Westward escape of the Aegean-Anatolian Microplate along the East and North Anatolian Transform faults represents a well-known tectonic escape zone along two major strike-slip fault systems. Şengör (1981) noted several pull-aparts along the North

and East Anatolian Transform faults. Following that idea, the deep roots of fault sets C and F are interpreted as master faults in a releasing bend (see Chapter1, Fig. 1.5) along the Kozan Fault splay from the East Anatolian Transform Fault. If fault set C is the principal deformation zone, then fault set F can either be Y-shears running parallel to the principal deformation zone, or R- shears that are usually the primary subsidiary deformation and lie at a small angle to the principal deformation zone (Figs. 5.10, also see Chapter1, Fig. 1.5b). However fault set F might also be master faults because they are still major basin bounding faults that have subsidence and collapse on them. These two approximately parallel fault sets, C and F, seem to bound a narrow zone that merges into the Kozan Fault zone to the north. Possibly the faults in each set converge at depth on two faults or narrow fault zones which are branches of the Kozan Fault zone. Fault sets C and F thus create a 'lazy S' shaped deformation that can be explained as the bounding faults of a pull-apart basin at a releasing bend (Fig. 5.13). The Kozan Fault zone would then be a transtensional zone with sinistral strike-slip motion and extension.

5.5.2.3.3. Fault Sets G and H

Extensional fault sets G and H initially seemed to be a conjugate set on seismic sections (Fig. 5.12); however, the map patterns showed that those two sets cannot be a conjugate set based on the different strike of the fault traces. According to Anderson's classification (Anderson, 1942), to have a conjugate set of high angle dip slip faults the strikes of the two fault sets need to be parallel to each other. In terms of stress orientation $\sigma 1$ needs to be vertical and $\sigma 2$ would be parallel to the line of intersection for extensional

faults (Figs. 5.10, also see Chapter 1, Fig. 1.5b). For extensional faults these two sets are separate generations of fault structures, but appear to be active over similar time intervals.

The relative dating of these sets cannot be simply identified, because they demonstrate multiple cutting and offset relationships. In many cases faults H terminate against the faults G, or faults G are offsetting faults H, but there are a few occasions that individual faults of the fault set H offset the faults G (see Chapter 4 section 4.4). The fault set G may have originated slightly earlier, but the two sets overlap in time. The two fault systems must be active at the same time. Faults G show evidence of growth strata in the Pliocene and Quaternary, and some of them create steps on the sea floor, suggesting that the faults are active in the present (Fig.5.12). Faults H also demonstrate minor growth strata in the Pliocene and Quaternary. The growth strata on these two fault systems seem to terminate their activity about at the same seismic stratigraphic level (Figs. 5.1, 5.12). They both are associated with growth strata successions within the same package, therefore there is basically synchronous activity on both of the fault systems.

These shallow faults of both sets are very low angle listric faults that affect almost the entire Pliocene-Quaternary succession (Figs. 5.11, 5.12). In an ideal dip slip system their strike should be parallel, and they are distinctly not. They are low angle extensional detachments. They do not demonstrate a truly negative flower behavior either; so they are not typical transtensional type of structures.

These two fault sets are contained between the two transtensional fault sets, C and F, described above and interpreted as major bounding faults of a pull-apart basin at a

releasing bend of the sinistral Kozan Fault zone. But the extensional stress system responsible is incompatible with the concurrent contractional deformation in the central basin floor. The 'lazy S' shaped transtensional strike-slip regime that observed in this part of the study area is expected to be complemented by a set of extensional faults bounded by these master faults of fault sets C and F. However the extension along the fault sets G and H cannot easily be explained in this setting because of the fault orientations. Extensional faults in the lazy-S pull-apart basins generally lie at an angle of 30-50° to the master faults (Mann et al., 1983). The faults H are nearly orthogonal to the fault set C, and faults G lie at a much larger angle to the master faults (Fig. 5.13).

In over-pressured wet shales as in Cilicia Basin sediments the main deformation may occur on R' and possibly P' (see Chapter 1, Fig. 1.5). In that concept fault set H can be explained as P' shears, but the fault set G still does not fit in this picture (Fig. 5.13). Because fault sets G and H are contained between fault sets C and F, a genetic relationship is likely. If C and F define a pull-apart basin at a releasing bend in the Kozan Fault zone, then G and H are symptomatic of extension within the pull-apart basin. That this orientation is quite different from that expected may indicate inheritance from earlier structures with those trends. It remains to be explained how the extension observed along the northwest continental margin relate to the concurrent contraction to the south. The conventional trends of pull-apart basins do not apply to the basin extension here in the northwest continental margin. Therefore the kinematics of these extensional faults may be related with something else.

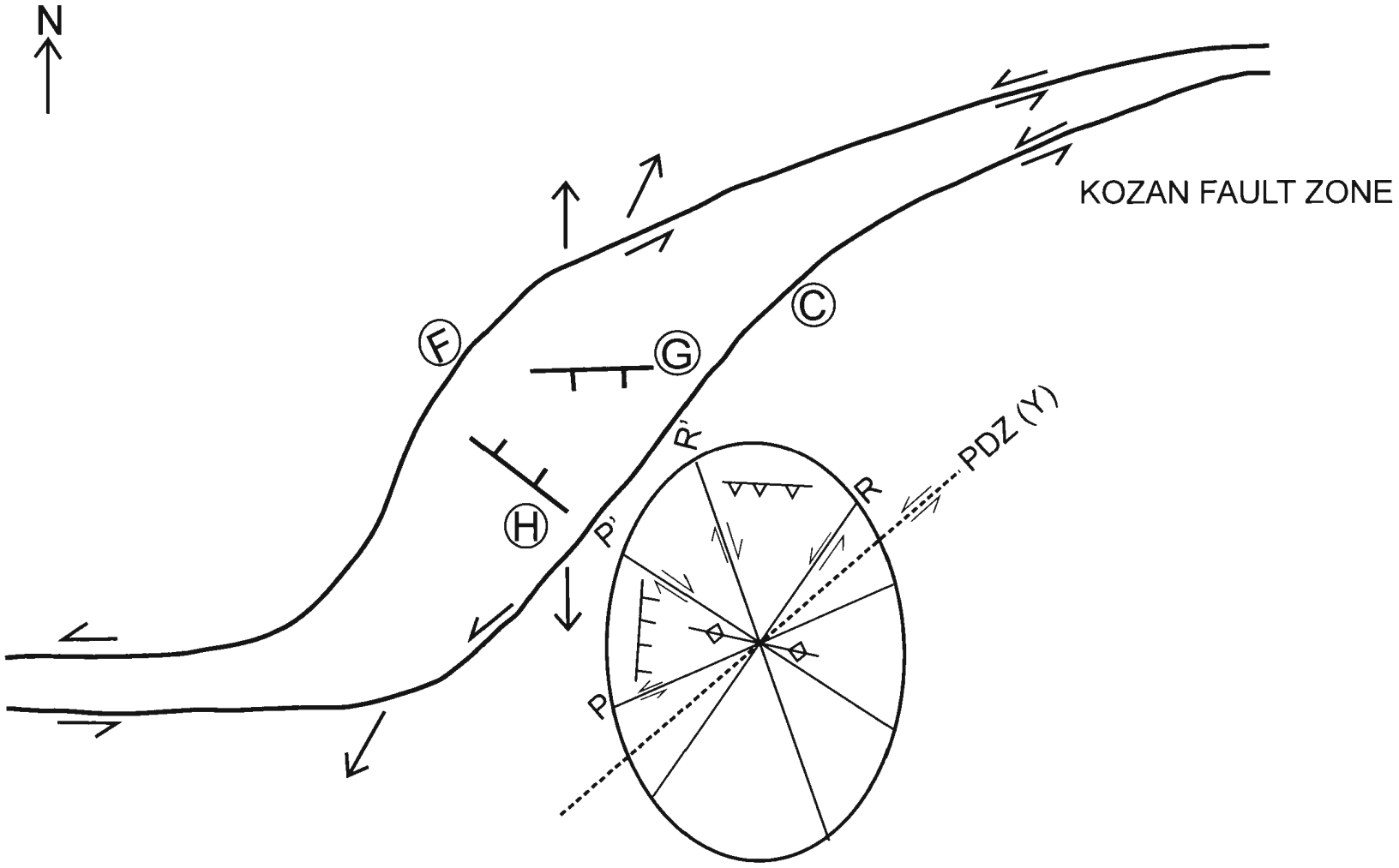

Figure 5.13: Schematic display of the fault systems in the northwest continental margin.

5.5.2.4. Possible Scenarios

For the Kozan Fault zone (i.e., fault sets C and F) the intermediate stress σ2 would be vertical and maximum and minimum stresses σ1 and σ3 would be horizontal with σ1 oriented approximately north-south and σ3 oriented east-west, respectively, given the transtensional nature of the principle deformation zone (Fig. 5.13). Within this system *en échelon* synthetic and antithetic parasitic faults such as R, R', P and P' shears should be vertical or have very steep dips and oriented at specific angles to the Y shears (Fig. 5.13). The predominantly extensional nature of the fault sets G and H as well as their relatively low dip angles preclude that these faults are genetically related to the strike slip deformation associated with the Kozan Fault zone. If the fault sets G and H are pure normal-sense dip-slip faults, they must represent two different extensional fault systems related to differently oriented stress fields. Despite the fact that the two systems have an overall north and south dipping polarities they cannot define contemporaneous conjugate fault sets because of the significant differences in their strike directions. The observed interactivity between the fault sets G and H and the demonstrable growth associated with each of these fault sets indicate that these faults are two independent systems in which one system overprints and reactivates the other in relation to the rotation of the principal tensile stress direction for these faults. The overall architecture of these two fault systems, notably their shallow dips, their prominent normal-sense dip separations with associated growth strata wedges and their listric fault plane geometries with associated bedding-parallel detachments collectively indicate that they might be part of a gravitationally-driven zone of widely distributed deformation.

Recent evolution of the eastern Mediterranean region is mainly controlled by relative motions of Eurasian and African plates, and Arabian Microplate. These relative motions are defined by subduction of the African Plate beneath the Eurasian Plate towards the Hellenic and Cyprus arcs, collision of Arabian and Eurasian plates across Bitlis-Zagros suture zone, and westward escape of the Aegean-Anatolian microplate along the North and East Anatolian Transform faults. Collision of the African and Eurasian plates with the Aegean-Anatolian Microplate and subduction of the African Plate along the Hellenic and Cyprus arcs create a N-S compression, but subducting roll-back drag is pulling the Aegean-Anatolian Microplate away from the Arabian Microplate. The Miocene history of the study area is explained in this N-S contractional setting. McClusky et al., (2000) suggested that the convergence between Africa and Eurasia plates is higher across the Hellenic Arc, and lower in the Cyprus Arc. They related the decrease in the convergence rates towards the Cyprus Arc to the subduction of the Eratosthenes Seamount beneath Cyprus. Dilek and Sandvol (2009) marked the existence of two distinct high velocity regions beneath the Aegean-Anatolian Microplate that might be evidence for two different slab break-off events caused by continuing convergence of the lithospheric mantle. They further stated that besides these break-off events the subduction was almost continuous. In case of a slab break-off or a slab detachment in the subducting African Plate there will be a change in the regional stress field. The gap between the attached and detached slabs will cause a relief in the stress field. The Aegean-Anatolian Microplate will not be forced westward by the collision anymore, and this will generate an areal extension observed in the Aegean back arc basin but possibly extension further east. A slab break in the subducting African Plate could basically cause

a rebound in the stress field, and the N-S compression will turn to a N-S extension, and this could explain the E-W trending normal faulting.

Another possible scenario is, if the convergence of the African Plate with the Aegean-Anatolian Microplate is continuing but now slowing due to collision of microcontinental blocks such as Eratosthenes Seamount below Cyprus, then compression (excluding the contractional features associated with gravitational sliding of the Pliocene-Quaternary sediments above the salt) may still characterise the southern part of the Cilicia Basin. However, slab detachment may induce extensional stress above which trajectory with continuing contraction to south may explain the duality of contraction and extension in this area.

CHAPTER 6

Conclusions

The processing and interpretation of ~ 850 km of high-resolution multi-channel seismic reflection data resulted in detailed mapping of a NW-SE transect across the middle of the Cilicia Basin. Age relationships of the specific events that occur in the area have been summarised with a special focus on the northwest continental margin. The following are the geological conclusions of this study.

- The Cilicia-Adana basin complex evolved in a foredeep setting in the Miocene. Tauride and Misis-Kyrenia fold-thrust belts are the major controls in this foredeep basin. During the Messinian salinity crisis, the study area became emergent and this event resulted in deposition of a thick evaporite succession in the Cilicia Basin.
- Seismic reflection profiles showed the co-occurrence of contractional, extensional and strike-slip deformation within the Cilicia Basin, all occurring during the Pliocene-Quaternary. The uplift of the Misis-Kyrenia Fault zone resulted in the tilting of the southern basin margin. The rapid deposition of deltaic sediments from the north caused the mobilization of the salt and resulted in a series of extensional faults in the Pliocene-Quaternary succession. The gravitational collapse of the Inner Cilicia Basin delta successions is complemented by the development of a contractional fold-thrust belt in the Outer Cilicia Basin.
- The northwest continental margin is mainly characterised by transtension in the Pliocene-Quaternary involving strike-slip faults, that are a reactivation of faults

related to Miocene transpression, and extensional faults that are confined to the northwest continental margin with fault activity in the Pliocene-Quaternary.

- The Kozan Fault zone appears to split in the Pliocene-Quaternary into two main strands that define the boundaries of a pull-apart basin at a 'lazy S' shaped releasing bend. Extensional faults within the pull-apart feature do not have orientations compatible with those expected and their trends may be inherited.
- The Quaternary and Recent fault activity on the Kozan Fault zone takes place along two different strands of the system which diverge in the Inner Cilicia Basin and converge again in the Outer Cilicia Basin. In late Quaternary time, the SE-strand dominates in the Inner Cilicia Basin, and the NW-strand dominates in the Outer Cilicia Basin. The late deformation thus appears to transfer from the one strand to the other along the Basin. This may be due to the stress system favouring particular orientations as the directions of the strands swing.
- Rebound from a slab break in the subducting African plate can explain the transtensional stress system in the northwest continental margin, while at the same time the collision of microcontinental blocks such as Eratosthenes Seamount below Cyprus, explains the contraction in the southern part of the Cilicia Basin.

6.2. Future Work

The existing data allowed us to delineate some of the main features in the study area, and answer some important questions about the Neogene evolution of the Cilicia Basin, however there are still questions to be answered that requires additional data acquisition.

A 3D seismic survey in the northwest continental margin could provide a better mapping of the extensional and transtensional features here with greater confidence, and help to answer some questions about the relative dating, slip rates of these features, and give a better idea about the primary and subsidiary deformations and the stress systems in the area.

A deeper penetrating seismic reflection survey in the central basin floor would also help to clarify the orientations and give a better image of the deeper geological features that may control shallow structures in the salt and overlying sediments.

References

Aksu, A.E., Calon, T.J., Piper, D.J.W, Turgut, S, Izdar, E.K., 1992a. Architecture of late orogenic basins in the eastern Mediterranean Sea. Tectonophysics, 210: 191·213.

Aksu, A.E., Uluğ, A., Piper, D.J.W., Konuk, T, Turgut, S., 1992b. Quaternary sedimentary history of Adana, Cilicia and Iskenderun Basins, Northeast Mediterranean Sea. Marine Geology, 104: 55·71.

Aksu, A.E., Hall, J. and Yaltırak, C., 2005a. Editorial - Miocene to Recent tectonic evolution of the eastern Mediterranean: new pieces of the old Mediterranean puzzle. Marine Geology, 221: 1-13.

Aksu, A.E., Calon, T.J., Hall, J., Mansfield, S., and Yaşar, D., 2005b. The Cilicia–Adana Basin complex, Eastern Mediterranean: Neogene evolution of an active fore-arc basin in an obliquely convergent margin. Marine Geology, 221: 121–159.

Aksu, A.E., Calon, T.J., Hall, J., and Yaşar, D., 2005c. Origin and evolution of the Neogene Iskenderun Basin, northeastern Mediterranean Sea. Marine Geology 221: 161-187.

Anderson, E. M., 1942. The Dynamics of Faulting and Dyke Formation. Oliver and Boyd, London.

Ben Avraham, Z., Kempler, D., Ginzburg, A., 1988. Plate convergence in the Cyprean Arc Tectonophysics, 146: 231-240.

Ben Avraham, Z., Tiber, G., Limanov, A. F., Leybov, M. B., Ivanov, M. K., Tokarev, M. Y., Woodside, J. M., 1995. Structural and tectonics of the eastern Cyprus Arc. Marine and Petroleum Geology, 12.263·271.

Ben-Avraham., J. Woodside, E. Lodolo, M. Gardosh, M. Grasso, A. Camerlenghi and G.B. Vai, 2006. Eastern Mediterranean Basin Systems, in: Gee, D.E. and Stephenson, R.A. (eds.), European Lithosphere Dynamics, Geological Society, London, Memoirs, 32, 263–276.

Biju-Duval, B, and L Montadert, comps. Structural History of the Mediterranean Basin. Paris: Editions Technips, 1978.

Bridge, C., Calon, T.J., Hall, J. and Aksu, A.E., 2005. Salt tectonics in two convergent margin basins of the Cyprus Arc, northeastern Mediterranean. Marine Geology, 221: 223-259.

Burchfiel B. C., and Stewart J. H., 1966. "Pull-apart" origin of the central segment of the Death Valley, California. The Geological Society of America, 77: 439-442

Burton-Ferguson, R., Aksu, A.E., Calon, T.J., and Hall, J., 2005. Seismic stratigraphy and structural evolution of the Adana Basin, Eastern Mediterranean. Marine Geology, 221: 189-222.

Calon, T.J., Hall, J. and Aksu, A.E., 2005a. The Oligocene-Recent evolution of the Mesaoria Basin (Cyprus) and its western marine extension, Eastern Mediterranean. Marine Geology, 221: 95-120.

Calon, T.J., Aksu, A.E. and Hall, J., 2005b. The Neogene evolution of the Outer Latakia Basin and its extension into the Eastern Mesaoria Basin (Cyprus), Eastern Mediterranean. Marine Geology, 221: 61-94.

Cosentino, D., Darbaş, G., and Gürbüz, K., 2010. The Messinian salinity crisis in the marginal basins of the peri-Mediterranean orogenic systems: examples from the central Apennines (Italy) and the Adana Basin (Turkey). EGU General Assembly, Geophysical Abstracts, 12: EGU2010-2462.

Cosentino, D., Schildgen, T. F., Cipollari, P., Faranda, C., Gliozzi, E., Hudackova, N., Lucifora, S., and Strecker, M. R., 2011. Late Miocene surface uplift of the southern margin of the Central Anatolian Plateau, Central Taurides, Turkey. Geological Society of America Bulletin, 124: 133-145.

Crowell, J. C., 1974. Origin of late Cenozoic basins in southern California. In: Dickinson, W. R. (Edt.) Tectonics and Sedimentation. SEPM Special Publications, 22: 190-204.

Cunningham, W. D., and Mann, P., 2007. Tectonics of strike-slip restraining and releasing bends. Geological Society, London, Special Publications, 290: 1-12.

Dewey, J.F., Hempton, M.R., Kidd, W.S.F., Şaroğlu, F. and Şengör, A.M.C., 1986. Shortening of continental lithosphere: the neotectonics of eastern Anatolia - a young collision zone. *In*: M.P. Coward and A.C. Ries (Eds.), Collision Tectonics. Geological Society Special Publication, 19: 3-36.

Dilek Y., and Sandvol E., 2009. Seismic structure, crustal architecture and tectonic evolution of the Anatolian-African Plate Boundary and the Cenozoic Orogenic Belts in the Eastern Mediterranean Region. The Geological Society, London, Special Publications, 327:127-160.

Ergin M., Aktar M., and Eyidoğan H., 2004. Present-Day Seismotectonics of the Cilician Basin: Eastern Mediterranean. Bulletin of the Seismological Society of America, 94: 930-939.

Evans, G., Morgan, P., Evans, W.E., Evans, T.R. and Woodside, J.M., 1978. Faulting and halokinetics in the northeastern Mediterranean between Cyprus and Turkey. Geology, 6: 392-396.

Ge, H., Jackson, M.P.A. and Vendeville, B.C., 1997. Kinematics and dynamics of salt tectonics driven by progradation. American Association Petroleum Geologists Bulletin, 81: 398-423.

Gökçen, S.L., Kelling, G., Gökçen, N. and Floyd, P.A., 1988. Sedimentology of a late Cenozoic collisional sequence: the Misis Complex, Adana, southern Turkey. Sedimentary Geology, 59: 205-235.

Hall, J., Aksu, A.E., Calon, T.J. and Yaşar, D., 2005a. Varying tectonic control on basin development at an active microplate margin: the Iskenderun - Latakia Basin complex, Eastern Mediterranean. Marine Geology, 221: 15-60.

Hall, J., Calon, T.J., Aksu, A.E., and Meade, S.R., 2005b. Structural evolution of the Latakia Ridge and Cyprus Basin at the front of the Cyprus Arc, Eastern Mediterranean Sea. Marine Geology, 221: 261-297.

Hsü, K.J., Cita, M.B. and Ryan, W.B.F., 1973. The origin of the Mediterranean evaporites. In: W.B.F. Ryan, K. Hsü, et al., Initial Reports of the Deep Sea Drilling Project, XIII, Part I, 1203-1231. U.S. Government Printing Office, Washington.

Hsü, K.J. Montadert, L., Bernoulli, D., Cita, M.B., Erickson, A., Garrison, R.E., Kidd, R.B., Mélières, F., Müller, C. and Wright, R., 1978. History of the Mediterranean salinity crisis. In: K. Hsü, L. Montadert et al., Initial Reports of the Deep Sea Drilling Project, XLII, Part I, 1053-1078. U.S. Government Printing Office, Washington.

International Commission on Stratigraphy (ICS), 2009. International Stratigraphic Chart.web.archive.org/web/20091229003212/http://www.stratigraphy.org/upload/ISChart 2009.pdf)

Işler, F.I., Aksu, A.E., Hall, J., Calon, T.J. and Yaşar, D., 2005. Neogene development of the Antalya Basin, Eastern Mediterranean: an active fore-arc basin adjacent to an arc junction. Marine Geology, 221: 299-330.

Jackson, M.P.A., Vendeville, B.C. and Schultz-Ela, D.D., 1994. Structural dynamics of salt systems. Annual Reviews Earth Planetary Sciences, 22: 93-117.

Jaffey, N. and Robertson, A. H. F., 2001. New sedimentological and structural data from the Ecemiş Fault Zone, southern Turkey: implications for its timing and onset

and the Cenozoic tectonic escape of Anatolia. Journal of the Geological Society, London, 158, 367-378

Karig, D.E. and Kozlu, H., 1990. Late Paleogene - Neogene evolution of the triple junction region near Mara_, south-central Turkey. Journal of the Geological Society, London, 147: 1023-1034.

Kelling, G., Gökçen, S.L., Floyd, P.A., Gökçen, N., 1987. Neogene tectonics and plate convergence in the eastern Mediterranean: new data from southern Turkey. Geology, 15: 425-429.

Kempler, D. and Garfunkel, Z., 1994. Structure and kinematics in the northeastern Mediterranean: a study of irregular plate boundary. Tectonophysics, 234: 19-32.

Kennedy, Susan, 2012. Miocene to Recent Evolution of the Cilicia Basin with Emphasis on the Pliocene-Quaternary Sedimentary Relationship Between the Göksu River and the Cilicia Basin. MSc Dissertation, Memorial University of Newfoundland, 269 pp.

Koçyiğit, A. and Beyhan, A., 1998. An intracontinental transcurrent structure: the Central Anatolian Fault Zone, Turkey. Tectonophysics, 284: 317-336.

Kozlu, H., 1987. Structural development and stratigraphy of Misis-Andirin region. *In*: Proceedings of the 7th Petroleum Congress of Turkey, Turkish Association of Petroleum Geologists, p. 104-116.

Mann P., Hempton M. R., Bradley D. C., and Burke K., 1983. Development of Pull-Apart Basins. The Journal of Geology, 91: 529-554

Mansfield, Stacey, 2006. Neogene Tectonic and Sedimentary Evolution of the Outer Cilicia Basin, Eastern Mediterranean Sea. MSc Dissertation, Memorial University of Newfoundland, 247 pp.

McClusky, S., Balassanian, S., Barka, A., C. Demir, S. Ergintav, I. Georgiev, O. Gürkan, M. Hamburger, K. Hurst, H.-G. Hans-Gert, K. Karstens, G. Kekelidze, R. King, V. Kotzev, O. Lenk, S. Mahmoud, A. Mishin, M. Nadariya, A. Ouzounis, D. Paradissis, Y. Peter, M. Prilepin, R. Relinger, I. Sanli, H. Seeger, A. Tealeb, M.N. Toksöz, G. Veis, 2000. Global positioning system constraints on plate kinematics and dynamics in the eastern Mediterranean and Caucasus. Journal of Geophysical Research, 105: 5695-5719.

McKenzie, D. and Yılmaz, Y., 1991. Deformation and volcanism in western Turkey and the Aegean, Bulletin of the Istanbul Technical University, pp. 345-373.

Mitchum, M. R., Jr., Vail, P. R. and Sangree, J. B., 1977a. Seismic stratigraphy and global changes of sea level, Part 6: Stratigraphic interpretation of seismic reflection patterns in depositional sequences. *In*: C. E. Payton (Editor), Seismic Stratigraphy Applications to Hydrocarbon Exploration. Memoir of the American Association of Petroleum Geologists, 26: 117-135.

Mitchum, R.A.Jr., Vail, P.R. and Thompson III, S., 1977b. Seismic stratigraphy and global change of sea level. Part 2: The depositional sequence as a basic unit for stratigraphic analysis. *In*: C.E. Payton (Editor), Seismic Stratigraphy Applications to

Hydrocarbon Exploration. American Association of Petroleum Geologists. Memoir, 25: 53-62.

Mulder, C.J., 1973. Tectonic framework and distribution of Miocene evaporites in the Mediterranean. *In*: Drooger, C.W. (Ed.), Messinian Events in the Mediterranean. Koninklijke Nederlandse Akademic von Weterschappen, North-Holland Publishing Company, Amsterdam, 44-59 pp.

Mulder, C.J., Lehner, P. and Allen D.C.K., 1975. Structural evolution of the Neogene salt basins in the eastern Mediterranean and the Red Sea. Geologie en Mijnbouw, 54: 208-221.

Özer, B., Biju·Duval, B., Courrier, P., Letouzey, J., 1974. Geology of Neogene Basins of

Antalya, Mut and Adana. Proceedings of the 3rd Petroleum Congress of Turkey, Turkish Association of Petroleum Geologists, p. 57-84.

Piercey, Tiffany, 2011. A Seismic Reflection Study of the Neogene Sedimentary History of the Outer Cilicia Basin, Eastern Mediterranean. MSc Dissertation, Memorial University of Newfoundland, 183 pp.

ProMAX© 3D Reference Guide, 1998. A reference guide for ProMAX© Geophysical Processing Software, V1 and V2.

Riba, O., 1976. Syntectonic unconformities of the Alto Cardener, Spanish Pyrenees: a genetic interpretation. Sedimentary Geology, 15: 213-233.

Robertson, A.H.F, 1998. Mesozoic–Tertiary tectonic evolution of the Easternmost Mediterranean area: integration of marine and land evidence. In: Robertson, A.H.F., Emeis, K.-C., Richter, C., and Camerlenghi, A. (Eds.), 1998 Proceedings of the Ocean Drilling Program, Scientific Results, V. 160: 723-782.

Robertson A.H.F. and Woodcock, N.H., 1986. The role of Kyrenia Range lineament, Cyprus, in the geological evolution of the eastern Mediterranean area. Royal Society of London Philosophical Transactions, Series A, V. 317: 141-177.

Robertson, A. H. F., Parlak, O., and Ustaömer, T., 2012. Overview of the Palaeozoic–Neogene evolution of Neotethys in the Eastern Mediterranean region (southern Turkey, Cyprus, Syria). Petroleum Geoscience, 18: 381-404.

Ryan, W. B. F., Hsu, K.J., 1973. lnitial Reptorts. DSDP, 13 (pts. 1 and 2), Washington (U.S. Govt printing office)

Ryan, W. B. F., 1969. The floor of the Mediterranean Sea. PhD Thesis. Columbia University, New York. 236 pp.

Schildgen, T.F., Cosentino, D., Bookhagen, B., Niedermann, S., Yıldırım, C., Echtler, H., Wittmann, H., and Strecker, M. R., 2012. Multi-phased uplift of the southern margin of the Central Anatolian plateau, Turkey: A record of tectonic and upper mantle processes. Earth and Planetary Science Letters, 317-318: 85-95

Sellier, N. C., Loncke, L., Vendeville., B.C., Mascle, J., Zitter, T., Woodside, J., Loubrieu, B., 2012 (in press.). Post-Messinian evolution of the Florence Ridge area (Western Cyprus Arc), Part I: Morphostructural analysis. Tectonophysics.

Şengör, A. M. C., 1979. Northern Anatolian fault: its age offset and tectonic significance. Geological Society, London, 136: 269-282.

Şengör, AM.C., Görür, N., Şaroğlu, F., 1985. Strike-slip faulting and related basin formation in zones of tectonic escape: Turkey as a case study. Society of Economic Palaeontologists and Mineralogists, Special Publication, 37: 227-264.

Şengör A. M. C., and Yılmaz Y., 1981. Tethyan evolution of Turkey: a plate tectonic approach. Tectonophysics, 75:181-241.

Smith, S.G., 1977. Diapiric structures in the eastern Mediterranean Cilicia Basin. Geology, 5: 705-707.

Spakman, W. and Wortel, R., 2004. A tomographoic view of the Western Mediterranean Geodynamics. In: Cavvaza, W., Roure, F., Spakman, W., Stampfli, G.M. and Ziegler, P.A. (Editors), The TRANSMED Atlas - The Mediterranean Region from Crust to Mantle. Springer-Verslag, Berlin, Heidelberg: 31-52.

Uffenorde H., Lund J. J., and Georgi, K. H., 1990. Biostratigraphy of the Neogene in the Iskenderun Basin. Turkish Association of Petroleum Geologists. 8th Petroleum Congress of Turkey, pp. 363–370.

Vendeville, B.C. and Jackson, M.P.A., 1992a. The rise of diapirs during thin-skinned extension. Marine and Petroleum Geology, 9: 331-353.

Vendeville, B.C. and Jackson, M.P.A., 1992b. The fall of diapirs during thin-skinned extension. Marine and Petroleum Geology, 9: 354-371.

Weiler, Y., 1969. The Miocene Kythrea flysch basin in Cyprus. Giornale di Geologia, 35: 213-229.

Williams, G.D., Ünlügenç, U.C., Kelling, G. and Demirkol, C., 1995. Tectonic controls on stratigraphic evolution of the Adana Basin, Turkey. Journal of Geological Society of London, 152: 873-882.

Woodside, J.M., 1977. Tectonic elements and crust of the eastern Mediterranean Sea. Marine Geophysical Research, 3: 317-354.

Woodside, J. M., Mascle, J., Zitter, T. A. C., Limonov, A. F., Ergün, M., Volkonskaia, A., Shipboard scientists of the PRISMEO IT Expedition, 2002. The Florence Rise, the western bend of the Cyprus Arc. Marine Geology, 185: 177-194.

Yalçin M. N., and Gorur N., 1984. Sedimentological evolution of the Adana Basin. In: Tekeli O, Göncüoğlu M. C. (Eds.), Proceedings of the International Symposium on the Geology of the Taurus Belt, Ankara, pp. 165–72.

Yetiş, C., Kelling, G., Gökçen, S.I. and Baroz, F., 1995. A revised stratigraphic framework for Late Cenozoic sequences in the northeastern Mediterranean region. Geologische Rundschau, 84: 794-812.

Yildirim C., Schildgen T. F., Echtler H., Melnick D., and Strecker M. R., 2011. Late Neogene and active orogenic uplift in the Central Pontides associated with the North Anatolian Fault: Implications for the northern margin of the Central Anatolian Plateau, Turkey. Tectonics, 30, TC5005, doi:10.1029/2010TC002756.

Yılmaz, Ö., 2001. Seismic Data Analysis: Processing, Inversion and Interpretation of Seismic Data (2 Volumes). Investigations in Geophysics No: 10. Society of Exploration Geophysicists.

Yılmaz, Y., Gürpınar, O. and Yiğitbaş, E., 1988. Tectonic evolution of the Miocene basins at the Amanos Mountains and the Maraş region. Bulletin Turkish Association of Petroleum Geologists 1/1: 52-72.

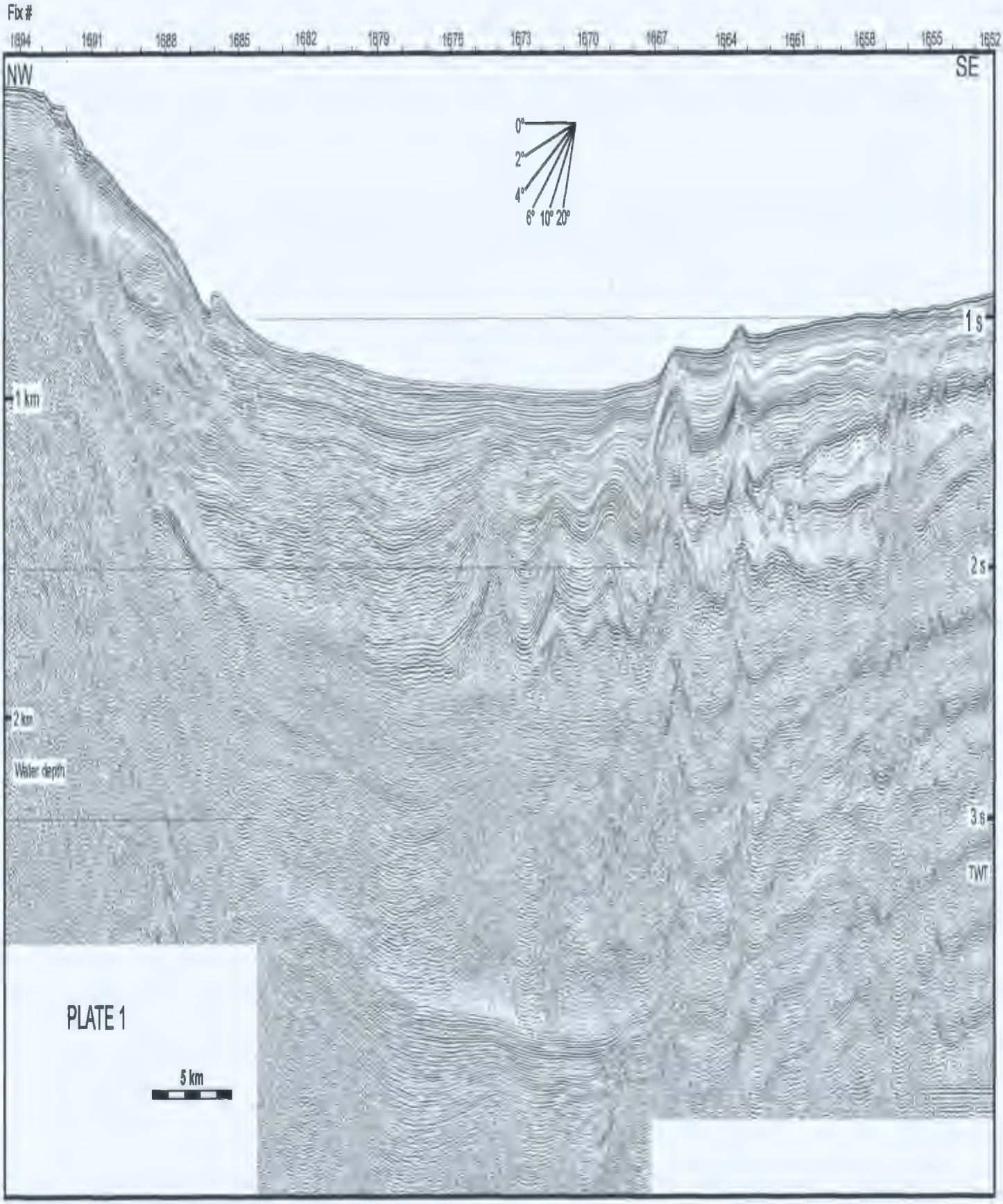
Fix #
1694
1691
1688
1685
1682
1679
1676
1673
1670
1667
1664
1661
1658
1655
1652
NW
SE
0°
2°
4°
6°
10°
20°
1 s
2 s
3 s
TWT
1 km
2 km
Water depth
PLATE 1
5 km

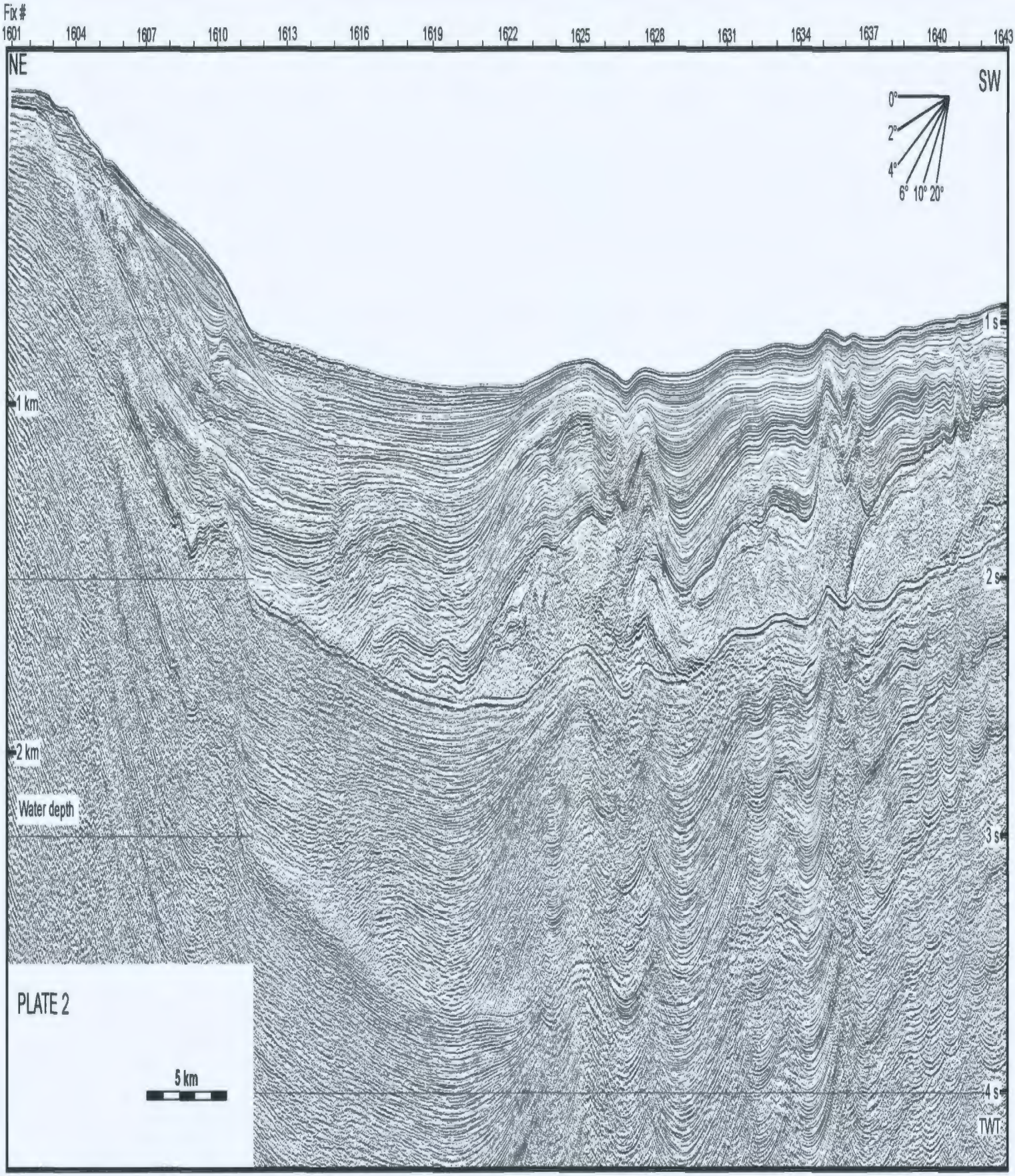
Fix #
1601
1604
1607
1610
1613
1616
1619
1622
1625
1628
1631
1634
1637
1640
1643
NE
SW
0°
2°
4°
6°
10°
20°
1 s
2 s
3 s
4 s
TWT
1 km
2 km
Water depth
PLATE 2
5 km

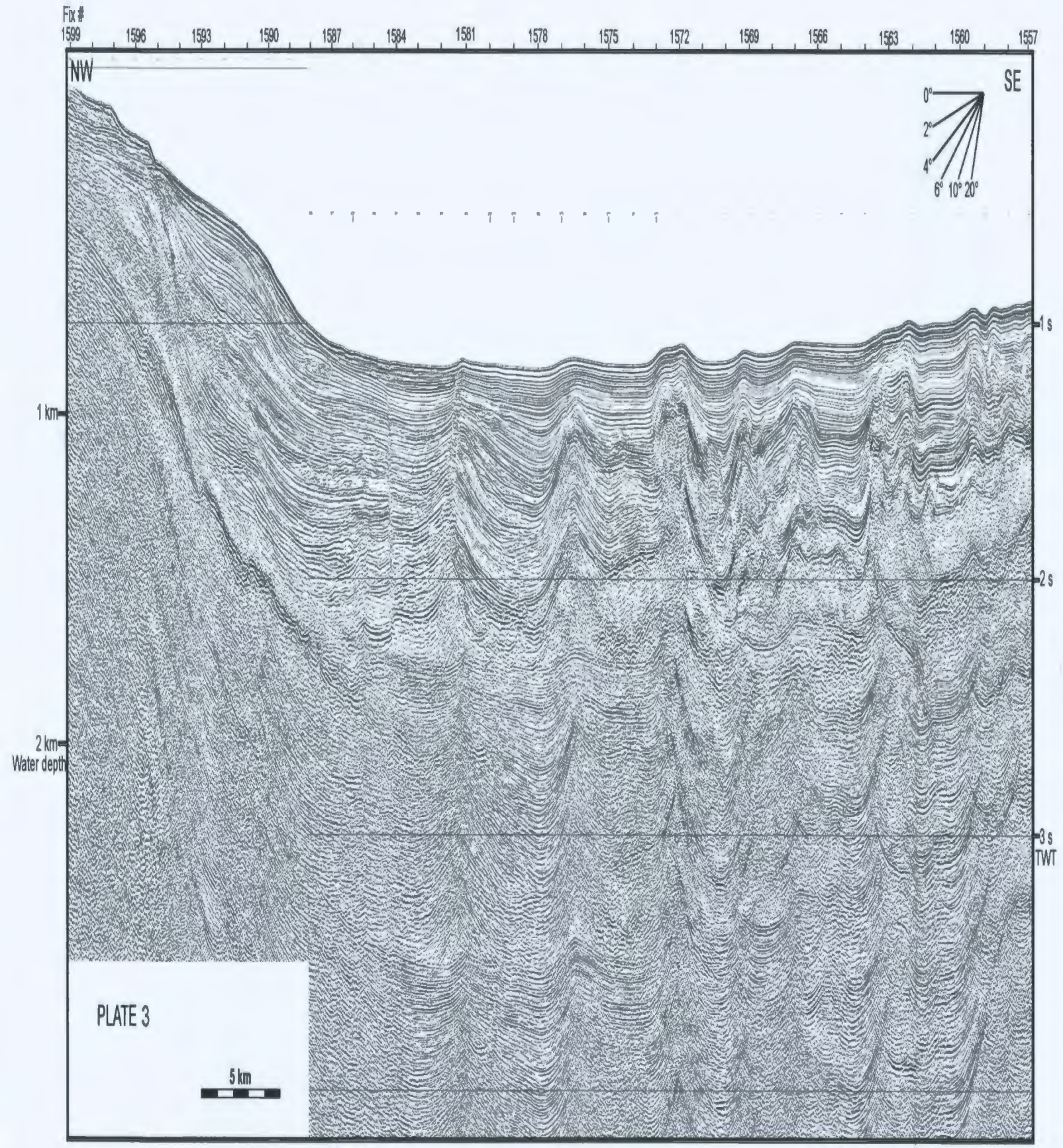
Fix #
1599
1596
1593
1590
1587
1584
1581
1578
1575
1572
1569
1566
1563
1560
1557
NW
SE
0°
2°
4°
6°
10°
20°
1 s
2 s
3 s
TWT
1 km
2 km
Water depth
PLATE 3
5 km

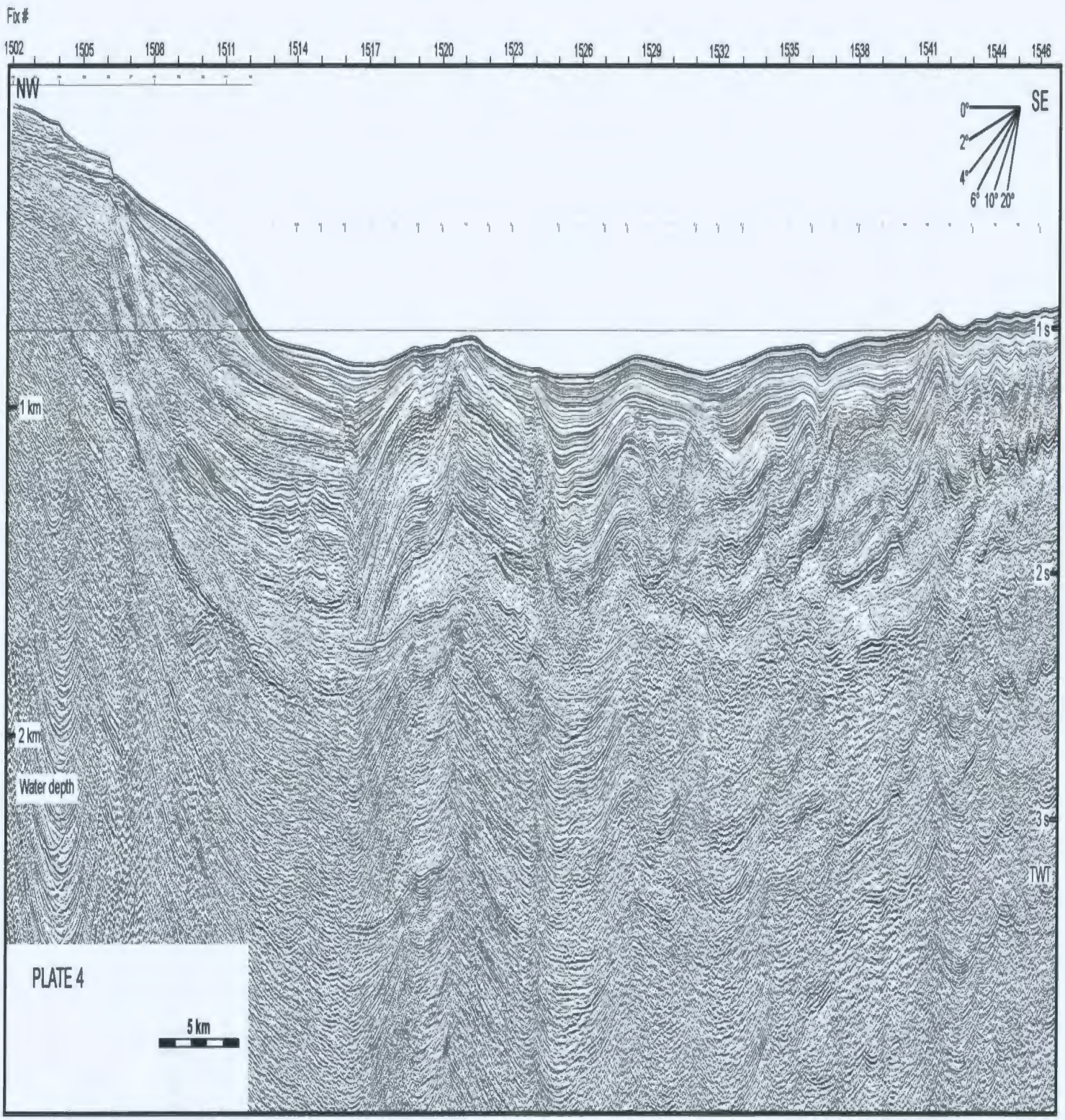
Fix #
1502
1505
1508
1511
1514
1517
1520
1523
1526
1529
1532
1535
1538
1541
1544
1546
NW
SE
0°
2°
4°
6°
10°
20°
1 s
2 s
3 s
TWT
1 km
2 km
Water depth
PLATE 4
5 km

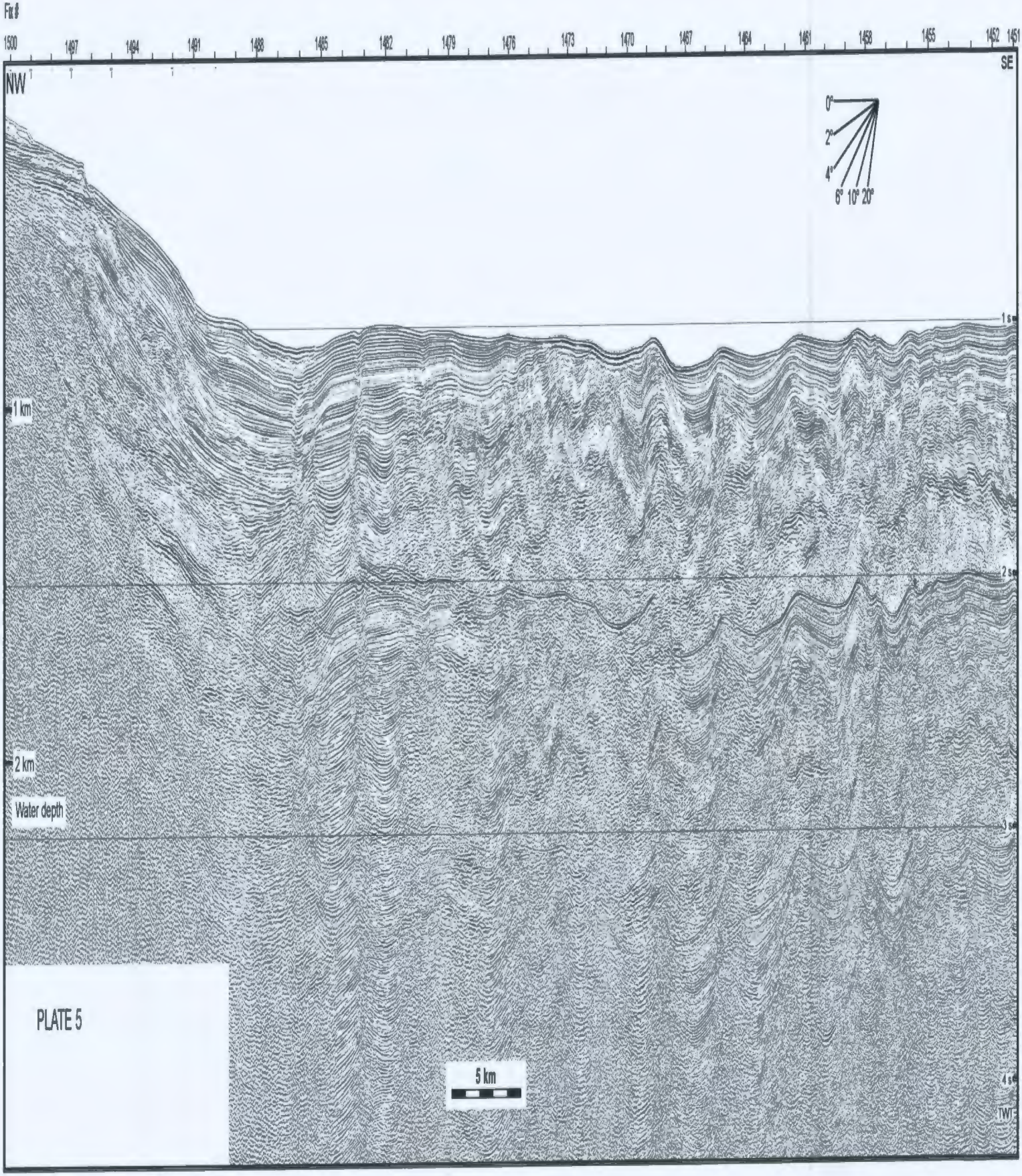
Fig 8
1500
1497
1494
1491
1488
1485
1482
1479
1476
1473
1470
1467
1464
1461
1458
1455
1452
1451
NW
SE
0°
2°
4°
6°
10°
20°
1 s
2 s
3 s
4 s
1 km
2 km
Water depth
5 km
TWT
PLATE 5

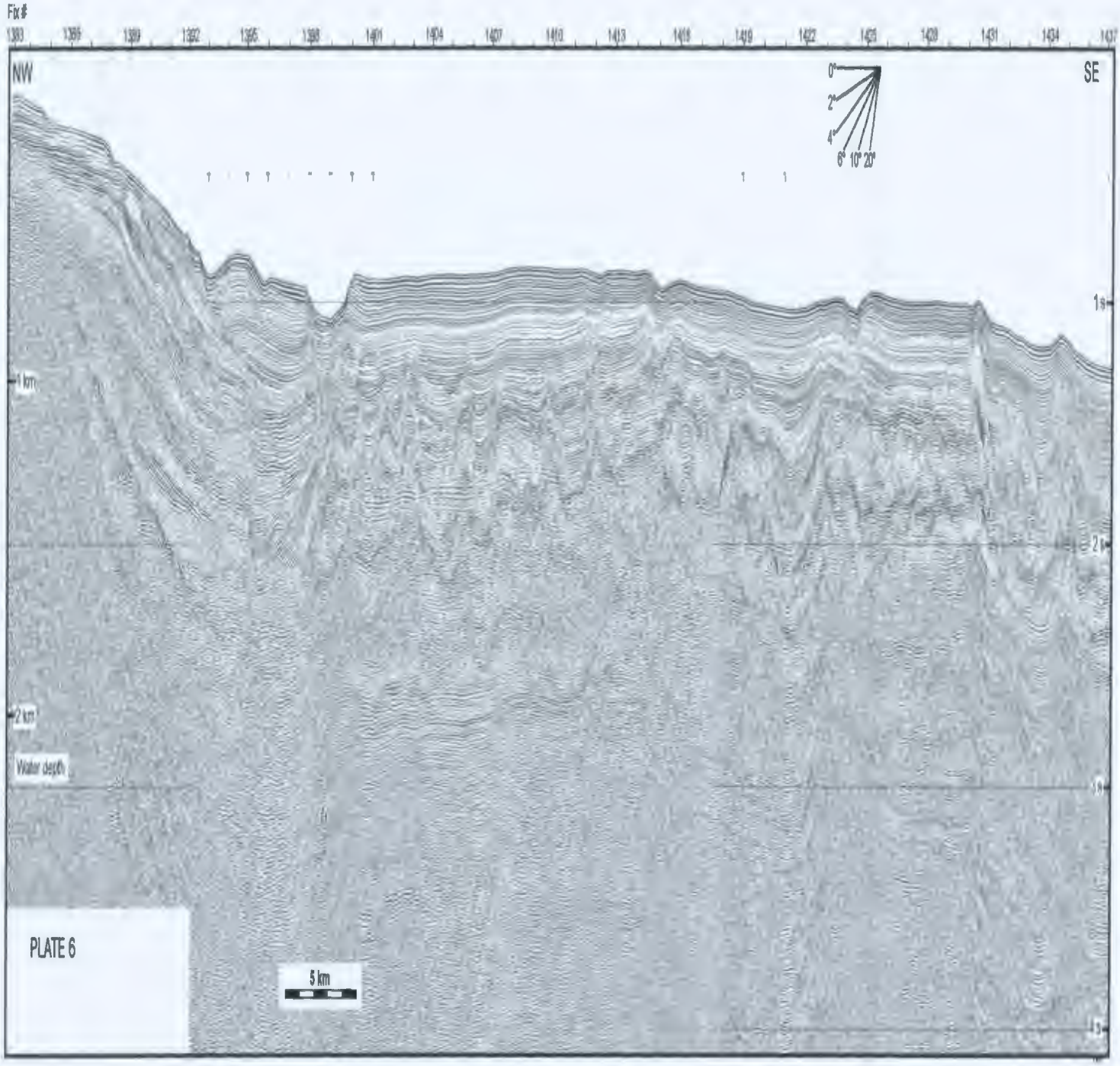
Fix #
1383
1386
1389
1392
1395
1398
1401
1404
1407
1410
1413
1416
1419
1422
1425
1428
1431
1434
1437
NW
SE
0°
2°
4°
6°
10°
20°
1 s
2 s
1 km
2 km
Water depth
PLATE 6
5 km

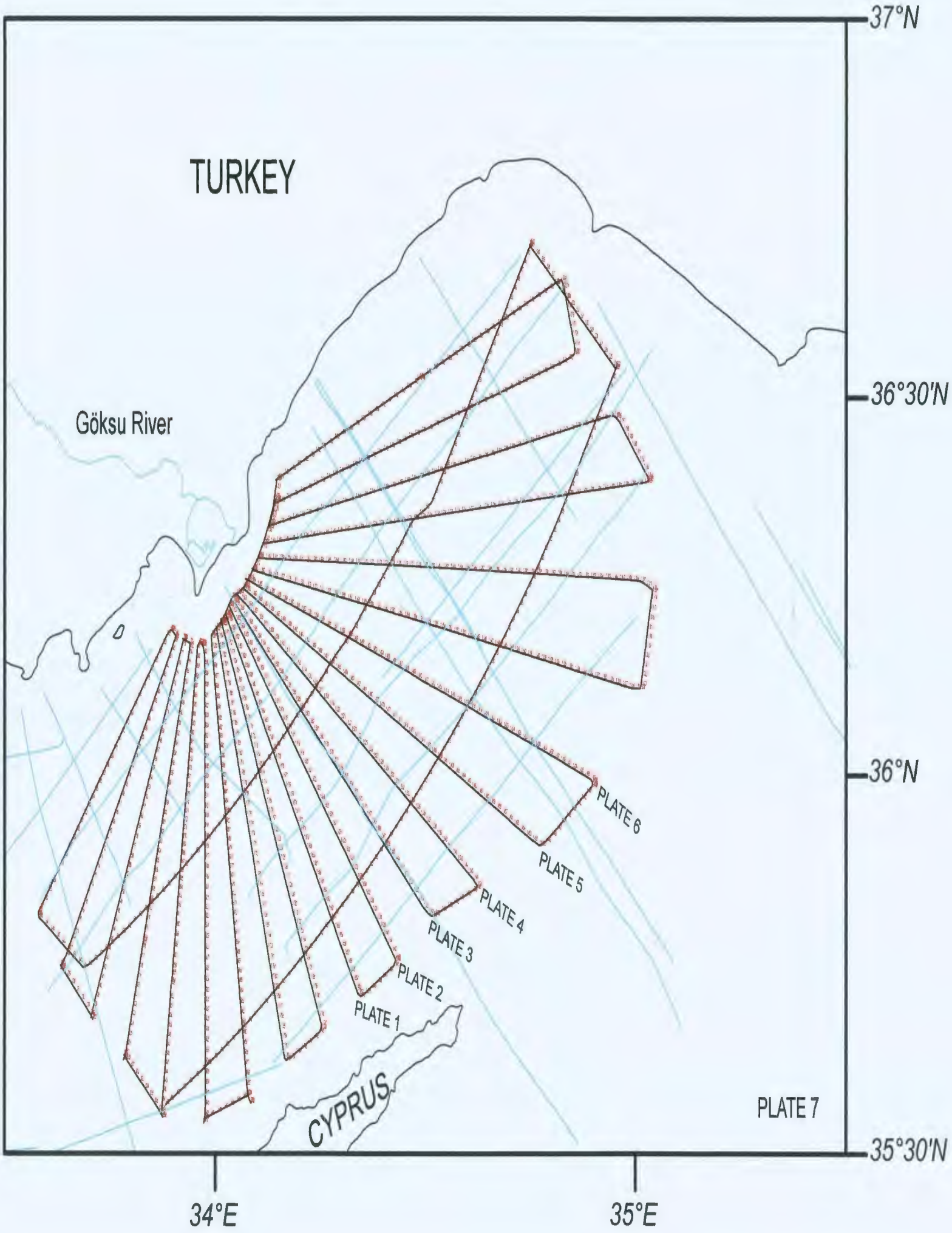
37°N
TURKEY
Göksu River
36°30'N
36°N
PLATE 6
PLATE 5
PLATE 4
PLATE 3
PLATE 2
PLATE 1
CYPRUS
PLATE 7
35°30'N
34°E
35°E